ISSN 2233-9485(Print)
ISSN 2233-9574(Online)

한국자기학회 2019년도 임시총회 및 하계학술연구발표회

KMS 2019 Summer Conference

논문개요집

일시 2019. 5. 22(수) ~ 24(금)

장소 한화리조트 해운대 티볼리

주최 한국자기학회

Digests of the KMS 2019 Summer Conference

The Korean Magnetics Society

사단법인 한국자기학회

한국자기학회 2019년도 임시총회 및 하계학술연구발표회

KMS 2019 Summer Conference

논문개요집

일시 2019. 5. 22(수) ~ 24(금)

장소 한화리조트 해운대 티볼리

주최 한국자기학회

공지사항

1. 포스터발표를 하시는 회원은 아래의 사항을 지켜주시기 바랍니다.

1) 포스터보드 크기는 한 명당 가로 100cm X 세로 180cm 사용할 수 있습니다.

2) 포스터는 수요일 오후 14:30~18:30까지 부착하시면 되고, 포스터 발표 Discussion은 20:00~21:00 사이에 별도로 진행됩니다.

2. 일정

5월 22일(수)	13:00~	참가자 등록			
	14:30~18:30	강습회 프로그램 (마나롤라)		포스터발표 (베르나차)	
	18:30~18:50	구두발표 (마나롤라)			
	18:50~20:00	저녁식사			
	20:00~21:00	포스터발표 Discussion & Bierstube (베르나차)			
5월 23일(목)	08:30~	참가자 등록			
	09:00~09:50	Plenary Session(IEEE DL) I (마나롤라)			
	09:50~10:00	Coffee Break			
	10:00~12:30	Special Session I (마나롤라)	Special Session II (베르나차)	Special Session III (코닐리아)	Special Session IV (리오마조레)
	12:30~14:00	점심식사			
	14:00~14:50	Plenary Session II (마나롤라)			
	14:50~15:00	Coffee Break			
	15:00~17:30	Special Session V (마나롤라)	Special Session II (베르나차)	Special Session III (코닐리아)	Special Session VI (리오마조레)
	17:30~18:00	한국자기학회 임시총회 및 시상식 (마나롤라)			
	18:00~20:00	Dinner (블루시걸)			
5월 24일(금)	08:30~	참가자 등록			
	09:00~09:50	Half-plenary Session I (마나롤라)	Half-plenary Session II (베르나차)		
	09:50~10:00	Coffee Break	Coffee Break		
	10:00~12:30	Special Session VII (마나롤라)	Special Session VIII (베르나차)	Special Session IX (코닐리아)	Special Session X (리오마조레)
	12:30~13:00	포스터 시상 및 경품, 폐회 (마나롤라)			

3. 『Best Poster 시상』이 5월 24일(금) 12:30부터 있을 예정이오니, 회원 여러분의 많은 참여를 바랍니다.
(단, 수상자(발표자)가 불참 시에는 수상이 취소됩니다.)

5월 22일[수]

시간	프로그램	
13:00 ~	참가자 등록	
	강습회 프로그램 (마나롤라) 좌장: 임성현(울산대)	포스터발표 (베르나차)
14:30 ~ 15:20	T-1. 미소자기 전산모사(micromagnetic simulation)의 이해와 실전 이기석(UNIST)	[1] Magnetic theory and calculations [2] Magnetization dynamics [3] Hard-magnetic Materials [4] Soft-magnetic Materials [5] Semiconductor spintronics [6] Spin orbit coupling and related phenomena [7] Nano-structured materials [8] Spin transfer torque for magnetic memory [9] Nanoscale Magnetism [10] Magnetic Oxides and Multiferroics [11] Biomedical Magnetics [12] Sensor and Applications [13] Others
15:20 ~ 15:30	Coffee Break	
15:30 ~ 16:20	T-2. Advanced TEM techniques for magnetic materials 박현순(인하대)	
16:20 ~ 16:30	Coffee Break	
16:30 ~ 18:30	T-3. Topology in magnetism Hans-Benjamin Braun(University College Dublin)	
18:30 ~ 18:50	구두발표 (마나롤라) O-1. Magnetics and History 김희중(KIST)	
18:50 ~ 20:00	저녁식사	
20:00 ~ 21:00	포스터발표 Discussion & Bierstube (베르나차) 좌장: 김상훈(울산대) / 이억재(KIST)	

5월 23일[목]

시간	프로그램			
08:30 ~	참가자 등록			
	Plenary Session I (마나롤라) 좌장: 이경진(고려대)			
09:00 ~ 09:50	P-1. (IEEE DL) Spin-Orbit Technologies: From Magnetic Memory to Terahertz Generation 양현수(National University of Singapore)			
09:50 ~ 10:00	Coffee Break			
	Special Session I (마나롤라) 'Magnetism in reduced dimension' 좌장: 유정우(UNIST)	Special Session II (베르나차) 'Hard & Soft Magnetic Materials: 고성능 모터용 자석 개발' 좌장: 이우영(연세대)	Special Session III (코닐리아) 'Bio-Neuro Convergence with Spin Magnetism' 좌장: 이재동(DGIST)	Special Session IV (리오마조레) 'Magnetization Dynamics' 좌장: 최석봉(서울대)
10:00 ~ 10:25	초S-I-1. Electron spin resonance on individual atoms on surfaces 최태영(이화여대)	초S-II-1. Revisit conventional magnets for tips on finding new permanent magnet material 권해웅(부경대)	초S-III-1. Enhancement of sensitivity of planar Hall effect sensors by optimization of geometry and layer composition: limitations and possibilities A. D. Talantsev(DGIST)	초S-IV-1. 수평자성과 좔로신스키-모리야 상호작용 문경웅(한국표준과학연구원)
10:25 ~ 10:50	초S-I-2. Novel scanning magnetic imaging based on diamond NV centers 이동헌(고려대)	초S-II-2. Progress in ceramic permanent magnets based on M-type hexaferrites 유상임(서울대)	초S-III-2. PHR 센서의 2차 고조파를 이용한 자성비드 측정 김동영(안동대)	초S-IV-2. 페리자성체/중금속 이종접합에서 마그논(magnon)에 의한 단방향 자기이방성의 거동 이수길(KAIST)
10:50 ~ 11:15	초S-I-3. Antiferromagnetic Van der Waals materials $TMPS_3$ and its Potentials 박제근(서울대)	초S-II-3. 1차원 구조를 갖는 교환자기결합형 Sm-Co/Fe-Co 코어쉘 나노섬유의 구현 및 자기적특성 김종렬(한양대)	초S-III-3. Extremely Low Perpendicular Magnetic Anisotropy and Sustainable Dzyaloshinskii-Moriya Interaction with a Palladium Underlayer 김준서(DGIST)	초S-IV-3. Long-range chiral interlayer exchange coupling in synthetic antiferromagnets 한동수(KIST)
11:15 ~ 11:40	초S-I-4. Physical properties of 2D magnetic materials 이창구(성균관대)	11:15 ~ 11:25 Coffee Break	초S-III-4. Valley magnetic domain as a pathway to the valleytronic current processing 이재동(DGIST)	초S-IV-4. Low magnetic damping of ferrimagnetic GdFeCo alloys 김덕호(Kyoto Univ.)
11:40 ~ 12:05	초S-I-5. Room temperature ferromagnetism in a magnetic-metal-rich van der Waals metal 김준성(포항공대)	11:25 ~ 11:50 초S-II-4. Development Status of Rare Earth magnets for Vehicle Motors 이재령(현대자동차)	초S-III-5. Accurate, Hysteresis Free Temperature Sensor for Health Monitoring Using a Magnetic Sensor and Pristine Polymer 정우성(DGIST)	초S-IV-5. Electric field induced spin waves on the CoFeB disk-shaped nanomagnet 조재훈(한국표준과학연구원)
12:05 ~ 12:30	초S-I-6. Electrically induced valley orbital magnetization in 2D semiconductor 이지은(아주대)	11:50 ~ 12:15 초S-II-5. Anisotropic Rare-earth Bulk Magnet produced by Hot-deformation Process 차희령(재료연구소)	초S-III-6. Magneto-optical properties of Bi-YIG thin films prepared by metal-organic decomposition 정종율(충남대)	초S-IV-6. Role of the topological singularity in magnetic-vortex dynamics 이기석(UNIST)
12:30 ~ 14:00	Lunch			

5월 23일[목]

시간	프로그램			
	Plenary Session II (마나롤라) 좌장: 김철기(DGIST)			
14:00 ~ 14:50	P-2. Nanomembranes: From basic concepts to paradigm shifting technologies Oliver Schmidt(Leibniz-Institut für Festkörper-und Werkstoffforschung Dresden)			
14:50 ~ 15:00	Coffee Break			
	Special Session V (마나롤라) 'Advanced Information Technology based on spin-orbit coupling' 좌장: 이경진(고려대) / 구현철(KIST)	Special Session II (베르나차) 'Hard & Soft Magnetic Materials: 고성능 모터용 자석 개발' 좌장: 이현숙(연세대)	Special Session III (코닐리아) 'DGIST-IFW Dresden 공동 협력연구 확대 방안 모색' 좌장: 이재동(DGIST)	Special Session VI (리오마조레) '뫼스바우어 분광분석을 활용한 융합연구' 좌장: 엄영랑(한국원자력연구원)
15:00 ~ 15:30	(Invited)S-V-1. PMA, SOT, and DMI in Non-Centrosymmetric Artificial Superlattices Teruo Ono(Kyoto Univ.)	15:00 ~ 15:25 초S-II-6. Microstructures and Magnetic Properties of Fe-rich Compounds with $ThMn_{12}$ Structure 박지훈(재료연구소)	비공개 세션	초S-VI-1. Electrochemically activated cobalt nickel sulfide for an efficient oxygen evolution reaction: partial amorphization and phase control 민성욱(한국생산기술연구원)
15:30 ~ 16:00	초S-V-2. Interface-generated spin current and spin-orbit torques 박병국(KAIST)	15:25 ~ 15:50 초S-II-7. Magnetic Properties of Rare-earth (NdFeB) and Rare-earth-free (Mn-based) Permanent Magnets 김수민(연세대)		초S-VI-2. Study of exchange interaction strength of $Y_{3-x}R_xFe_5O_{12}$ (R=La, Na, and Gd) using Mössbauer spectroscopy 엄영랑(한국원자력연구원)
16:00 ~ 16:30	초S-V-3. Bulk-likespin – orbit torques in ferrimagnets 양현수 (National University of Singapore)	15:50 ~ 16:15 초S-II-8. Selective Laser Melting Processing of Soft Magnetic Bulk Metallic Glass 정재원(재료연구소)		초S-VI-3. Fe계 신영구자석 개발과 뫼스바우어 분광 연구 임정태(재료연구소)
16:30 ~ 17:00	초S-V-4. Abnormal asymmetric motion of magnetic solitons with multiple inversion asymmetries 김경환(KIST)	16:15 ~ 16:25 Coffee Break		초S-VI-4. Analysis and Control of Heat Generation of MNPs by Changes in Magnetization for Magnetic Hyperthermia 김성훈(원광대)
17:00 ~ 17:30	초S-V-5. Orbital Anisotropic Magnetoresistance 고혜원(고려대)	16:25 ~ 16:50 초S-II-9. Analysis techniques based on magneto-optical Kerr effect 김동현(충북대) 16:50 ~ 17:15 초S-II-10. High Performance Magnetic Materials based on Metastable Iron / Iron Oxides 백연경(재료연구소)		초S-VI-5. Frequency Dependence of Initial Heat Generation in Magnetite Nanoparticles 윤성현(군산대)
17:30 ~ 18:00	한국자기학회 임시총회 및 시상식 (마나롤라)			
18:00 ~ 20:00	Dinner (블루시걸)			

5월 24일[금]

시간	프로그램			
08:30 ~	참가자 등록			
	Half-plenary Session I (마나롤라) 좌장: 민병철(KIST)	Half-plenary Session II (베르나차) 좌장: 김동현(충북대)		
09:00 ~ 09:50	HP-I-1. Static and dynamical skyrmions and emergent electromagnetism of moving monopoles in nanowires Hans-Benjamin Braun (University College Dublin)	HP-II-1. 희토류 소재 저감형 신규 모터 설계 기술 연구 유세현(전자부품연구원)		
09:50 ~ 10:00	Coffee Break	Coffee Break		
	Special Session VII (마나롤라) 'スピン オビトロニクス: 이론과 실험' 좌장: 임성현(울산대) / 김상훈(울산대)	Special Session VIII (베르나차) 'Electro-Magnetic Energy Convergence' 좌장: 최장영(충남대)	Special Session IX (코닐리아) 'Medical Magnetics' 좌장: 한만석(강원대) / 안우상(울산의대)	Special Session X (리오마조레) 'Magnetics for IoT' 좌장: 손대락(한남대)
10:00 ~ 10:25	초S-VII-1. Emergence of robust 2D skyrmions in $SrRuO_3$ ultrathin film 김봉주(서울대)	초S-VIII-1. Size Reduction Design of Electric Machine for Rare-earth free applying BSMM 박현진(한양대)	초S-IX-1. Development of Gamma Camera with a Diverging Collimator Using DMLS 3D Print 원종훈(강원대)	초S-X-1. 함정 전자기 신호 피탐 성능 분석 기법 연구 양창섭(국방과학연구소)
10:25 ~ 10:50	초S-VII-2. Orbital Spintronics: Non-trivial charge-to-spin conversion in ferromagnetic metal/Cu/oxide trilayers 김준연(RIKEN)	초S-VIII-2. Asymmetric Rotor Shape Design for Interior Permanent Magnet Synchronous Motor using Advanced Inverse Cosine Function 임명섭(영남대)	초S-IX-2. MR-compatible DOI-PET detector providing multiple spatial resolution 홍성수(전남대)	초S-X-2. 3-축 Flux-gate 마그네토미터를 이용한 지하매설 불발병기(DXO)탐지에 관한 연구 손대락(한남대)
10:50 ~ 11:15	(Invited)S-VII-3. Linear-response-based DFT+U study on Co-based full Heusler alloy for half-metallic electronic structure Kenji Nawa(NIMS)	초S-VIII-3. Study on Slotless Axial Flux Synchronous Motor Using Ceramic Coating Coil 정경태(한양대)	초S-IX-3. Evaluation of Image Distortion according to Difference of Average and Partial Fourier in Gd Contrast Agent in 3D T1 SPACE 한용수(한림대)	초S-X-3. 함정용 소자장비 핵심기술 개발 표성영(대양전기공업(주))
11:15 ~ 11:40	(Invited)S-VII-4. Dynamics of noncollinear antiferromagnetic domain wall driven by spin current injection Yuta Yamane(SPICE and RIKEN)	초S-VIII-4. 해석적 기법을 이용한 마그네틱 랙-피니언 기어의 토크 특성 해석과 실험 장강현(충남대)	초S-IX-4. The use of Near Infrared Radiation (NIR) in Reconstructing 3D Oxygenated Images as Biomedical Evidence in Monitoring Diabetic Foot 정영진(동서대)	초S-X-4. 함정의 두께와 반자장에 따른 탈자 영향 분석 박관수(부산대)
11:40 ~ 12:05	(Invited)S-VII-5. Magnetic spin Hall effects in a non-colinear antiferromagnet Motoi Kimata(Tohoku Univ.)	초S-VIII-5. Magnet Shape Design for SPMSM of EPS System by Using Cycloid Curve 이충성(만도)	초S-IX-5. Radiation Dosimetry for medical field using Alanine/ESR System 장한기(한국방사선진흥협회)	초S-X-5. 선체 부식으로 인한 수중 전자기 신호 특성 및 감소 기법 연구 정현주(국방과학연구소)
12:05 ~ 12:30	초S-VII-6. First-Principles Materials Design of Magnetic Anisotropy Dorj Odkhuu(인천대)	초S-VIII-6. Design of IE4 Class Line Start Permanent Magnet motor 이정종(전자부품연구원)	초S-IX-6. 자기공명영상(MRI) 기반의 영상유도방사선치료 기법 및 응용 정도일((주)한빔테크놀로지)	초S-X-6. NextSAT2 호기용 TAM 및 EMTB에 관한 연구 김은애((주)센서피아)
12:30 ~ 13:00	포스터 시상 및 경품, 폐회 (마나롤라)			

CONTENTS

5월 22일(수) 14:30~18:30
Session : 강습회 프로그램 — 마나롤라

좌 장 : 임성현(울산대)

T-1 14:30 미소자기 전산모사(micromagnetic simulation)의 이해와 실전 ····· 3
이기석*, 한희성, 정대한, 김남규

T-2 15:30 Advanced TEM techniques for magnetic materials ····· 4
Hyun Soon Park*

T-3 16:30 Topology in Magnetism ····· 5
Hans-Benjamin Braun*

5월 22일(수) 14:30~18:30
Session : 포스터발표 — 베르나차

좌 장 : 김상훈(울산대) / 이억재(KIST)

○ Session MT[Magnetic theory and calculations]

MT01 Poster Temperature dependent magnetic properties of Bi-doped $Fe_{16}N_2$ for potential rare-earth-free permanent magnet applications ····· 9
Imran Khan, Sungkyun Park* and Jisang Hong†

MT02 Poster An ab-initio study of C-doping effect on magnetocrystalline anisotropy of τ-MnAl ····· 10
Jin Sik Park, S. H. Rhim* and Soon Cheol Hong†

MT03 Poster First Principles Calculation on Magnetic properties and MCA of $L1_0$- FeNiX(X= B, C, N, O) ····· 11
Mun Bong Hong, S. H. Rhim and S. C. Hong*

MT04 Poster The Energy Product of Hard- and Soft-magnetic Cylindrical Core/shell ····· 12
Namkyu Kim*, Hee-Sung Han, Soo Seok Lee, Ki-Suk Lee

MT05 Poster Comparison of the deformation behavior and magnetic properties of Nd-Fe-B magnets made from isotropic melt-spun and HDDR powders ····· 14
Jae-Gyeong Yoo*, Ga-Yeong kim, Hee-Ryoung Cha, Jung-Goo Lee

MT06 Poster Electronic and Magnetic Structures of Insulating β-$V_2O(PO_4)$ with Quasi-one-dimensional Ferrimagnetic Spin Chain ····· 15
Seo-Jin Kim* and Kwan-Woo Lee

MT07 Poster On chip manipulation of particle/ cells on varied thickness of the magnetic diode for bio applications ····· 16
Keonmok Kim*, Jongwan Yoon, Hyeonsal Kim, Cheol Gi Kim†

MT08 Poster Magnetic property of bilayer CrI_3 ····· 17
Fazle Subhan*, Imran Khan and Jisang Hong†

MT09 Poster Effects of Structural Defects on Magnetic Properties of MgO/Pt(100) and MgO/Pt(110) Junctions: An *Ab-initio* Study ····· 18
Thi H. Ho, S. H. Rhim* and S. C. Hong†

MT10 Poster First principles study on half-metallicity of alkali-metal- based half-Heusler XCrZ (X = Li, Na, K; Z = As, Sb) ····· 19
Hoang Thu Thuy*, S. H. Rhim and S. C. Hong

MT11 Poster First principles studies of antiferromagnetic layered square lattice of spin S=1 Ni^{2+} ····· 20
Mi-Young Choi* and Kwan-Woo Lee†

MT12 Poster Multiple topological characters in room-temperature half-metallic antiferromagnet Cr_2CoAl ····· 21
Hyo-Sun Jin*, Young-Joon Song and Kwan-Woo Lee

MT13 Poster Influences of Substitutional Cobalt in Magnetic Properties of Tetragonal $D0_{22}$ Mn_3Ga ····· 22
Quynh Anh T. Nguyen, Thi H. Ho, S. C. Hong† and S. H. Rhim*

MT14 Poster Revisiting the complex magnetic structures of ultrathin fcc Fe/Cu(001) film ·· 23
Qurat-ul-ain*, S. H. Rhim, S. C. Hong and Jaejun Yu†

MT15 Poster Two-dimensional materials in curved geometry ····· 24
Minkyu Park* and Sung Hyon Rhim

MT16 Poster Influence of permeability according to packing rate of soft magnetic particles ··· 25
Ji Eun Lee*, Seok Hwan Huh†

MT17 Poster A resonated breaking of time-reversal symmetry: a first-principles TDDFT study for the case of 2-dimensional semiconductors ····· 26
Adem Halil Kulahlioglu*, Mahmut Sait Okyay, Bumseop Kim, Min Choi, Dongbin Shin, Noejung Park

MT18 Poster Intrinsic Spin Hall Conductivity of Heavy Metals: a First Principles Study ····· 27
Do Duc Cuong, Soon Cheol Hong* and S. H. Rhim*

MT19 Poster Robust cos theta dependence of Current shift to normal geomagnetic field ·· 28
Changjin Yun*, Mingu Kim, Jiho Kim and Kungwon Rhie

MT20 Poster Dynamics characteristics of ferrimagnetic GdFeCo alloy Atomistic simulation study ····· 30
Jaegun Sim*, Jae-Hyeok Lee, Sang-Koog Kim

MT21 Poster 마그노닉 결정 속 스핀파 프랙탈 ····· 32
박규영*, 김상국

○ Session MD[Magnetization dynamics]

MD01 Poster Highly efficient energy dissipation in soft magnetic and spherical nanoparticles in a single-domain state for hyperthermia bio-applications ····· 33
Min-Kwan Kim, Jaegun Sim, Jae-Hyeok Lee* and Sang-Koog Kim†

MD02 Poster In-plane field control of coupled-vortex oscillations in magnetic-dot-networks ····· 35
Young-Jun Cho*, Jaegun Sim and Sang-Koog Kim†

MD03 Poster Coupling of spin waves propagating along domain walls and a magnetic vortex in a thin-film nanostrip cross structure ····· 36
Hyeon-Kyu Park*, Jong-Hyuk Lee, Jaehak Yang and Sang-Koog Kim

MD04 Poster Stochastic Domain Wall Motion and Thermal Field Characterization ····· 37
Geun-Hee Lee* and Kab-Jin Kim

MD05 Poster Photon-magnon coupling in planar-geometry hybrid structure of Stub line resonator with YIG films ····· 38
Haechan Jeon*, Sang-Koog Kim

MD06 Poster Spin-wave excitation and critical angles in a photon-magnon-coupled hybrid system ····· 40
Bosung Kim*, Biswanath Bhoi and Sang-Koog Kim

MD07 Poster Abnormal anti-crossing effect in photon-magnon coupled system ····· 42
Biswanath Bhoi*, Bosung Kim and Sang-Koog Kim

MD08 Poster Dynamic modes of magnetic skyrmions in magnetic nanotubes ····· 44
Jaehak Yang*, Junhoe Kim, Claas Abert, Dieter Suess and Sang-Koog Kim†

MD09 Poster Huge Spin-Transfer Torque in Ferromagnetic Pd/Co/Pd Film ····· 45
Dae-Yun Kim, Seong-Hyub Lee*, Yune-Seok Nam, Ji-Sung Yu, Yong-Keun Park, Byoung-Chul Min and Sug-bong Choe†

○ Session HM[Hard-magnetic Materials]

HM01 Poster Effect of iron deficiency and Co substitution on the magnetic properties of Ca-La M-type hexaferrites ····· 47
Kang-Hyuk Lee* and Sang-Im Yoo†

HM02 Poster Growth temperature dependence on magnetism and crystallization of $SmFe_{12}$ thin films ····· 48
Daegill Cho*, Hyun Jung Kim, Sangkyun Ryu, Jae S. Lee, Jun Kue Park, Jaekwang Lee, Hyoungjeen Jeen

HM03 Poster Magnetic properties and hot-deformation behavior of Nd-lean magnets ····· 49
Ga-Yeong Kim*, Hee-Ryoung Cha, Yang-Do Kim, Jung-Goo Lee

HM04 Poster Synthesis of ε-Fe_2O_3 Nanopowder Substituted with Non-magnetic Elements based on Spray-Drying Process ····· 50
Kyung Min Kim*, Seung Min Lee, Min Ji Pyo, Jung Goo Lee, Youn-Kyoung Baek†

HM05 Poster Near theoretical ultra-high magnetic performance of rare-earth nanomagnets via synergetic combination of calcium-reduction and chemoselective dissolution ····· 51
이지민*, 김종렬, 좌용호

HM06 Poster Development of texture in (Nd,Ce)-Fe-B-type die-upset hybrid magnet composed of two constituents with/without Ce ····· 52
M. S. Kang*, Dagus R. Djuanda, H. W. Kwon, J. G. Lee and H. J. Kim

HM07 Poster Epitaxial growth of $SrFe_{12}O_{19}$ thin films and their magnetism ····· 54
Sangkyun Ryu*, Kung wan Kang, June Hyuk Lee, Jaekwang Lee, Jin-Hyung Cho, Hyoungjeen Jeen†

HM08 Poster Enhancing the coercivity and thermal stability of Nd-Fe-B sintered magnets by grain boundary diffusion process ····· 55
Sumin Kim*, Hyun-Sook Lee, Donghwan Kim, Jong Wook Roh and Wooyoung Lee†

HM09 Poster 영구자석 착자를 고려한 컴프레서용 모터 설계 ····· 56
김규섭*, 김수철, 김규식, 이병화

HM10 Poster Artificially produced rare earth free $L1_0$-FeNi phase through annealing of the FeNiPC amorphous alloy ····· 58
Jonghee Han*, Jihye Kim and Haein Choi-Yim

HM11 Poster 가스분무된 희토류 소결자석 소성변형능에 미치는 Ti 첨가의 영향 ····· 59
조주영*, 좌용호, 남선우, 김택수

○ Session SM[Soft-magnetic Materials]

SM01 Poster Modulating magnetism of polycrystalline $PrBaCo_2O_{5.7\pm x}$ through oxygen vacancy engineering ····· 60
Yun-Seok Heo* and Hyoungjeen Jeen†

SM02 Poster Enhance of Saturation Magnetic Flux Density of the Soft magnetic Core, with Maintaining Low Core loss and High Permeability ····· 61
Seoyeon Kwon* and Haein Yim

SM03 Poster Al 이온을 소량치환한 Y-type hexaferrite의 자기적 성질 연구 ····· 62
김정훈*, 김철성

SM04 Poster 다중스캔 기반 SLM법으로 제조된 FeSiBCCr 연자성 조형체의 미세 조직 및 자기적 특성 ····· 64
남영균*, 양상선, 유지훈, 정재원†

SM05 Poster 교차된 일축이방성 효과에 의한 NiO층 기반 이층 구조형 거대자기저항-스핀밸브 다층박막의 자기저항 특성 비교 ····· 66
최종구*, 카지드마, 강병욱, 이상석

SM06 Poster 보온재 비해체식 배관 감육평가를 위한 비파괴검사와 신호처리 ····· 68
박예라*, 신정우, 김경모, 손대락, 박덕근†

○ Session SS[Semiconductor spintronics]

SS01 Poster Current-induced magnetization change in a ferromanget/$Ge_2Sb_2Te_5$ interface ····· 71
Sung Jong Kim*, Tae-Eon Park, Oukjae Lee, Suyoun Lee and Hyun Cheol Koo

SS02 Poster Electrical transport along the surface of InAs nanowire ····· 72
Jeehoon Jeon*, Taeyueb Kim, Sangsu Kim, Sungjung Joo, Jae Cheol Shin, Hyun Cheol Koo, Jinki Hong

SS03 Poster $Ta_{1-x}W_x$/CoFeB/MgO 구조의 수직자기이방성과 스핀궤도토크 ····· 73
차인호*, 김태현, 김용진, 김규원, 김영근

○ Session SO[Spin orbit coupling and related phenomena]

SO01 Poster Variation of Interfacial Structure and Chemistry at Pt/Fe_3O_4 interfaces ····· 74
Thi Nga Do*, Thi Kim Hang Pham, Tae Hee Kim†

SO02 Poster Fluorophosphates $Na_2Fe_{0.9}Mn_{0.1}PO_4F$ 양극물질의 결정구조 및 자기적 특성 ····· 75
서재연*, 박승영, 김철성

SO03 Poster Li 이온의 결핍에 따른 $Li_xFe_{0.95}Mg_{0.05}PO_4$ 양극물질의 뫼스바우어 분광학적 연구 ·· 77
최현경*, 김철성

SO04 Poster Artifact-free optical spin-orbit torque magnetometry ····· 79
김주성, 박용근, 황현석, 박정현*, 민병철, 최석봉

○ Session NS[Nano-structured materials]

NS01 Poster $Mn_{1+b}Fe_{2-b}O_{4-\delta}$ 나노입자의 구조 및 자기적 특성 ····· 80
Y. J. Choi*, N. Tran, T. L. Phan, B. W. Lee†

NS02 Poster Fe_3O_4-ZnO 나노입자-나노선 계층구조 복합체의 합성 및 특성 분석 ····· 81
Min Jun Ko*, Bum Chul Park, Sang Won Byun and Young Keun Kim†

NS03 Poster Structural, Magnetic and Electrical Properties of $MnFe_2O_4$-$BiFeO_3$ Nanocomposite ····· 82
Inna Yusnila Khairani*, Anindityo Nugra Arifiadi, Biswanath Bhoi, Trivoramai Jiralerspong, Jaehyeok Lee, Jaegun Sim and Sang-Koog Kim†

○ Session BM[Biomedical Magnetics]

BM01 Poster 협착이 있는 마이크로채널 내에서 혈류흐름에 대한 펄스자기장의 영향 ····· 84
목진원*, 한승현, 방승환, 이현숙

BM02 Poster 저주파 자극에 따른 자성 홀소자 맥진파형 특성에 관한 연구 ····· 86
강병욱*, 최종구, 이상석

○ Session SA[Sensor and Applications]

SA01 Poster 칼만필터를 이용한 자기센서의 노이즈제거 ····· 88
김민석*, 김경원, 신광호

SA02 Poster Low Current sensing Planar Hall Resistance Sensors module for automobile ··· 89
J. H. Lee*, S. J. Kim, C. G. Kim

SA03 Poster Microwave absorption properties of Co-Mn substituted Sr-La M-type hexaferrite in Ka band (26.5-40 GHz) ····· 90
Sungjoon Choi*, Jae-Hyoung You, Seung-Young Park, Seong Jin Choi and Sang-Im Yoo

SA04 Poster Controllable Actuation of Magnetic Kirigami Patterns ····· 91
Trivoramai Jiralerspong*, Geonhee Bae and Sang-Koog Kim

SA05 Poster Magneto-transport effect in CoSiB thin films ····· 93
Y. K. Kim*, H. N. Lee, T. W. Kim†

5월 22일(수) 18:30~18:50
Session : 구두발표
마나틀라

좌 장 : 임성현(울산대)

O-1 18:30 Magnetics and History ····· 97
Hi-Jung Kim*

5월 23일(목) 09:00~09:50
Plenary Session Ⅰ (IEEE DL)
마나틀라

좌 장 : 이경진(고려대)

P-1 09:00 Spin-Orbit Technologies: From Magnetic Memory to Terahertz Generation ··· 101
Hyunsoo Yang*

5월 23일(목) 10:00~12:30
Special Session Ⅰ 'Magnetism in reduced dimension'
마나틀라

좌 장 : 유정우(UNIST)

초S-I-1 10:00 Electron spin resonance on individual atoms on surfaces ····· 105
Taeyoung Choi*

초S-I-2 10:25 Novel scanning magnetic imaging based on diamond NV centers ····· 106
Donghun Lee*

초S-I-3 10:50 Antiferromagnetic Van der Waals materials $TMPS_3$ and its Potentials ····· 107
Je-Geun Park*

초S-I-4 11:15 Physical properties of 2D magnetic materials ····· 108
Changgu Lee*

초S-I-5 11:40 Room temperature ferromagnetism in a magnetic-metal-rich van der Waals metal ····· 109
Jun Sung Kim*

초S-I-6 12:05 Electrically induced valley orbital magnetization in 2D semiconductor ····· 110
Jieun Lee*

5월 23일(목) 10:00~12:15
Special Session Ⅱ 'Hard & Soft Magnetic Materials: 고성능 모터용 자석 개발'
베르나차

좌 장 : 이우영(연세대)

초S-Ⅱ-1 10:00 Revisit conventional magnets for tips on finding new permanent magnet material ····· 113
Hae-Woong Kwon*, Jung Gu Lee

초S-Ⅱ-2 10:25 Progress in ceramic permanent magnets based on M-type hexaferrites ····· 114
Sang-Im Yoo*, Kang-Hyuk Lee and Sung-Jun Choi

초S-Ⅱ-3 10:50 1차원 구조를 갖는 교환자기결합형 Sm-Co/Fe-Co 코어쉘 나노섬유의 구현 및 자기적특성 ····· 115
김종렬*

초S-Ⅱ-4 11:25 Development Status of Rare Earth magnets for Vehicle Motors ····· 116
Jaeryung Lee*

초S-Ⅱ-5 11:50 Anisotropic Rare-earth Bulk Magnet produced by Hot-deformation Process ·· 117
Hee-Ryoung Cha*, Jae-Gyeong Yoo, Ga-Yeong Kim, Youn-Kyoung Baek, Hae-Woong Kwon, Jung-Goo Lee

5월 23일(목) 10:00~12:30
Special Session Ⅲ 'Bio-Neuro Convergence with Spin Magnetism'

코닐리아

❀ 좌 장 : 이재동(DGIST)

초S-Ⅲ-1 10:00 Enhancement of sensitivity of planar Hall effect sensors by optimization of geometry and layer composition: limitations and possibilities ····· 121
A. D. Talantsev*, S. J. Kim, M. J. Kim, K. W. Kim, A. A. Elzwawy, S. Oh, T. Q. Hung, C. G. Kim

초S-Ⅲ-2 10:25 PHR 센서의 2차 고조파를 이용한 자성비드 측정 ····· 123
김동영*, 윤석수, 이재훈, 김철기

초S-Ⅲ-3 10:50 Extremely Low Perpendicular Magnetic Anisotropy and Sustainable Dzyaloshinskii-Moriya Interaction with a Palladium Underlayer ····· 124
June-Seo Kim*

초S-Ⅲ-4 11:15 Valley magnetic domain as a pathway to the valleytronic current processing ··· 126
Youngjae Kim and Jae Dong Lee*

초S-Ⅲ-5 11:40 Accurate, Hysteresis Free Temperature Sensor for Health Monitoring Using a Magnetic Sensor and Pristine Polymer ····· 127
Wooseong Jeong*, Mijin Kim, Jae-Hyun Ha, Wooseong Jeong, Nora Asyikin Binti Zulkifli, Jung-Il Hong, Cheol Gi Kim and Sungwon Lee

초S-Ⅲ-6 12:05 Magneto-optical properties of Bi-YIG thin films prepared by metal-organic decomposition ····· 130
Viet Dongquoc, Jong-Ryul Jeong*

5월 23일(목) 10:00~12:30
Special Session Ⅳ 'Magnetization Dynamics '

리오마조레

❀ 좌 장 : 최석봉(서울대)

초S-Ⅳ-1 10:00 수평자성과 좔로신스키-모리야 상호작용 ····· 133
문경웅*, 김창수, 윤정범, 김동석, 전병선, 이상선, 김동옥, 조재훈, 양승모, 황찬용

초S-Ⅳ-2 10:25 페리자성체/중금속 이종접합에서 마그논(magnon)에 의한 단방향 자기이방성의 거동 ····· 134
이수길*, 강준호, 이재욱, 김정목, 김상훈, 이년종, 김창수, 문경웅, 황찬용, 박승영, 박병국, 김갑진

초S-Ⅳ-3 10:50 Long-range chiral interlayer exchange coupling in synthetic antiferromagnets ····· 135
Dong-Soo Han*

초S-Ⅳ-4 11:15 Low magnetic damping of ferrimagnetic GdFeCo alloys ····· 136
Duck-Ho Kim*, Takaya Okuno, Se Kwon Kim, Se-Hyeok Oh, Tomoe Nishimura, Yuushou Hirata, Yasuhiro Futakawa, Hiroki Yoshikawa, Arata Tsukamoto, Yaroslav Tserkovnyak, Yoichi Shiota, Takahiro Moriyama, Kab-Jin Kim, Kyung-Jin Lee and Teruo Ono

초S-Ⅳ-5 11:40 Electric field induced spin waves on the CoFeB disk-shaped nanomagnet ··· 137
조재훈*

초S-Ⅳ-6 12:05 Role of the topological singularity in magnetic-vortex dynamics ····· 138
Hee-Sung Han, Mi-Young Im, Young-Sang Yu, Min-Seung Jung, Sooseok Lee, Jung-Il Hong and Ki-Suk Lee*

5월 23일(목) 14:00~14:50
Plenary Session Ⅱ
마나롤라

좌 장 : 김철기(DGIST)

P-2 14:00 Nanomembranes: From basic concepts to paradigm shifting technologies ··· 141
Oliver G. Schmidt*

5월 23일(목) 15:00~17:30
Special Session Ⅴ
'Advanced Information Technology based on spin-orbit coupling
마나롤라

좌 장 : 이경진(고려대) / 구현철(KIST)

초S-Ⅴ-1 15:00 PMA, SOT, and DMI in Non-Centrosymmetric Artificial Superlattices ····· 147
Teruo Ono*

초S-Ⅴ-2 15:30 Interface-generated spin current and spin-orbit torques ····· 148
Seung-heon Chris Baek, Young-Wan Oh, Kyung-Jin Lee and Byong-Guk Park*

초S-Ⅴ-3 16:00 Bulk-like spin-orbit torques in ferrimagnets ····· 149
Hyunsoo Yang*

초S-Ⅴ-4 16:30 Abnormal asymmetric motion of magnetic solitons with multiple inversion asymmetries ····· 150
Kyoung-Whan Kim*, Seo-Won Lee, Kyoung-Woong Moon, Jung-Hwan Moon, Gyungchoon Go, Nico Kerber, Jonas Nothhelfer, Aurélien Manchon, Hyun-Woo Lee, Karin Everschor-Sitte and Kyung-Jin Lee

초S-V-5 17:00 Orbital Anisotropic Magnetoresistance ····· 151
Hye-Won Ko*, Hyeon-Jong Park, Gyungchoon Go, Jung Hyun Oh,
Kyoung-Whan Kim, Hyun Cheol Koo and Kyung-Jin Lee

5월 23일(목) 15:00~17:15
Special Session Ⅱ 'Hard & Soft Magnetic Materials: 고성능 모터용 자석 개발'

베르나차

좌 장 : 이현숙(연세대)

초S-Ⅱ-6 15:00 Microstructures and Magnetic Properties of Fe-rich Compounds with $ThMn_{12}$ Structure ····· 155
Jihoon Park*, Hui-Dong Qian, Jung-Tae Lim, Jong-Woo Kim and Chul-Jin Choi†

초S-Ⅱ-7 15:25 Magnetic Properties of Rare-earth (NdFeB) and Rare-earth-free (Mn-based) Permanent Magnets ····· 156
Sumin Kim*, Hyun-Sook Lee, Donghwan Kim, Jong Wook Roh and Wooyoung Lee†

초S-Ⅱ-8 15:50 Selective Laser Melting Processing of Soft Magnetic Bulk Metallic Glass ····· 157
Jae Won Jeong*, Yeong Gyun Nam, Mi Se Chang, Sangsun Yang, Jung-Goo Lee,
Yong-Jin Kim and Ji Hun Yu

초S-Ⅱ-9 16:25 Analysis techniques based on magneto-optical Kerr effect ····· 158
Dong-Hyun Kim*

초S-Ⅱ-10 16:50 High Performance Magnetic Materials based on Metastable Iron / Iron Oxides ··· 159
Youn-Kyoung Baek*, Kyung Min Kim and Jung-Goo Lee

5월 23일(목) 15:00~17:30
Special Session Ⅵ '뫼스바우어 분광분석을 활용한 융합연구'

리오마조레

좌 장 : 엄영랑(한국원자력연구원)

초S-Ⅵ-1 15:00 Electrochemically activated cobalt nickel sulfide for an efficient oxygen evolution reaction: partial amorphization and phase control ····· 163
Sungwook Mhin*, Hyuksu Han

초S-Ⅵ-2 15:30 Study of exchange interaction strength of $Y_{3-x}R_xFe_5O_{12}$ (R=La, Na, and Gd) using Mössbauer spectroscopy ····· 164
Young Rang Uhm*, Gwang Min Sun and Chul Sung Kim

초S-Ⅵ-3 16:00 Fe계 신영구자석 개발과 뫼스바우어 분광 연구 ····· 165
임정태*, 천휘동, 박지훈, 김종우, 김철성, 최철진

초S-Ⅵ-4 16:30 Analysis and Control of Heat Generation of MNPs by Changes in Magnetization for Magnetic Hyperthermia ····· 166
Sung Hoon Kim*

초S-Ⅵ-5 17:00 Frequency Dependence of Initial Heat Generation in Magnetite Nanoparticles ····· 167
Sunghyun Yoon* and Chul Sung Kim

5월 24일(금) 09:00~09:50
Half-plenary Session Ⅰ
마나롤라

좌 장 : 민병철(KIST)

HP-1 09:00 Static and dynamical skyrmions and emergent electromagnetism of moving monopoles in nanowires ····· 171
Hans-Benjamin Braun*

5월 24일(금) 09:00~09:50
Half-plenary Session Ⅱ
베르나차

좌 장 : 김동현(충북대)

HP-2 09:00 희토류 소재 저감형 신규 모터 설계 기술 연구 ····· 175
유세현*

5월 24일(금) 10:00~12:30
Special Session Ⅶ '스핀 오비트로닉스: 이론과 실험'
마나롤라

좌 장 : 임성현(울산대) / 김상훈(울산대)

초S-Ⅶ-1 10:00 Emergence of robust 2D skyrmions in $SrRuO_3$ ultrathin film ····· 179
Bongju Kim*, Byungmin Sohn, Hai Huang, Sang-Jun Lee, Se Young Park, Taeyang Choi, Hua Zhou, Seo Hyoung Chang*, Jung Hoon Han*, Jun-Sik Lee* and Changyoung Kim*

초S-Ⅶ-2 10:25 Orbital Spintronics: Non-trivial charge-to-spin conversion in ferromagnetic metal/Cu/oxide trilayers ····· 180
Junyeon Kim*, Dongwook Go, Hanshen Tsai, Kouta Kondou, Hyun-Woo Lee, YoshiChika Otani

초S-Ⅶ-3 10:50 Linear-response-based DFT+U study on Co-based full Heusler alloy for half-metallic electronic structure ····· 181
Kenji Nawa*, Yoshio Miura

초S-Ⅶ-4 11:15 Dynamics of noncollinear antiferromagnetic domain wall driven by spin current injection ····· 183
Yuta Yamane*, Olena Gomonay and Jairo Sinova

초S-Ⅶ-5 11:40 Magnetic spin Hall effects in a non-colinear antiferromagnet ····· 185
Motoi Kimata*

초S-Ⅶ-6 12:05 First-Principles Materials Design of Magnetic Anisotropy ····· 186
D. Odkhuu*, D. Tuvshin, T. Ochirkhuyag, Chang Geun Park, T. Tsevelmaa, S. H. Rhim and S. C. Hong

5월 24일(금) 10:00~12:30
Special Session Ⅷ 'Electro-Magnetic Energy Convergence'

베르나차

❀ 좌 장 : 최장영(충남대)

초S-Ⅷ-1 10:00 Size Reduction Design of Electric Machine for Rare-earth free applying BSMM ····· 189
Hyeon-Jin Park*, Kyung-Tae Jung, Myung-Seop Lim, Yun-Yong Choi and Jung-Pyo Hong

초S-Ⅷ-2 10:25 Asymmetric Rotor Shape Design for Interior Permanent Magnet Synchronous Motor using Advanced Inverse Cosine Function ····· 190
Young-Hoon Jung, Myung-Seop Lim*

초S-Ⅷ-3 10:50 Study on Slotless Axial Flux Synchronous Motor Using Ceramic Coating Coil ····· 191
Kyung-Tae Jung*, Hyeon-Jun Park, Yun-Yong Choi, Myung-Seop Lim and Jung-Pyo Hong

초S-Ⅷ-4 11:15 해석적 기법을 이용한 마그네틱 랙-피니언 기어의 토크 특성 해석과 실험 ····· 192
장강현*, 김창우, 서성원, 신경훈, 윤익재, 최장영

초S-Ⅷ-5 11:40 Magnet Shape Design for SPMSM of EPS System by Using Cycloid Curve ··· 194
Chung-Seong Lee*, Hyeon-Jin Park, Yun-Yong Choi

초S-Ⅷ-6 12:05 Design of IE4 Class Line Start Permanent Magnet motor ····· 195
Jeong-Jong Lee*, Ki-Doek Lee and Se-Hyun Rhyu

5월 24일(금) 10:00~12:30
Special Session Ⅸ 'Medical Magnetics'

코닐리아

❀ 좌 장 : 한만석(강원대) / 안우상(울산의대)

초S-Ⅸ-1 10:00 Development of Gamma Camera with a Diverging Collimator Using DMLS 3D Print ····· 199
Jong-Hun Won*, Dong-Hee Han, Seung-Jae Lee, Cheol-Ha Baek

초S-Ⅸ-2 10:25 MR-compatible DOI-PET detector providing multiple spatial resolution ····· 200
Sungsoo Hong*, Jingyu Yang, Jihoon Kang

초S-Ⅸ-3 10:50 Evaluation of Image Distortion according to Difference of Average and Partial Fourier in Gd Contrast Agent in 3D T1 SPACE ····· 203
Yong Soo Han*, Cheol Soo Park, Man Seok Han

초S-Ⅸ-4 11:15 The use of Near Infrared Radiation (NIR) in Reconstructing 3D Oxygenated Images as Biomedical Evidence in Monitoring Diabetic Foot ··· 204
Mezie Laurence B. Ortiz, Axel Yen C. Garcia and Youngjin Jung*

초S-Ⅸ-5 11:40 Radiation Dosimetry for medical field using Alanine/ESR System ····· 207
Han-Ki Jang*, Ki-Tak Han, Woo-sang Ahn

초S-Ⅸ-6 12:05 자기공명영상(MRI) 기반의 영상유도방사선치료 기법 및 응용 ····· 208
정도일*, 오성훈

5월 24일(금) 10:00~12:30

Special Session Ⅹ 'Magnetics for IoT'

리오마조레

좌 장 : 손대락(한남대)

초S-X-1 10:00 함정 전자기 신호 피탐 성능 분석 기법 연구 ····· 211
양창섭*, 정현주, 배기웅, 정우진, 이현진, 표성영

초S-X-2 10:25 3-축 Flux-gate 마그네토미터를 이용한 지하매설 불발병기(DXO)탐지에 관한 연구 ····· 213
손대락*, 김은애, 김상준

초S-X-3 10:50 함정용 소자장비 핵심기술 개발 ····· 214
표성영*, 이현진, 정봉출, 정현주, 양창섭

초S-X-4 11:15 함정의 두께와 반자장에 따른 탈자 영향 분석 ····· 216
박관수*, 임상현, 이호영, 정현주

초S-X-5 11:40 선체 부식으로 인한 수중 전자기 신호 특성 및 감소 기법 연구 ····· 218
정현주*, 양창섭

초S-X-6 12:05 NextSAT2 호기용 TAM 및 EMTB에 관한 연구 ····· 220
김은애*, 김상준, 손대락

KMS 2019 Summer Conference

강습회 프로그램

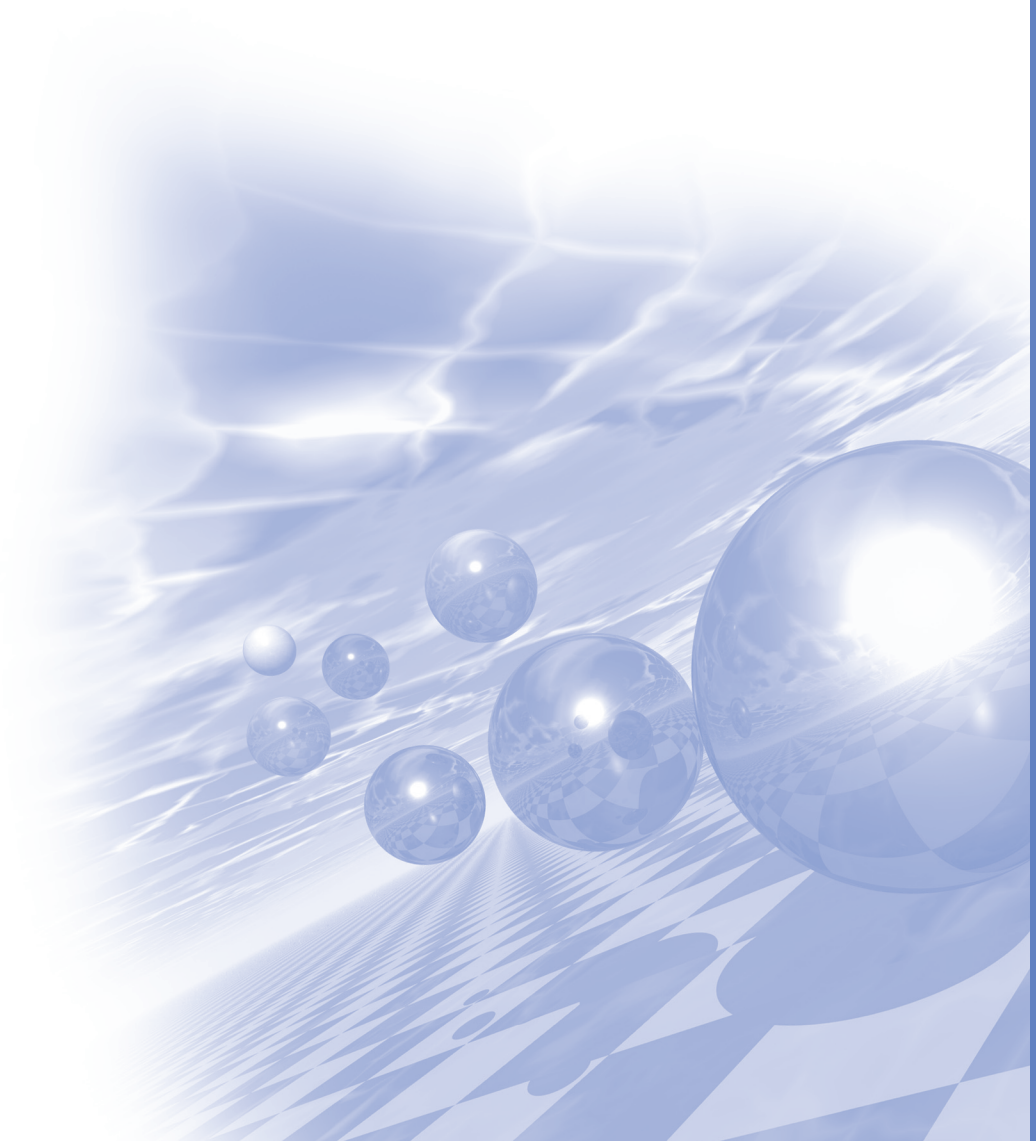

미소자기 전산모사(micromagnetic simulation)의 이해와 실전

이기석*, 한희성, 정대한, 김남규
울산과학기술원 (UNIST), 신소재공학부

본 강습회에서는 자성체의 자기적 거동, 특히 외부 자기장에 대한 반응인 자기이력곡선, 자기 모멘트의 시간에 따른 거동을 이해하는데 오늘날 널리 이용되는 모델인 미소자기학(micromagnetism)을 다루고자 한다. 미소자기학은 블로흐(Bloch)의 개념적 아이디어[1]에 란다우(Landau)와 리프쉬츠(Litshitz)가 물리적 기초를 다진 것[2]에서 출발했다고 볼 수 있다. 브라운(Brown)이 처음에 몇개의 원자 단위 거리를 연속체로 표현[3]하기 위해 사용한 '마이크로(micro)'라는 말 때문에 오해를 받기도 하지만, 미소자기학은 수 나노미터에서 마이크로미터 크기의 자성체의 거동을 무리없이 모사할 수 있는 모델이다. 최근에는 이 미소자기학을 원자단위까지 확장하여 원자단위의 자기 모멘트 거동을 이해하는데 쓰기도 한다.

본 강습회에서는 미소자기학 모델의 기초에 대해 살펴보고 여러가지 전산모사방법으로 미소자기학을 계산하는 대표적인 오픈소스 코드들, 그리고 실제로 연구에서는 어떻게 사용되고 있는지에 대한 몇가지 예들을 소개한다. 그리고 가장 많이 사용되고 있는 OOMMF 코드[4]를 중심으로 초보자가 처음 계산을 시작하는 방법과 계산에서 얻은 데이터의 분석 방법을 몇가지 예시를 통해 실습한다.

References

[1] F. Bloch, Z. Phys. 70, 295 (1932).
[2] L. Landau and E. Lifshitz, Phys. A. Sowjetunion 8, 153 (1935).
[3] W. F. Brown, Micromagnetics, Wiley, New York (1936).
[4] M.J. Donahue and D.G. Porter, OOMMF User's Guide, Version 1.0, National Institute of Standards and Technology, Gaithersburg, MD (1999) (http://math.nist.gov/oommf).

Advanced TEM techniques for magnetic materials

Hyun Soon Park*
Department of Materials Science and Engineering, Inha University, Incheon 22212, Korea
*hsparkinha@inha.ac.kr

Observations of the magnetic microstructures on a nanometer scale are very important for understanding material property and its application to engineering. Among the repertoire of so-called “magnetic imaging” methods, imaging techniques in transmission electron microscope (TEM) are Lorentz microscopy and electron holography, which can be implemented in a standard TEM. These techniques have been widely utilized to image magnetic microstructures and the magnetization process in situ. In the Fresnel (out-of-focus) method of Lorentz microscopy, domain walls (DWs), vortices and skyrmions (nanoscale spin vortex) are imaged, and these place a lower limit of tens of nanometers on the requirement for spatial resolution. The Fresnel method has been used to capture DWs nucleation/motion and the dynamics of vortices and skyrmions, spanning from the millisecond to the nanosecond regime. Electron holography, using the wave nature of electrons, provides opportunities for directly detecting and visualizing, in real space, the phase shifts ϕ of electron waves due to electromagnetic fields. In this tutorial, I introduce the principle of magnetic imaging and applications on various materials using Lorentz microscopy and/or electron holography [1-3].

Keywords: Magnetic microstructure, Microstructures, TEM, Magnetic imaging

References

[1] H. S. Park, J. Spencer Baskin, A. H. Zewail, 4D Lorentz electron microscopy imaging: magnetic domain wall nucleation, reversal, and wave velocity, **Nano Letters 10**, 3796 (2010)

[2] D. Shindo, T. Tanigaki, H. S. Park, Advanced electron holography applied to electromagnetic field study in materials science, **Advanced Materials 29**, 1602216 (2017)

[3] S. J. Lee, H.-J. Lee, K. Song, S.-Y. Choi, H. S. Park, In situ observation of domain wall motion in electroplated Ni_{80}-Fe_{20} thin film by Lorentz TEM and DPC imaging, J. Magnetics **22**(4), 563 (2017)

Topology in Magnetism

Hans-Benjamin Braun*
University College Dublin

Topological spin textures in real space such as skyrmions, merons, vortices and domain walls have attracted a lot of interest recently. Similar to a knot in a rope, they inherit the stability from the fact that the magnetization cannot be undone without violating the continuity of the magnetization field. In this lecture, it an overview of topological defects in magnetism is given and as an example, it is shown how topological constraints affect both helicity switching in skyrmions and the thermal stability of bits in high anisotropy materials. Finally, it is shown that geometric ideas such as Berry's phase play an important role in the quantum dynamics of single spins, of entire domain walls, and of electrons propagating in the background of topologically nontrivial spin textures. In half-integer spin systems without parity breaking interactions such as Dzyaloshinski-Moriya exchange, this gives rise to the spontaneous emergence of chirality and spin currents associated with propagating domain walls which can be measured via neutron scattering.

포스터발표

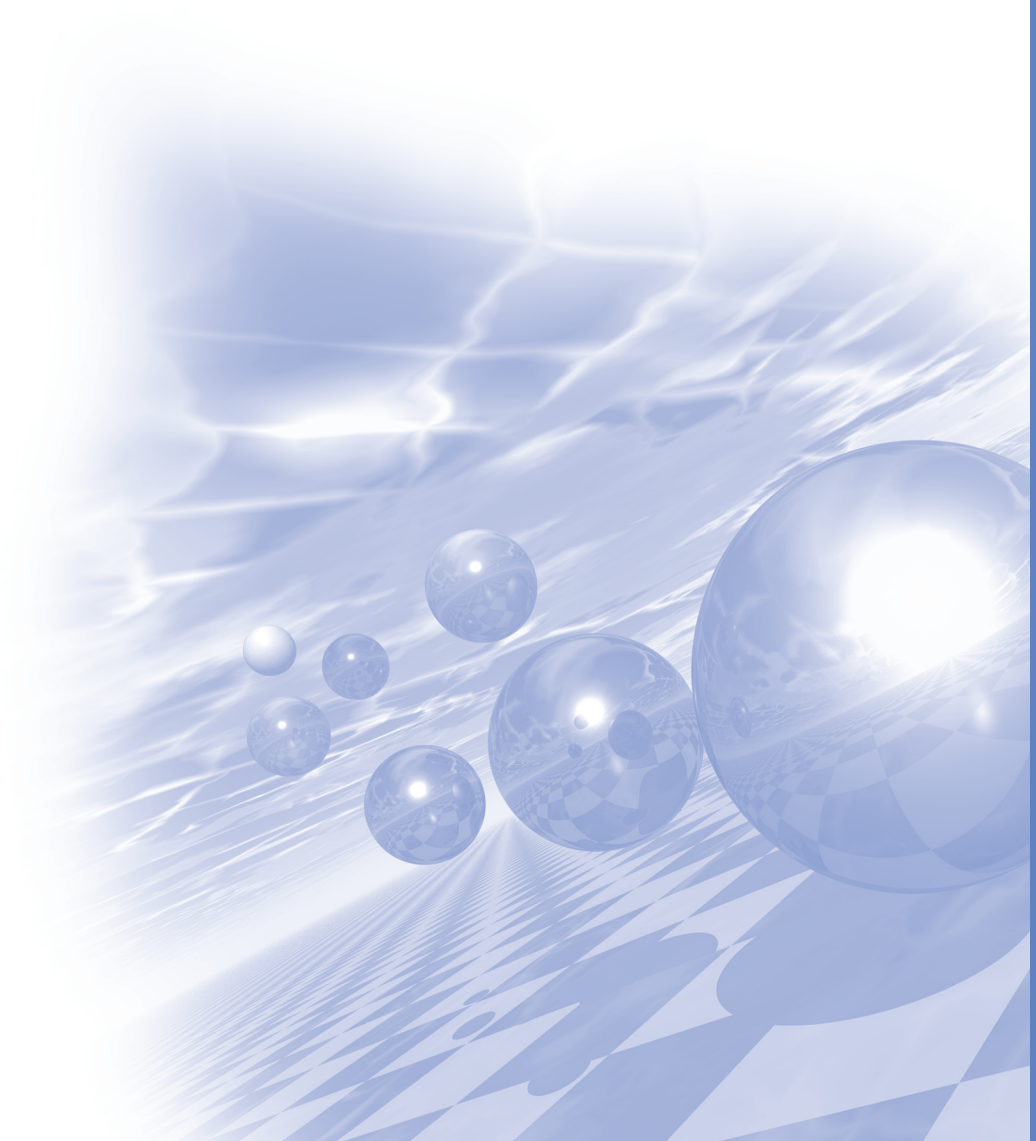

Temperature dependent magnetic properties of Bi-doped $Fe_{16}N_2$ for potential rare-earth-free permanent magnet applications

Imran Khan[1], Sungkyun Park[1*] and Jisang Hong[2†]
[1]Department of Physics, Pusan National University, 46241, Korea
[2]Department of Physics, Pukyong National University, Busan 48513, Korea
E-mails: *psk@pusan.ac.kr and †hongj@pknu.ac.kr

The feasibility of the rare-earth-free Bi-doped $Fe_{16}N_2$ magnet and its electronic and magnetic properties has been studied using first principle calculations within generalized gradient approximation. Bi doping increases the interatomic distances, thereby lead to a lattice distortion. Due to nonmagnetic Bi atom, lattice distortion and volume expansion we found a suppression of around 12% in the saturation magnetization of Bi-doped system compared to pristine $Fe_{16}N_2$. However, the hybridization between Fe 3d and Bi 6p orbitals were very helpful for enhancing the magnetocrystalline anisotropy from 0.73 meV/cell in pristine $Fe_{16}N_2$ to 1.57 meV/cell in Bi-doped system. In addition, the temperature dependent magnetic properties were also calculated by incorporating the ab initio results in atomistic simulations. The Monte Carlo (MC) metropolis simulations revealed an enhancement in the Curie temperature up to 860 K with Bi doping. In addition, the enhancement in uniaxial anisotropy with Bi doping results in an enhancement of the coercive field at finite temperature. For instance we obtained a coercive field of 9.63 kOe for Bi-doped system at 300 K which is almost three times enhancement compared to the pristine $Fe_{16}N_2$ alloy (3.61 kOe). Furthermore, the maximum energy product of 70.2 MGOe in Bi-doped alloy at 300 K was even larger than the value in Dy-doped Nd-based magnet (40 MGOe). Overall, we propose that the Bi-doped system could be a potential rare-earth-free permanent magnet.

Keywords: Permanent magnet, $Fe_{16}N_2$, substitutional doping, Magnetization, Magnetic anisotropy, Curie temperature, Coercive Field

Acknowledgments

This research was supported by Basic Science Research Program through the National Research Foundation of Korea (NRF) funded by the Ministry of Science, ICT and future planning (2016R1A2B4006406) to J. Hong, NRF-2018R1D1A1B07045663) and a KBSI grant (C38529) to S. Park.

An ab-initio study of C-doping effect on magnetocrystalline anisotropy of τ-MnAl

Jin Sik Park, S. H. Rhim* and Soon Cheol Hong†
Department of Physics and Energy Harvest Storage Research Center,
University of Ulsan, Ulsan 44610, Republic of Korea
Corresponding authors: *sonny@ulsan.ac.kr, †schong@ulsan.ac.kr

Ferromagnetic $L1_0$ structured τ-MnAl is one of candidates for rare-earth free permanent magnets. Its magnetic moment was measured in experiments to be 1.94 μ_B/f.u. and its lattice constants are a=3.91 Å and c=3.56 Å. However, τ-MnAl is just metastable at room temperature. The metastable τ-MnAl is stabilized by doping of elements such as C in MnAl [1]. And it is reported that 1.7% C-substitution is optimal [2].

In this study, we reveal the C-doping effects on magnetism and magnetocrystalline anisotropy (MCA) of the τ-MnAl, adopting the first-principles calculational method of Vienna Ab-initio Simulation Package (VASP). For the exchange-correlation potential, the generalized gradient approximation(GGA) is employed as parametrized by Perdew, Burke, and Ernzerhof (PBE). We choose supercell of 2x2x2 for calculating doping effect. The k-mesh of 11x11x11 is used in the Monkhorst-Pack scheme for the supercell. For the wave function expansion, a plane-wave basis set with a cutoff energy 450 eV is used. First, equilibrium lattice constants of a=3.89 Å and c=3.49 Å are obtained from total energy calculations. They are a little bit smaller compared to the experimental values(a=3.91 Å, c=3.56 Å), but consistent with a previous DFT calculation [3]. We got magnetic moment of 2.30 μ_B/f.u. and MCA energy of +0.27 meV/f.u. without doping (magnetic moment of 2.29 μ_B/f.u. and MCA energy +0.27 meV/f.u. [3]). We pound that after substitution 6.25% for the Al site, Magnetization was decreases 1.01 T to 0.90 T, but enhances MCA constant 1.6 MJ/m^3 to 1.9 MJ/m^3. We will discuss the origin of the enhanced MCA by the C-doping and variation of the magnetic moment and the MCA with amount of the C-doping.

References

[1] A. Pasko, M. LoBue, E. Fazakas, L. K. Varga, and F. Mazaleyrat, J. Phys.: Condens. Matter **26**, 064203 (2014).
[2] Q. Zeng, I. Baker, J.B. Cui, and Z.C. Yan, J. Magn. Magn. Mater. **308**, 214 (2007).
[3] A. Edstrom, J. Chico, A. Jakobsson, A. Bergman, and J. Rusz, Phys. Rev. B **90**, 014402 (2014)

First Principles Calculation on Magnetic properties and MCA of $L1_0$- FeNiX(X= B, C, N, O)

Mun Bong Hong, S. H. Rhim and S. C. Hong*
Department of Physics and Energy Harvest Storage Research University of Ulsan, Ulsan 44610 Republic of Korea

In magnetism, permanent magnets have been always important topic in both science and industry perspective. Recently, it has been a key issue to avoid rare earth metals, which are susceptible to change of supply and demand in market. As an alternative of rare earth (RE), alloys in $L1_0$ structure such as FePt, FePd, and CoPt have attracted with strong perpendicular magnetic anisotropy (PMCA). Among those, since Pd and Pt are rather expensive, $L1_0$-FeNi without rare earth and precious metals has been explored next generation permanent magnets. The $L1_0$ structured $L1_0$-FeNi contains two iron and nickel per unit cell, where lattice constants are a = 3.556 Å, c = 3.584 Å. In this work, we study $L1_0$-FeNiX (X= B, C, N, O) using density functional calculations. The magnetic moments of Fe and Ni are 2.58 μ_B and 0.62 μ_B, respectively. For the 0% strain case, the saturation magnetization are 1.6514 T with the MCA of 0.182 meV. When instituting B, C, N, O into $L1_0$-FeNi, C and O atoms have the smallest decrease rate of saturation magnetization with the maximum anisotopy constant value.

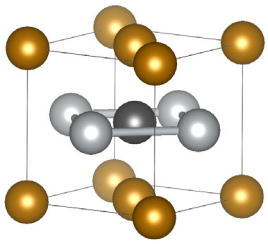

Fig. 1. $L1_0$- FeNiX structure

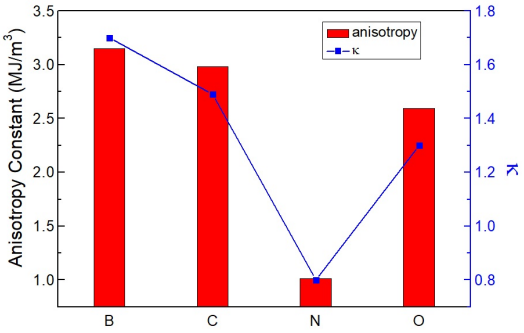

Fig. 2. Anisotropy constant and κ of $L1_0$- FeNiX

The Energy Product of Hard- and Soft-magnetic Cylindrical Core/shell

Namkyu Kim*, Hee-Sung Han, Soo Seok Lee, Ki-Suk Lee
Ulsan National Institute of Science and Technology (UNIST), Korea

As importance of permanent magnet in daily-life is increased for energy conversion ranging from electric cars to wind power generators, research on the development of new high-efficiency and low-cost permanent magnet is actively being carried out [1]. The exchange-coupled hard and soft magnet has been considered as one of the prominent candidates for high-efficiency permanent magnet since it can compensate for relatively low magnetization of hard magnet and very low crystalline anisotropy of soft magnet and thus, it improves the energy product [2,3]. In order to apply this prospect for high performance permanent magnet, various types of exchange-coupled magnet are proposed including multi-layer [4], mixture [5], and core/shell structure [6,7]. The cylindrical core/shell structure are particularly advantageous owing to large interface for exchange coupling and versatility at controlling composition and demagnetization factor by the dimensions [8]. In this work, we adopted cylindrical core/shell structure composed of the soft magnetic shell (FeCo) and the hard-magnetic core (Sm_2Co_{17}) as a model system. To obtain hysteresis loop and the energy product, we computed equilibrium magnetization configuration of local energy minimum under external magnetic field by using a finite differential micromagnetic solver, Mumax [9]. The hysteresis loops were obtained from applying external magnetic field ranging from -10 T to 10 T along easy axis. Since the energy product corresponds to the energy stored in the stray field produced by the magnet itself, it should be calculated from H_d and B at the remanent state (zero external magnetic field). Thus, we obtained the maximum energy product for each cylindrical core/shell structure directly from the calculations of the remanent states for various aspect ratio of the cylinder. For finding optimized core/shell structure, the energy product is expressed as phase diagrams. We expanded the model to iterative array structure of the cylindrical core/shell, and the results show great prospect for applying to bulk permanent magnet with high value of energy product.

References

[1] R. W. McCallum, L. Lewis, R. Skomski, M. J. Kramer, and I. E. Anderson, “Practical Aspects of Modern and Future Permanent Magnets,” Annu. Rev. Mater. Res., vol. 44, no. 1, pp. 451-477, 2014.

[2] E. F. Kneller and R. Hawig, “The exchange-spring magnet: A new material principle for permanent magnets,” IEEE Trans. Magn., vol. 27, no. 4, pp. 3588-3600, 1991. [2] S. Mechanics, “Magnetic properties of core/shell nanoparticles with magnetic or nonmagnetic shells,” vol. 4, pp. 0-20, 2012.

[3] R. Skomski and J. M. D. Coey, “Giant energy product in nanostructured two-phase magnets,” Phys. Rev. B vol. 48, no. 21, pp. 15812-15816, 1993.

[4] T. H. Rana et al., “Micromagnetism of MnBi:FeCo thin films,” J. Phys. D. Appl. Phys., vol. 49, no. 7, pp. 3-8, 2016.

[5] W. Zhanyong et al., “High coercivity Nd2Fe14B/α-Fe nanocomposite magnets,” Phys. B Condens. Matter, vol. 404, no. 8-11, pp. 1321-1325, 2009.

[6] W. Liu, Z. Zhang, J. Fischbacher, and A. Kovacs, “Rational design of the exchange-spring permanent magnet,” 2014.

[7] E. Lottini et al., “Strongly Exchange Coupled Core|Shell Nanoparticles with High Magnetic Anisotropy: A Strategy toward Rare-Earth-Free Permanent Magnets,” Chem. Mater., vol. 28, no. 12, pp. 4214-4222, 2016.

[8] N. Kim, H.-S. Han, and K.-S. Lee, “A Limit to Predict Maximum Energy Product (BHmax) from the Magnetization Hysteresis Loop,” J. Korean Magn. Soc., vol. 28, no. 5, pp. 205-211, 2018.

[9] A. Vansteenkiste, J. Leliaert, M. Dvornik, M. Helsen, F. Garcia-Sanchez, and B. Van Waeyenberge, “The design and verification of MuMax3,” AIP Adv., vol. 4, no. 10, 2014.

Comparison of the deformation behavior and magnetic properties of Nd-Fe-B magnets made from isotropic melt-spun and HDDR powders

Jae-Gyeong Yoo[1,2*], Ga-Yeong kim[1,2], Hee-Ryoung Cha[1], Jung-Goo Lee[1]
[1]Powder&Ceramic Division, Korea Institute of Materials Science, Changwon, Korea
[2]Department of Material Engineering, Pusan National University, Busan, Korea

The hot-deformation technique is an important method for fabricating nanocrystalline anisotropic Nd-Fe-B bulk magnets using ultra-fine grains such as melt-spun (~50nm) and HDDR (~300nm) powder to obtain high maximum energy product (BH)max. Compared to conventional sintered Nd-Fe-B magnets with micrometer-scale grain size, the hot-deformed Nd-Fe-B magnets bear huge potential to obtain high coercivity and improve its temperature dependence without using heavy rare-earth (HRE) elements owing to its ultrafine grain size. The mechanism of texture formation by the interface-controlled solution-precipitation-creep process during hot-deformation has been extensively studied for melt-spun powder. However, there were only a few studies examining texture formation during hot-deformation with HDDR powder. Thus, to understand texturing mechanism of HDDR powder during hot-deformation, we compared hot-deformation behavior between HDDR powder and commercial melt-spun powder which have the same composition as $Nd_{13.6}Fe_{73.6}Co_{6.6}Ga_{0.6}B_{5.6}$ during hot-deformation under the same deformation condition. Deformation behavior shows that dependence of strain-stress behavior on strain rate was significantly different between melt-spun and HDDR powder, also in magnetic properties, the remanence enhancement trend of hot-deformed magnet between HDDR and melt-spun powder as increasing strain was different which depends on strain rate. In microstructure, the grain shape and aspect ratio of hot-deformed magnet between HDDR and melt-spun powder shows also difference. Based upon these results, the magnetic properties and deformation behavior of Nd-Fe-B magnets melt-spun and HDDR powders will be discussed.

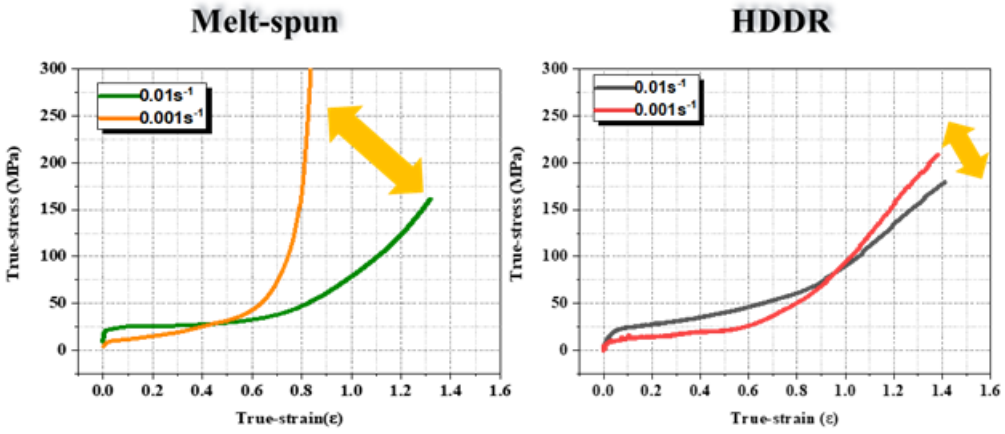

Fig. True stress-strain curves of hot-pressed compacts with melt-spun and HDDR powder during die-upsetting process at two different strain rates.

Electronic and Magnetic Structures of Insulating β-$V_2O(PO_4)$ with Quasi-one-dimensional Ferrimagnetic Spin Chain

Seo-Jin Kim[1*] and Kwan-Woo Lee[1,2]

[1]Department of Applied Physics, Graduate School, Korea University, Sejong

[2]Division of Display and Semiconductor Physics, Korea University, Sejong

Initially, the vanadium oxide phosphate V_2OPO_4, based on quasi-one-dimensional V-V chains, was suggested to have a tetragonal crystal structure. Presuming this structure and ferromagnetic state, a magnetic Weyl semimetallic character was predicted by a first principles study. Recently, however, a structure transition of tetragonal to monoclinic at T_s= 605 K has been observed[1,2]. The monoclinic phase shows two different V−O bond lengths in the face-sharing VO_6 octahedra, resulting in the V^{2+}/V^{3+} charge ordering along the chain. Additionally, a ferromagnetic order happens at T_C=165 K. Remarkably, the observed net moment is only one third of our calculated value for the ferrimagnetic order of V^{2+}($3d^3$, S=2/3) and V^{3+} ($3d^2$, S=1)[1,2]. This is very unusual, since a tiny spin-orbit coupling is expected in the 3d system.

Using the conventional and correlated band theories, we have investigated the electronic and magnetic structures of the low temperature monoclinic V_2OPO_4 phase to unveil the origin of the unusual magnetic characters. The pure structure transition leads to the charge-ordering of V^{2+}–V^{3+}, regardless of magnetic ordering. Applying the on-site Coulomb repulsion, a metal to insulator transition occurs at the effective critical value of U^c_{eff} ≈3.5eV. Our calculations show that the magnetic ground state significantly depends on strength of the on-site Coulomb replusion. Using the hopping parameters obtained from the Wannier function technique, our calculated exchange integrals J's suggest a frustration in the weakly-linked pyrochlore-like V4 tetrahedral structure. In this presentation, we will address its magnetic properties in detail.

The research was supported by NRF of Korea Grant No. NRF-2019R1A2C1009588.

References

[1] E. Pachoud, J. Cumby, C. T. Lithgow, and J. P. Attfield, J. Am. Chem. Soc. 140, 636 (2018)

[2] J. Xing, H. Cao, A. Paul, C. Hu, H.-H. Wang, Y. Lua, R. Chaklashiya, J. M. Allred, S. Brown, T. Birol, and N. Ni, arXiv: 1712.09973 (2017).

[3] S.-J. Kim, K.-W. Lee, arXiv:1902.10359 (2019)

On chip manipulation of particle/ cells on varied thickness of the magnetic diode for bio applications

Keonmok Kim*, Jongwan Yoon, Hyeonsal Kim, Cheol Gi Kim†
Department of Emerging Materials Science, DGIST, Republic of Korea
†cgkim@dgist.ac.kr

In recent years, controlling and transporting micron and sub-micron particles/cells have gained significant interest for myriad biological applications. In comparison with competing strategies based on optical and electrical fields, magnetic fields offer the most scalable and stable method for single cell analysis and separation. The inherent advantage of magnetic manipulation is that it avoids several undesirable side effects associated with optical or electrical field-based manipulation techniques, which are of particular concern for biological materials and living cells.

In this study, we fabricated permalloy micro-magnetic patterns in the form of magnetophoretic circuit, which has the ability to introduce and retrieve single cells from precise locations of the chip to perform with the level of integrated computer circuits and we have observed the particle/cell behavior by varying the distance between the particle and the magnetic pattern, thickness of the micro-magnetic pattern and size of the micro-magnetic particle. In addition, we predict the magnetic potential energy of a particle theoretically and experimentally.

Keywords: Micro particles, cells, magnetic fields, manipulation, permalloy thickness

Magnetic property of bilayer CrI_3

Fazle Subhan[1*], Imran Khan[2] and Jisang Hong[1†]
[1]Department of Physics, Pukyong National University, Busan 48513, Korea
[2]Department of Physics, Pusan National University, 46241, Korea

Using the first principles calculations, we explored the pressure dependent magnetic properties of CrI_3 bilayer CrI_3 for AB and AA type stacking. We found an anti-ferromagnetic ground state in both pristine bilayer systems with indirect band gaps of 1.71 and 1.68 eV for AB and AA type system. However, the transition from anti-ferromagnetic to ferromagnetic state was achieved with the pressure and the band gap was decreased although the indirect band gap nature remains unchanged. We obtained a substantially enhanced perpendicular magnetic anisotropy with pressure. In the pristine anti-ferromagnetic bilayer, both Cr and iodine atoms almost equally contributed to the perpendicular magnetic anisotropy. However, the contribution from the iodine atoms was almost four times larger than the Cr contribution with increasing the pressure. Particularly, the interface iodine atoms played a major role for the enhancement of the perpendicular magnetic anisotropy. We found that both AB and AA type bilayer displayed the same tendency.

Keywords: Chromium (III) iodide, stacking, pressure, magnetic semiconductor, magnetic anisotropy

Effects of Structural Defects on Magnetic Properties of MgO/Pt(100) and MgO/Pt(110) Junctions: An *Ab-initio* Study

Thi H. Ho, S. H. Rhim* and S. C. Hong†
Department of Physics and Energy Harvest Storage Research Center,
University of Ulsan, Ulsan 44610, Republic of Korea
Corresponding authors: *sonny@ulsan.ac.kr, †schong@ulsan.ac.kr

Defected-induced room-temperature ferromagnetism have been observed in MgO, a classical metal-oxide. [1,2,3] On the other hand, Pt is widely studied in spintronics, which is nearly ferromagnetic. With MgO ultra-thin film deposited on Pt surface, the combination effects of interface and defect may lead to the change of magnetic properties. A better understanding on the effects can offer more opportunity to control the stability and characterize the structural properties of MgO/Pt junctions.

Here, *ab-initio* calculations based on density functional theory have been employed to study the electronic and structural characteristics of ultra-thin MgO films on Pt(100) and Pt(110) surfaces. Furthermore, the influence on the magnetic properties of O and Mg defects at the interface are also investigated. The energetics reveals that oxygen atom on top of Pt is the most favorable. Interestingly, only Mg vacancy brings about the magnetic moments of 0.5 μ_B and 0.1 μ_B, which originates from the spin polarization of the 2*p* electrons of O atoms and the 5*d* electrons of Pt atoms surrounding the vacancies, respectively. The results are discussed in detail by the electronic structure perspective.

Keywords: magnetism, Mg vacancy, MgO/Pt junction, magnetic moments

References

[1] J. Li et at., Appl. Phys Lett **102**, 072406 (2013).
[2] L. Balcells et al., Appl. Phys. Lett. **97**, 252503 (2010).
[3] J. Guo et al., Appl. Phys. Lett. **111**, 192402 (2017).

First principles study on half-metallicity of alkali-metal-based half-Heusler XCrZ (X = Li, Na, K; Z = As, Sb)

Hoang Thu Thuy*, S. H. Rhim and S. C. Hong
Department of Physics and Energy Harvest-Storage Research Center, University of Ulsan, Republic of Korea
schong@ulsan.ac.kr, sonny@ulsan.ac.kr

Even though metastable zinc-blende(zb) CrZ (Z = As and Sb) are possible candidates for spintronic applications thanks to their half-metallicity(HM), thermal instability has limited real applications to devices [1]. To improve their physical properties such as thermal stability and magnetic moment without destroying HM, alkali-metal-based half-Heusler XCrZ have been suggested [2]. In addition, their lattice constants can be engineered by controlling the concentration of the alkali-metals.

We investigate magnetism and electronic structure of alkai-metal-based half-Heusler XCrZ system (X = Li, Na, and K; Z=As and Sb) using first principles calculational method of VASP to search for applicable new HM materials. Equilibrium lattice constants are calculated to be a_0= 6.00 Å, 6.42 Å, 6.37 Å, 6.94 Å, 6.74 Å, and 7.29 Å for LiCrAs, LiCrSb, NaCrAs, NaCrSb, KCrAs, and KCrSb, respectively. Wide band gaps of 2.16 eV, 2.27 eV, 1.67 eV and 1.86 eV in the minority spin states for NaCrAs, NaCrSb, KCrAs, and KCrSb exhibit HM at the equilibrium lattice constants except the Li-based ones. One more electron donation from the alkali-metals to Cr enhances magnetic moment of Cr to 4 μ_B from 3 μ_B of CrZ, compatible with the modified Slater-Pauling rule.

We also reveal strain effects on the electronic structures to consider lattice mismatch with III-V semiconductors for epitaxial growth. The half-metallicity of NaCrZ and KCrZ is quite robust under the severe strain of -10% to +10%. However, KCrZ, from formation energy calculations, turns out thermally unstable. In conclusion, we suggest that NaCrZ are most proper half-metals for spintronic applications with robust half-metallicity as well as low lattice mismatches of +1.71% and +4.03% for NaCrAs and NaCrSb, respectively, with a popular semiconductor substrate InSb.

References

[1] S. Javad Hashemifar, Peter Kratzer and Matthias Scheffler. Phys. Rev. B 82. 214417 (2010)
[2] L. Damewood, B. Busemeyer, M. Shaughnessy, C. Y. Fong, L. H. Yang, and C. Fesler. Phys. Rev. B. **91**. 064409 (2015).

First principles studies of antiferromagnetic layered square lattice of spin S=1 Ni^{2+}

Mi-Young Choi[1*] and Kwan-Woo Lee[1,2†]

[1]Department of Applied Physics, Graduated School, Korea University, Sejong 33010, Korea

[2]Division of Display and Semiconductor Physics, Korea University, Sejong 33010, Korea

After the discovery of high T_c cuprates, the layered square lattice has been extremely of interest and intensively investigated. Since Ni^{2+} systems have one more valence electrons than in the curpartes, it has been expected that these are hosts of a novel superconductor, when appearing an antiferromagnetic spin order. However, spin-ordered Ni^{2+} systems are very rare.

Very recently, a layered oxychalcogenide $Sr_2NiO_2Ag_2Se_2$ was synthesized by high pressure and high temperature techniques. This system shows two magnetic transitions of antiferromagnetic at T_N=150 K and spin-glass-like behaviors at T= 50 K. Although no experimental data is available, this system is experimentally claimed to be semiconducting.

Here, we have investigated its electronic and magnetic properties, as a starting point, by first principles calculations including correlation effects. In the GGA level, the) orbital has a band width narrower than that of the cuprates, leading to smaller hopping parameters. This indicate a weaker AFM tendency estimated by the superexchange, consistent with the observed lower Neel temperature. Applying the on-site Coulomb repulsion *U*, a transition of metal to insulator occurs above the critical value of effective eV. Additionally, as expected, inclusion of SOC leads to a tiny anisotropy of less than several tenths meV. In this presentation, we will discuss similarities and contrasts to cuprates in detail.

Acknowledgements: This research was supported by NRF-2019R1A2C1009588.

Multiple topological characters in room-temperature half-metallic antiferromagnet Cr_2CoAl

Hyo-Sun Jin[1*], Young-Joon Song[1] and Kwan-Woo Lee[1,2]
[1]Department of Applied Physics, Graduate School, Korea University, Sejong, Korea
[2]Division of Display and Semiconductor Physics, Korea University, Sejong, Korea

In condensed matters, multipole unconventional characters often lead to more exotic phenomena and abundant application capabilities in various field. Here, we will address the system, which shows both novel topological and half-metallic characters with no macroscopic magnetic field.

The half-metallic antiferromagnets, also called compensated half-metals (CHMs), have only one conducting spin channel with the zero net magnetic moment. CHMs are expected to be a good candidate for the spintronics application, since these show a high ordering temperature and no stray magnetic field due to the antiferromagnetic nature. In spite of many theoretical suggestions for the last 20 years, only one material realization has been achieved.

Our first principle calculations suggest that the inverse-Heusler Cr_2CoAl is a precisely compensated half-metal with a high Curie temperature of $T_c \sim 750K$ [1]. In addition, we have found that this system is another route of topological properties which are experimentally measurable. Cr_2CoAl, possessing no inversion and time-reversal symmetries, shows multiple topological characters; 12 pairs of Weyl points, three sets of triple nodal points (TNPs), and nexus fermion near the Fermi level E_F [2]. The nexus fermions, having TNPs interconnected to nodal lines, remains very new. These topological characters may be common in the inverse-Heusler systems. Although SOC can break some of these characters, compared with the observed high Curie temperature the strength of SOC of ~10meV in Cr_2CoAl is negligible. Thus, in addition to the zero macroscopic magnetic moment, the nearness to E_F makes this nexus fermion experimentally measurable. Our results suggest that Cr_2CoAl is not only feasible room temperature CHM, but also a promising candidate of novel topological states.

Acknowledgements: This research was supported by NRF Grants No. NRF-2016R1A2B4009579.

References

[1] H.-S. Jin and K.-W. Lee, Curr. Appl. Phys. **19**, 193 (2019).
[2] H.-S. Jin, Y.-J. Song, W. E. Pickett, and K.-W. Lee, Phys. Rev. Materials 3, 021201(R) (2019).

Influences of Substitutional Cobalt in Magnetic Properties of Tetragonal $D0_{22}$ Mn_3Ga

Quynh Anh T. Nguyen, Thi H. Ho, S. C. Hong† and S. H. Rhim*
Department of Physics and Energy Harvest Storage Research Center,
University of Ulsan, Ulsan 44610, Republic of Korea
Corresponding authors: †schong@ulsan.ac.kr, *sonny@ulsan.ac.kr

Heusler compounds have recently attracted interests among researcher because of rich physics and broad possibility of application, where Mn_3Ga is one of them. Here, magnetism of $Mn_{3-x}Co_xGa$ (x=0~1) is studied using of density functional theory. Mn_3Ga (x=0) crystallizes in tetragonal $D0_{22}$ structure, which exhibits ferrimagnetic ordering. Two Mn sites, octahedral and tetrahedral ones denoted as Mn-I and Mn-II, respectively, have different moments. Co substitution into different Mn sites demonstrates different magnetic trend. When Co concentration $x \leq 0.5$, substitution into Mn-I with enhanced magnetic moment, whereas that into Mn-II with reduce moment. After crossing from the phase transition point (x = 0.5), substitution into Mn-I drops sharply in comparison with that into Mn(II) increase again. When x>0.5 cubic phase is stable, which is unstable without Co substitution, become more energetically favored over tetragonal phase. The underlying difference is discussed in terms of low- and high spin competition and different symmetry of two Mn sites.

Keywords: Heusler compound, density functional theory, tetragonal $D0_{22}$ structure, low spin state, high spin state

Revisiting the complex magnetic structures of ultrathin fcc Fe/Cu(001) film

Qurat-ul-ain[1*], S. H. Rhim[1], S. C. Hong[1] and Jaejun Yu[2†]
[1]Department of Physics and Energy Harvest Storage Research Center (EHSRC),
University of Ulsan, Ulsan 44610, Korea
[2]Center for Theoretical Physics, Department of Physics and Astronomy,
Seoul National University, Seoul 08826, Korea

Magnetic structures of fcc Fe/Cu(001) have remained a subject of great interest for several decades. Here, we revisit the problem of the structural and magnetic properties of γ-Fe. we carry out non-collinear-spin density-fucntional-theory calculations for free-standing fcc Fe films and epitaxial Fe films on Cu(001) substrat using the OpenMX code. Various magnetic configurations are taken into account, including FM, stripe AFM (AFM-A), single-layer AFM (AFM-G), double-layer AFM (AFM-2G), and non-collinear spin spiral (SS) states. The topmost two surface layers of Fe are always found to be ferromagnetically coupled regardless of the film thickness, while the magnetic coupling among other Fe layers varies depending on the layer thickness n. The magnetic ordering of Fe shows five diverse regions: For $n \leq 3$ ML, FM state is most stable, while the ground mangetic structure shifts to AFM-2G state for 4 ML $\leq n \leq$ 8 ML. Moving further, 9 and 10 ML shows a mixed state of AFM-A and AFM-2G, which evolves to AFM-A state for 11 and 12ML. For $n \geq 13$ ML, the fcc Fe turns into a bcc lattice. Contrary to the recent claim of the SS ordering originating from the out-of-plane Fermi surface (FS) nesting [1], no such nesting is found in our calculation. Also our total energy results exclude a non-collinear ordering in the ultrathin fcc Fe film on Cu (001).

Reference

[1] J. Miyawaki, A. Chainani, Y. Takata, M. Mulazzi, M. Oura, Y. Senba, H. Ohashi, and S. Shin, Phys. Rev. Lett. **104**, 066407 (2010).

Two-dimensional materials in curved geometry

Minkyu Park[1*] and Sung Hyon Rhim[2]
[1]Research Institute of Basic Sciences, University of Ulsan, Ulsan, 44610, Republic of Korea
[2]Department of Physics and Energy Harvest Storage Research Center,
University of Ulsan, Ulsan, 44610, Republic of Korea

In this work, we consider curved two-dimensional materials and study how electronic band structures are altered by curvature. A single-particle Green function which contains the in-formation of single-particle density of states is a relatively accessible object that is aected by the curvature. Based on the work of [1], we calculate the Green function in momentum space where rst-order perturbation correction is proportional to the curvature. A tunneling spectroscopy experiment can be employed to verify the change in the density of states since the dierential conductance dI=dV is proportional to the density of states at low temperatures.

Reference

[1] T. S. Bunch and L. Parker, Feynman propagator in curved spacetime: a momentum-space representation, Phys. Rev. D20 (1979) 2499-2510.

Influence of permeability according to packing rate of soft magnetic particles

Ji Eun Lee[1*], Seok Hwan Huh[2†]
[1]Department of Materials Science and Engineering, Changwon National University, Changwon, Gyungsangnam-do 51140, Republic of Korea
[2]Department of Mechatronics Conversion Engineering, Changwon National University, Changwon, Gyungsangnam-do 51140, Republic of Korea

Recently, soft magnetic materials have been used in various industrial fields as materials for transformers for automobiles, electric motors, and inductors. With the development of portable electronic devices, these components are focused on miniaturization and light weight, which necessitates the development of high permeability materials. Therefore, in this study, we observed the change of permeability according to the packing rate of soft magnetic particles. Fe-Si, Permalloy(Fe-Ni), Sendust(Fe-Si-Al) were used as soft magnetic powders and Fe_3O_4, which is a fine particles, was used to increase the packing rate. The soft magnetic powder was dispersed in epoxy and place in a holder and dried at about 60 to 80 degrees to obtain a sample. The structural properties and morphology of the samples were measured by XRD and SEM, and the saturation magnetization values were measured by using VSM. The permeability was measured using an impedance analyzer and the initial permeability was calculated using the Bruggman equation. From this equation, it is possible to deduce μ_i, which is the permeability of the fine particles, from the permeability measurement value μ_e of the sample having the packing rate q. Also, we compared the permeability graph measured by using the equation that μ_i, the permeability of one particle, is μ_{eddy} by the eddy current. As a result of permeability measurement, the permeability of the soft magnetic powder was higher at low frequencies and the permeability increased as the packing rate increased. It is considered that, at a low filling rate, the static magnetic coupling between the fine particles is weak and the effect of the demagnetizing field is large, but the higher the packing rate, the stronger the static magnetic coupling between the fine particles.

Keywords: Soft magnetic, Permeability, Fine particles, Bruggman equation, Eddy current

A resonated breaking of time-reversal symmetry: a first-principles TDDFT study for the case of 2-dimensional semiconductors

Adem Halil Kulahlioglu[1*], Mahmut Sait Okyay[1], Bumseop Kim[1], Min Choi, Dongbin Shin[1,2], Noejung Park[1,2]

[1]Department of Physics, Ulsan National Institute of Science and Technology, Ulsan, 689-798 Korea

[2]Max Planck Institute for the Structure and Dynamics of Matter, Luruper Chaussee 149, 22761 Hamburg, Germany

Time-reversal symmetry (TRS) in a static condensed matter enforces two electrons of opposite spins to be matched as a Kramers pair, which can only be altered by a substantially strong external magnetic field. In dynamical situations, however, a circularly polarized electric field can be utilized as a more efficient breaker of the TRS, which possibly provoke transient or even unceasing magnetism[1-3]. We have particularly focused on the effect of applied electric fields in resonance with the intrinsic spin oscillation of the system. We performed the real-time time-dependent density functional theory (rt-TDDFT) calculations. We found that in diamagnetic materials with substantial spin-orbit couplings (SOCs), a circularly polarized light with energy far below the band gap effectively breaks the TRS, thereby resulting in the emergence of a considerable amount of magnetic moment (remanence). We present that a finite remanence can be evidence of a novel phase transition from diamagnet to a magnetic order, which can further be utilized to introduce a magnetoelectric hysteresis. In this selected example systems of transitional metal dichalcogenides (TMDC) with various strength of SOC, we varied simulation conditions (driver's frequencies, field strengths, and pulse durations) in the pursuit of the maximum remanence under the resonant frequency. Our results indicate that the resonated behaviors between the external electric driver and the SOC system can open a new path for ultrafast control of all-optical magnetization.

References

[1] Ziel, J. P. van der, Pershan, P. S. & Malmstrom, L. D. Optically-induced magnetization resulting from the inverse Faraday effect. Phys. Rev. Lett. **15**, 190 (1965).

[2] Kimel, A. V. et al. Ultrafast non-thermal control of magnetization by instantaneous photomagnetic pulses. Nature **435**, 655-657 (2005).

[3] Choi, G. M., Schleife, A. & Cahill, D. G. Optical-helicity-driven magnetization dynamics in metallic ferromagnets. Nat. Commun. **8**, 1-7 (2017).

Intrinsic Spin Hall Conductivity of Heavy Metals: a First Principles Study

Do Duc Cuong, Soon Cheol Hong* and S. H. Rhim*
Department of Physics and Energy Harvest Storage Research Center, University of Ulsan, Ulsan 44610, South Korea
*email: schong@ulsan.ac.kr, sonny@ulsan.ac.kr.

The spin Hall effect is a phenomenon that converts charge current into spin current, where spin orbit coupling is proposed to play one of important roles. In this study, intrinsic spin Hall conductivities (SHC) of *5d* transition metals and bismuth (Bi), which have strong spin orbit coupling, have been investigated using first principles calculations. We found that the SHCs of the early *5d* transition metals show negative values while those of the late 5d metals show positive values, which follow the sign of the spin orbit polarization at the Fermi level. The SHC of the early and late *5d* transition metals follow the V- and L-shape behavior, where the maximal SHC values (in the sense of absolute) are -783 $(W\cdot cm)^{-1}$ and 2043 $(W\cdot cm)^{-1}$ for W and Pt, respectively. Calculated spin Berry curvature reveals that SHC was found to be maximized when the Fermi level is located within the energy gap induced by the spin orbit coupling. On the other hand, the SHC of the low symmetry heavy metal Bi is obtained to be 340 $(W.cm)^{-1}$.

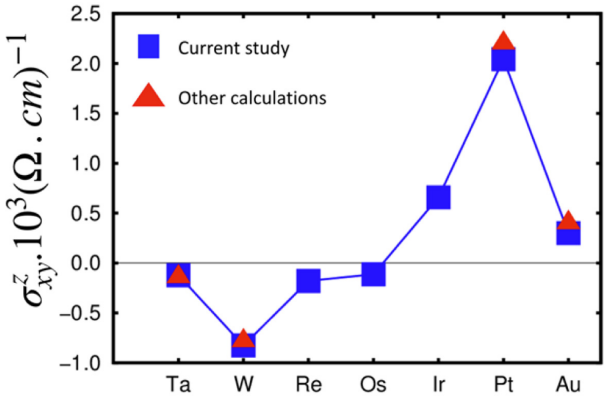

Fig. 1. Spin Hall conductivities of 5d transition metals.

Robust cos theta dependence of Current shift to normal geomagnetic field

Changjin Yun[1*], Mingu Kim[1], Jiho Kim[1] and Kungwon Rhie[2]
[1]Applied physics, Korea University, Sejong, 30019, Korea
[2]Department of Display and Semiconductor Physics, Korea University, Sejong, 30019, Korea

In our study, the magnetic field were exerted on sample y and z direction at the same time. Y-direction magnetic field was 200 Oe, and z-direction magnetic field(H_z) was changed from -10 Oe to 10 Oe. The current switching hysteresis which moved to left or right depends on the z-direction field sign. From this experiment, the I_{shift} vs H_z linear graph was obtained.

The measurement of spin Hall angle is well explained by Liu[1] by spin torque equation. In Liu's study, the spin Hall effect torque is considered only x-direction. However, due to the existence of domain wall motion, the effective spin Hall effect torque must be divided to two component y and z direction. From this theory, the I_{shift} vs H_z linear graph slope was confirmed $\frac{dh_z}{d\tau} = \cos\theta$.

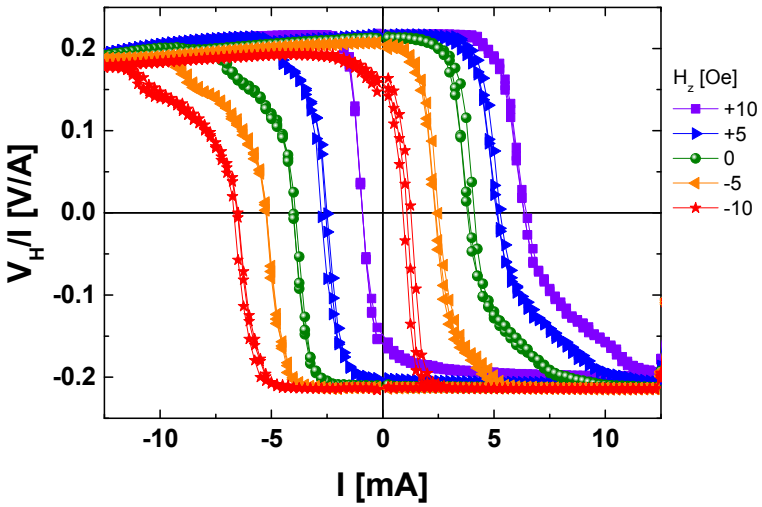

Fig. 1. Current switching hysteresis are moved depend on z-directional magnetic field. When the positive magnetic field is exerted on sample, hysteresis moved to right. If negative magnetic field is applied, hysteresis shifted to left.

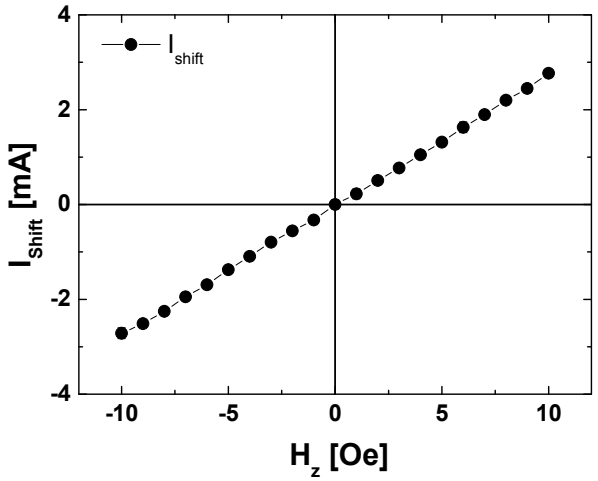

Fig. 2. From the figure 1, the average value(I_{shift}) of the points which V_H = 0 is slightly moved dependent on z-directional magnetic field. The linear graph slope is $2.8\left[\frac{mA}{Oe}\right]$.

Sample info.

The Pt(4)/Co(0.8)/Pt(1) in nm was sputtered in chamber, which base pressure is $5.0\times10^{-9}\,torr$, on thermally oxidized Si wafers. After sputtering, sample was annealed at 300℃ in high vacuum chamber for 30 minutes.

The perpendicular magnetic anisotropy (PMA) characteristics of the sample are well implemented. Bar-pattern on the sample was photo-lithographed by $25\times640\,um^2$

The sample magnetization saturation value was $1.35MA/m$and anisotropy field was 4 kOe, which were measured by VSM

Reference

[1] Luqiao Liu et al., Phys. Rev. Lett. 109, 096602 (2012)

Dynamics characteristics of ferrimagnetic GdFeCo alloy Atomistic simulation study

Jaegun Sim*, Jae-Hyeok Lee, Sang-Koog Kim
National Creative Research Initiative Center for Spin Dynamics and Spin-Wave Devices,
Nanospinics Laboratory, Research Institute of Advanced Materials,
Department of Materials Science and Engineering, Seoul National University, Seoul 151-744, Republic of Korea

1. 서론

A central motivation for antiferromagnetic spintronics is the expectation that antiferromagnetic spin dynamics are much faster than their ferromagnetic counterpart[1] and that the antiferromagnet has no magnetic stray field, which properties are beneficial for integrated circuits due to the fact that the stray field is the primary source of detrimental magnetic perturbations.[2] However, for realization of such magnetic memory devices in the future, it is necessary to understand the intrinsic mechanism of the dynamics. The fast dynamics of the antiferromagnet also are observed in the ferrimagnet, which fact is very helpful for understanding antiferromagnetism, owing to its ease of measurement.[3] Ferrimagnetic GdFeCo[4] material is one of the robust model systems for the study of the ferrimagnetic resonance (FMR) dynamic modes as a function of Gd atomic content across the magnetization and angular momentum compensation points. The experimental observations of FMR near both compensation points are not consistent with the theoretical predictions.[5]

2. 실험방법과 결과

Here, as further work, we calculated the temperature dependence of sublattice magnetizations and resonant magnetization dynamics over a given Gd-concentration range (0-48%) [6]. In this calculation, we used the VAMPIRE software package, which uses a simple text file format to define and run an atomistic simulation [7].

3. 고찰

The magnetization directions of FeCo and Gd are opposite to each other, and therefore they exhibit antiferromagnetic coupling between the sublattices. The magnetization (T_M) and angularmomentum (T_A) compensation points exist within a Gd-concentration range of 24-44% and increase linearly with that concentration [8]. According to the literature,[9-11] g_{FeCo}(~2.2) is slightly larger than g_{Gd}(~2), owing to the spin-orbit coupling of FeCo and the zero orbital angular momentum of the half-filled 4f shell of Gd. T_A is expected to be higher than T_M in GdFeCo

4. 결론

We confirmed that the correlation of the resonance frequency of magnetization dynamics is a function of the sublattice composition and thermal fluctuations and found that the common equations dose not predict FMR frequency close to Curie temperature due to assumption. Then, we confirmed that atomistic simulations of magnetic materials are useful for understanding the mechanism of the fast dynamics of the ferrimagnet and their applications to other systems.

5. 참고문헌

[1] F. Keffer, C. Kittel, Phys. Rev. 85, 329 (1952).

[2] T. Shiino, S. H. Oh, P. M. Haney, S. W. Lee, G. Go, B. G. Park, and K. J. Lee, Phys. Rev, Lett. 117, 087203 (2016).

[3] S. Kim, Y. Tserkovnyak, Appl. Phys. Lett. 111, 032401 (2017).

[4] K. Vahaplar, A. M. Kalashnikova, A. V. Kimel, D. Hinzke, U. Nowak, R. Chantrell, A. Tsukamoto, A. Itoh, A. Kirilyuk, and Th. Rasing, Phys. Rev. Lett. 103, 117201 (2009).

[5] A. Tuskamoto, T. Sato, S. Toriumi, and A. Itoh, J. Appl. Phys. 109, 07D302 (2011).

[6] T.A. Ostler, R.F.L. Evans, R.W. Chantrell, Phys. rev. B. 84, 024407 (2011).

[7] R.F.L. Evans, W.J. Fan, P. Chureemart, T.A. Ostler, M.O.A. Ellis, R.W. Chantrell, J. Phys.: Condens. Matter 26, 103202 (2014).

[8] P. Hansen, C.Clausen, G.Much, M. Rosenkranz, J. Appl. Phys. 66, 756 (1989).

[9] C. Kittel, Phys. Rev. 76, 743-748 (1949).

[10] G. G. Scott, Rev. Mod. Phys. 347, 102-109 (1962).

[11] B. I. Min and Y. R. Jang, J. Phys. Condens. Matter 3, 5131-5141 (1991).

마그노닉 결정 속 스핀파 프랙탈

박규영*, 김상국
서울대학교 재료공학부

1. 서론

프랙탈은 관측 대상의 사이즈 변화에 따라 자기유사성을 보이는 비선형적 특성으로, 다양한 영역에서 그 특성을 가지는 시스템들이 보고되고 있다. 마그노닉스 분야에서, 프랙탈적인 주파수 특성을 가지는 시스템은 대표적으로 두 가지가 보고되어 있는데, 하나는 피드백 회로가 구현된 박막에서의 스핀파이고 다른 하나는 주기적으로 패턴 된 스트립에서의 인가 에너지에 따른 스핀파 전달이다. 이러한 프랙탈 주파수 특성은 정보 통신 분야에서 큰 이점을 가지게 되는데, 첫 번째는 공명 주파수 영역의 확장이고, 두 번째는 공명 모드의 증가이다. 특히 마그노닉스 분야의 자기장을 통한 제어 가능성은 정보 전달 및 저장에 더 유리한 측면이 있다. 본 발표에서는 새로운 자성 박막 시스템에서 발견한 프랙탈 주파수 특성을 보고하고자 한다.

2. 실험방법과 결과

본 연구에서는 유한차분법을 사용하여 란다우-립시츠-길버트 방정식의 해를 구하고, 그 계산 과정을 그래픽 처리 장치를 이용 하여 가속하는 Mumax^3 소프트웨어를 사용하여 계산하였다. 안정화된 해당 마그노닉 시스템을 Sinc field로 여기하고, 그 자화 변화를 고속 푸리에 변환하여 분석하였다. 그 결과, 해당 시스템의 공명 모드가 프랙탈 특성에 맞게 진화해가는 과정에 대한 주파수 영역 결과를 얻을 수 있었다.

3. 고찰

해당 시스템의 FMR 모드를 중심으로 좌, 우로 미세하게 여기 되어 나타나는 영역에서, 프랙탈이 진화함에 따라 Repetition peaks가 형성되게 된다. 다음 프랙탈에서는 이 Repetition 모드를 중심으로 Daughter peaks이 형성되고, 차례대로 새로운 모드가 나타나는 것을 확인할 수 있다. 이에 따라 각 Repetition 모드를 중심으로 전체 주파수 특성이 해당 모드를 중심으로 유사하게 나타나는 현상을 분석하였다.

4. 결론

특정 마그노닉 시스템에서 프랙탈 공명 주파수 특성을 보이고, 그 특성이 어떤 양상으로 진화하는지 설명한다.

5. 참고문헌

[1] Daniel Richardson et al., Physical Review Letters 121, 107204 (2018)
[2] Aaron M. Hagerstrom et al., Physical Review Letters 102, 207202 (2009)
[3] Mingzhong Wu et al, Physical Review Letters 96, 187202 (2006)

Highly efficient energy dissipation in soft magnetic and spherical nanoparticles in a single-domain state for hyperthermia bio-applications

Min-Kwan Kim, Jaegun Sim, Jae-Hyeok Lee* and Sang-Koog Kim†
National Creative Research Initiative Center for Spin Dynamics and Spin-Wave Devices,
Nanospinics Laboratory, Research Institute of Advanced Materials,
Department of Materials Science and Engineering, Seoul National University, Seoul 151-744, South Korea
†Corresponding author: sangkoog@snu.ac.kr

Magnetic nanoparticles are of increasing interest due to their unique physical properties such as superparamagnetism, the exchange-bias effect, and particle-size-dependent static and dynamic properties [1-3]. These novel characteristics make magnetic nanoparticles very attractive for bio-applications including magnetic hyperthermia and MRI contrast agents. As an example, soft magnetic nanoparticles in single-domain states exhibit collective Larmor precession of individual spins. In cases where the frequency of time-varying magnetic fields equals the Larmor precession frequency, individual magnetic moments efficiently absorb energies that are transferred from externally applied AC magnetic fields, after which those energies dissipate into other forms due to their intrinsic damping of given magnetic materials. Such energy dissipations of magnetic nanoparticles are of crucial importance in hyperthermia bio-applications for high specific loss power (SLP). Larmor precession motions of individual spins in magnetic particles excited by relatively high-frequency (several hundred MHz) AC magnetic fields can give rise to a higher efficiency of energy dissipation than those by Brownian rotation of nanoparticles and/or by Néel relaxation of nanoparticles' magnetizations.

In the present study, we explored robust non-linear magnetization dynamics and their associated high-efficiency energy-dissipation effect using soft single-domain-state magnetic nanospheres excited by oscillating magnetic fields of different frequencies and amplitudes under given static magnetic fields. We conducted micromagnetic simulations to explore the novel magnetization dynamics of soft magnetic particles and additional analytical derivations of the energy-dissipation rate in the steady-state regime by varying the frequency and strength of rotating magnetic fields for different Gilbert damping constants and static magnetic field strengths. The energy-dissipation rate was found to have its maximum value at resonance in cases where the frequency of the rotating magnetic fields is equal to that of the Larmor precession of uniform magnetizations for a given Gilbert damping constant. The resonant energy-dissipation rate in the steady state, $\overline{Q}_{RES}$, is simply given in terms of AC field strength, H_{AC}, and DC field strength, H_{DC}, for a given damping constant, α. For the cases of $H_{AC} \geq \alpha H_{DC}$, the quantity of $\overline{Q}_{RES}$ reaches its maximum value of $\overline{Q}_{RES}^{MAX} = \alpha(\gamma M_s {H_{DC}}^2/\rho)$. This explicit form provides the highest SLP value, on the order of 10^4 - 10^5 W/g, and enables a reliable controllability of the SLP by externally applying magnetic fields to single-domain magnetic particles for magnetic hyperthermia bio-applications.

This work provides further insights into the fundamentals of magnetization dynamics in magnetic particles and the associated energy dissipation effect, and suggests a highly efficient means of magnetic-hyperthermia-applicable energy dissipation.

References

[1] M.-K. Kim et al., Appl. Phys. Lett. 2014, 105, 232402.

[2] S.-K. Kim et al., Sci. Rep. 2015, 5, 11370.

[3] S.-K. Kim et al., Sci. Rep. 2016, 6, 31513.

In-plane field control of coupled-vortex oscillations in magnetic-dot-networks

Young-Jun Cho*, Jaegun Sim and Sang-Koog Kim†
Department of Materials Science and Engineering, Seoul National University, South Korea
†Corresponding author: sangkoog@snu.ac.kr

Magnetic vortices are characterized by a clockwise or counter-clockwise in-plane curling magnetization (chirality) around a single core being magnetized perpendicularly either upward or downward (polarity). The potential for device applications, which include information storage and microwave oscillators [1-5], has strongly motivated studies of the gyration and its resonance of vortex cores. In particular, coupled vortices in network comprising vortex-state disks have been intensively studied both theoretically and experimentally as robust mechanisms of signal transfer and logic operations [6].

In the present study, we demonstrate an in-plane magnetic field controlling of the gyration signal propagation in magnetic-dot-networks by micromagnetic simulation and electrical measurement experiment. We used a Permalloy ($Ni_{81}Fe_{19}$) model system of vortex-state disks of diameter D=1000nm, thickness t=40nm, and edge-to-edge distance D_{int} = 100nm. The shortest distance from the chopped disk's center to the flat edge is 700nm. The resonance behavior of the vortex core gyration in the single round and chopped disk are studied. Depending on the vortex chirality, the in-plane magnetic field can drive the core either towards the disk's round edge or towards the its flat edge. When the core is located near to the flat edge, the core's directional dynamic stiffness for movement parallel to the edge is reduced. This leads to the gyrotropic frequency being less than when the core is centered or located near the round edge [7]. We examined the effect of in-plane magnetic field on the magnetic-dot-networks consisting of dipolar-coupled round and chopped disks. The dynamic behavior of the cores in magnetic-dot-networks strongly depend on the direction of the in-plane magnetic field. This work provides an understanding of the effects of in-plane magnetic fields on coupled-vortex arrays as well as an efficient practical means of dynamically manipulating collective vortex gyrations applicable to information-processing devices.

References

[1] H. Jung, K.-S. Lee, D.-E. Jeong, Y.-S. Choi, Y.-S. Yu, D.-S. Han, A. Vogel, L. Bocklage, G. Meier, M.-Y. Im, P. Fischer, and S.-K. Kim, Sci. Rep. 1, 59 (2011).

[2] B. Pigeau, G. de Loubens, O. Klein, A. Riegler, F. Lochner, G. Schmidt, L. W. Molenkamp, V. S. Tiberkevich, and A. N. Slavin, Appl. Phys. Lett. 96, 132506 (2010).

[3] S. Bohlens, B. Krueger, A. Drews, M. Bolte, G. Meier, and D. Pfannkuche, Appl. Phys. Lett. 93, 142508 (2008).

[4] S.-K. Kim, K.-S. Lee, Y.-S. Yu, and Y.-S. Choi, Appl. Phys. Lett. 92, 022509 (2008).

[5] Y.-S. Yu, H. Jung, K.-S. Lee, P. Fischer, and S.-K. Kim, Appl. Phys. Lett. 98, 052507 (2011)

[6] H. Jung, Y.-S. Choi, K.-S. Lee, D.-S. Han, Y.-S. Yu, M.-Y. Im, P. Fischer, and S.-K. Kim, ACS Nano 6, 3712 (2012)

[7] M. Sushruth, J. P. Fried, A. Anane, S. Xavier, C. Deranlot, V. Cros, and P. J. Metaxas, Phys. Rev. B 96, 060405(R) (2017)

Coupling of spin waves propagating along domain walls and a magnetic vortex in a thin-film nanostrip cross structure

Hyeon-Kyu Park*, Jong-Hyuk Lee, Jaehak Yang and Sang-Koog Kim
National Creative Research Initiative Center for Spin Dynamics and Spin-Wave Devices,
Nanospinics Laboratory, Research Institute of Advanced Materials,
Department of Materials Science and Engineering, Seoul National University, Seoul 151-744, South Korea

Spin wave is the collective excitation occurring in lattice of spins. It was recently demonstrated that the energy density required to switch or transfer single-digit information in spin-wave-based devices is less than that in conventional electronic transistors[1]. With aid of nanotechnology[2], quite long feature size of current magnonic devices fabricated by optical lithography might be downscaled to several nanometers. Thus, spin waves provide a new pathway for future information processing devices in regard with energy-cost efficiency. Furthermore, spin-wave modes confined in narrow potential wells of magnetic domain walls have been intensively studied owing to its fundamental interest as well as possible applications to logic gates[3]. Confinements of spin waves inside sub-100nm narrow channels such as domain walls[4] promise to further reduce power consumption in magnonic devices, as well as to enhance relatively low group velocities of spin waves[5].

Here, we report on a micromagnetic simulation study of interactions between spin waves propagating along narrow domain-wall channels and a magnetic vortex in a thin-film nanostrip cross structure. The specific modes of spin` waves propagate well in the narrow potential well of domain walls, then interact with a magnetic vortex when they go through the vortex soliton. Via this interaction, characteristic eigenmodes of vortex motions appeared, resulting in elliptical gyration motions of several specific frequencies[6]. The gyration motions can be interpreted by the sum of clockwise and counter-clockwise circular eigenmodes excited by spin waves of corresponding resonance frequencies[7]. According to action-reaction effect, the phase and amplitude of spin waves after their interaction with the vortex are modified differently in the three different arms.

References

[1] A. V. Chumak, A. A. Serga, & B. Hillebrands, Nature Commun. 5, 4700 (2014).
[2] J. A. Briggs, G. V. Naik, T. A. Petach, B. K. Baum, D. Goldhaber-Gordon, and J. A. Dionne, Appl. Phys. Lett. 108, 051110 (2016).
[3] F. Garcia-Sanchez, et al. Phys. Rev. Lett. 114, 247206 (2015).
[4] E. Albisetti, et al. Commun. Phys. 1, 56 (2018).
[5] G. Duerr, K. Thurner, J. Topp, R. Huber, and D. Grundler, Phys. Rev. Lett. 108, 227202 (2012).
[6] B. Krüger, A. Drews, M. Bolte, U. Merkt, D. Pfannkuche, and G. Meier, Phys. Rev. B 76, 224426 (2007).
[7] K.-S. Lee and S.-K. Kim, Phys. Rev. B 78, 014405 (2008).

Stochastic Domain Wall Motion and Thermal Field Characterization

Geun-Hee Lee* and Kab-Jin Kim
Department of Physics, Korea Advanced Institute of Science and Technology, Daejeon 34141, Republic of Korea

Magnetic domain wall (DW) motion has been attracting much interest for the fundamental study [1] as well as technological application [2]. Despite the importance, however, our understanding of the DW motion is far from complete. In particular, the physical mechanism of thermally activated DW motion is still a debating issue because the stochastic nature due to the finite temperature effect. Therefore, it is of great importance how to understand the thermally-induced magnetic field. In this work, we try to characterize the thermally-induced magnetic field. We first set the mathematical model to analyze stochastic domain wall motion with multiple pinning site. From this model, we obtain depinning probability of DW by varying the driving external field. (Fig.1) Finally, we characterize thermally-induced magnetic field based on both Gaussian distribution [3] and Arrhenius law. We find some discrepancy between Gaussian thermal field model and Arrhenius' thermal activation model, which suggests that we need further controlled experiments to understand the mechanism underlying the thermally activated DW motion.

Key words: Thermal activation, Domain wall, Stochastic motion

References

[1] Kab-Jin Kim, et al., Nat. Mater. **16**, 1187 (2017)
[2] S.S. P. Parkin, M. Hayashi, and L. Thomas, Science **320, 5873 (2008)**
[3] W. Brown, IEEE. Trans. Magn. **15, 5 (1979)**

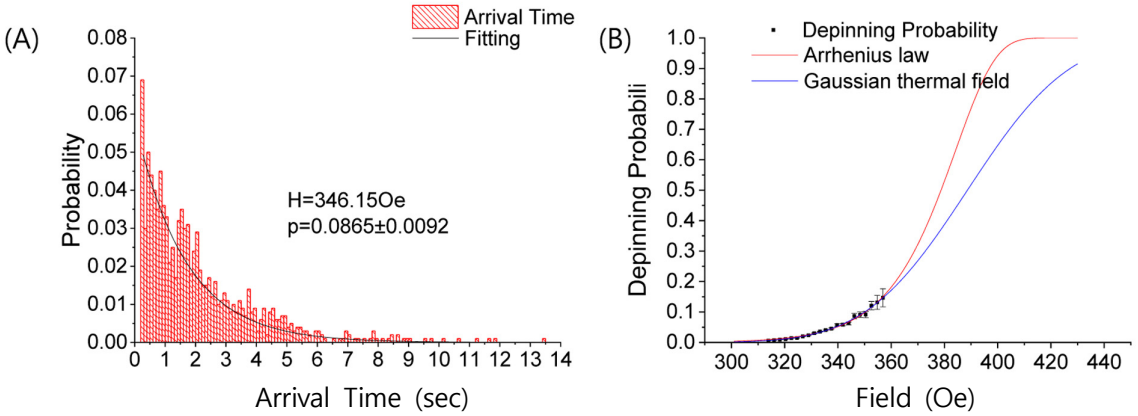

Fig. 1. DW arrival time distribution(A) and obtained depinning probability at certain external field(B).

Photon-magnon coupling in planar-geometry hybrid structure of Stub line resonator with YIG films

Haechan Jeon*, Sang-Koog Kim
National Creative Research Initiative Center for Spin Dynamics and Spin-Wave Devices,
Nanospinics Laboratory, Research Institute of Advanced Materials,
Department of Materials Science and Engineering, Seoul National University, Seoul 151-744, Republic of Korea

1. 서론

보존 특성을 가지면서 일관된 정보를 교환하는 것은 양자 정보 전달 시스템에서 필수적이다. 이 시스템을 실현시키기 위한 자기 역학과 자화 동역학 사이의 강력한 결합은 통신 과학 및 기술 분야에서 오랜 관심 주제였다[1]. 두 영역의 결합은 빛과 물질로 이루어진 두 개의 하위 시스템 간 결합 강도로 나타낼 수 있고, 공진 시스템 적용으로 평균 에너지 손실보다 커진다[2-4]. 빛의 전기 역학과 물질 역학의 결합으로 준입자 형태인 폴라리톤이 다양하게 발생하게 되며, 이 중 스핀의 집단적 거동으로 발생하는 마그논과 광자의 결합은 양자 정보 기술을 위한 마그논과 광자의 결합은 양자 정보 기술을 위한 핵심 연구로 진행되고 있다[5]. 양자 정보 전달을 달성하기 위해 두 하위 시스템의 강력한 결합이 요구되는데, 단일 스핀과 광자 결합은 요구하는 수준의 세기에 도달하지 못 한다. 따라서 스핀들의 집단적 거동을 통한 광자와의 효과적인 결합 강도 달성이 필요하다.

이러한 면에서 강자성체 및 페리자성 물질의 강한 자속 밀도는 강하게 결합된 마그논 모드를 형성시키는데 적합하다. 특히 낮은 감쇠 상수와 높은 스핀 밀도를 가지는 페리자성 물질인 Yittrium-Iron-Garnet(YIG)는 마이크로 스트립 라인 기술과 결합되었을 때 강한 광자-마그논 결합을 형성할 수 있음이 관찰되었다.[6,7]

Cavity 양자 전기 역학의 발달로 YIG를 고품질 마이크로파 cavity에 구나 입자 형태로 삽입하여 강한 photon-magnon coupling을 쉽게 형성시킬 수 있게 되었다[8-10]. 특히 YIG cavity를 사용한 연구들 중, FMR 공진을 형성하는 Kittel mode와 photon-magnon coupling 간의 상호작용을 관찰함으로써 더 강한 결합을 형성시키는 연구들이 진행되었다. 그 결과 강한 결합뿐만 아니라 강한 자성 전류도 형성시킬 수 있었으나 3차원 형태의 구, 박막을 사용했기 때문에 MTJ나 MRAM와 같은 기존의 스핀트로닉스 디바이스들이 가지는 2차원 구조에 적용할 수 없다는 한계를 가지고 있었다. [11]

2. 실험방법과 결과

본 연구는 마이크로 스트립 라인 기술에 2차원 평면 형상의 Stub line Resonator를 적용하여 YIG와 하이브리드 결합 구조를 통한 광자-마그논 결합을 연구하였다. YIG는 Pulsed Laser Deposition(PLD) 증착법을 사용하여 직접적으로 제작되었으며 서로 다른 두께의 박막을 사용하여 YIG의 두께와 광자-마그논 결합 간의 연관성을 관찰하였다. 2포트-Vector Network Analyzer를 이용하여 Stub Line Resonator의 광자 모드와 YIG의 마그논 모드 사이에 강한 Anti-crossing 상호작용을 실험적으로 관찰하였다.

3. 고찰

이 연구에서는 Stub line resonator를 가진 광자 모드를 이용하여 YIG의 마그논 모드와 결합을 발생시키는 실험을 진행하였다. 먼저 기존 3차원 형태의 Cavity 공진기 대신 2차원 형태의 Stub line resonator를 마이크로 스트립 라인 기술에 적용함으로써 소형의 2차원 평면 형상 공진기를 설계하였다. LC회로와 등가 형태를 가진 Stub line resonator의 간단한 형태를 이용하여 광자-마그논 결합을 상대적으로 쉽게 형성하였고 이로써 스핀

전류와 같은 스핀트로닉스 현상을 관찰할 수 있는 가능성을 발견하였다. 본 연구실에서 YIG 박막을 상업적으로 구매하지 않고 직접 PLD 시스템을 통하여 박막을 제작하였고 이를 사용하여 표준화된 광자-마그논 결합 강도를 측정해본 결과 기존의 LPE 공법을 통해 제작된 상업적 YIG 박막만큼 충분히 강한 결합 강도를 측정할 수 있었다.

4. 결론

결과적으로 간단한 형태의 Stub line resonator와 PLD 공법으로 제작된 YIG 박막을 사용하여 충분히 강한 광자-마그논 결합을 측정하였고 이는 Stub line resonator를 YIG 박막 위에 직접적으로 패턴함으로써 진정한 의미의 소형 집적화된 2차원 하이브리드 시스템의 가능성을 보여주고 있다.

5. 참고문헌

[1] A. Imamoglu, Cavity QED based on collective magnetic dipole coupling : spin ensembles as hybrid two-level systems, Physical Review Letters, 102, 083602 (2009).

[2] A. A. Serga, A. V. Chumak, and B. Hillebrands, YIG magnonics, Journal of Physics D : Applied Physics, 43, 264002 (2010).

[3] T. Ueda and M. Tsutsumi, Left-handed transmission characteristics of rectangular waveguides periodically loaded with ferrite, IEEE Transactions on Magnetics, 41, 3532 (2005).

[4] Y. He, et al., Tunable negative index metamaterial using yttrium iron garnet, Journal of Magnetism and Magnetic Materials, 313, 187 (2007).

[5] E. L. Albuquerque and M. G. Cottam, Polaritons in periodic and quasiperiodic structures, Elsevier, (2004).

[6] Y. Tabuchi, et al., Hybridizing ferromagnetic magnons and microwave photons in the quantum limit, Physical Review Letters, 113, 083603 (2014).

[7] X. Zhang, et al., Strongly coupled magnons and cavity microwave photons, Physical Review Letters, 113,

[8] O. O. Soykal and M. E. Flatte, Strong field interactions between a nanomagnet and a photonic cavity, Physical Review Letters, 104, 077202 (2010).

[9] C. Braggio, et al., Optical Manipulation of a Magnon Photon Hybrid System, Physical Review Letters, 118, 107205 (2017).

[10] Y. Cao, et al., Exchange magnon-polaritons in microwave cavities, Physical Review B, 91, (2015).

[11] R. Hisatomi, et al, Bidirectional conversion between microwave and light via ferromagnetic magnons, PHYSICAL REVIEW B 93, 174427 (2016)

Spin-wave excitation and critical angles in a photon-magnon-coupled hybrid system

Bosung Kim*, Biswanath Bhoi and Sang-Koog Kim
National Creative Research Initiative Center for Spin Dynamics and Spin-Wave Devices,
Nanospinics Laboratory, Research Institute of Advanced Materials,
Department of Material Science and Engineering, Seoul National University, Seoul 151-744, South Korea

1. Introduction

Magnons represent quanta of spin-wave modes of coupled dynamic motions of individual magnetizations excited in ferro-, ferri-, and anti-ferromagnets. In particular, spin waves of wavelengths lying within the micrometer-to-millimeter range, the so-called magnetostatic spin waves (MSWs) [1-3], can propagate over long distances in low-damping magnetic materials, e.g. yttrium iron garnets (YIG). Therefore, magnonics has been attracting significant interest owing both to its novel underlying physics and potential applications to information processing technologies. It has been reported that there exist certain critical angles [4] whereby all excited spin-wave modes look like the ferromagnetic resonance (FMR) mode as found at its single frequency. Earlier theoretical and experimental studies on the critical angles of spin-wave modes having been focused mostly on in-plane magnetizations, the critical angles of spin waves excited in out-of-plane magnetizations remain elusive. In the present study, therefore, we studied multiple-mode spin-wave excitation under more general arbitrary magnetic-field directions with respect to the wave vector of the spin waves. We then explored the dispersion characteristics, and found the critical angles of all of the spin waves excited in the YIG film for various magnetic-field directions at room temperature.

2. Method and Results

The sample used in this study consisted of a YIG film coupled to a specially designed inverted split-ring photon resonator (ISRR). For microwave excitations in both the ISRR and the YIG film, a microstrip feeding line was placed on the front side of the sample. To investigate the weak signals of the multiple spin-wave modes excited in the YIG film, we coupled them to the ISRR's photon mode using a magnon-photon-coupled hybrid system. We measured transmission coefficient S_{21} using a calibrated two-port vector network analyzer. The static magnetic fields applied are defined as $\mathbf{H} = \mathbf{H}_x + \mathbf{H}_y + \mathbf{H}_z$ with arbitrary orientation denoted as (θ, ϕ) where θ and ϕ are the polar and azimuthal angles from the $+z$ and $+x$ direction, respectively. We observed three representative spin-wave modes of backward volume magnetostatic waves, magnetostatic surface waves, and forward volume magnetostatic waves as well as their mixed modes along with their transitions across very specific angles, defined as critical angles where the group velocity of spin waves approaches zero with the appearance of a single FMR peak.

3. Discussion

Using the dispersion curves, we replotted the group velocities ($v_g = d\omega/dk$) for the different angles of (θ, ϕ). The resultant group velocity curves contrast strongly for the indicated field directions. For the cases of θ = 90°,

the υ_g values are positive above a certain ϕ angle but negative below it. Such a behavior is similar to that for the case of ϕ = 0: υ_g is positive for θ = 0 and negative for θ = 90°. More interestingly, at certain angle sets, υ_g is almost 0 in the given k range. On the other hand, for ϕ = 90°, υ_g is always positive, independent on θ. We analytically calculated the phase diagram of all of the excited spin waves and their critical angles relative to some experimental data points. From experimental measurements, we found that there exist certain characteristic angles, which is to say critical angles (θ_c, ϕ_c), whereby the group velocity of the excited spin-wave modes reaches zero, along with a single ferromagnetic resonance peak. Further, we analytically derived the critical angles as $\sin\theta_c = (H_{eff}/H)\{2-(1+\mu_0 M_s/H_{eff})\sin^2\phi_c\}^{-1/2}$ where H_{eff} is the effective magnetic-field strength, H the externally applied field strength, and $\mu_0 M_s$ is the saturation magnetization. This analytical form is in quantitative agreement with estimations from experimentally observed spin-wave modes.

4. Conclusion

The disappearance of multiple peaks of spin-wave modes at the critical angles implies the reduction of a magnon's various channels with which a single photon mode can exchange energy via coupling. Therefore, the change in the external magnetic-field direction could play a role, as an on/off switch or a pass-band filter, in the control of the number of information exchange channels in quantum information processing and quantum computing devices. Also, such signal enhancements in a magnon-photon-coupled system imply that this hybrid system enables the study of many higher-mode spin-wave measurements. Although further studies are necessary to clarify the strength of magnon-photon coupling according to the wave number and the magnetic-field direction, the present work can be extended to patterned YIG films and various resonators of different quality factors for the study of spin waves and photon-magnon coupling.

5. References

[1] J. R. Eshbach and R. W. Damon, Phys. Rev., 118, 1208 (1960).

[2] R. W. Damon and J. R. Eshbach, J. Phys. Chem. Solids, 19, 308 (1961).

[3] R. W. Damon and H. Van De Vaart, J. Appl. Phys., 36, 3453 (1965).

[4] P. E. Wigen, C. F. Kooi, and M. R. Shanabarger, Phys. Rev. Lett., 9, 206 (1962).

Abnormal anti-crossing effect in photon-magnon coupled system

Biswanath Bhoi*, Bosung Kim and Sang-Koog Kim
National Creative Research Initiative Center for Spin Dynamics and Spin-Wave Devices,
Nanospinics Laboratory, Research Institute of Advanced Materials,
Department of Material Science and Engineering, Seoul National University, Seoul 151-744, South Korea

1. Introduction

Understanding and exploiting the interactions of excited modes in hybrid quantum systems are the keys to achieve the ambitious goal of quantum information processing [1-2]. Therefore, collectively excited modes (i.e., magnons) in ferromagnets, being coupled to elementary excitations of electromagnetic waves (photons), have increasingly been studied in a variety of hybrid structures of two or more different systems [3-5]. The interaction (coupling) between the magnon and photon modes usually demonstrated by showing the modes' splitting near their common resonant frequency within the so-called anti-crossing region or the level repulsion, as described well by a classical model for coupled oscillators [4] and also by a two-level quantum model [5]. In this work, we report the experimental demonstration of an abnormal, opposite anti-crossing dispersion (or level attraction) in a photon-magnon-coupled system that consists of an yttrium iron garnet (YIG) film and an inverted pattern of split-ring resonator structure (noted as ISRR) in a planar geometry.

2. Method and Results

The dimensions of the ISRR and the YIG film are exactly the same as those reported for previous experiments [4]. We designed two different ISRRs of equal dimensions but different split-gap positions/orientation i.e. orthogonal (case-I) and parallel (case-II) with respect to the microstrip line axis. The details on the fabrication of the ISRRs and the measurement of photon-magnon coupling were reported in Ref. [4]. From the two different orientations of the ISRR's split gap in the ISRR-YIG hybrid, we obtained transmission coefficient $|S_{21}|$ as a function of microwave frequency of oscillating currents flowing along the microstrip line and the strength H of a static magnetic field applied along the film plane. For case-I wherein the ISRRs' split gap is perpendicular to the microstrip line, the anti-crossing effect appeared at the common resonant frequency, which represents two higher and lower coupled branches on the ω/ω_{ISRR}-H/H_{cent} plane. On the other hand, for case-II wherein the ISRR's split gap is parallel to the microstrip line, a completely opposite anti-crossing shape was observed. Here ω_{ISRR} and H_{cent} represent the resonant angular frequency of the ISRR and the field center of the anti-crossing dispersion, respectively.

3. Discussion

To understand the experimentally observed contrasting behaviors of the normal and abnormal anti-crossing shapes, we made analytical derivations based on fundamental electromagnetic interactions (Faraday's induction and Ampere's circuit laws) between the YIG film and the ISRR, taking into account the orientation of the ISRR's split gap. The magnetizations in the YIG are influenced by the effective field, which is the sum of two

time-dependent rf magnetic fields from the feeding line (h_{line}) and from the ISSR split gap (h_{ISRR}), where ϕ is the phase difference between them, and δ is the ratio between their amplitudes. For the case of ISRRs' split gap being perpendicular to the microstrip line, both h_{line} and h_{ISRR} are in the equal phase. On the other hand, for the case of ISRRs' split gap being parallel to the microstrip line, both the fields are out of (π) phase. We derive an analytical expression to estimate the strength of coupling of the ISRR mode to the magnon mode for different types of anti-crossing. By fitting the lower and higher frequency branches of the experimental data to our analytical expression we obtained the value of net coupling strength Δ = 90 and 90i MHz the normal and opposite anti-crossing respectively. The opposite anti-crossing effect can be explained by the compensation of both intrinsic damping and coupling induced damping in the magnon modes. This compensation is achievable by controlling the relative strengths and phases of oscillating magnetic fields generated from the ISRR's split gap and the microstrip feeding line. The behavior of anti-crossing effect was further investigated by plotting the analytical $|S_{21}|$ spectra on the ω/ω_{ISRR}-H/H_{cent} plane for different values of δ and ϕ. Importantly, we provided a phase diagram of the dispersion type in the photon-magnon coupling region. The shapes of anti-crossing effect, including the dispersion, linewidth, and net coupling strength of the two coupled modes are found remarkably variable and controllable with changing the relative strength and phase of the oscillating magnetic fields generated from both the ISRR's split gap and the microstrip feeding line.

4. Conclusion

The abnormal opposite anti-crossing effect (or level attraction), which has been so-far considered as challenging, is experimentally demonstrated at room temperature by using a photon-magnon-coupled system that consists of a YIG film and an ISRR in a planar geometry. The experimentally observed opposite anti-crossing and the analytically calculated abnormal anti-crossing of various dispersion types demonstrate the potential and great flexibility of photon-magnon systems for exploration of the not-yet-revealed phenomena of light-matter interaction.

5. References

[1] H. J. Kimble, Nature, 453, 1023 (2008).

[2] Z. Xiang, et al., Rev. Mod. Phys., 85, 623 (2013).

[3] L. Bai, et al., Phys. Rev. Lett., 114, 227201 (2015).

[4] B. Bhoi, et al., Sci. Rep., 7, 11930 (2017).

[5] M. Harder, et al., Sci. China Phys. Mech. Astron., 59, 117511 (2016).

Dynamic modes of magnetic skyrmions in magnetic nanotubes

Jaehak Yang[1*], Junhoe Kim[1], Claas Abert[2], Dieter Suess[2] and Sang-Koog Kim[1†]

[1]National Creative Research Initiative Center for Spin Dynamics and Spin Wave Devices, Nanospinics Laboratory, Research Institute of Advanced Materials, Department of Materials Science and Engineering, Seoul National University, Seoul 151-744, Republic of Korea

[2]Christian Doppler Laboratory - Advanced Magnetic Sensing and Materials, University of Vienna, Austria

[†]Correspondence and requests for materials should be addressed to S.-K. K. (sangkoog@snu.ac.kr).

Magnetic skyrmions are among the topologically protected magnetization textures that are promisingly applicable to information processing devices [1] owing to their nanosize and low-power-consumption motions. Fundamental dynamic modes of skyrmions for two-dimensional (2D)-geometry elements have been demonstrated theoretically by M. Mochizuki [2] and experimentally by Y. Onose et al. [3]; these modes include skyrmion-core gyrations in either the clockwise (CW) or counter-clockwise (CCW) rotation sense, as excited by in-plane ac magnetic fields or currents, as well as the breathing mode excited by out-of-plane ac magnetic fields or currents. To date, there have been no reports of skyrmion dynamic modes in curved-geometry structures.

Since the dynamic behaviors of skyrmions in 3D elements are expected to differ from their known dynamic modes in 2D elements, we investigated, as reported herein, skyrmions' dynamic modes and motions in short-length nanotubes. The model nanotubes were assumed to have the magnetocrystalline anisotropy axis and the Dzyaloshinskii-Moriya Interaction (DMI) vector in the direction normal to their surface. Unlike the case in 2D flat systems, the skyrmions formed in the nanotubes had rather an elliptical shape and asymmetry between the longitudinal and transverse directions. This geometrical asymmetry results in an additional curvature-induced interaction terms. The long axis of elliptical shape is parallel (perpendicular) to the tube's longitudinal axis for the positive (negative) DMI constant.

For in-plane applications of resonant ac magnetic fields, there exist either CCW or CW gyration motions. For the CCW gyration, the skyrmion's core rotates in a vertical oval orbit. In the case of CW gyration, the core of the skyrmion rotates in a nearly circular orbit. The breathing mode, as in 2D elements, is also excited by out-of-plane application of resonant ac magnetic fields. Unlike the case in 2D elements, with increasing strength of in-plane ac field above its critical strength, the CCW gyration motion becomes a periodic translational motion in the circumferential direction. The critical field strength is about 400 Oe for a given dimension, and the velocity of the skyrmion is about 22.9 m/s irrespective of ac magnetic field strength. The rotation sense of this periodic translational motion is determined by the skyrmion helicity that is governed by the sign of the interfacial DMI constant. This work provides a new physical insight into skyrmion dynamics in curved-geometry systems and also might prove applicable to potential skyrmion-based 3D racetrack memories.

References

[1] Fert, A., Cros, V., and Sampaio, J. Skyrmions on the track. Nature Nanotech. **8**, 152 (2013).

[2] Mochizuki, M. Spin-wave modes and their intense excitation effects in skyrmion crystals. Phys. Rev. Lett. **108**, 017601 (2012).

[3] Onose, Y. et al. Obervation of magnetic excitations of skyrmion crystal in a helimagnetic insulator. Phys. Rev. Lett. **109**, 037603 (2012).

Huge Spin-Transfer Torque in Ferromagnetic Pd/Co/Pd Film

Dae-Yun Kim[1], Seong-Hyub Lee[1*], Yune-Seok Nam[1], Ji-Sung Yu[1], Yong-Keun Park[1,2], Byoung-Chul Min[2] and Sug-bong Choe[1†]

[1]Department of Physics & Astronomy, Seoul National University, Seoul 151-742, Republic of Korea

[2]Spin Convergence Research Center, Korea Institute of Science and Technology, Seoul 136-791, Republic of Korea

[†]sugbong@snu.ac.kr

Electric currents generate spin-orbit torque (SOT) and/or spin-transfer torque (STT) into the magnetization, enabling the switching or the DW motion. In ferromagnetic thin film with perpendicular magnetic anisotropy, the SOT is observed frequently and thus, various relevant studies have been reported. On the other hand, observation of STT, as well as its relevant studies are rare [1, 2]. Here we report observation of huge STT in ferromagnetic Pd/Co/Pd film. For this study, 5.0-nm Ta/2.5-nm Pd/0.3-nm Co/1.5-nm Pd films were fabricated on a Si/100-nm SiO_2 substrate by using DC magnetron sputter. The total spin-torque efficiency ε_{ST} (sum of ε_{SOT} and ε_{STT}) was determined by deppining field measurement, proposed by P. P. J. Haazen *et al.* [3], as a function of longitudinal magnetic field H_x. Then, in order to decouple ε_{SOT} and ε_{STT} from ε_{ST}, the Dzyaloshinskii-Moriya-interaction-induced field H_{DMI} was independently determined by asymmetric DW speed measurement, proposed by Je *et al.* [4]. Fig.1 shows the plots of decoupled ε_{SOT} and ε_{STT} as a function of H_x for t_{Co}=0.3 nm, respectively. Interestingly, huge STT was observed in this film, of which magnitude even dominates SOT. Moreover, its magnitude is much larger than that of Pt/Co/Pt film for given t_{Co}. We concluded that this huge STT attributes to the narrow DW width λ_{DW}, because ε_{STT} is known to be inversely proportional to λ_{DW}, which will be discussed in the presentation.

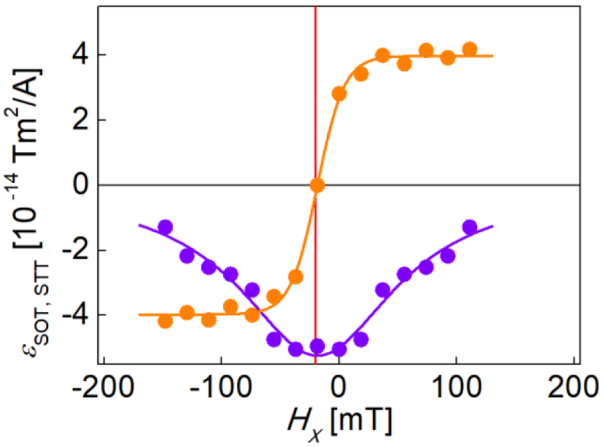

Fig. 1. Plot of ε_{SOT} (orange symbol) and ε_{STT} (purple symbol) with respect to H_x. Solid lines guide typical antisymmetric and symmetric nature of ε_{SOT} and ε_{STT}. The red vertical line indicate H_{DMI}, which is determined by measurement of asymmetric DW speed measurement.

References

[1] Soong-Geun Je, Sang-Cheol Yoo, Joo-Sung Kim, Yong-Keun Park, Min-Ho Park, Joon Moon, Byoung-Chul Min, and Sug-Bong Choe. Emergence of Huge Negative Spin-Transfer Torque in Atomically Thin Co layers. Phys. Rev. Lett. **118**, 167205 (2017).

[2] Fanny C. Ummelen, Tijs A. Wijkamp, Tom Lichtenberg, Rembert A. Duine, Bert Koopmans, Henk J.M. Swagten, and Reinoud Lavrijsen. Anomalous direction for skyrmion bubble motion. arXiv:1807.07365 (2018).

[3] P. P. J. Haazen, E. Murè, J. H. Franken, R. Lavrijsen, H. J. M. Swagten, and B. Koopmans. Domain wall depinning governed by the spin Hall effect. Nat. Mater. **12**, 299 (2013).

[4] S.-G. Je, D.-H. Kim, S.-C. Yoo, B.-C. Min, K.-J. Lee, and S.-B. Choe. Asymmetric magnetic domain-wall motion by the Dzyaloshinskii-Moriya interaction. Phys. Rev. B **88**, 214401 (2013).

Effect of iron deficiency and Co substitution on the magnetic properties of Ca-La M-type hexaferrites

Kang-Hyuk Lee* and Sang-Im Yoo†
Department of Material Science and Engineering, Research Institute of Advanced Materials (RIAM), Seoul National University, Seoul, Korea

Recently, $Ca_{0.5}La_{0.5}Fe_{12}O_{19}$ (Ca-La M-type) hexaferrites have been reported to possess higher crystalline anisotropy compared with $SrFe_{12}O_{19}$ (Sr M-type) hexaferrite without reducing its saturation magnetization (M_s), resulting in higher coercivity (H_c). Previous reports have mainly focused on La^{3+}substitution for the Ca^{2+} site and transition metals substitution for the Fe^{3+} sites of M-type hexaferrites. However, the effects of iron deficiency and Co substitution on the magnetic properties of the Ca-La M-type hexaferrites remain unexplored. In this study, therefore, we tried to investigate the effect of iron deficiency and Co substitution on the magnetic properties of $Ca_{0.5}La_{0.5}Fe_{12-y}O_{19-\delta}$ ($9 \leq 12-y \leq 11.25$) and $Ca_{0.5}La_{0.5}Fe_{12-z}Co_zO_{19}$ ($0 \leq z \leq 2$) hexaferrites, respectively, prepared by solid state reaction. Samples were characterized by powder X-ray diffraction (XRD), vibrating sample magnetometer (VSM), and scanning electron microscope (SEM). In the case of iron-deficient Ca-La M-type hexaferrties, as-calcined powder was pressed into pellets and sintered at 1275~1325℃ for 4 h in air. Powder XRD analyses revealed that M-type single phase were obtained with Fe contents of 10.25 and 10 at sintering temperature of 1300℃, and Fe contents from 9.5 to 11.25 at sintering temperature of 1325℃. The saturation magnetization (M_s) of the Ca-La M-type hexaferrite samples was around 70 emu/g. The maximum M_s was obtained for the sample sintered at 1300 ℃ and a Fe content of 10.25 at 76.8 emu/g. However, the coercivity (H_c) decreased with higher Fe content because the grain size was larger than the single domain size. In the case of Co-substituted Ca-La M-type hexaferrties, powder XRD analyses revealed that M-type single phase was obtainable from the samples with the Co contents of 0.5 and 1 at sintering temperature of 1195℃ for 2 h in air. The M_s and H_c values of $Ca_{0.5}La_{0.5}Fe_{11.5}Co_{0.5}O_{19}$ samples sintered at 1195 ℃ was 71.5emu/g and 3850 Oe. Detailed microstructures and magnetic properties of Ca-La M-type hexagonal ferrites will be presented for a discussion. This research was supported by Future Materials Discovery Program through the National Research Foundation of Korea (NRF) funded by the Ministry of Science and ICT (2017M3D1A1013748).

Keywords: Ca-La Hexaferrite, magnetic property, iron deficiency, M-type hexaferrite

Growth temperature dependence on magnetism and crystallization of $SmFe_{12}$ thin films

Daegill Cho[1*], Hyun Jung Kim[1], Sangkyun Ryu[1], Jae S. Lee[2],
Jun Kue Park[2], Jaekwang Lee[1], Hyoungjeen Jeen[1]

[1]Department of Physics, Pusan National University, Busan 46242, Korea

[2]Korea Multi-purpose Accelerator Complex, Korea Atomic Energy Research Institute, Gyeongju 38180, Korea

Nd-Fe-B-based permanent magnets have dominated magnet market for several decades. However, high cost of rare earth elements motivates to develop new type of permanent magnets, i.e. rare-earth free permanent magnets and/or rare-earth lean permanent magnets. In this regard, $SmFe_{12}N$ is an interesting material, since it has less rare-earth elements and higher performing temperature than those of Nd-Fe-B-based permanent magnets. In this presentation, we show growth temperature dependence on magnetism and structure of meta-stable $SmFe_{12}$ thin films buffered on crystalline Ag. The main reason to use thin film is possible stabilization of a meta-stable phase through lattice mismatch control and non-equilibrium growth process. Thus, thin film approach is necessary not only to study fundamental properties but also to find a potential route, i.e. strain to enhance properties before bulk approach. RF magnetron sputtering with two guns is used to growth of a buffered Ag layer, $SmFe_{12}$ layer, and Ag capping layer. This growth approach is beneficial to prevent potential oxidation of $SmFe_{12}$ films. In addition, it may reduce lattice mismatch. Grown films were characterized by high resolution x-ray diffractometer and vibrating sample magnetometer to study film orientation and magnetization. We observed crystallization temperature, orientation evolution, and magnetism evolution as a function of temperature. To crystallize $SmFe_{12}$, growth temperature should be higher than 500^{o}C. However, the film grown at 700^{o}C clearly showed reduced magnetism indicating possible Sm loss during high temperature growth process. Lastly, we will briefly introduce our approach on nitridation of $SmFe_{12}$ with nitrogen ion beam implantation. This work is supported by the National Research Foundation of Korea (NFR) (NRF-2018M2A2B3A01071859).

Magnetic properties and hot-deformation behavior of Nd-lean magnets

Ga-Yeong Kim[1,2*], Hee-Ryoung Cha[1], Yang-Do Kim[2], Jung-Goo Lee[1]
[1]Powder&Ceramics Division, Korea Institute of Materials Science, Changwon, Korea
[2]Department of Materials Science and Engineering, Pusan National University, Busan, Korea

Nd-Fe-B permanent magnets have been widely used in various applications. However, Nd, Pr and Dy are less abundant in the natural rare earth resources and rapidly increasing cost for rare earth elements hinders their application widely. Considering the cost reduction and the unbalanced use of rare earth metals, there is an urgent and growing requirement for usage of abundant rare earth metals such as Ce, La, and misch-metal in Nd-Fe-B magnets. Therefore, we need to develop RE-Fe-B magnets using abundant rare-earth. On the other hand, for the fabrication of anisotropic nanocrystalline magnets with high maximum energy density, they should be subjected to hot-deformation (hot pressing and subsequent die upsetting) process. The hot-deformation process is a potential alternative method to prepare anisotropic Nd-Fe-B magnets without oxidation issue and which causes grain alignment along the c-axis parallel to the pressing direction and high (BH)max. In this study, we investigated the magnetic properties and the hot-deformation behavior of the Nd-lean magnets. Initial melt-spun ribbons with the nominal compositions of $(Nd_{1-x}M_x)_{13.6}Fe_{bal}B_{5.6}Ga_{0.6}Co_{6.6}$(x=0, x=0.2/M=Ce, x=0.3/M=Ce, Ce+La,wt.%), named as ND, CE0.2, CE0.3, CELA0.3, respectively, were prepared at a wheel speed of 28m/s in an argon atmosphere by a single-roller melt-spinning machine and pulverized into powders. The powders were then pressed at 700℃ in vacuum under 100MPa and deformed at 700℃ in argon atmosphere until the height reduction 75% achieved. The grain size of the initial melt-spun powders was independent on the composition. After hot-deformation process, the magnetic properties of hot-deformed magnets was decreased due to the intrinsic magnetic properties of cerium and lanthanum, which is the same tendency as initial melt-spun powder. On the other hand, the grain morphology was changed from sphere to platelet. However, the aspect ratio strongly depended on the composition, which decreased with Ce, La content. It is reported that high aspect ratio facilitate grain sliding during hot-deformation process, which induce high grain alignment. In other words, Ce, La substitution decrease the ability of hot-deformation of Nd-Fe-B melt-spun powder. The magnetic anisotropy was decreased with Ce and La content too. Especially, the magnetic anisotropy of CELA0.3 magnet was much lower than that of CE0.3 magnet.

Synthesis of ε-Fe_2O_3 Nanopowder Substituted with Non-magnetic Elements based on Spray-Drying Process

Kyung Min Kim[1*], Seung Min Lee[1,2], Min Ji Pyo[1,3], Jung Goo Lee[1], Youn-Kyoung Baek[1†]

[1]Korea Institute of Materials Science, Changwon 51508, South Korea

[2]Department of Materials Science and Engineering, Pusan National University, Pusan 46241, South Korea

[3]Department of Materials Science and Engineering, Pukyong National University, Pusan 48513, South Korea

Magnetic materials are required in various industrial fields, especially, they are applied variously in the fields of communication electronic devices. With the development of information technology, the demand is rising for sending heavy data such as high-resolution images at high speed. It is necessary to develop a high frequency electromagnetic wave absorbing material applicable to the next generation communication electronic devices. In order to effectively suppress electromagnetic interference (EMI) in millimeter waves range (30-300 GHz), development of a next-generation electromagnetic wave shielding/absorber in the millimeter wave range is considered to be essential. Since the resonance frequency is proportional to the anisotropy field, the high coercivity ε-Fe_2O_3 nanopowder(>20 kOe) can absorb electromagnetic wave at high frequencies(~190 GHz). In addition, the non-magnetic elements substituted ε-Fe_2O_3 nanopowder can absorb the electromagnetic wave of wide range because the coercivity of ε-Fe_2O_3 nanopowder substituted with non-magnetic elements is reduced. In this study, we investigated the magnetic properties of ε-Fe_2O_3 nanopowder substituted with non-magnetic elements by spray drying process as a pilot study of next generation electromagnetic wave shielding/ absorber.

칼슘환원법과 선택적 용해를 통한 고순도 희토류 나노자석의 제조 및 그 특성

Near theoretical ultra-high magnetic performance of rare-earth nanomagnets *via* synergetic combination of calcium-reduction and chemoselective dissolution

이지민*, 김종렬, 좌용호
한양대학교 재료화학공학과

Rare earth permanent magnets with superior magnetic performance have been generally synthesized through many chemical methods incorporating calcium thermal reduction. However, a large challenge still exists with regard to the removal of remaining reductants, byproducts, and trace impurities generated during the purifying process, which serve as inhibiting intermediates, inducing productivity and purity losses, and a reduction in magnetic properties. Nevertheless, the importance of a postcalciothermic reduction process has never been seriously investigated. Here, we introduce a novel approach for the synthesis of a highly pure samarium-cobalt (Sm-Co) rare earth nanomagnet with near theoretical ultra-high magnetic performance *via* consecutive calcium-assisted reduction and chemoselective dissolution. The chemoselective dissolution effect of various solution mixtures was evaluated by the purity, surface microstructure, and magnetic characteristics of the Sm-Co. As a result, NH_4Cl/methanol solution mixture was only capable of selectively rinsing out impurities without damaging Sm-Co. Furthermore, treatment with NH_4Cl led to substantially improved magnetic properties over 95.5% of the M_s for bulk Sm-Co. The mechanisms with regard to the enhanced phase-purity and magnetic performance were fully elucidated based on analytical results and statistical thermodynamics parameters. We further demonstrated the potential application of chemoselective dissolution to other intermetallic magnets.

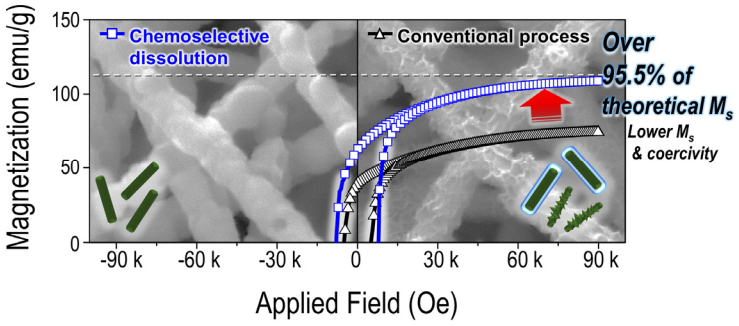

Reference

[1] Scientific Reports 8(1), December 2018

Development of texture in (Nd,Ce)-Fe-B-type die-upset hybrid magnet composed of two constituents with/without Ce

M. S. Kang[1*], Dagus R. Djuanda[1,2], H. W. Kwon[1], J. G. Lee[3] and H. J. Kim[4]
[1]Pukyong National University, Busan, Republic of Korea 48513
[2]Metal Industries Development Center, Bandung, Indonesia 40135
[3]Korea Institute of Materials Science, Changwon, Republic of Korea 51508
[4]Korea Institute of Industrial Technology. Cheonan, Republic of Korea 31056

When it comes to the supply risk of rare-earth for Nd-Fe-B-type magnet, what has emerged from permanent magnet community is so-called 'rare-earth balanced magnet', which advocates exploitation of abundant and cheap light rare-earths as coping strategy for supply risk of rare-earth metals and helps maintain a balance between supply and demand of the rare-earth resources. The light rare earths such as La, Ce, Pr and Nd are mostly refined from rare-earth ores of Bastnasite and Monazite, and the most abundant rare-earth element in those ores is cerium (Ce), thus Ce metal is available with much more affordable price than Nd and Pr. An extensive research has been made to exploit Ce as a substituent for Nd and Pr in the (Nd,Pr)-Fe-B-type magnet. Our previous report revealed that fabrication of Ce-substituted Nd-Fe-B-type die-upset magnet with good magnetic performance was feasible by hybridisation of two different Nd-Fe-B-type materials with and without Ce-substitution. Texture in the die-upset hybrid magnet was dependent upon the mixing ratio of the two constituent materials for hybridization. In the present study, we did go into in great detail about the texture development in Nd-Fe-B-type die-upset hybrid magnet composed of two Nd-Fe-B-type materials with and without Ce-substitution. Nd-Fe-B-type alloy flakes (MQU-F) and HDDR-treated (Nd,Ce)-Fe-B-type alloy powders were thoroughly mixed, and the mixture was first hot-pressed at 670 ^{o}C and then die-upset at 735 ^{o}C with 75 % thick reduction. Texture in the hybrid magnet was evaluated by means of x-ray diffraction (XRD, CuK_{a}) and magnetic measurement. Texture in the die-upset magnet prepared using only HDDR-treated powder was noticeably smaller than that of the magnet from

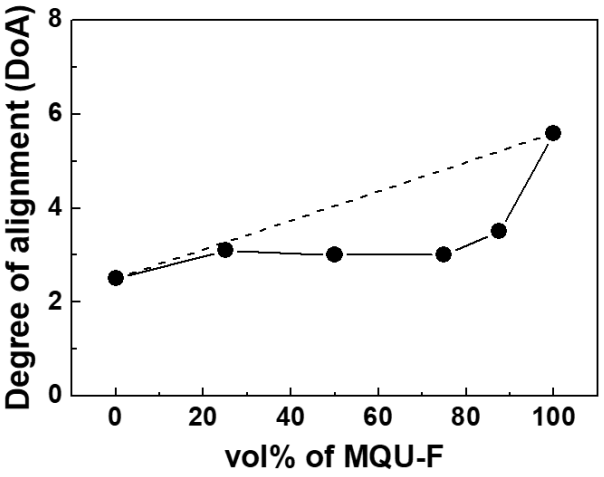

Fig. 1. Dependence of texture in the hybrid die-upset magnet on mixing ratio of constituent materials of HDDR-treated powder and MQU-F flakes.

only MQU-F flakes. If texture in each constituent part in the hybrid magnet would be same as that in single alloy die-upset magnet, texture of the hybrid magnet would be given following mixture law: overall texture (degree of alignment: DoA) of the hybrid magnet would lie on the corresponding value on the straight dotted line connecting the DoA values for the die-upset magnets from only HDDR-treated powder and only MQU-F flakes (see Fig.1). Texture of the hybrid magnet, however, was measurably lower with respect to that expected from the mixture law. This indicates that texture in each constituent region in the hybrid magnet may be less developed with respect to that formed in the die-upset magnet from only HDDR-treated powder and only from MQU-F flakes. Texture development in the hybrid magnet is discussed in relation to microstructure of the two constituent parts of HDDR-treated powder and MQU-F flakes in the hybrid magnet.

Epitaxial growth of $SrFe_{12}O_{19}$ thin films and their magnetism

Sangkyun Ryu[1*], Kung wan Kang[1], June Hyuk Lee[2], Jaekwang Lee[1], Jin-Hyung Cho[1], Hyoungjeen Jeen[1†]

[1]Department of Physics, Pusan National University, Busan, 46241, Korea

[2]KAERI, Daejeon, 34057, Korea.

Hexaferrite-based permanent magnet are widely used due to its low cost. However, there is a need to increase of magnetism like increase of saturation magnetization in these conventional materials. Currently, industries heavily rely on doping strategy to enhance their magnetism, i.e. doping of cobalt, alkali metals, and etc. In contrast to conventional approaches, we rather focused on structure-property relation in hexaferrites, since magnetic ground state is ferromagnetic. For detailed study on the relation, it is necessitated to grow either single crystals or epitaxial thin films. In this presentation, we will address our effort to create epitaxial $SrFe_{12}O_{19}$ (SFO) thin films and show physical properties of the epitaxial thin films. We synthesized SFO ceramic target through conventional solid-state reaction. For epitaxy, we used pulsed laser deposition with two different substrates, providing hexagonal lattices: (0001) Al_2O_3 and (111) $SrTiO_3$. By varying growth temperature and oxygen partial pressure, we could see the film is crystalized at least 700^{o}C or higher. After determined the optimal growth condition, we performed magnetometry using vibrating sample magnetometer. From the result, we could obtained 500 emu/cm^3 saturation magnetism and 2901 Oe coercivity. Note that saturation magnetization and coercivity of SFO on (001) Al_2O_3 are 608 emu/cm^3 and 2932 Oe. This is higher than those from SFO on (111) $SrTiO_3$. We additionally studied surface morphology wit atomic force microscopy and x-ray rocking curve to see crystallinity. This work is supported by the National Research Foundation of Korea (NFR) (NRF-2018M2A2B3A01071859).

Enhancing the coercivity and thermal stability of Nd-Fe-B sintered magnets by grain boundary diffusion process

Sumin Kim[1*], Hyun-Sook Lee[1], Donghwan Kim[2], Jong Wook Roh[3] and Wooyoung Lee[1†]

[1]Department of Materials Science and Engineering, Yonsei University, Seoul 03722, Republic of Korea

[2]R&D center, Star Group, Daegu 42714, Republic of Korea

[3]School of Nano & Materials Science and Engineering, Kyungpook National University, Gyeongsangbuk-do 37224, Republic of Korea

The realization of efficient electric vehicle motors or power generation systems for wind turbines necessitates the development of high-performance permanent magnets, which is associated with a number of challenges. Since their discovery in 1984, high-coercivity sintered Nd-Fe-B magnets have found numerous practical and industrial applications, e.g., as components of actuators, motors, and generators. However, the above applications require long-term magnet operation in high-temperature environments without any coercivity decrease, which is a non-trivial criterion. Generally, the coercivity of Nd-Fe-B magnets at room temperature can be enhanced by the partial replacement of Nd by Dy, Tb, or both; however, the high cost and scarcity of these rare earths preclude the widespread application of this method and necessitate the development of more economically viable alternatives. One of such alternatives is the reduction of heavy rare earth elements (e.g., Dy and Tb) usage and minimization of remanence and energy product loss via the utilization of the grain boundary diffusion process. For application in a high-temperature environment, we should consider both coercivity and thermal stability of Nd-Fe-B magnets.

Herein, we enhance the not only coercivity, but also thermal stability by grain boundary diffusion process and consecutive heat treatments for application in a high-temperature environment such as electric motors.

영구자석 착자를 고려한 컴프레서용 모터 설계

김규섭*, 김수철, 김규식, 이병화
자동차부품연구원

1. 서론

영구자석형 동기전동기 모터는 자동차, 생활가전, 로봇 등과 같은 다양한 분야에서 사용되고 있다. 모터의 생산성을 높이기 위해 회전자에 삽입되는 영구자석에 대한 다양한 조립 공법이 적용되고 있으며 그중 착자되지 않은 영구자석을 삽입한 후에 착자되는 방법도 고려되고 있다. 특히, 후착자 방법으로 회전자 조립시 회전자 형상이 복잡할 때에는 착자 프로세를 고려한 해석적인 방법이 필요하다. 본 논문에서는 후착자 조립을 고려한 컴프레서용 모터 회전자의 역기전력을 비교하였다.

2. 해석방법과 결과

영구자석의 착자 프로세스를 고려하기 위하여 초자화곡선과 착자정도에 따른 감자곡선을 활용하여 착자전류가 인가될 때 최종 잔류자속밀도를 계산하였다. 회전자 형상에 따라 영구자석에 미치는 자계강도가 다르므로 초기자화 곡선에 도달하는 값을 추정하여 최종 잔류자속 밀도를 산정하였다.

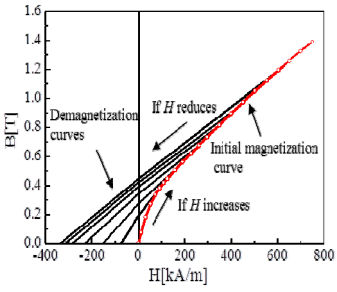

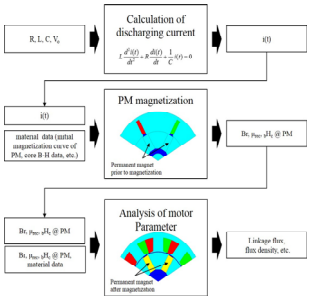

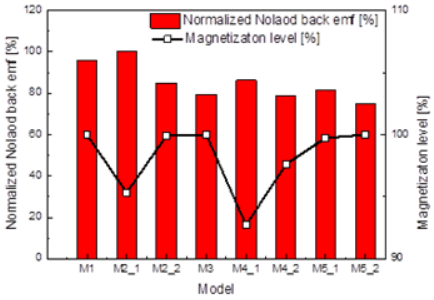

3. 고찰

회전자 형상에 따라 착자되는 자계 강도 양이 다르며 이를 통해 확보 가능한 역기전력의 양이 다른 것을 파악할수 있었다.

4. 결론

조립후 착자과정을 통해 생산되는 회전자의 경우 영구자석의 모든 부분이 착자가 잘 되었는지 착자프로세스를 고려한 해석이 필요하다.

5. 사사

본 연구는 대구광역시에서 시행중인 미래형자동차 선도기술 개발사업(준중형급 전기자동차 공조용 전동식 컴프레셔 구동 시스템 개발, DG-2017-02)의 지원하에 수행되었습니다.

6. 참고문헌

[1] M.-F. Hsieh, Y.-M. Lien, and D. G. Dorrell, “Post-assembly magnetization of rare-earth fractional-slot surface permanent-magnet machines using a two-shot method,” IEEE Trans. Ind. Appl., vol. 47, no. 6, pp. 2478-2486, Nov./Dec. 2011.

[2] H.-J. Kim, D.-Y. Kim, and J.-P. Hong, “Structure of concentrated flux-type interior permanent-magnet synchronous motors using ferrite permanent magnets,” IEEE Trans. Magn., vol. 50, no. 11, Nov. 2014, Art. ID 8206704.

[3] D. G. Dorrell, M.-F. Hsieh, and Y.-C. Hsu, “Post assembly magnetization patterns in rare-earth permanent magnet motors,” IEEE Trans. Magn., vol. 43, no. 6, pp. 2489-2491, Jun. 2007.

Artificially produced rare earth free $L1_0$-FeNi phase through annealing of the FeNiPC amorphous alloy

Jonghee Han*, Jihye Kim and Haein Choi-Yim
Department of Physics, Sookmyung Women's University

The rare-earth-free hard magnetic $L1_0$-FeNi phase has excellent magnetic properties such as a high saturation magnetization (M_s ~1270 emu/cm3) and a large uniaxial magnetic anisotrophy (K_u ~1.3 107 erg/cm3). However, it is very difficult to artificially produce the $L1_0$-FeNi phase due to the low atomic diffusion coefficients of Fe and Ni near the order-disorder temperature (~320℃). Therefore, FeNiPC amorphous alloy systems were investigated. The thermal properties of FeNiPC amorphous alloy systems were measured by using differential scanning calorimetry (DSC), including crystallization temperature (T_x). It exhibit T_x near the transition temperature. After measuring thermal properties, the amorphous alloys were annealed at T_x resulting in high atomic diffusion. The structural and micro structural characterizations of annealed ribbons revealed the formation of $L1_0$-FeNi phase through observation of the superlattice peak by using X-ray Diffraction (XRD). Transmission Electron Microscopy (TEM) and Energy Dispersive X-ray Spectroscopy (EDS) were utilized in order to determine additional supporting evidence of the formation of the $L1_0$-FeNi phase. The magnetic property measured by a vibrating sample magnetometer (VSM), such as M_s and coercivity (H_c), also indicated the formation of L10 FeNi phase.

가스분무된 희토류 소결자석 소성변형능에 미치는 Ti 첨가의 영향

조주영[1*], 좌용호[2], 남선우[1], 김택수[1,3]
[1]한국생산기술연구원 한국희소금속산업기술센터
[2]한양대학교 재료화학공학과
[3]과학기술연합대학원 대학교

현재까지 발견된 영구자석 중 가장 우수한 자성특성으로 다양한 산업분야에 널리 사용되고 있는 Nd-Fe-B 계 희토류 영구자석 제조를 위한 새로운 시도로 가스분무를 통해 Nd-Fe-B 계 구형 분말을 만들고 이를 이용하여 자석을 제조하는 방법이 연구되었으나 분말의 크기가 상대적으로 크고, 등방성이므로 산업적으로 본드자석에만 일부 사용되고 있다. 이러한 한계를 극복하고자 소성변형을 통해 이방성을 부여하는 연구가 수행되었으나 강자성상인 $Nd_2Fe_{14}B$ 상의 적은 슬립시스템으로 인해 상온에서 소성변형이 불가능하며, 고온에서는 $Nd_2Fe_{14}B$ 상 사이에 존재하는 REE-rich 상의 낮은 융점으로 인해 REE-rich상이 액상으로 존재하여 $Nd_2Fe_{14}B$ 상의 소성변형을 방해하기 때문에 REE-rich 상의 제어가 필수적이다.

따라서 본 연구에서는 Nd-Fe-B 계 영구자석의 소성변형능을 향상시키기 위한 연구를 수행하였다. 소성변형 시 REE-rich 상의 융점을 향상시키기 위해 열역학 프로그램을 통하여 합금원소를 결정하였으며 Ti을 Nd-Fe-B 합금에 첨가하여 가스분무된 분말을 열분석함으로써 REE-rich 상의 융점 변화를 확인했다. 그 후 최적화된 가성형 및 고온변형을 통해 소성변형 함으로써 소결 자석을 제조하였고 SEM 및 XRD를 통해 소성 변형 후 빌렛의 종횡비 및 이방성 형성을 확인함으로써 소성변형능 변화를 확인함으로써 소성변형 가능성을 판단하였다.

Keywords: Nd-Fe-B magnet, gas atomization, plastic deformation, anisotropic, refractory metal

Modulating magnetism of polycrystalline $PrBaCo_2O_{5.7\pm x}$ through oxygen vacancy engineering

Yun-Seok Heo* and Hyoungjeen Jeen†
Department of Physics, Pusan National University, Busan 46241 Korea

A-site double perovskites have gotten great attentions, since they have been believed as a promising cathode material for solid oxide fuel cells due to fast oxygen exchange behavior. Moreover, Such oxygen desorption and absorption characteristics of the double perovskites can often trigger their modulation in magnetic ground states through complex magnetic interaction as well as electronic ground states. Thus, it would be interesting to see the relation between oxygen vacancy and magnetism. Among many double perovskites, we chose $PrBaCo_2O_{5.7\pm x}$ (PBCO), since it is known that it has spin state transition in specific composition, superior oxygen exchange behavior, and tunable magnetism by oxygen contents. In this presentation, we will provided relation among oxygen vacancy, crystal structure, and magnetism in PBCO. We used solid state reaction to prepare polycrystalline PBCO. From SQUID data, we could stabilized the oxygen contents of our air-sintered PBCO is at least x = 5.7. To address the oxygen-content-driven variations in structure and magnetism, we used temperature and time control annealing apparatus, powder x-ray diffraction and SQUID magnetometry. For tuning oxygen content, we used thermal treatments under 3% H_2 forming gas and O_2 to stabilize different oxygen contents in between x = -0.4 and 0.1 at relatively low temperatures (200°C and 300°C). We also observed composition-driven structural transition from tetragonal to orthorhombic. This work is supported by the National Research Foundation of Korea (NFR) (NRF-2018R1D1A1B07045462).

Enhance of Saturation Magnetic Flux Density of the Soft magnetic Core, with Maintaining Low Core loss and High Permeability

Seoyeon Kwon* and Haein Yim
Department of Physics, Sookmyung Women's University, Seoul 04310, Korea
Fax: +82-(30)-3079-90362 E-mail address: sykwon39@sookmyung.ac.kr

The refinement of FINEMET type alloy with an experiment stretching over various stages was reported. It was carried out on new composition soft magnetic core, this alloy can be ubiquitously utilized in various applications such as motors, common mode choke, actuators, and so forth. This experiment was performed with the aim at increasing saturation magnetization (B_s) while keeping low core loss (P_{cv}) and high permeability (μ). The amorphous core $Fe_{80}Si_7B_9Nb_3Cu_1$ has been fabricated by rapid cooling on a single copper wheel. The values of thermal properties were measured by using differential scanning calorimetry (DSC), including crystallization temperature (T_x). The microstructure properties were confirmed by X-ray diffraction (XRD) and transmission electron microscopy (TEM). The magnetic characteristics were measured by AC B-H loop tracer. The B_s and coercivity (H_c) were measured under a maximum applied field (H_m) of 800 A/m, the μ was observed in the frequencies (f) of 10 kHz and 100 kHz, and the P_{cv} was measured at constant condition. The core annealed at 560 ℃ showed the improvement in B_s with value of 1.57 T compare to conventional value of FINEMET core (Bs = 1.23 T). The combination of high B_s with excellent magnetic properties at 560 ℃ in this paper, promised this soft magnetic alloys an outstanding economical application in high frequency region.

Al 이온을 소량치환한 Y-type hexaferrite의 자기적 성질 연구

김정훈*, 김철성
국민대학교 물리학과

1. 서론

투자율을 가지는 연자성 물질인 ferrite는 다양한 영역의 주파수에서 사용할 수 있는 RF 디바이스의 소자로 주목받고 있다. 그 중 hexaferrite는 자기기억소자, 영구자석, 정보저장장치 등 많은 종류의 장치에서 사용될 수 있는 물질이다. Y-type hexaferrite는 spin-current 모델에 기초한 magnetoelectric(ME) 효과를 나타내며 Sr 이온의 높은 평면 이방성으로 인해 스핀구조가 변형될 수 있다. 또한 Al 이온의 치환은 저자장 하에 상온에 근접하는 온도에서 ME 효과를 나타낼 수 있다. 본 연구에서는 $Ba_{0.5}Sr_{1.5}Ni_2(Fe_{0.99}Al_{0.01})_{12}O_{22}$ 물질의 자기적 성질을 연구하고자 한다.

2. 실험방법

시작물질로 $BaCo_3$, $SrCo_3$, $Ni(NO_3)_2 \cdot 6H_2O$, $Fe(NO_3)_3 \cdot 9H_2O$, $Al(NO_3)_3 \cdot 9H_2O$를 사용하여 polymerizable complex 방법을 이용하여 $Ba_{0.5}Sr_{1.5}Ni_2(Fe_{0.99}Al_{0.01})_{12}O_{22}$ 물질을 제조하였다. 증류수에 시작물질을 정확한 당량비에 맞추어 계산한 후 넣고 60 ℃에서 1시간 유지하고, 1 : 2.5 (총 금속 : 시트르산)의 비율로 시트르산을 첨가하여 70 ℃로 승온하여 1시간 유지한다. 그 후 에틸렌 글리콜을 첨가하여 80 ℃에서 1시간 교반시켜 준 뒤 120 ℃로 승온하여 gel 형태로 건조시켜 metal-citrate 복합체 사이의 중합을 실시한 뒤 320 ℃에서 하소하였다. 하소된 분말을 압축 성형하여 1100 ℃에서 10시간 동안 소결하여 $Ba_{0.5}Sr_{1.5}Ni_2(Fe_{0.99}Al_{0.01})_{12}O_{22}$ 시료를 획득하였다. 획득한 시료의 결정학적 특성을 확인하기 위해 X-선 회절기를 이용하였으며 전기역학적 등가속도형 Mössbauer 분광기, Vibrating sample magnetometer(VSM)을 이용하여 자기적 특성을 확인하였다. 또한 Network Anlayzer를 이용하여 50 MHz부터 4 GHz까지의 유전율, 투자율을 측정하였다.

3. 실험결과 및 고찰

Y-type hexaferrite $Ba_{0.5}Sr_{1.5}Ni_2(Fe_{1-x}Al_x)_{12}O_{22}$ 물질을 X-선 회절 실험한 결과 R-3m의 공간군을 가지는 rhombohedral 구조를 갖는 것으로 확인되었으며, 격자상수는 a_0 = 5.829, c_0 = 43.238 Å, V = 1272.45 Å^{3}으로 분석되었다. 상온에서의 Mössbauer 결과는 18h_{VI}, 3b_{VI}, 6c_{IV}, 6c_{IV}*, 6c_{VI}, 3a_{VI}의 결정학적 구조를 바탕으로 초미세자기장은 18h_{VI} 격자가 가장 큰 초미세 자기장을 가지며 6 격자의 평균 이성질체 이동치는 0.31 mm/s로 확인되었고 각 격자의 Fe 이온은 Fe^{3+} 상태임을 확인하였다. 온도에 따른 자화곡선은 100 Oe하에 4.2에서 300 K까지 측정하였으며 시료의 상온에서의 포화자화는 20.40 emu/g 이며 보자력은 63 Oe으로 확인되었다. NA측정을 통해 얻은 유전율은 50 MHz에서 9.4, 투자율은 2.4이며 주파수가 증가할수록 감소하여 4 GHz에서의 유전율은 8.9, 투자율은 1.5로 확인하였다.

4. 참고문헌

[1] Y. Y. Song, J. Zheng, M. Sun, S. Zhao, J. Mater. Sci.-Mater. Electron. **27**, 4131 (2016).

[2] A. Nikzad, A. Ghasemi, M. K. Tehrani, G. R. Gordani, J. Supercond. Nov. Magn. **28**, 3579 (2015).

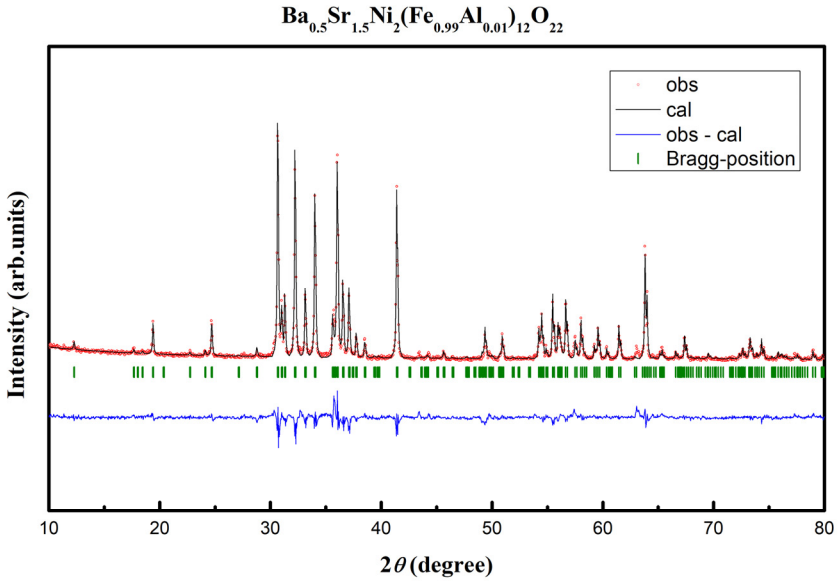

Fig. 1. The refined X-ray diffraction patterns of the $Ba_{0.5}Sr_{1.5}Ni_2(Fe_{0.99}Al_{0.01})_{12}O_{22}$ at room temperature.

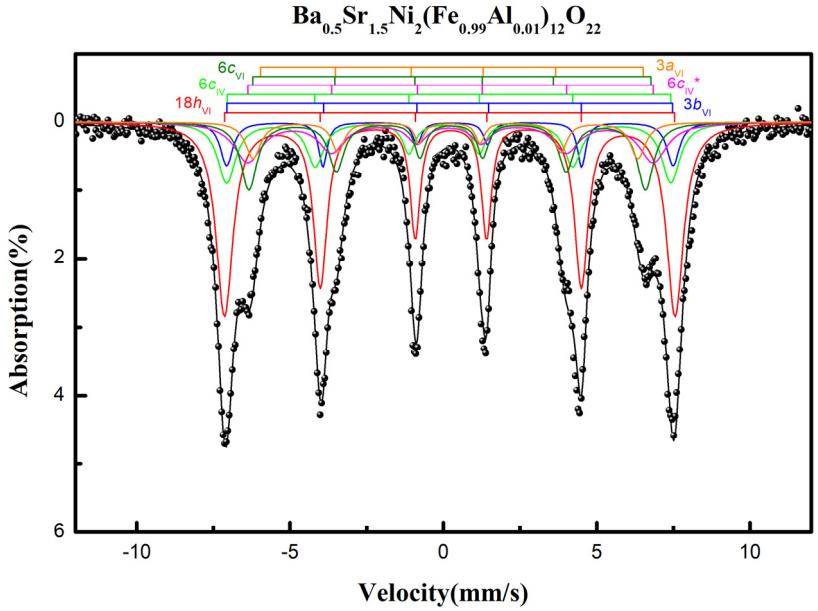

Fig. 2. Mössbauer spectrum of the $Ba_{0.5}Sr_{1.5}Ni_2(Fe_{0.99}Al_{0.01})_{12}O_{22}$ at room temperature.

다중스캔 기반 SLM법으로 제조된 FeSiBCCr 연자성 조형체의 미세 조직 및 자기적 특성

남영균[1*], 양상선[1], 유지훈[2], 정재원[1†]
[1]재료연구소 분말/세라믹연구본부 금속분말연구실
[2]재료연구소 분말/세라믹연구본부 3D프린팅소재센터

1. 서론

전기강판(Fe-Si)으로 대표되는 연자성 합금은 모터, 발전기 및 변압기를 포함한 다양한 전자기 응용분야에서 널리 사용되고 있다. 대표적 응용 분야 중 하나로 모터가 있으며, 모터의 경우에 있어 출력과 효율 성능에 크게 영향을 미치는 연자성 합금의 세 가지 중요한 특성으로 포화 자화, 투자율 및 코어손실이 있다. 대표적인 모터용 연자성 소재인 전기강판의 경우, 1.8 T 이상의 높은 포화자화를 나타내어 모터의 출력 특성을 맞추기 위해 폭넓게 활용되고 있다. 하지만, 일반적으로 전기강판은 압연 공정으로 0.1 ~ 0,5 mm 두께의 시트 형태로 제조되기 때문에 3차원 설계에 한계가 있을 수밖에 없으며, 철손 감소를 위한 박판화에도 한계가 있다. 반면, Fe계 비정질 연자성 합금은 기존의 전기강판과 비교하여 결정 이방성이 없기 때문에 높은 투자율을 가지며, 높은 전기저항으로 인해 매우 낮은 철손(Core loss)을 가지면서, 압연 공정이 적용되지 않기 때문에 3차원 설계에 기반한 부품 제조가 가능하여 모터에 적용할 경우 출력과 효율을 향상 시킬 수 있을 것으로 기대된다. 그러나 비정질 상을 형성하기 위해서는 급랭 공정이 요구되기 때문에 와이어나 필름 형태로 소형으로 제작되는 등 제작 가능한 형상에 제한이 따른다. 대표적 비정질 합금 제조 기술인 구리 몰드 흡입 주조(Copper mold Suction casting) 혹은 멜트스피닝(Melt spinning)으로 제조된 비정질 합금의 크기는 최대 수 mm 수준으로 제한되며, 포화자화 또한 1.56 T 미만으로 보고되고 있다. 이러한 문제점의 대안으로, 얇은 금속분말 층에 레이저를 조사하여 적층제조하는 방식인 선택적 레이저 용융 공정(Selective Laser Melting: SLM)이 떠오르고 있다. SLM 공정은 10^3-10^8 K/s의 높은 냉각속도를 나타내며 3차원의 자유설계 구현이 가능해 Fe계 비정질 연자성 부품 제조에 적합한 공정일 수 있다. 하지만 SLM 공정을 이용해 비정질 합금을 제조하는데 있어 Melt pool의 화학적 불균일성으로 인해 균일한 비정질 상의 형성이 어려운 것으로 보고되고 있다.

이에 본 연구에서는 기존 SLM 공정에 문제점을 해결하고자 화학적 균일성을 향상시켜 비정질 상을 안정적으로 형성시킬 수 있는 다중스캔 기법을 적용하였다. FeSiBCr 비정질 연자성 합금 분말을 이용하여, 일반스캔과 다중스캔 방식을 적용하고 각각의 방식에서 에너지 밀도에 따른 비정질 분율과 자기적 특성, 기계적 특성을 비교 분석하였다.

2. 실험방법과 결과

본 연구에서는 FeSiBCCr 비정질 연자성합금의 비정질 상 분율을 향상하기 위해 다중스캔법을 적용하였다. SLM 공정은 분말이 제공되는 Dose chamber에서 분말을 이송하여 Building state에 한 층을 도포하고 설정이 인식된 설계 도면을 따라 레이저를 조사하는 방식으로 시편을 제작하였다. 레이저 출력(Laser power: p)은 50 W, 70 W, 90 W의 조건으로, 스캔 속도(Scan Speed: v)는 1200 mm/sec, 1600 mm/sec의 조건으로 시편을 제작하였으며, 일반스캔(Normal scan)과 다중스캔(Multiple scan) 두 가지 방식을 적용하여 각각 6가지의 시편을 제작하였다. 해치간격(hatch spacing: h), 레이어두께(Layer thickness: t), 오버랩(overlap)은 각각 80 ㎛, 25 ㎛, 30%로 고정하였다. 레이저 스캔 패턴은 일방향 조사 방법인 Continuous 방식이고, 다중스캔 시에는 Cross-section 방식으로 교차 스캔을 사용하였다. 시편크기는 10 mm x 10 mm x 5 mm로 cubic 형상으로 제작 하였으며, 철손(Core

loss)특성 분석을 위해서 원형시편(Toroid)을 내경 10 mm, 외경 20 mm, 높이 5 mm으로 추가로 제작하였다.

실험결과 비정질 연자성합금의 상대밀도는 다중스캔 전략 적용시 일반스캔보다 높게 나타나는 것을 확인하였다. 다중스캔 적용시 기공이 감소하면서 상대밀도가 상승하였다. XRD 분석시 다중스캔이 일반스캔보다 결정피크가 완화되는 것을 확인하였고, FE-TEM분석 결과 비정질상 영역과 비정질/결정질 상 혼재 영역이 같이 존재함을 확인하였다. 열분석 결과 다중스캔의 경우가 일반스캔보다 더 높은 결정화 엔탈피를 나타내었으며, 화학적균일성은 전자빔미세분석(EPMA) 을 통하여 확인한 결과 다중스캔이 일반스캔보다 조성 균일도가 높은 것을 확인하였다. 자기특성 분석 결과 다중스캔이 일반스캔보다 높은 포화자속밀도와 투자율을 나타내며, 낮은 보자력을 나타내었다. 철손(Core loss) 특성 분석 결과 역시다중스캔이 일반스캔 보다 철손 감소에 효과적이었다. 다중스캔과 열처리를 모두 진행한 소재가 가장 낮은 철손과 가장 높은 투자율을 나타내었으며, 항절력(Transverse test) 측정을 통한 기계적 특성 분석경우 다중스캔이 일반스캔 보다 높은 기계적 강도를 나타냄을 확인하였다. 이는 다중스캔 적용 시 기공의 감소로 인한 밀도 향상 때문인 것으로 사료된다.

3. 고찰

다중스캔적용 시 일반스캔보다 높은 포화자화, 포화자기분극 값을 나타내고, 보자력또한 다중스캔에서 감소하는 것을 확인하였다. 이는 밀도 향상과 함께 비정질상의 증가로 결정자기이방성이 감소되어 자구의 이동이 용이해졌기 때문이다. FeSiBCCr 비정질 연자성합금의 철손(Core loss) 특성 분석 결과 다중스캔이 일반스캔보다 철손 감소에 효과적이었다. 이는 비정질상 분율 향상으로 보자력 감소에 따른 히스테리시스 손실감소에 기인한 것으로 사료된다. FeSiBCCr 비정질 연자성합금의 열처리에 따른 자성 특성 향상 효과를 확인하였다. 다중스캔과 열처리를 모두 진행한 소재가 가장 낮은 철손과 가장 높은 투자율을 나타내었으며, 이는 열처리 시 잔류응력 감소로 응력장에 잡혀있던 자벽구조가 원활 해지면서 자화이동이 원활 해졌다고 볼 수 있다. FeSiBCCr 비정질 연자성합금의 항절력(Transverse test) 측정을 통한 기계적 특성 분석을 진행하였으며, 다중스캔이 일반스캔 보다 높은 기계적 강도를 나타냄을 확인하였다. 이는 다중스캔 적용 시 기공의 감소로 인한 밀도 향상 때문인 것으로 사료된다.

4. 결론

본 연구에서는 FeSiBCCr 합금의 SLM 적층제조 공정에서 다중스캔법을 이용함으로써 화학적 조성 균일성을 확보하였고, 이를 통해 비정질 분율을 향상시켜 보자력과 철손은 감소시키고 투자율 특성은 향상시킨 결과를 확인하였다.

5. 참고문헌

[1] H.Y. Jung, S.J. Choi, K.G. Prashanth, M. Stoica, S. Scudino, S. Yi, U. Kuhn, D.H. Kim, K.B. Kim, J. Eckert, Fabrication of Fe-based bulk metallic glass by selective laser melting: A parameter study, Mater Design, 86 (2015) 703-708.

[2] G. Herzer, Modern soft magnets: Amorphous and nanocrystalline materials, Acta Mater, 61 (2013) 718-734.

교차된 일축이방성 효과에 의한 NiO층 기반 이층 구조형 거대자기저항-스핀밸브 다층박막의 자기저항 특성 비교

최종구[1*], 카지드마[2], 강병욱[1], 이상석[1]
[1]상지대학교 한방의료공학과
[2]상지대학교 대학원 동서의료공학과

1. 서론

바이오소자로 활용하는 거대자기저항-스핀밸브 (giant magnetoresiatance spin valve, GMR-SV) 다층박막에서 가장 중요한 역할을 하는 반강자성체는 주로 Mn계 금속 합금박막인 IrMn, FeMn, PtMn, NiMn 타겟들로 사용되어 왔다. 산화계 반강자성체로써 결정학적으로 단순한 스핀 구조를 띠고 있으며 화학적으로 안정된 NaCl 구조인 부도체이자 반도체의 특성을 가지고 있는 NiO 박막과 인접한 강자성체인 NiFe 박막 층 사이의 계면에서는 큰 이방성 교환결합력이 유도된다. NiO 박막은 상온으로 290 K 부근에서 보다 저온으로 77 K에서 분자형 자성체는 전이금속과 산소원자로 이루어진 클러스터 원자가 기본적으로 자성을 나타내고 있으므로 2차원 상에서 원자 위치의 인위적 변화에 따른 다양한 차원에서 자기이방성 에너지 값 산출의 필요성과 더불어 자기적 특성의 향상을 위하여 NiO 박막에 대한 연구가 다시 대두되고 있다. GMR-SV 다층박막 구조에서 바닥층과 보호층이 금속박막일 경우에는 누설효과로 하여금 거대자기저항적 특성의 감소를 방지하고 자기저항비를 높이기 위해서는 스펙큘러 (specular) 전자산란을 향상시키는 표면 개질 기술의 개발이 중요하다.

2. 실험방법

본 연구는 순수한 금속 자성체 간의 스핀 의존산란 효과와 스펙큘러(specular) 효과를 동시에 적용하여 나노자성을 감지할 수 있는 바이오센서로 활용하기 위하여 두께가 10 nm = 100 Å인 NiO 층의 이중구조를 갖는 GMR-SV 다층박막을 단일 구조 다층박막이 서로 반평행이 되게 Fig. 1와 같이 서로 교차된 일축자기이방성을 적용하여 이층구조 GMR-SV 다층박막을 제작하였다. GMR-SV 다층박막에 따른 자기적 특성으로 고정층과 자유층 사이의 교환결합세기 (exchange coupling field, H_{ex}), 보자력 (coercivity, H_c), 자기저항비 그리고 자장감응도 (magnetic sensitivity, MS)의 값을 상온과 액체질소 상의 온도 77 K에서 각각 4-단자법으로 측정된 자기저항 곡선을 분석하여 결정하였다.

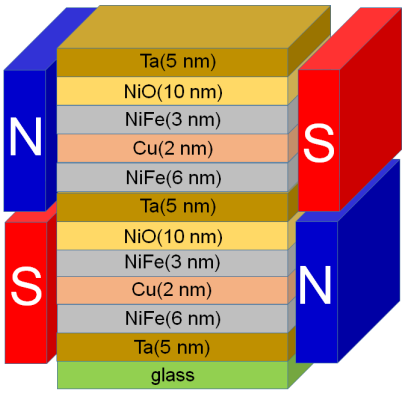

Fig. 1.

3. 실험결과 및 토의

Fig. 2는 glass/Ta(5 nm)/NiFe(6 nm)/Cu(2 nm)/NiFe(3 nm)/Ni0(10 nm)/Ta(2.5 nm)/∞(180°)/Ta(2.5 nm)/NiFe(6 nm)/Cu(2 nm)/NiFe(3 nm)/Ni0(10 nm)/Ta(5 nm) 다층 박막의 상온과 액체질소상의 온도 77 K에서 얻은 major 자기저항 곡선이다. 다층박막 시료 아래에 위치한 1개의 자유층으로 삽입한 상부의 자유층 NiFe(6 nm) 박막 사이에 두고 상부층의 NiO 박막과 적층한 후, 일축자기 이방성을 스위칭하기 위하여 영구자석을 180° 회전하였다. 그 위에 하부층 Ta(5 nm)/NiFe(6 nm)/Cu(2 nm)/NiFe(3 nm)/Ni0(10 nm)와 똑 같은 구조로 상부층 NiO-GMR-SV 박막이 적층되었다. 상온에서 측정된 자기저항 곡선인 Fig. 2(a)에 보여준 바와 같이 180° 교차되어 스위칭된 일축 자기이방성 효과를 나타내고 있지 않았다. 그러나 이중층 구조의 하부와 상부 NiO-GMR-SV

박막이 형성한 자기저항비는 5.6%이며 하부 NiO-GMR-SV 박막이 갖는 교환결합력 (H_{ex})와 보자력 (H_c)은 각각 18.0 Oe, 13.0 Oe 이었다. 반면에 이중층 구조의 상부 NiO-GMR-SV 박막이 형성한 교환결합력 (H_{ex})와 보자력 (H_c)은 각각 12.0 Oe, 5.0 Oe 이었다. 77 K에서 측정된 자기저항 곡선인 Fig. 2(b)에 보여준 바와 같이 180° 교차되어 스위칭된 일축 자기이방성 효과를 나타내고 있다. 또한 이중층 구조의 하부와 상부 NiO-GMR-SV 박막이 형성한 자기저항비는 10.0%이로 향상되었다. 하부 NiO-GMR-SV 박막의 교환결합력 (H_{ex})와 보자력 (H_c)은 각각 60.0 Oe, 50.0 Oe이었다. 반면에 이중층 구조의 상부 NiO-GMR-SV 박막이 일축 자기이방성 스위칭 효과에 의한 교환결합력 (H_{ex})와 보자력 (H_c)은 각각 -30.0 Oe, -45.0 Oe이었다.

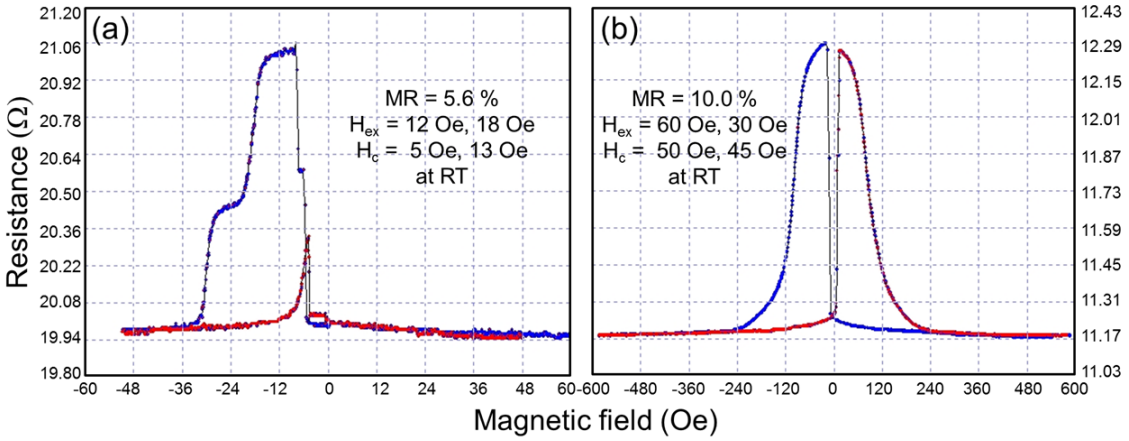

Fig. 2 (a). and 2 (b).

교차된 일축이방성 효과에 의한 3가지 조합으로 이루어진 NiO층 기반 이층 구조형 거대자기저항-스핀밸브 다층박막의 자기저항 특성 비교하기 위하여 비교 분석하였다. 3가지 이층 구조 조합은 Fig. 3과 같다.

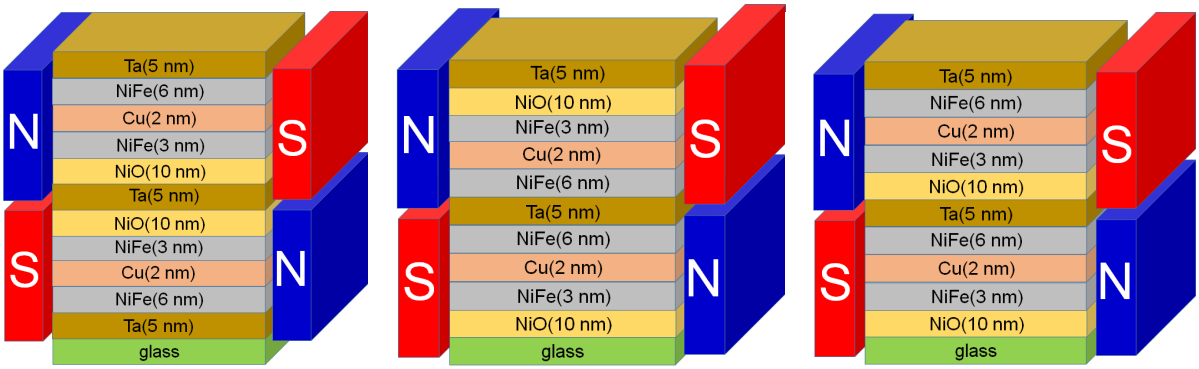

Fig. 3.

감사의 글

이 연구는 교육과학기술부의 재원으로 한국연구재단(NRF)의 기초연구사업 지원을 받아 수행된 연구(No. NRF-2016R1D1A1B03936289)의 결과이다.

보온재 비해체식 배관 감육평가를 위한 비파괴검사와 신호처리

박예라[1,3*], 신정우[2], 김경모[1], 손대락[3], 박덕근[1,2†]
[1]한국 원자력 연구원, 덕진동 유성 34057, 대전
[2]AIPIT, 덕진동 유성 34057, 대전
[3]광센서공학과, 한남대학교, 70 한남로, 대전

Nondestructive Testing for the Wall Thinning of insulated pipe and Signal Processing

Ye La park[1,3*], JeongWooShin[2], KyungMoKim[1], Derac Son[3], Duck-GunPark[1,2†]
[1]Nuclear Materials Research Division, Korea Atomic Energy Research Institute,
Dukjin-dong, Yuseong 34057, Daejeon
[2]AIPIT Inc., Dukjin-dong, Yuseong 34057, Daejeon
[3]Dept.of Photonics and Sensors, Hannam University, 70, Hannam-ro , Daedeok, Daejeon
[†]Corresponding author : dgpark@kaeri.re.kr

1. 서론

펄스와전류 검사 기술은 기존에 사용하는 와전류 검사 기술에서 파생된 기술로 근본 원리는 코일을 이용하는 점에서는 와전류 기술이지만, 기존의 와전류가 가지고 있는 단점을 보완해서 고완 된 기술이다.[1,2] 자기장이 가해질 때 도체에서 패러데이의 자기유도법칙에 의하여 와전류가 유도되어서 도체 근처에서 있는 코일을 통해서 전압신호로 관찰이 된다. 일반적으로 와전류에서의 자기장은 단일한 주파수로 진동하는 정상파에 의해서 생성된다. 반면에 펄스와전류는 정상파를 인가하는 대신 사각 펄스파를 인가하는 와전류를 발생시킨다. 전류 밀도가 낮은 사인파는 배관의 표면 근처의 정보만 알 수 있었다. 반면에 펄스전류는 전류 밀도를 높일 수 있다. 높임으로 배관의 내부의 정보까지 알 수 있다.[3,4] 펄스와전류의 기술에 대한 정확도와 신뢰도에 대해서 알아보기 위해 개발한 장비Programmable Pulsed Large Current Generator (PPLCG)를 이용하여 펄스와전류 Pulsed Eddy Current(PEC)로 배관을 측정해보고. 같은 배관을 기존성능이 검증된 상용 비파괴 검사 장비(38DL PLUS)로 초음파검사 Ultrasonic Test (UT)하여 측정한 결과 값을 비교 해보았다.

2. 실험방법과 결과

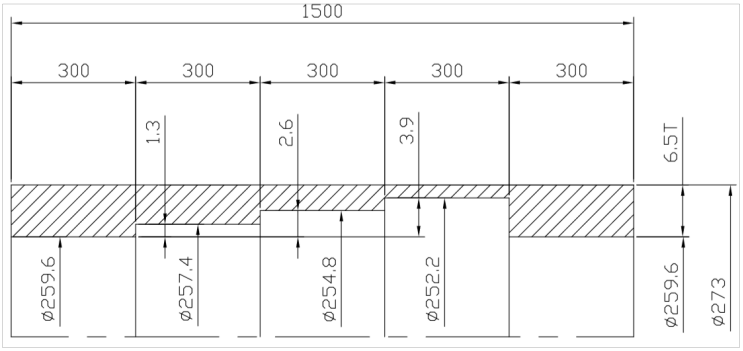

Fig. 1. 시험편의 도면 (10 I Step 6.5T)

그림 1인 시험편은 길이 1500mm, 시험편의 두께는 6.5mm이고, 시험편의 단차가 1.3mm씩 줄어들어 구분할 수 있다. 양끝은 동일하다. 단차간의 거리가 300mm 간격으로 가공했으며, 총 5단계로 나눌 수 있다. 파이프에 보온재두께 50mm을 덮고 앞서 말한 배관에 제작한 장비 PPLCG (최대 전류: 30A, 최대전압:18V)를 이용하여 5단계 각각의 150mm로 간격을 두고 측정하였고, 직접 제작한 PPLCG와 비교하기 위해서 기존성능이 확인된 초음파 검사 장비로 보온재를 빼고 시험편에 5단계 각각의 150mm간격을 두고 두께를 측정하여 비교해보았다.

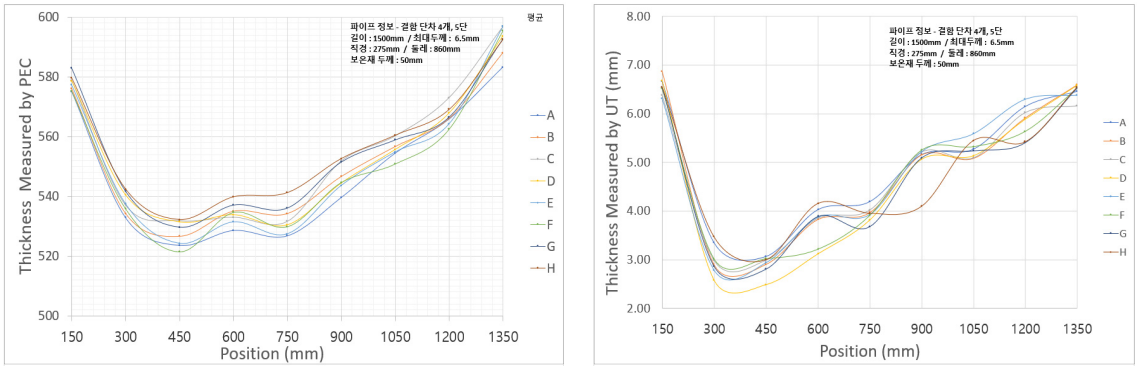

Fig. 2. PEC 장비 측정한 데이터 값과 UT장비로 측정한 데이터 값.

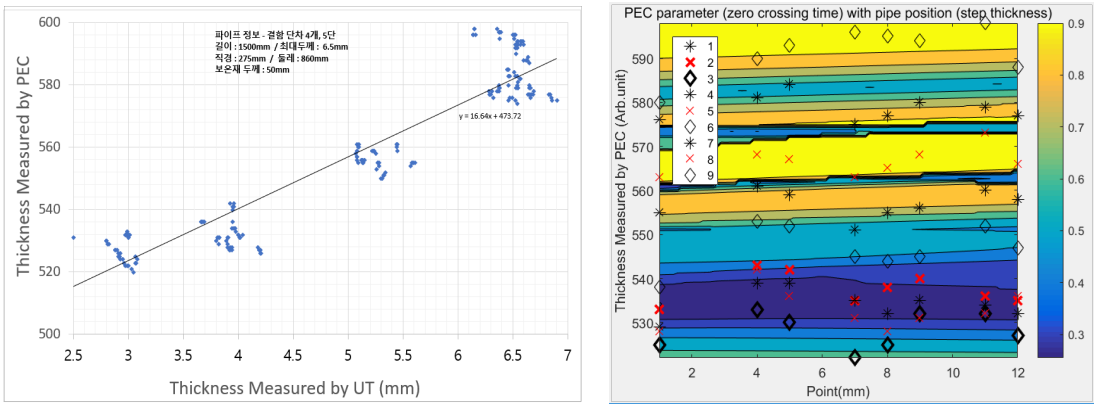

Fig. 3. x축을 초음파 두께에 따른 y축을 PEC 데이터 값 그래프와 SVM coding.

그림 2를 보면 PEC 장비로 보온재 50mm를 덮고 측정한 데이터 값이 실제 시험편의 두께와 거의 일치하였고, UT 장비로 측정한 데이터 값도 보온재를 빼고 파이프만 측정한 두께의 값이 실제 두께와 거의 일치한 값이 나온 것을 확인 할 수 있다. 그림 3을 보면, 보온재의 두께에 따라서 제작한 장비(PPLCG)를 이용해서 펄스와전류 기술로 측정해보니 그래프를 보면 x축에 따라 y축의 두께에 따라 달라지는 값들을 확인할 수 있다. 시험편의 두께에 따른 여러 번의 측정한 결과로 최소자승법을 이용해서 나타낸 그래프이다. x축에 초음파 두께이고 y축은 펄스와전류 측정값이다. 그래프를 보면 펄스와전류로 측정한 데이터와 초음파 탐상 검사로 측정한 결과를 보면 실제 시험편의 두께에 대한 변화에 따라 두께 데이터도 달라지는 것을 확인해 볼 수 있다. 그래프를 보면 두께에 따라서 결과 값이 약간의 오차가 보이나, 대부분의 경향은 거의 일치한다. 시험편의 두께 값에 따라서 MATLAB을 이용하여 펄스와전류 신호처리를 위해서 계단 단차의 다중분류를 위해서 SVM으로 분석하여 직접 Coding하여서 두께에 따라서 두께에 따른 다중분류를 확인해 보았다.

3. 고찰 및 결론

두꺼운 보온재로 덮여있는 시험편 배관에 펄스와전류 기술 장비와 초음파 탐상 검사 장비로 실제 두께 변화에 대해서 측정하였다. 본 연구를 통해서 보면 두께 그래프에 따르면, PEC의 기술은 이미 상용화가 된 UT의 기술과 거의 두께 데이터 값이 경향이 거의 일치하게 나오고, 실제 시험편과 비교를 해보면, 정확도와 신뢰도도 높게 평가된다. 결과적으로 강력한 펄스 자기장이 시험편에 인가되고 이에 따라서 펄스와전류를 유도하게 된다. PEC의 기술이 실제 현장에서도 적용 가능할 것으로 보여 진다. 이처럼 펄스와전류는 기존의 와전류의 한계점을 보완할 수 있는 기술로 각광받고 있다. 펄스와전류 기술이 더 세밀하고 정확도 또한 높여서 PEC의 성능을 한 단계 더 향상시키기 위해서는 다양한 데이터베이스의 확보와 신호처리 기술을 보완하여서 개발할 필요가 있다고 본다.

4. 참고문헌

[1] R.A. Smith, G.R. Hugo, Proc. 5th Joint NASA/FAA/DoD Aging Aircraft Conference (2002)

[2] S. Winnik, Corrosion-under-insulation (CUI) guidelines, European Federation of Corrosion Publications No. 55, Woodhead Publishing Limited (2008)

[3] G. Dobmann, R. Becker, M. Disque, Welding Research Abroad, 16 (1998).

[4] S. K. Burke and L. R. F. Rose, J. Phys. D: Applied Physics 20, 797 (1987).

Current-induced magnetization change in a ferromanget/$Ge_2Sb_2Te_5$ interface

Sung Jong Kim[1,2*], Tae-Eon Park[2], Oukjae Lee[2], Suyoun Lee[3] and Hyun Cheol Koo[1,2]
[1]KU-KIST Graduate School of Converging Science and Technology, Korea University, Korea
[2]Center for Spintronics, Korea Institute of Science and Technology, Korea
[3]Center for Electronic Materials, Korea, Institute of Science and Technology, Korea

Spin-orbit coupling is one of the major concerns because it can be utilized for switching the magnetization of the ferromagnetic cells. The phase-change material is good candidate for generating spin current because it has a strong spin-orbit coupling. In addition, this material has special electrical and magnetic characteristics as a function of the crystallinity. For example, depending on annealing temperature, the various phases of amorphous, cubic (190 ℃), and hexagonal (400 ℃) structures are observed in a $Ge_2Sb_2Te_5$ film.

To observe the current-induced magnetization change of the ferromagnet, we utilized anisotropic magnetoresistance (AMR) which is determined by the vector alignment between the magnetization direction and the bias current. The device consists of permalloy (30 nm)/$Ge_2Sb_2Te_5$ (100 nm) hybrid structure and the lateral dimension is 8 μm by 3 μm. A $Ge_2Sb_2Te_5$ channel has a strong spin Hall effect and subsequently spin current is injected to the permalloy layer. As shown in Figure 1, the channel resistance is measured with a rotational magnetic field of 2 T in the plane which is large enough to saturate the permalloy patterns.

The charge current induces a spin current which changes the magnetic anisotropy and switching process of the ferromagnetic layer. The orientation of induced spin is transverse direction of the current and this spin current increases the magnetic anisotropy of the ferromagnet along the transverse direction at the interface. This induced anisotropy increases the anisotropic magnetoresistance of the ferromagnetic pattern. Furthermore, the magnitude of spin current is a function of crystallinity so at room temperature the AMR enhancement of amorphous, cubic and hexagonal channels show 3.56%, 6.02% and 8.97%, respectively.

These results provide an efficient way for manipulating magnetic anisotropy and magnetization switching process. We also demonstrate the channel crystallinity dependence of spin Hall effect and anisotropic magnetoresistance in a ferromagnet/$Ge_2Sb_2Te_5$ interface.

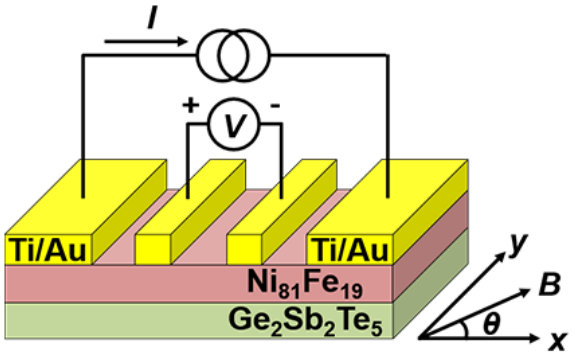

Fig. 1. Device structure and AMR measurement geometry.

Electrical transport along the surface of InAs nanowire

Jeehoon Jeon[1,2*], Taeyueb Kim[1], Sangsu Kim[1], Sungjung Joo[3], Jae Cheol Shin[4], Hyun Cheol Koo[2,5], Jinki Hong[1]

[1]Department of Applied Physics, Korea University, Sejong, 30019, Korea
[2]Spin Convergence Research Center, Korea Institute of Science and Technology, Seoul, 02792, Korea
[3]Center of Electricity and Magnetism, Korea Research Institute of Standards and Science, Daejeon, 34113, Korea
[4]Department of Physics, Yeungnam University, Gyeongsan 38541, Korea
[5]KU-KIST Graduate School of Converging Science and Technology, Korea University, Seoul, 02792, Korea

The controlled generation, manipulation and detection of spin-polarized currents in semiconductor is an important issue in spintronic devices [1]. The great variety of spin related techniques have been demonstrated so far. All of them, however, make use of the classical electromagnetic force or torque acting locally on the magnetic moment associated with the spin.

Semiconductor nanowires have attracted high interest because they offer the study of fundamental quantum effect in electron and spin transport of nanostructure. In addition, these semiconductor nanowires has occurred a surface accumulation due to the Fermi level pinning in the conduction band. The two-dimensional electron gas (2DEG) have formed at the surface. In the case of InAs nanowire, it is known that the electrons in the accumulation layer are also subject to the impact of a strong spin orbit coupling. [2], [3] Rashba effect induced by spin orbit coupling is of relevance for spin electronic devices since it can be employed for gate controlled spin manipulation. [4], [5]

In this work, we study the control of the geometric phase of an electron spin in InAs nanowire using purely quantum-mechanical and nonlocal method by adopting wave interference effect. The principal mechanism of the proposed spin geometric phase contains Aharonov-Bohm (AB) and Aharonov-Casher (AC) phase. AB effect relies on the electron's charge under magnetic field while AC effect comes from electron's magnetic moment with electric field. The Rashba spin-orbit interaction is responsible for AC effect in our device and provides the geometric phase factor of a spin.

Here, we show AB and AC oscillation induced by the magnetic field and the gate voltage in InAs nanowire, providing transport evidence of the surface state in one-dimensional non-magnetic nanowire. Moreover, the quantum transport can be modulated by tuning the Fermi level using a gate voltage, enabling a deeper understanding of the rich physics residing in III-V semiconductor nanowire.

References

[1] Mikio Eto, Tetsuya Hayashi and Yuji Kurotani, J. Phys. Soc. Jpn. 74, 7, 1934 (2005)
[2] S. Estevez Hernández et al., Phys. Rev. B 82, 235303 (2010)
[3] Ch. Blomers et al., Nano Lett. 11, 3550 (2011)
[4] S. Datta and B. Das, Appl. Phys. Lett. 56, 665 (1990)
[5] Koo H. C. et al., Science 325, 1515-1518 (2009).

$Ta_{1-x}W_x$/CoFeB/MgO 구조의 수직자기이방성과 스핀궤도토크

차인호*, 김태현, 김용진, 김규원, 김영근
고려대학교 공과대학 신소재공학과

1. 서론

최근 스핀트로닉스(spintronics)와 스핀오비트로닉스(spin-orbitronics) 분야에서는 스핀궤도결합(spin-orbit coupling)에 의해 발생하는 스핀궤도토크(spin-orbit torque)에 관한 연구가 활발히 진행되고 있다. 비자성중금속/자성체 구조에서 전하전류가 비자성중금속의 면 방향으로 흐를 때 스핀전류가 비자성중금속의 수직방향으로 발생하게 된다. 이때 발생한 스핀전류는 자성체의 자화방향을 반전 시킬 수 있으며 이 방식은 기존의 스핀전달토크 방식보다 더 빠른 속도로 자화 방향을 반전 시킬 수 있어 많은 연구가 진행되고 있다. 최근에는 비자성중금속층을 단일 금속이 아닌 Pt/Au, Ta/Pt, Ta/W 와 같은 이중층 또는 W_xHf_{1-x}, $Pd_{1-x}Pt_x$ 와 같은 합금층으로 사용하여 스핀궤도토크를 측정하는 연구결과들이 발표되고 있다. 본 연구에서는 TaW 합금을 비자성중금속층으로 사용하여 TaW 합금의 조성에 따른 수직자기이방성과 스핀궤도토크 변화를 관찰하였다.

2. 실험방법과 결과

모든 시편은 초고진공 마그네트론 스퍼터링 시스템으로 증착하였으며 스퍼터링 시스템의 초기진공도는 5x10-9 Torr이다. 증착 후 고진공 열처리 시스템에서 6 kOe의 자기장 하에서 1시간동안 300도 열처리를 진행하였다. 샘플의 자성특성은 진동시료자력계로 측정하였으며 노광공정으로 소자를 만들어 하모닉스 시스템과 프로브스테이션으로 전기적 특성을 평가하였다.

3. 고찰

$Ta_{1-x}W_x$/CoFeB/MgO 구조는 W의 조성에 상관없이 열처리 후 수직자기이방성이 발현되었으며 유효수직자기이방성에너지는 W의 조성이 작은 부분과 W의 조성이 큰 부분에서 서로 다른 경향성을 보이고 있다. 하모닉스 시스템으로 측정한 damping-like torque efficiency (ζ_{DLT})는 W의 조성에 따라 변하였으며 W의 조성이 작은 부분과 W의 조성이 큰 부분이 서로 확연한 차이를 보였다. 이러한 변화의 경향성은 프로브스테이션에서 전류인가자화반전 실험에서 유사하게 나타나는 것을 확인하였다.

4. 결론

본 연구에서 $Ta_{1-x}W_x$/CoFeB/MgO 구조에서 W의 조성에 따른 수직자기이방성과 스핀궤도토크의 변화를 관찰하였다. 단일 중금속이 아닌 합금을 이용할 경우 합금의 조성비를 조절하여 수직자기이방성과 스핀궤도토크 조절할 수 있는 것을 확인하였다.

5. 참고문헌

[1] Y. Chen, Q. Zhang, J. Jia, Y. Zheng, Y. Wang, X. Fan, and J. Cao, Appl. Phys. Lett. 112, 232402 (2018)
[2] K. Fritz, S. Wimmer, H. Ebert, and M. Meinert, Phys. Rev. B 98, 094433 (2018)

Variation of Interfacial Structure and Chemistry at Pt/Fe_3O_4 interfaces

Thi Nga Do[1,2*], Thi Kim Hang Pham[1,2], Tae Hee Kim[1,2†]

[1]Center for Quantum Nanoscience, Institute for Basic Science, Ewha Womans University, Seoul, 120-750, Korea

[2]Department of Physics, Ewha Womans University, Seoul, 120-750, Korea

In this work, we investigated the correlation of electrical characteristics with interface chemistry and structures in Pt/Fe_3O_4 hybrid structures. Using different growth conditions, the different levels of surface/interface roughness ranging from 0.4 to 1.2 nm were provided. The chemical variation was introduced between Fe_3O_4 and Pt layers by inserting a 2-nm-thick Al_2O_3, MgO, and SiO_2 thin film. The Fe_3O_4 films were prepared by oxide-MBE technique under different deposition parameters on substrate and substrate temperature, and then followed by vacuum annealing. We report magnetoresistance (MR) behaviors on 3-nm-thick Pt Hall bars. Based on the results of resistivity versus temperature measurements of Pt, we clearly observed the impact of the interface on the change of the magnetoelectric effect of Fe_3O_4 (T_V = 125 K) [1,2]. The careful analysis of the surface properties of Fe_3O_4 was also performed using AFM and TEM. As the interface roughness increases, we observed a significant enhancement of spin-mixing conductance that is extracted from the SMR effect measured at low temperature (77 K lower than the Verway transition temperature of magnetite), and the MR effect persists even in the hybrid structure with a thin interlayer.

Our results suggest that bilayer systems consisting of a non-magnetic noble metal deposited on a magnetic film can be used as a probe to explore the complex magnetic properties of magnetic hybrid structures, paving the way for a better and consistent understanding of spin Hall magnetoresistance behaviors in magnetic hybrid structures to develop highly effective spintronic devices.

References

[1] Verwey EJW. Electronic Conduction of Magnetite (Fe_3O_4) and its Transition Point at Low Temperatures. Nature. 1939;144:327. doi: 10.1038/144327b0.

[2] Phase DM, et al. Raman study across Verwey transition of epitaxial Fe_3O_4 thin films on MgO (100) substrate grown by pulsed laser deposition. Journal of Applied Physics. 2006;100:123703. doi: 10.1063/1.2403849.

Fluorophosphates $Na_2Fe_{0.9}Mn_{0.1}PO_4F$ 양극물질의 결정구조 및 자기적 특성

서재연[1*], 박승영[2], 김철성[1]
[1]국민대학교 물리학과
[2]한국기초과학지원연구원 스핀공학물리연구팀

1. 서 론

$NaFePO_4$는 친환경적이며 저비용이라는 상업적 이점을 지닌 전기 화학적 성능과 열적 안정성을 가지고 있으나 낮은 전도성과 에너지밀도를 지니고 있다.[1] 이를 해결하기 위하여 transition metal 물질을 치환하여 Fe 물질보다 산화 환원 전위가 높은 Mn 물질을 치환하고 이온전도도와 화학적 성능의 개선을 위해 Fluorine 물질을 첨가하여 그 특성을 향상시키고자 하는 많은 연구가 이루어지고 있다.[2] 본 연구 에서는 $Na_2Fe_{0.9}Mn_{0.1}PO_4F$ 양극물질의 저온에서 스핀 궤도 결합에 의해 발현되는 특이한 자기적 성질을 연구하고자 한다.

2. 실험방법

Maricite 구조를 가지는 $NaFePO_4$ 양극물질에 Mn물질을 치환하여 $NaFe_{0.9}Mn_{0.1}PO_4$ 물질을 ball mill법으로 제조하였다. 출발 물질인 $Na(CH_3COO)$, $FeC_2O_4{\cdot}2H_2O$, $MnCO_3$ 및 $NH_4H_2PO_4$의 1: 0.9: 0.1: 1의 비율로 혼합하여 Ar 분위기에서 350 ℃에서 3시간 동안 하소시켰다. 하소된 시료를 pellet으로 제작 후 Ar 분위기에서 675 ℃에서 10시간 동안 소결시켰다. 그 후, 제조된 $NaFe_{0.9}Mn_{0.1}PO_4$를 적절한 양의 NaF와 혼합하고, pellet으로 제작 후, Ar 분위기에서 625 ℃에서 6시간 동안 소결하였다. Cu-$K\alpha$ 선에 의한 X-선 회절장치(XRD)를 통하여 시료의 결정학적 특성을 측정하였으며, Rietveld 분석법을 이용한 full prof 프로그램을 통해 회절 pattern을 분석하였다. 저온구간에서 초전도양자간섭장치(SQUID) 및 뫼스바우어 분광기(Mössbauer spectroscopy)를 통하여 본 양극물질의 자기적 특성을 확인하였다.

3. 실험결과 및 고찰

$Na_2Fe_{0.9}Mn_{0.1}PO_4F$ 양극물질을 X-선 회절 실험한 결과, 그림 1과 같이 orthorhombic 구조의 *Pbcn* 공간 그룹을 갖는 것으로 확인되었으며, 격자상수는 a_0 = 6.866 Å, b_0 = 8.988 Å, c_0 = 5.047 Å, and V = 311.544 Å^{3}으로 분석되었다. 1.8 K에서 295 K까지 초전도양자간섭 실험을 측정한 결과, 그림 2와 같이 해당물질의 닐 온도는 2.5 K로 결정되었으며, 닐 온도 이하에서는 반강자성체 거동을 보이는 것으로 확인되었다. 4.2 K에서 295 K까지의 뫼스바우어 분광실험을 측정한 결과는, 4.2 K에서 전기 4중극자 분열치(Electric quadrupole splitting)는 2.94 mm/s, 이성질체 이동치(isomer shift)는 1.25 mm/s로 확인되었다. 모든 온도 구간에서 doublet 형태의 흡수선으로 나타났으며, Fe 이온은 $FeO_4F_2(MnO_4F_2)$ 팔면체 위치에서 Fe^{2+}상태를 가지는 비대칭 구조임을 확인하였다.

4. 참고문헌

[1] T. Boyadzhieva, V. Koleva and R. Stoyanova, Phys. Chem. Chem. Phys. **19**, 12730 (2017).
[2] X. Wu, J. Zheng, Z. Gong and Y. Yang, J. Mater. Chem. **21**, 18630 (2011)

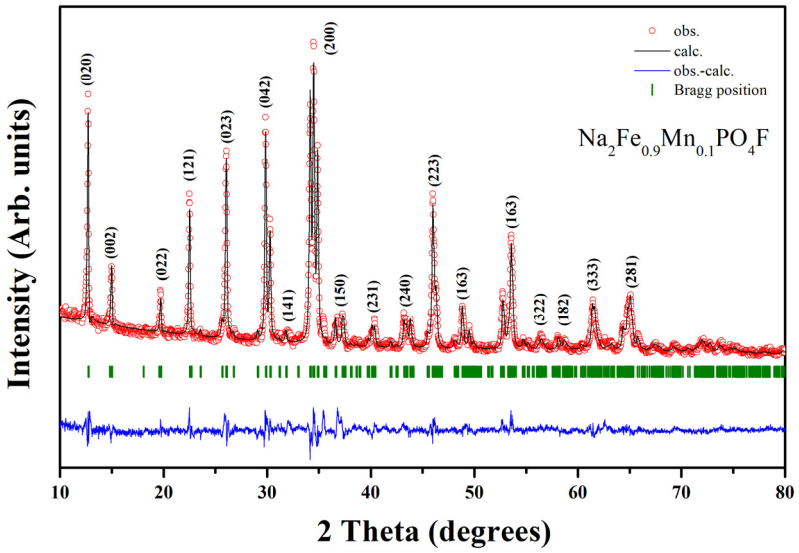

Fig. 1. Refined x-ray diffraction pattern of $Na_2Fe_{0.9}Mn_{0.1}PO_4F$ at room temperature.

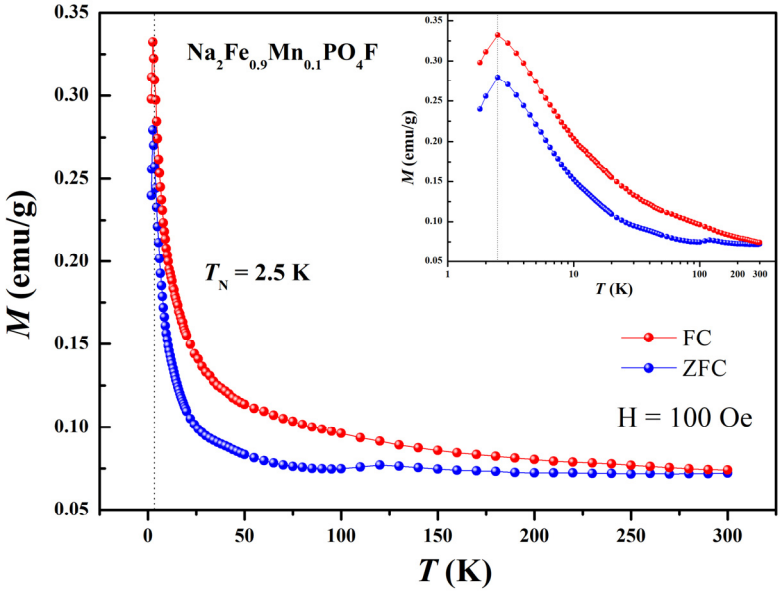

Fig. 2. Temperature dependences of the ZFC and the FC magnetizations for $Na_2Fe_{0.9}Mn_{0.1}PO_4F$ at an applied field of 100 Oe.

Li 이온의 결핍에 따른 $Li_xFe_{0.95}Mg_{0.05}PO_4$ 양극물질의 뫼스바우어 분광학적 연구

최현경*, 김철성
국민대학교 물리학과

1. 서 론

이차전지 산업의 발달에 따른 고효율 특성의 양극물질 소재 연구가 활발히 진행되고 있으며, 이들 소재는 PO_4 구조 단위에 기초한 polyanion framework 화합물로서 충방전 효율을 향상시키기 위하여 화합물에 전이금속을 치환한 연구가 수행되고 있다. 본 연구에서는 리튬 결핍에 따른 $Li_xFe_{0.95}Mg_{0.05}PO_4$ 양극물질을 제조하여 뫼스바우어 분광 실험을 이용하여 자기적 특성을 연구하였다.

2. 실험방법

올리빈 구조의 $LiFe_{0.95}Mg_{0.05}PO_4$ 양극물질은 직접합성법(Solid-state reaction method)을 사용하여 제조하였다. 출발물질로는 Li_2CO_3, $FeC_2O_4{\cdot}2H_2O$, $NH_4H_2PO_4$, 그리고 $(CH_3COO)_2Mg{\cdot}4H_2O$를 이용하였으며, 당량비에 맞게 그라인딩 하였다. 제조된 혼합물을 350 ℃에서 3시간 동안 하소였으며, 하소된 시료를 다시 그라인딩 한 후에 700 ℃에서 10시간 동안 소결하였고, 모든 열처리는 Ar 분위기에서 진행하였다. 최종적으로 얻어진 $LiFe_{0.95}Mg_{0.05}PO_4$ 양극물질의 리튬 이온의 결핍을 유도하기 위하여 화학적 산화방법(Chemical deintercalation method)을 이용하여 $Fe_{0.95}Mg_{0.05}PO_4$ 양극물질을 제조하였다. 합성된 $LiFe_{0.95}Mg_{0.05}PO_4$과 NO_2BF_4 산화제를 30 ml의 acetonitrile 용액에 넣은 후 상온에서 24 h동안 반응시켰다. 합성된 $Li_xFe_{0.95}Mg_{0.05}PO_4$ 양극물질의 결정학적 및 자기적 특성을 연구하기 위하여, X-선 회절기 (XRD), 진동시료형 자화율측정기 (VSM), 그리고 뫼스바우어 분광기를 이용하여 실험을 수행하였다.

3. 실험결과 및 고찰

$Li_xFe_{0.95}Mg_{0.05}PO_4$ 양극물질의 결정구조는 *Pnma* 공간군을 갖는 orthorhombic 구조로 확인되었으며, $LiFe_{0.95}Mg_{0.05}PO_4$의 격자상수는 a_0 = 10.3103 Å, b_0 = 5.9997 Å, c_0 = 4.6914 Å, $Fe_{0.95}Mg_{0.05}PO_4$의 격자상수는 a_0 = 9.8295 Å, b_0 = 5.7949 Å, c_0 = 4.7810 Å로 분석되었다. VSM 실험을 통하여 온도에 따른 자화율 곡선을 측정한 결과, $LiFe_{0.95}Mg_{0.05}PO_4$의 닐 온도는 49.5 K, 리튬이 결핍된 $Fe_{0.95}Mg_{0.05}PO_4$의 닐 온도는 106 K로 확인되었으며 두 시료 모두 닐 온도 아래에서 antiferromagnetic 거동을 보였다. 또한, 미시적인 자기 특성을 확인하기 위하여 온도에 따른 뫼스바우어 분광 실험을 실시하였으며, 닐 온도 아래에서는 비대칭적인 8-line 형태의 스펙트럼을 확인하였다. 합성된 $Li_xFe_{0.95}Mg_{0.05}PO_4$ 양극물질의 경우, Li_xFePO_4보다 감소된 antiferromagnetic 거동을 보였는데, 이는 Fe—O—Fe link 보다 ㅁ상대적으로 약한 Fe—O-Mg link에 의한 초교환 상호작용 때문으로 해석될 수 있다.

4. 참고문헌

[1] S. Yaroslavtsev, S. Novikova, V. Rusakov, N. Vostrov, T. Kulova, A. Skundin, A. Yaroslavtsev, Solid State Ionics **317**, 149-155, (2018).

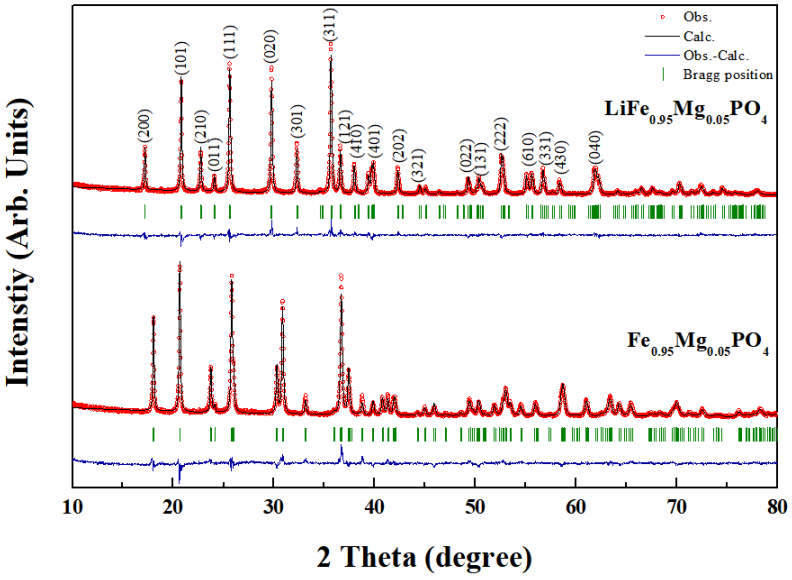

Fig. 1. XRD patterns of $Li_xFe_{0.95}Mg_{0.05}PO_4$ at 295 K.

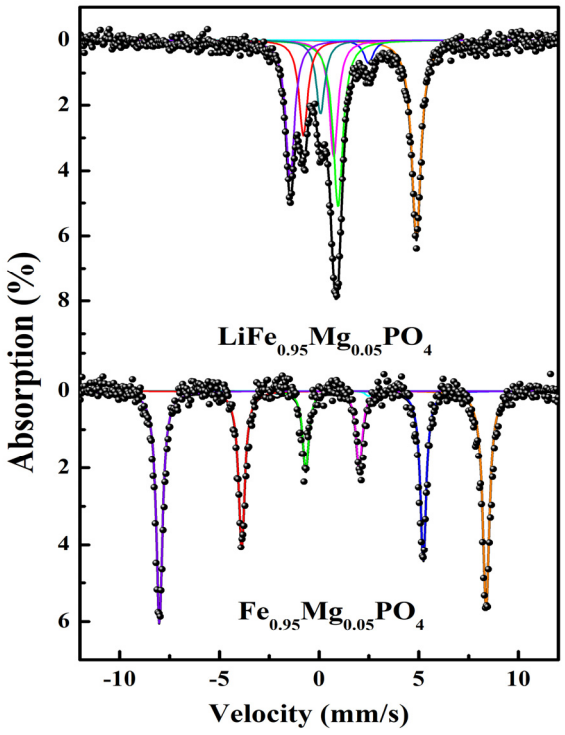

Fig. 2. Mössbauer spectrum of $Li_xFe_{0.95}Mg_{0.05}PO_4$ at 4.2 K.

Artifact-free optical spin-orbit torque magnetometry

김주성[1], 박용근[1,2], 황현석[1], 박정현[1*], 민병철[2], 최석봉[1]
[1]서울대학교 물리학부
[2]한국과학기술연구원

Current control of magnetization via the spin-orbit torque (SOT) has opened a new horizon for magnetic memory devices. SOT causes magnetization switching and domain wall motion that enable read/write operations in spintronic memory devices. For more efficient operation of such spintronic devices and further investigation of underlying SOT mechanisms, a precise and artifact-free SOT quantification method is required. In this circumstance, however, planar Hall effect (PHE) and anomalous Nernst effect (ANE) signals complicate SOT analysis in the electrical harmonic measurement method. Our optical setup utilizes photoelastic modulation (PEM) and balanced detection (BD) to measure the polar magneto-optic Kerr effect (pMOKE) signal exclusively. We demonstrate an optical SOT measurement scheme that is free from artifacts such as the optic PHE and optic ANE. We verified the separation of the pMOKE signal in the Pt/Py bilayer sample with sizable optic PHE. Our method with single measurement principle reduces the analysis complexity, and thus, it could help expand the scope of SOT studies.

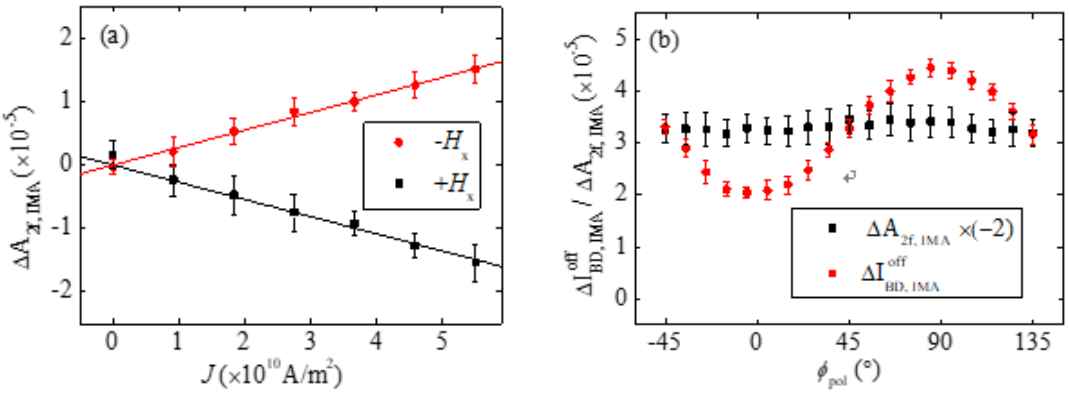

Fig. 1. Linear proportionality of the SOT-induced signal with respect to current density J at mT. Red and black lines are linear fits to the data with zero intercept.

Fig. 2. Comparison of the two SOT-induced signals and with respect to polarization angle at mT. has no dependence whereas has sinusoidal dependence from optic PHE

$Mn_{1+b}Fe_{2-b}O_{4-\delta}$ 나노입자의 구조 및 자기적 특성

Y. J. Choi*, N. Tran, T. L. Phan, B. W. Lee†
Department of Physics and Oxide Research Center, Hankuk University of Foreign Studies,
Yongin 17035, South Korea
†Corresponding author: bwlee@hufs.ac.kr

$Mn_{1+b}Fe_{2-b}O_{4-\delta}$ (MFO) 나노 입자 (NP)를 hydrothermal method로 제조하였다. 시료는 평균 25nm의 균일한 구형 입자들로 구성되었다. XRD 분석 결과, MFO NP는 a = 8.410 Å의 cubic-spinel 구조로 나타났다. MFO NP의 포화 자화 (M_s)는 300 K에서 30.7 emu/g, 15 K에서 40.3 emu/g)로, 다른 발표된 결과에 비해 상당히 낮은 것으로 나타났다. 반면, 무질서 상태의 형성으로 인해 15 K에서 보자력(H_c)은 347 Oe로, 300 K에서의 Hc = 116 Oe보다 3배 크게 나타났다. Energy dispersive X-ray spectroscopy, Raman scattering와 X-ray absorption spectroscopy 분석 결과, MFO NP는 $Mn_{1.12}Fe_{1.88}O_{3.74}$의 mixed spinel ferrite임을 알 수 있었다. 실험적으로 구한 magnetic moment (n_{exp} = 1.66 μ_B/f.u. ≈ 40.3 emu/g)는 계산한 값 (n_{cal} = 3.29 μ_B/f.u.)보다 작게 나타났다. 이는 MFO NP의 canted spin (Yafet-Kittle 모델에 기초, α_{YK} ≈ 36.5 °) 및/또는 자기적으로 dead layer (두께 t ≈ 3.5 nm)에 기인한 것으로 생각된다.

Key words: Manganese ferrites, energy dispersive X-ray spectroscopy X-ray absorption spectroscopy

Fe_3O_4-ZnO 나노입자-나노선 계층구조 복합체의 합성 및 특성 분석

Synthesis and characterization of Fe_3O_4-ZnO hierarchical nanospike

Min Jun Ko[1*], Bum Chul Park[1,2], Sang Won Byun[1] and Young Keun Kim[1†]

[1]Department of Materials Science and Engineering, Korea University, Seoul 02841, Korea

[2]Research Institute of Engineering and Technology, Korea University, Seoul 02841, Korea

산화철 나노입자는 고유한 자기적 성질을 바탕으로 이를 이용하는 복합체 연구가 활발히 진행되어 표적약물 전달시스템, 생체 내 이미징, 온열 치료, 생체분자 분리 등 다양한 분야에 응용하는 연구가 활발히 진행되고 있다[1]. 지금까지는 단순 이종 소재를 복합하여 각 소재 고유의 특성을 이용하는 연구가 활발했는데, 최근에는 특정 구조로 형성하여 소재 특성 이외에도 구조체의 형상에서 나타나는 효과를 조절하는 방향으로 연구가 진행되고 있다[2]. 본 연구에서는 스파이크형 산화철 나노입자-산화아연 나노선 계층구조를 합성하여 물리적 특성, 구조를 분석하였다. 먼저 단계적 화학반응을 이용하여 산화철 나노입자를 작은 크기의 산화아연 나노결정들으로 감싼 후, 이를 씨앗층으로 이용하여 산화아연 나노선을 성장시켰다[3]. 주사전자현미경(Scanning Electron Microscope), 투과전자현미경(Transmission Electron Microscope), 엑스선회절분석(X-ray diffraction, XRD)을 이용하여 계층구조 복합체의 형상 및 구조를 확인하였다. 또한 수열합성 이전 산화철-산화아연 콜로이달 나노결정 클러스터의 자성 및 광학 특성을 분석하였다. 이종 콜로이달 나노결정 클러스터는 내부에는 산화철 나노결정이, 외부에는 산화아연 나노결정이 뭉쳐있는 형태임을 확인하였고, 산화아연 클러스터가 다결정 또는 비정질 형태로 존재함을 분석하였다. 또한 기반이 되는 산화철-산화아연 나노결정 클러스터의 자기적, 광학적 특성을 진동시편자력계와 형광분광계를 이용하여 분석하였다.

참고문헌

[1] N. H. Cho et al., Nat. Nanotechnol., 6, p. 675 (2011)

[2] M. Fang et al., Adv. Energy Mater., 7, 1700559 (2017)

[3] P. Sharma et al., Nanoscale, 11, 4591 (2019)

Structural, Magnetic and Electrical Properties of $MnFe_2O_4$-$BiFeO_3$ Nanocomposite

Inna Yusnila Khairani*, Anindityo Nugra Arifiadi, Biswanath Bhoi, Trivoramai Jiralerspong, Jaehyeok Lee, Jaegun Sim and Sang-Koog Kim†

National Creative Research Initiative Center for Spin Dynamics and Spin-Wave Devices,
Nanospinics Laboratory, Research Institute of Advanced Materials,
Department of Materials Science and Engineering, Seoul National University, Seoul 151-744, Republic of Korea
†Correspondence and requests for materials should be addressed to S.-K. K (sangkoog@snu.ac.kr).

Device miniaturization, making the device smaller without reducing the performance, is one of the objective of every device manufacturer. Nevertheless, shrinking the size of the device results in adverse impact of the magnetic component itself, since coils to produce the magnetic field are highly dependent on the diameter of the coils. When the coils are made smaller, it cannot withstand the large current flow due to the resistance of the coils, and therefore excess heat might accumulate and set damage to the device. To overcome this problem, magnetoelectric multiferroic materials are a good candidate. This material shows a coupling behavior of magnetic properties and electrical properties, therefore, we can simply change the magnetization direction of a material by applying electrical field into it, and vice versa. The use of coils becomes insignificant.

There are several known magnetoelectric multiferroics, however, most materials work at very low temperature[1]. Only bismuth ferrite, $BiFeO_3$, that retains the ability of magnetoelectric coupling at room temperature. But since the magnetic properties of $BiFeO_3$ is too low, several approaches have been done to increase the magnetic property of $BiFeO_3$, including by making the material in nanosize[3], doping, and making composite of two different phases[4], [5]. By making composite of $BiFeO_3$ with another material with high magnetization, there will be overall enhancement of ferroelectricity, magnetism, and magnetoelectric coupling[2].

Spinel ferrite is one of the candidate to enhance the magnetization of $BiFeO_3$ due to the high magnetization value of this group. One of the potential candidate for the composite is $MnFe_2O_4$. This material shows the highest magnetization in the group and small coercivity, which are valuable to make magnetoelectric coupling in a composite.

In this work, we presented the fabrication of $MnFe_2O_4$ and $BiFeO_3$ nanoparticles through chemical synthesis method of coprecipitation and sol-gel method, respectively, and the fabrication of nanocomposite through mechanosynthesis process by pressing and sintering at low temperature. Compared to the other published work on the fabrication of composite $MnFe_2O_4$ and $BiFeO_3$[6], our FESEM results shows less pores with qualitatively better densification of the composite pellet. WHen less pores are form, there is an increase of interfacial interaction, and therefore we expect an enhanced coupling of magnetoelectric multiferroic properties. Raman spectroscopy also shows no changes of phases after the sintering by compared the spectra of sintered composite to the individual $MnFe_2O_4$ and $BiFeO_3$. Moreover, the reuslt was achieved by sintering at a very low temperature of 400°C in both ambient and inert atmosphere, compared to the published work with sintering temperature of 1000°C. Additionally, the $BiFeO_3$ was fabricated as nanoparticles, therefore it shows better magnetic properties compared to the bulk $BiFeO_3$ which is antiferromagnetic in nature. From this result, it is expected to see the enhancement of magnetic properties of $BiFeO_3$ and $MnFe_2O_4$ composite, along with higher magnetoelectric coupling.

참고문헌

[1] W. Eerenstein, N. D. Mathur, and J. F. Scott, “Multiferroic and magnetoelectric materials,” Nature, vol. 442, no. 7104, pp. 759-765, 2006.

[2] J. Wu, Z. Fan, D. Xiao, J. Zhu, and J. Wang, “Multiferroic bismuth ferrite-based materials for multifunctional applications: Ceramic bulks, thin films and nanostructures,” Prog. Mater. Sci., vol. 84, pp. 335-402, 2016.

[3] T. J. Park, G. C. Papaefthymiou, A. J. Viescas, A. R. Moodenbaugh, and S. S. Wong, “Size-dependent magnetic properties of single-crystalline multiferroic $BiFeO_3$ nanoparticles,” Nano Lett., vol. 7, no. 3, pp. 766-772, 2007.

[4] X. M. Liu, S. Y. Fu, and C. J. Huang, “Synthesis and magnetic characterization of novel $CoFe_2O_4$-$BiFeO_3$ nanocomposites,” Mater. Sci. Eng. B Solid-State Mater. Adv. Technol., vol. 121, no. 3, pp. 255-260, 2005.

[5] S. Kuila et al., “Study of magnetization and magnetoelectricity in $CoFe_2O_4$/$BiFeO_3$core-shell composites,” J. Appl. Phys., vol. 123, no. 6, 2018.

[6] A. Kumar and K. L. Yadav, “Synthesis and characterization of $MnFe_2O_4$ $BiFeO_3$ multiferroic composites,” Phys. B Condens. Matter, vol. 406, no. 9, pp. 1763-1766, 2011.

협착이 있는 마이크로채널 내에서 혈류흐름에 대한 펄스자기장의 영향

목진원*, 한승현, 방승환, 이현숙
상지대학교 보건과학대학 한방의료공학과, 강원 원주시, 26339

1. 서론

오늘날 고령화 사회에 접어들면서 혈액순환장애로 인한 질병 또한 증가하고 있어 혈액순환관리 필요성이 높아지고 있다. 다양한 병리적 현상과 생리학적 요인에 의해 모세혈관에 협착이 생기면 혈액순환장애로 인한 고혈압, 당뇨병 등 심혈관질환이 발생한다. 또한 혈류역학에서 혈류속도와 적혈구의 변형성은 혈액순환에 중요한 요인으로 알려져 있다. 이러한 혈액순환 치료에 대하여 비침습적인 치료법이 고안되고 있는데, 그 중 펄스자기장 자극이 혈류속도 개선에 긍정적인 영향을 미친다고 보고되었다[1]. 따라서 본 연구에서는 실제혈관과 유사한 모사혈관모델을 PDMS를 사용하여 제작하여 펄스자기장 자극 유무에 따른 혈류유동특성을 연구하고자 한다. 특히 모사혈관모델에서 협착 구간을 통과한 후 혈류속도 개선에 대한 자기장의 효과와 적혈구 변형성 등을 관찰하고자 한다.

2. 실험방법과 결과

직경이 15um인 직선 모양의 마이크로채널과 15um에서 10um로 점차 좁혀지다가 다시 15um로 넓어지는 협착 모양의 길이 200um인 마이크로채널을 MEMS 공정 기술과 PDMS를 이용하여 제작한다. 실험을 위해 필요한 혈액은 IRB면제 심의 후 강원혈액원에서 공급받아 적혈구만을 추출하기 위해 3 ml의 혈액을 원심분리(3000rpm, 10분)를 2회함으로써 혈장과 부유물을 제거하였다. 단일 적혈구의 관측을 용이하게 하기 위해 PBS를 사용하여 HTC 5%로 맞추었다. 실린지 펌프와 현미경을 이용하여 혈액을 1ul/min의 유량으로 마이크로채널에 주입하여 0.1T세기의 펄스자기장을 3분간 인가 전후의 혈류 속도 변화와 변형성을 관찰하였다. 직선 형태의 마이크로채널에서의 혈류속도는 PMF 자극 전 761um/s, PMF자극 후 1060um/s로 1.4배 증가하였다. 협착이 있는 채널내에서 협착통과전과 후의 혈류속도를 측정하였는데, 각각 904.2um/s와 937.7um/s로 협착을 통과한 후 혈류 속도가 3.7% 증가하였다. PMF자극 후 협착 통과 전후의 혈류속도는 각각 1332.4um/s와 1422.6um/s로 협착 통과한 후 6.7% 증가하여 자기장 자극전보다 자극 후의 혈류속도가 빨라지는 것이 관측되었다. 또한 적혈구 변형성에 자기장의 효과를 알아보기 위해 타원형 형태로 변형된 적혈구의 장축과 단축을 측정하여EI지수를 계산하였다[2]. 협착전과 협착구간은 각각 PMF자극 전에는 0.05, 0.02로 변화 하였고, PMF자극 후에는 0.18, 0.47로 변화 하였다

3. 고찰

많은 선행 연구들이 혈액의 유변학적 관점에서 혈액유동에 대한 특성을 보고하고 있으나, 협착이 있는 마이크로채널 내에서의 자기장의 효과는 현재까지 보고되어 있지 않다. 그러므로 본 연구에서는 비교적 간단한 모사혈관모델을 사용하여 펄스자기장 전후의 혈류속도를 관측하였다. 하지만 실제 인체의 매우 복잡한 모세혈관을 모사하기 위해서는 다양한 형태의 마이크로채널을 제작할 필요가 있다. 또한 적혈구 변형성 측정 시 현미경시야에서 2차원으로만 장축과 단축을 측정할 수밖에 없는데, 추후 3차원적으로 정확한 변형성을 측정할 수 있는 방법을 모색하여야 한다. 본 연구방법을 통해 자기장이 다양한 질병치료의 도구로 사용되기 위해서는 혈

액의 신장흐름률 변화에 따른 변형성과 자기장세기와 주파수 변화에 따른 혈액유동에 대해 자세한 연구가 필요할 것으로 사료된다.

4. 결론

본 연구에서는 실제혈관과 유사하게 직선과 협착이 있는 모사혈관모델을 PDMS를 사용하여 제작하여 펄스자기장 자극 유무에 따른 혈류유동특성을 연구하였다. 직선 채널에서뿐만 아니라 협착부분을 포함하는 마이크로채널 내에서 펄스자기장 자극으로 인한 혈류흐름의 개선 효과를 관찰하였다. 또한 적혈구가 협착부위의 채널을 통과할 때 적혈구 변형성을 관측하였고, 펄스자기장이 자극 전에 비해 변형성이 개선되는 것을 확인하였다. 펄스자기장의 인가조건을 최적화 한다면 고혈압, 당뇨병 및 동맥경화 등 모세혈관이 막히면서 병증을 유발하는 심혈관질환 치료에 펄스자기장이 혈액순환 개선의 비침습적 치료법으로 제안될 수 있을 것이라 기대된다.

5. 참고문헌

[1] Y. Jo, H. Ahn, K. Shin, and H. Lee, IEEE Trans. magn, **99,** 1-3 (2018).

[2] M. Grau, S. Pauly, J. Ali, K. Walpurgis, M. Thevis, W. Bloch, and F. Suhr, PloS one, **8(2),** e56759 (2013).

BM02

저주파 자극에 따른 자성 홀소자 맥진파형 특성에 관한 연구

강병욱*, 최종구, 이상석
상지대학교 한방의료공학과

1. 서론

본 연구는 “저주파 치료기 라고 하는 의료기기가 사람의 건강에 어떤 영향을 줄 수 있을까?”를 알아보기 위한 것이다. 저주파 자극기로 사람의 질병의 원인이 되는 혈관 상태를 완화 시킬 수 있는지에 대해 알아보기 위한 연구를 진행하였다. 즉, 저주파 자극기로 치료를 하게 되면 사람의 혈관 순환에 대한 질병을 완화 할 수 있게 되는 것을 한방의료기기인 자성 홀소자 맥진기를 사용해서 저주파 자극에 따른 맥진파형을 확인하여 수축기 시간의 변화를 조사하였다. 본 연구실험의 결과를 사람이 보다 건강하게 살아 갈 수 있게 되는 것을 기대해 볼 수 있을 것이다.

2. 실험방법

본 연구에서 사용된 저주파 침전기자극기(GP-302N)는 경피신경 자극기 (Transcutaneous electrical nerve stimulation, TENS)라고 불린다. 그 특징들로서는 250 Hz 미만의 펄스전류를 흐르게 하며, 직접 통증부위에 통하게 하여 자극한다. 그리고 통증부위의 반복적인 수축과 이완은 신경을 안정시키고 혈행을 촉진시켜 통증을 치료한다. 근육의 수축과 이완을 반복시킴으로서 효과를 주어 근육의 수축운동은 쇠약된 신체기능을 강화시키고 지방세포에 작용하여 비만을 치료한다. 전기적 근육자극 (Electrical muscle stimulation, EMS) 운동기도 같은 종류이다.

Fig. 1은 침전기자극기의 실제 실험중 사용 장비와 실습과정을 촬영한 사진이다. 환부에 전류를 흘려 전기자극을 가하는 2인용 기기이며, 스위치 조작을 통해 저주파 파형, 세기, 동작시간, 저주파가 발생되며, 저주파 전류의 주파수 등을 조절기능과 CPU로 제어되는 자동 프로그램 (Auto mode, Manual mode) 기능, Touch 패널 적용과 안전기능 등이 있다.

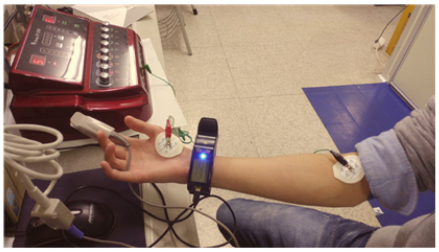

수소음 심경의 두 경혈점
“소해”와 “소부”에 저주파 전기자극

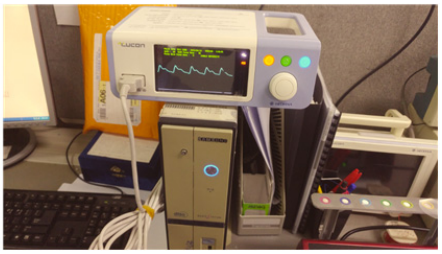

저주파 자극기, 집게형맥진기, PPG

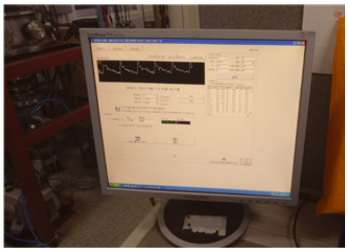

집게형맥진기:
요골동맥 맥진파형분석

<Fig. 1>

실험 방법과 순서는 다음과 같다. ① 먼저 혈압을 측정한다. ② 측정한 것을 기록지에 적는다. ③ 자성홀소자 맥진기로 맥진 파형을 측정한다. ④ 맥진 파형이 나온 그림을 저장한다. ⑤ 저주파 자극기의 전원을 누른다. ⑥ 저주파 자극기의 전극을 경혈점에서 “소해”라는 경혈점에 전극을 부착하고 또 경혈점에서 “소부”라고 부르는 곳에 전극을 또 하나 부착한다. 여기서 “소해”와 “소부”의은 손목과 팔목 부위에 위치는 수소음 심경인 겨드랑이 중앙의 극천혈에서 시작하여 팔뚝 안쪽을 지나 새끼손가락 안쪽 소충혈에 이른다. 이 두 경혈점을 자극

함으로써 심혈관 질환과 상열(위가 뜨겁다-머리/심장/폐는 차가워야 한다), 불면증, 정신질환을 치료한다 ⑦ 맥진기를 왼쪽 손목에 부착하고 광욕적 맥파기를 왼손의 검지에 부착한다. ⑧ 저주파 자극기를 통해서 측정을 하는데 먼저 5분 동안 주파수를 8 Hz로 선택해 측정한다. ⑨ 측정을 하면서 맥진 파형이 정확하게 나온 것을 선택해서 그림파일로 저장한다. ⑩ 주파수를 15 Hz로 맞추고 측정을 하고 마친 가지로 모양이 정확하게 나온 파형을 그림파일로 저장한다. ⑪ 주파수를 30 Hz로 맞추고 측정한 다음 정확하게 나온 파형을 그림파일로 만들어서 저장한다. ⑫ 저주파 자극기로 측정이 끝났으면 저주파 자극기의 전원을 끄고 저주파 자극기의 전극을 때어내고 맥진 파형을 측정한다. ⑬ 측정한 파형을 그림파일을 만들어서 저장한다. ⑭ 마지막으로 팔에 부착한 기기를 때어내고 혈압을 측정하고 측정한 혈압을 기록지에 적고 저장한 파일을 분석해서 새로 파일을 만들어 저장한다. ⑮ 매주 3번 측정 정례화하고 6개월의 70번 이상의 데이터를 확보하여 분석한다.

3. 실험결과 및 토의

먼저 주 3회 4주 동안 임상실험을 행한 20대 건강한 남학생의 경우에는 수축기 혈압의 측정은 오른손과 왼손의 상완 팔 측정 및 분석하였다. 그 이유는 왼손과 오른손 중에 주로 오른손의 혈압이 정확하기 때문에 오른손으로 분석했고 측정 순번 수와 혈압을 Fig. 2(a)에 나타냈다. 저주파 전기 자극 치료 전과 후 차의 수축기 혈압을 분석해본 결과 13개의 데이터 중 12개의 데이터가 저주파 치료 후 혈압이 감소한 데이터임을 알 수 있었다. 저주파 전기자극 치료 전과 후의 모든 수축기 혈압 데이터의 평균혈압 값은 각각 138 mmHg, 132 mmHg이었다. 즉, 7.6%가 수축기 혈압이 온열치료 후가 치료 전보다 줄어들었음을 알 수 있다. 또한 저주파 전기자극 전과 후에 대한 요골동맥의 맥진파형을 집게형 맥진기로 측정하고 그 맥진파형을 분석한 결과에서 주요인자인 수축기 시간인 S.time에 대해 수축기 혈압 데이터 분석과 같은 방법으로 수행한 결과를 Fig. 2(b)에 나타냈다. 저주파 전기 자극주파수는 3가지로 8 Hz, 15 Hz, 30 Hz로 강도세기는 팔뚝의 두 단자인 경혈점 소해와 소부에서 느끼는 자극이 떨림이 안정화되는 최대 10 단계를 택하였다. 그리고 각 주파수별로 5분간 자극시간을 유지하였다. 각 주파수별로 S.time의 차이 분석 결과로는 S.time이 가장 크게 증가한 주파수는 15 Hz이었고, 저주파 자극전보다 평균 107.75 ms에서 평균 1.49 ms이 증가하여 평균 0.84 ms 증가하였다. 따라서 요골동맥의 맥진파형를 활성화하여 혈류를 개선하는 데 알맞은 저주파 전기자극 효과는 주파수가 15 Hz 임을 알 수 있다.

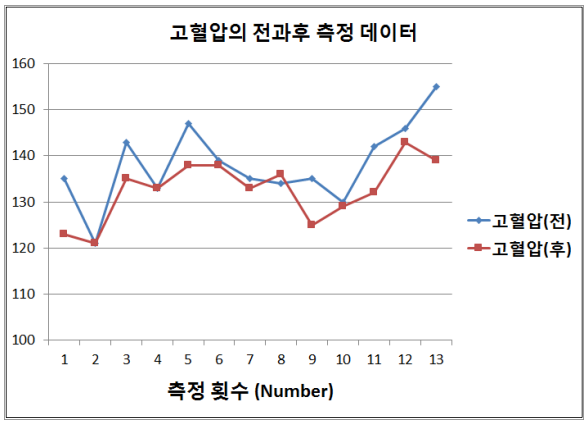

<Fig. 2(a)>

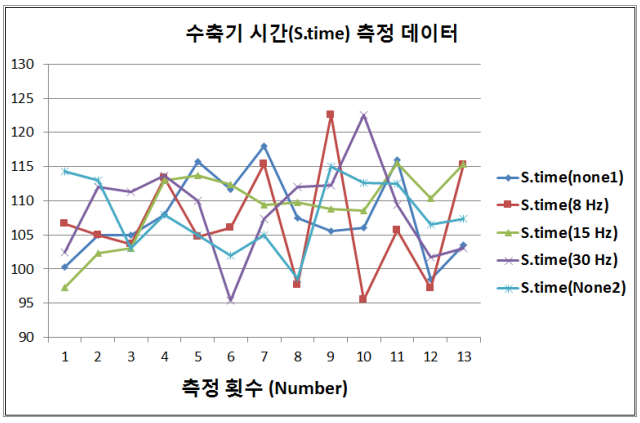

<Fig. 2(b)>

감사의 글

이 연구는 상지대학교의 공학인증 한방의료공학과 심화프로그램 및 캡스톤디자인의 지원을 받아 수행된 연구의 결과이다.

칼만필터를 이용한 자기센서의 노이즈제거

김민석*, 김경원, 신광호
경성대학교 정보통신공학과

2.8인치 LCD모니터, Bluno Nano, 3개의 홀센서를 이용하여서 3축 자기센서를 제작하였다. 제작된 자기센서에 있어서, 잡음제거 용 필터의 성능을 비교하기 위해 실제 측정 데이터에 이동평균필터, LPF, 칼만 필터를 각각 적용한 후 노이즈의 제거 효과를 비교하였다. 이동평균필터는 평균구간을 정하고 최신 센서값을 추가할 때 가장 오래된 센서값을 제거한 후 평균을 구하는 반복 제어문을 이용하였다. LPF필터는 높은 주파수인 잡음을 걸러내고 낮은 주파수만 통과시켜 완만한 신호를 얻기 위해 식 $\overline{x_k} = a\overline{x_{k-1}} + (1-a)x_k \ (a<1)$에서의 이전 추정값 ($\overline{x_{k-1}}$)과 측정값($x_k$)에 적절한 가중치를 부여해 현재의 추정값을 나타내는 방법을 이용하였다. 칼만 필터는 초기값를 선정한 후 식 $\widehat{x_k^-} = A\widehat{x_{k-1}}$을 이용해 시각이 t_k에서 t_{k+1}로 바뀔 때 추정값 예측하고, 추정값의 척도인 오차 공분산 예측한 값을 이용해 다음 단계 칼만 이득을 구하는데 사용하였다. 칼만 이득 계산 단계에서는 칼만 이득 값을 새로 계산해 가중치를 새롭게 조정한 칼만 이득의 가중치로 최종 추정값, 오차공분산을 얻을 수 있다. 이러한 알고리즘들을 반복 적용할 수 있는 프로그램을 C를 이용하여 제작한 후, Atmega328 마이크로컨트롤로와 TI CC2540 BLE칩이 일체화 되어 있는 Bluno Nano에 업로드하여 실행시켰다. 자계 측정 센서는 홀센서를 이용하였고, 필터링 방법을 비교하기 위해서 아날로그 증폭이나 필터링은 사용하지 않았다. 그림 1은 측정된 센서데이터, 이동평균필터적용 데이터, LPF적용 데이터, 칼만필터적용 데이터를 비교하여서 보여주고 있다.

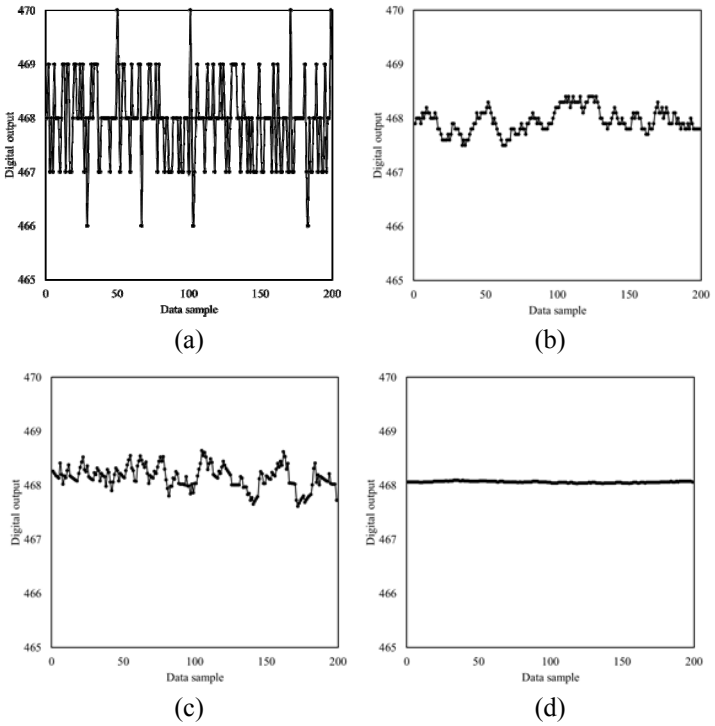

Fig. 1. 센서 출력 데이터 비교. (a)센서출력데이터 (b)이동평균필터적용데이터
(c)LPF적용데이터 (d)칼만필터적용데이터

Low Current sensing Planar Hall Resistance Sensors module for automobile

J. H. Lee*, S. J. Kim, C. G. Kim
Emerging Materials Science, DGIST, Daegu, Republic of South Korea

In modern industry, various types of sensors are actively studied in the industrial and medical fields. In particular, in the industrial and medical fields, studies of magnetic sensors based on magnetic materials are being conducted in a variety of ways. Among these studies, the development of high-resolution sensors is a very important part of signal analysis. Therefore, in this study, we conducted a study on the low current detection module using the PHR (Planar Hall Resistance) [1] sensor, which is a type of magnetic sensor. High resolution low current sensing sensor is manufactured using PHR sensor. The designed PHR sensor is designed to control external magnetic interference and use high resolution to detect current. In this study, a three-story structural vessel [2] was constructed using a DC magnetron sputter. The PHR sensor used Ta/NiFe/Cu/IrMn/Ta[3]. The manufactured PHR sensor was finished in chip form through calibration circuit and a metal oxide semiconductor (CMOS) process after completion. Manufactured PHR current sensors were designed to measure current at levels 1 to 100 A and measured self-resolution 0.148 mG, 1% precision and 0.46% nonlinear characteristics.

References

[1] N. T. Thanh, B. Parvatheeswara Rao, N. H. Duc, and C-G Kim phys. stat. sol. (a) 204, 12, 4053-4057 (2007)

[2] N. J. Gökemeijer, T. Ambrose, and C. L. Chien[3] N. J. Gökemeijer, T. Ambrose, and C. L. Chien, Phys. Rev. Lett. **79**, 4270 (1997).

[3] Christian D. Damsgaard, Susana C. Freitas, Paulo P. Freitas, and Mikkel F. Hansen Journal of Applied Physics **103**, 07A302 (2008)

Microwave absorption properties of Co-Mn substituted Sr-La M-type hexaferrite in Ka band (26.5-40 GHz)

Sungjoon Choi[1*], Jae-Hyoung You[1], Seung-Young Park[2], Seong Jin Choi[3] and Sang-Im Yoo[1]

[1]Department of Materials Science and Engineering, and Research Institute of Advanced Materials, Seoul National University, Seoul 151-744, Korea

[2]Spin Engineering Physics Team, Division of Scientific Instrumentation, Korea Basic Science Institute, Daejeon 34133, Korea

[3]Chang Sung Co Ltd, R&D Ctr, 11-9 Namdong Ind Area, Inchon 405100, Republic of Korea

In the recent years, much attention has been paid to microwave absorbers, because of a solution of electromagnetic pollution and special usage in military and aerospace field in modern society. The hexagonal ferrites (or hexaferrites) are well known for electromagnetic interference (EMI) suppression. Hexaferrites can be used in the frequency region of gigahertz (GHz) because they have high magnetic anisotropy values. We fabricated Co-Mn substituted Sr-La M-type with the chemical formula of $Sr_{0.85}La_{0.15}Co_{0.15-x}Mn_xFe_{11.85}O_{19}$ (x = 0, 0.075). Structural, morphological, and magnetic properties were investigated by using x-ray diffraction (XRD), field-emission scanning electron microscopy (FE-SEM), vibrating sample magnetometer (VSM), respectively. The complex permittivity and permeability measurements result in the Ka band (26.5-40 GHz). The microwave absorbing properties will be evaluated including reflection loss (RL) and presented for a discussion.

The research fund for this study is from Chang Sung Co.

Controllable Actuation of Magnetic Kirigami Patterns

Trivoramai Jiralerspong*, Geonhee Bae and Sang-Koog Kim
National Creative Research Initiative Center for Spin Dynamics and Spin-Wave Devices,
Nanospinics Laboratory, Research Institute of Advanced Materials,
Department of Materials Science and Engineering, Seoul National University, Seoul 151-744, Republic of Korea

The ancient paper cutting art, kirigami, consists of cuts that are made on a single sheet of material, where planar mechanical deformations could induce shape transformations in both two-dimensional (2D) and three-dimensional (3D) space [1]. Due to this remarkable property, kirigami patterns could give rise to complex material properties such as auxetics and mechanical metamaterials in which materials expand when subjected to tensile loading [2]. However, the mechanical deformations of these structures are usually performed physically by hand or machine, limiting its application [3]. Therefore, external stimuli such as magnetic fields could be used to realize the remote actuation of kirigami patterns due to its safe and effective control [4].

In this study, the remote actuation of kirigami patterns in 2D and 3D are explored, by utilizing the magnetic anisotropy of magnetic nanoparticle (MNP) chains within the magnetic-elastomer composite, a soft material composed of an elastomer matrix and MNPs, to bring about motion. The shape morphologies are demonstrated by utilizing simple kirigami patterns consisting of connected square units that are linked together by rotating hinges [5], forming a sheet of horizontal and vertical cuts. Depending on the cut designs and the MNP chain orientation in-plane and out-of-plane within each square unit, 2D and 3D actuation can be achieved, respectively, as illustrated in Figure 1a and 1b. The kirigami patterns are fabricated by means of a uniform magnetic field and a 3D printed mold (see Figure 1c), where the MNPs within the composite self-assemble to form chains along the direction of the applied field. The in-plane and out-of-plane chain orientation are achieved by aligning the

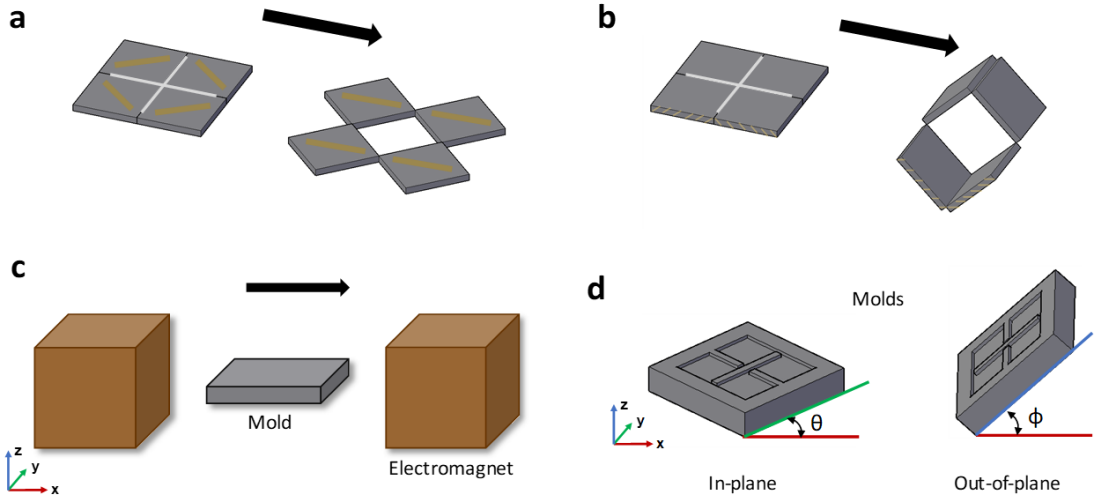

Fig. 1. Schematic drawing of the kirigami patterns, the shape deformations, and the fabrication method. a) 2D and b) 3D actuation of the kirigami patterns, c) chain alignment method of the kirigami patterns using an electromagnet, d) mold orientation to create the in-plane and out-of-plane chain alignment. Black arrows indicate the uniform magnetic field and its direction.

mold and hence the MNPs along the xy-plane or the xyz-axis, respectively, as shown in Figure 1d. Once the elastomer is cured, the chains are permanently fixed within the composite, even after the removal of the field. The experiment is conducted under a uniform magnetic field of 300 mT that is produced by an electromagnet. Experimental results show that the embedded chains within the kirigami patterns respond quickly to align its magnetic moment along the direction of the applied magnetic field, demonstrating the remote actuation in 2D and 3D. This untethered actuation of kirigami patterns therefore show promising potential applications in areas such as drug delivery, medical patches, and artificial valves.

References

[1] X. Ren, R. Das, P. Tran, T. D. Ngo, and Y. M. Xie, "Auxetic metamaterials and structures: A review," Smart Mater. Struct., vol. 27, no. 2, 2018.

[2] A. Rafsanjani and K. Bertoldi, "Buckling-Induced Kirigami," Phys. Rev. Lett., vol. 118, no. 8, pp. 1-11, 2017.

[3] K. Bertoldi, V. Vitelli, J. Christensen, and M. Van Hecke, "Flexible mechanical metamaterials," Nat. Rev. Mater., vol. 2, 2017.

[4] R. M. Erb, J. J. Martin, R. Soheilian, C. Pan, and J. R. Barber, "Actuating Soft Matter with Magnetic Torque," Adv. Funct. Mater., vol. 26, no. 22, pp. 3859-3880, 2016.

[5] V. Kunin, S. Yang, Y. Cho, P. Deymier, and D. J. Srolovitz, "Static and dynamic elastic properties of fractal-cut materials," Extrem. Mech. Lett., vol. 6, pp. 103-114, 2016.

Magneto-transport effect in CoSiB thin films

Y. K. Kim*, H. N. Lee, T. W. Kim†
Department of Nanotechnology & Advanced Materials Engineering, Sejong University, Seoul, Korea

Magnetic multilayer films with perpendicular magnetic anisotropy (PMA) have been widely investigated and expected to be used for magnetic recording media, magnetic sensor, and magnetic memories. We have studied PMA magnetic multilayer films with amorphous materials due to their smooth surface and soft magnetic properties. The CoSiB 1000 Å single layer film shows soft magnetic properties with 1.6 Oe coercivity and 407 emu/cm^3 saturation (M_s). The as-deposited CoSiB 1000 Å film has amorphous structure even with post-annealing treatment up to 350 ℃. The Hall effect in [CoSiB/Pt] multilayer films were measured by using Van der Pauw method and showed spontaneous Hall angle (ρ_H/ρ). Even though the observed Hall resistivity in [CoSiB/Pt] multilayer is smaller than that in amorphous rare earth-transition metal (RE-TM) alloy films, the Hall angle of 8% is much larger than amorphous RE-TM alloy films. The trilayer films of the structure [CoSiB 15 Å/Pt (t) Å/CoSiB 15 Å] (t_{Pt} from 11 Å to 39 Å) have out-of-plane easy axes and show strong antiferromagnetic exchange coupling especially for the films of t_{Pt} = 22 Å and 27 Å. Hall voltage curve show two hysteresis loops. This is a clear evidence of antiferromagnetic coupling. This is a clear evidence of antiferromagnetic coupling. It is believed that the CoSiB/Pt/CoSiB is a candidate system for use in hall sensor.

This work was supported by sejong Univ.(20180417)

구두발표

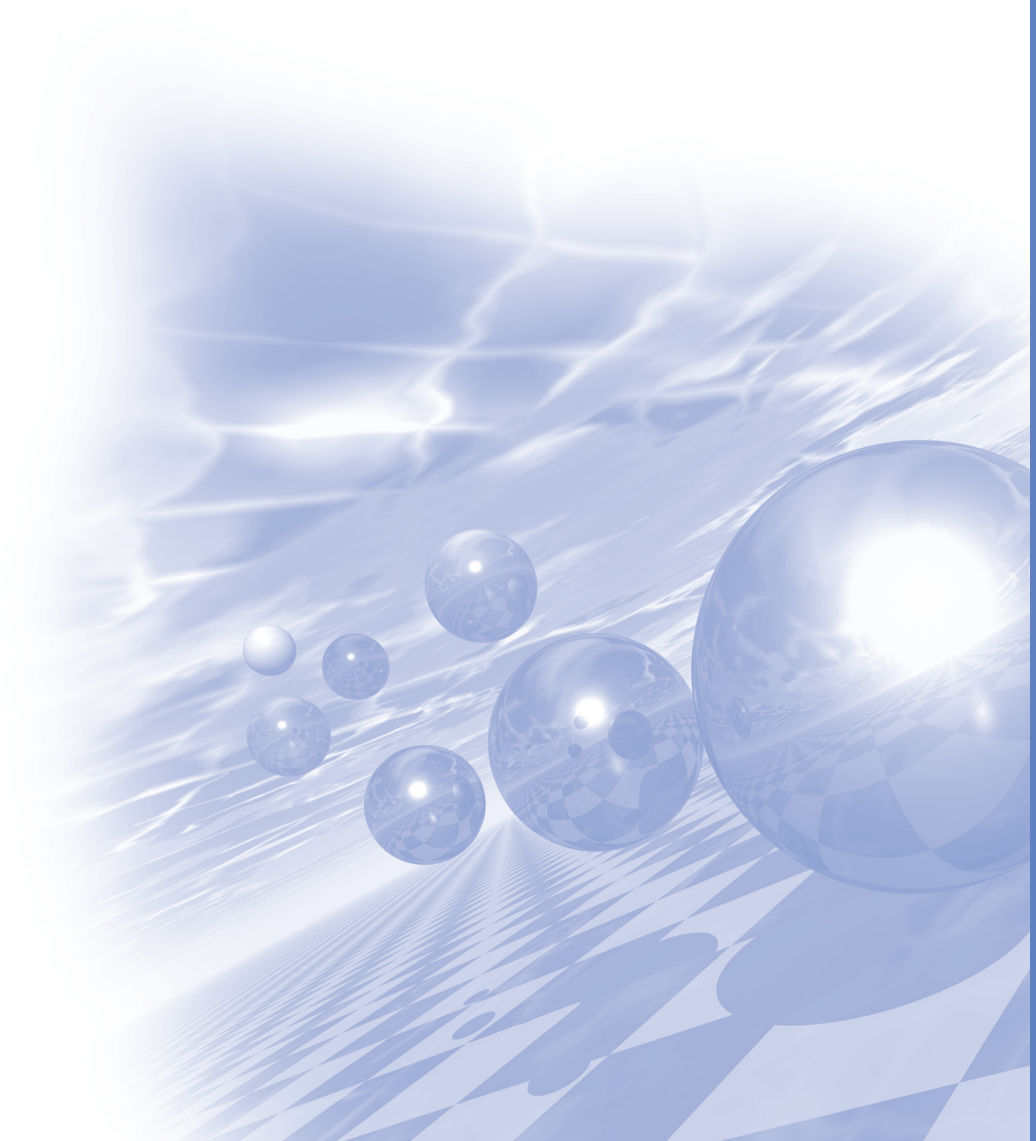

Magnetics and History

Hi-Jung Kim*
Korea Institute of Science and Technology

Ancient people thought that magnetic phenomena were very strange and amaging. In 5-6C B.C., rocks containing iron oxide are discovered in the district of Magnesia, Greeks and the words such as “magnetite”, “magnet”, “magnetism” were derived from the name of Magnesia land.

In 1100 A.D., the Chinese used needles of magnetite to make compasses indicating the north and south poles. The compass technology were delivered to the Arabia and then transfered to Europe during the Crusades.

The compass promoted the Pelagic voyage and open the Age of Uncharted.

C. Columbus discovered the new land and F. Magellan succeed the voyage of Around the world using the compass.

In 16C, Gilbert discovered that the earth was a giant magnet and mapped out the earth’s magnetic field.

I will briefly introduce the beginning history of magnetics and the historical revolutions influenced from the magnetics.

Plenary Session I

'IEEE DL'

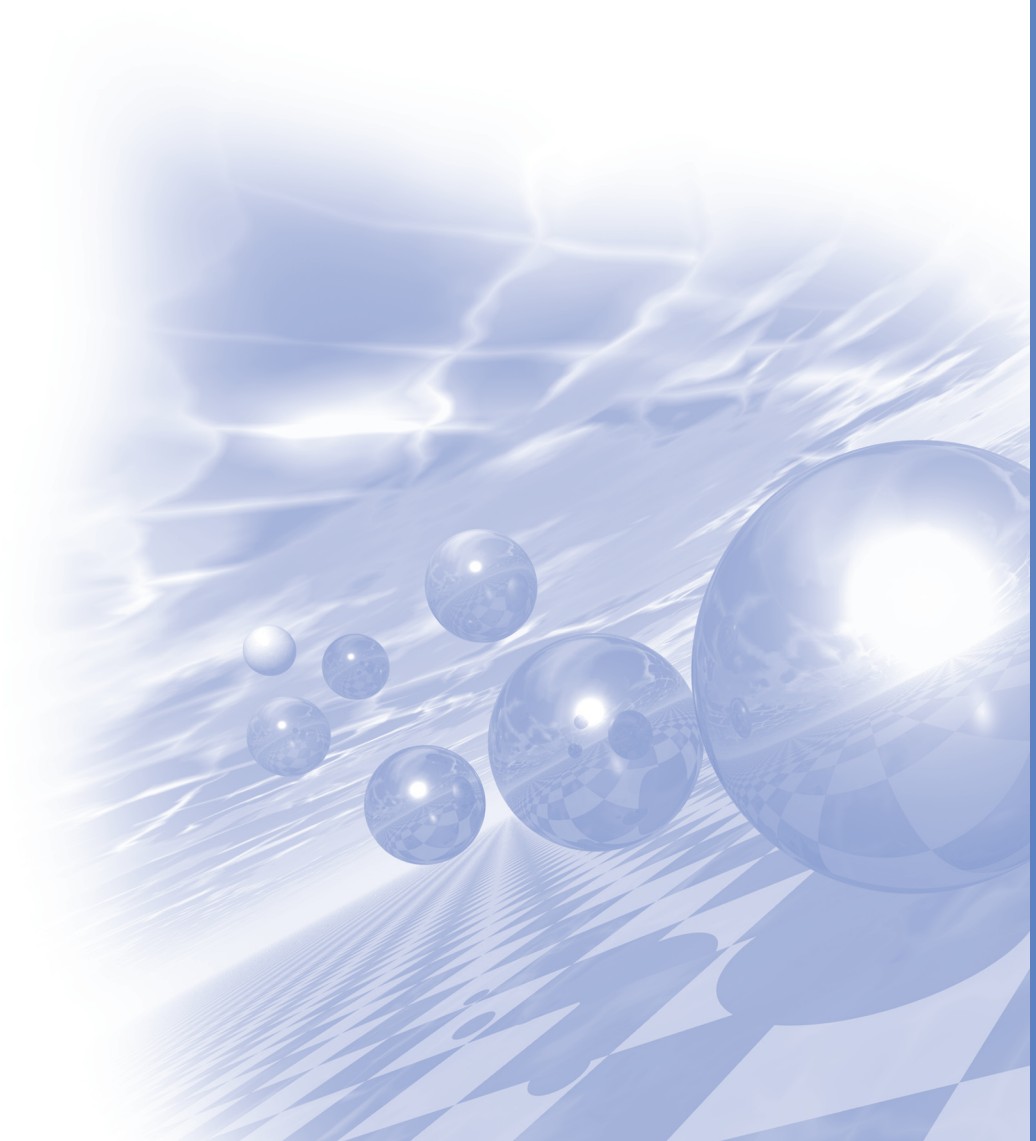

Spin-Orbit Technologies: From Magnetic Memory to Terahertz Generation

Hyunsoo Yang*
Department of Electrical and Computer Engineering, National University of Singapore, Singapore
e-mail: eleyang@nus.edu.sg

Spintronic devices utilize an electric current to alter the state of a magnetic material and thus find great applications in magnetic memory. Over the last decade, spintronic research has focused largely on techniques based on spin-orbit coupling, such as spin-orbit torques (SOTs), to alter the magnetic state. The phenomenon of spin-orbit coupling in magnetic heterostructures was also recently used to generate terahertz emission and thus bridge the gap between spintronics and optoelectronics research.

I will introduce the basic concepts of SOTs, such as their physical origin, the effect of SOTs on a magnetic material, and how to quantitatively measure this effect [1,2]. Next, I will discuss the latest trends in SOT research, such as the exploration of novel material systems like topological insulators and two-dimensional materials to improve the operation efficiency [2,3]. Following this, some of the technical challenges in SOT-based magnetic memory will be highlighted [3]. Moving forward, I will introduce the process of terahertz generation in magnetic heterostructures [4], where the spin-orbit coupling phenomenon plays a dominant role. I will discuss the details of how this terahertz emission process can be extended to novel material systems such as ferrimagnets [5] and topological materials [6]. The final section will focus on how the terahertz generation process can be used to measure SOTs in magnetic heterostructures, thus highlighting the interrelation between terahertz generation and the SOTs, which are linked by the underlying spin-orbit coupling.

References

[1] X. Qiu et al., "Characterization and manipulation of spin orbit torque in magnetic heterostructures," Adv. Mater., **30**, 1705699 (2018).

[2] Y. Wang et al., "FMR-related phenomena in spintronic devices" J. Phys. D: Appl. Phys., **51**, 273002 (2018).

[3] R. Ramaswamy et al., "Recent advances in spin-orbit torques: Moving towards device applications" Appl. Phys. Rev., **5**, 031107 (2018).

[4] Y. Wu et al., "High-performance THz emitters based on ferromagnetic/nonmagnetic heterostructures" Adv. Mater., **29**, 1603031 (2017).

[5] M. Chen, et al., "Terahertz emission from compensated magnetic heterostructures," Adv. Opt. Mater., **6**, 1800430 (2018).

[6] X. Wang, et al., "Ultrafast spin-to-charge conversion at the surface of topological insulator thin films" Adv. Mater. **30**, 1802356 (2018).

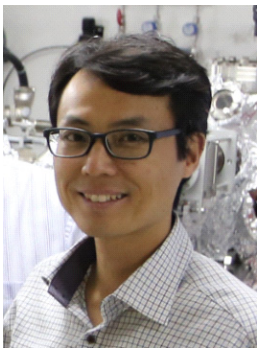

Hyunsoo Yang obtained the bachelor's degree from Seoul National University and the PhD degree from Stanford University. He worked at C&S Technology, Seoul; LG Electronics, San Jose, CA; and Intelligent Fiber Optic Systems, Sunnyvale, CA, USA. From 2004 to 2007, he was at the IBM-Stanford Spintronic Science and Applications Center, IBM Almaden Research Center. He is currently a GlobalFoundries chaired associate professor in the Department of Electrical and Computer Engineering, National University of Singapore, working on various magnetic materials and devices for spintronics applications. He has authored 170 journal articles, given 100 invited presentations, and holds 15 patents. Prof. Yang was a recipient of the Outstanding Dissertation Award for 2006 from the American Physical Society's Topical Group on Magnetism and Its Applications and the IEEE Magnetic Society Distinguished Lecturer for 2019.

KMS 2019 Summer Conference

Special Session I

‘Magnetism in reduced dimension’

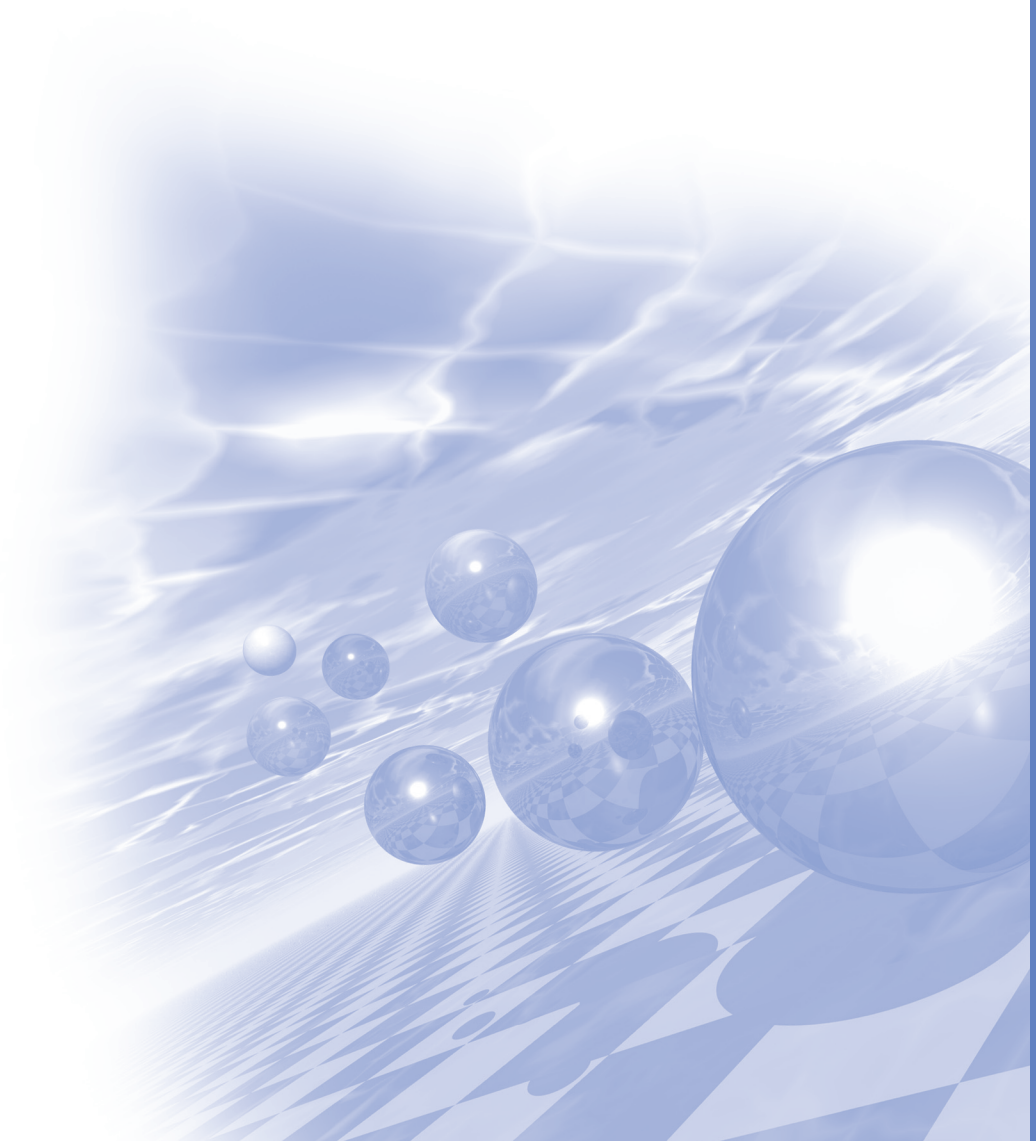

Electron spin resonance on individual atoms on surfaces

Taeyoung Choi*
Center for Quantum Nanoscience, Institute for Basic Science (IBS), Seoul 03760, Republic of Korea
Department of Physics, Ewha Womans University, Seoul 03760, Republic of Korea

Understanding, controlling, and utilizing nanoscale quantum systems have been one of major research interests across fields of physics, chemistry, and material science. Recently, we successfully combined microwave technique to a Scanning Tunneling Microscopy (STM) and demonstrated electron spin resonance (ESR) of individual Fe atoms on ultrathin insulating MgO. Coherent Quantum control of atoms on surfaces using STM is a highly interesting and a new Quantum architecture, enabling us to position qubits and control their interaction in nano-meter and nano-electron-volt resolution.

With this new tool (ESR-STM), we studied magnetic interaction of artificially built nanostructures. We found that an ESR signal from single Fe atom split into two different frequencies when we position an additional Fe atom nearby. We measure ESR energy splittings that decay as $1/r^3$ (where r is the separation of the two Fe atoms), indicating that the atoms are coupled through magnetic dipole-dipole interaction. This energy and distance relation enables us to determine magnetic moments of atoms and molecules on a surface with high precision in energy (~10MHz = ~40neV). Unique and advantageous aspects of ESR-STM compared to other quantum magnetic sensors (such as NV centers) are the atom manipulation and imaging capabilities, which allow us to build atomically precise nanostructures and examine their interactions. For instance, we construct a dice *cinque* arrangement of five Fe atoms, and probe their magnetic interaction and energy degeneracy. We demonstrate the ESR-STM technique can be utilized for quantum magnetic sensors.

Novel scanning magnetic imaging based on diamond NV centers

Donghun Lee*
Department of Physics, Korea University, Seoul, Republic of Korea

Probing and imaging magnetism at nanometer scale with high field sensitivity is of great interest in a wide range of fields, including solid-state physics, materials science and biomedical applications. In this talk, I will introduce a novel magnetic sensing and imaing method based on nitrogen-vacancy (NV) defect center in diamond. The diamond NV center has promising potential for nanometer and nanotesla magnetometry due to its atomic-scale size, long spin coherence times and high magnetic field sensitivity (e.g. < $nT/Hz^{1/2}$). Since these properties are robust against a wide range of operating temperature, it is also suitable for studying novel magnetic materials exhibiting temperature-dependent magnetic orders. I will present basic working principle of magnetic field sensing and introduce scanning magnetometer combined with diamond NV center. I will also show some examples of sensing and imaging magnetic samples including permalloy and spin-orbit-torque devices.

Antiferromagnetic Van der Waals materials $TMPS_3$ and its Potentials

Je-Geun Park*
Center for Correlated Electron Systems, Institute for Basic Science (IBS), Seoul 08826, Republic of Korea
Department of Physics & Astronomy, Seoul National University, Seoul 08826, Republic of Korea

Magnetic van der Waals materials has been fast emerging as a new exciting field just over the last few years. Among one of the few known examples, TMPS3 with TM=transition metal elements have attracted significant attentions as it can exhibit the three fundamental magnetic model of Ising, XY and Heisenberg Hamiltonian depending on the TM elements. In this talk, I will demonstrate how we can use this unique magnetic property of these materials to learn of the old physics.

References

[1] Je-Geun Park, J. Phys. Condens. Matter 28, 301001 (2016)
[2] Jae-Ung Lee, et al., Nano Lett. 16, 7433 (2016)
[3] Cheng-Tai Kuo, et al., Scientific Reports 6, 20904 (2016)
[4] So Yeun Kim, et al., Phys. Rev. Lett. 120, 136402 (2018)
[5] Kenneth S. Burch, David Mandrus, and Je-Geun Park, Nature 563, 47 (2018)
[6] Kangwon Kim, et al., Nature Communications 10, 345 (2019)

Physical properties of 2D magnetic materials

Changgu Lee*
Department of Mechanical Engineering, Sungkyunkwan University, Suwon, Republic of Korea
SKKU Advanced Institute of Nanotechnology (SAINT), Sungkyunkwan University, Suwon, Republic of Korea

The representative 2D materials, graphene, h-BN, and MoS2, have interesting mechanical, electrical and optical properties and have exhibited fascinating physical phenomena so far. However, they mostly lack one important physical property in physics, magnetism. The new 2D materials such as CrSiTe3, CrI3, and FePS3, which began to be studied recently, possess ferro- or antiferro-magentic properties even in atomic level thickness and are expected to reveal deep level of physics in 2-dimensional confinement.

In this talk, our recent works on thickness dependence of magnetic and optical properties of ternary 2D materials, Fe3GeTe2 and CrPS4, which are ferromagnetic and antiferromagnetic 2D materials, will be presented. Fe3GeTe2 was studied with hall measurement and STM methods. From the hall measurement, it exhibited the anomalous hall effect due to its intrinsic ferromagnetism. Interestingly, the magnetic properties such as coercivity changed significantly with decreasing thickness changing from weak ferromagnet to strong ferromagnet. STM study revealed some magnetic domains on the surface. The domain structures barely changed below Curie temperature, but disappeared above the critical temperature, which suggests they are magnetic structures. CrPS4, which is an antiferromagnet, was characterized with Raman and PL spectroscopies. Its bandgap was measured to be roughly 1.3 eV and its structure showed strong in-plane optical anisotropy.

Room temperature ferromagnetism in a magnetic-metal-rich van der Waals metal

Jun Sung Kim*
CALDES, IBS & Department of Physics, POSTECH, Pohang, Republic of Korea

Spintronics, one of the next-generation information technologies, exploits the spin degree of freedom for information storage and logic operations through three key components of spin controls, i.e. spin transport, manipulation, and generation. For these spin controls, two-dimensional (2D) van der Waals (vdW) crystals constitute a promising class of materials, including graphene for long-distance spin transport, and transition metal dichalcogenides (TMDCs) for effective spin manipulation by the strong spin-orbit coupling.

Despite these recent developments, stabilizing 2D spin-source has remained challenging so far, because of the lack of the stable metallic vdW ferromagnets at room temperature, which can generate highly spin-polarized current and be easily incorporated with other vdW crystals. Here we show that several-atom-thick and magnetic-metal-rich layers, designed by ab-initio calculations, can stack in the vdW structure and host the long-range itinerant ferromagnetism near the room temperature due to the enhanced exchange pair interaction. This design scheme is successfully realized in a new iron-based vdW ferromagnet Fe4GeTe2 showing a high Tc of 280 K, a large conductivity, and a large magnetization, favorable for spin source operation. Our findings highlight Fe4GeTe2 as a key component in all-vdW-material-based spintronic applications and hold a promise to further increase Tc in vdW ferromagnets with thick magnetic-metal-rich layers.

Electrically induced valley orbital magnetization in 2D semiconductor

Jieun Lee*
Department of Physics and Department of Energy Systems Research,
Ajou University, Suwon 16499, Republic of Korea

In 2D honeycomb lattices with broken inversion symmetry, electron's valley degree of freedom may emerge in addition to spin. The valley degree of freedom is manifested by the observation of the valley-contrasting orbital magnetization at K and K' valleys. The development of experimental methods to control the valley magnetization by external fields are not only fundamentally interesting, but may also find applications in valley-based electronic and memory devices. Here, I will introduce methods to control the valley magnetization in monolayer 2D semiconductors by using an electric field and strain. In the first part of the talk, I will discuss the valley magnetization generated by the valley Hall effect at the edges of monolayer semiconductors. The scanning Kerr rotation microscopy is employed to directly image the valley magnetization distribution with sub-micron spatial resolution. In the second part, I will introduce our recent work on the mechanical control of the valley magnetization using strain. The observed valley magnetization depends on the direction and magnitude of strain and is well explained using strain-induced modification of Berry curvature effects.

KMS 2019 Summer Conference

Special Session II

‘Hard & Soft Magnetic Materials:
고성능 모터용 자석 개발’

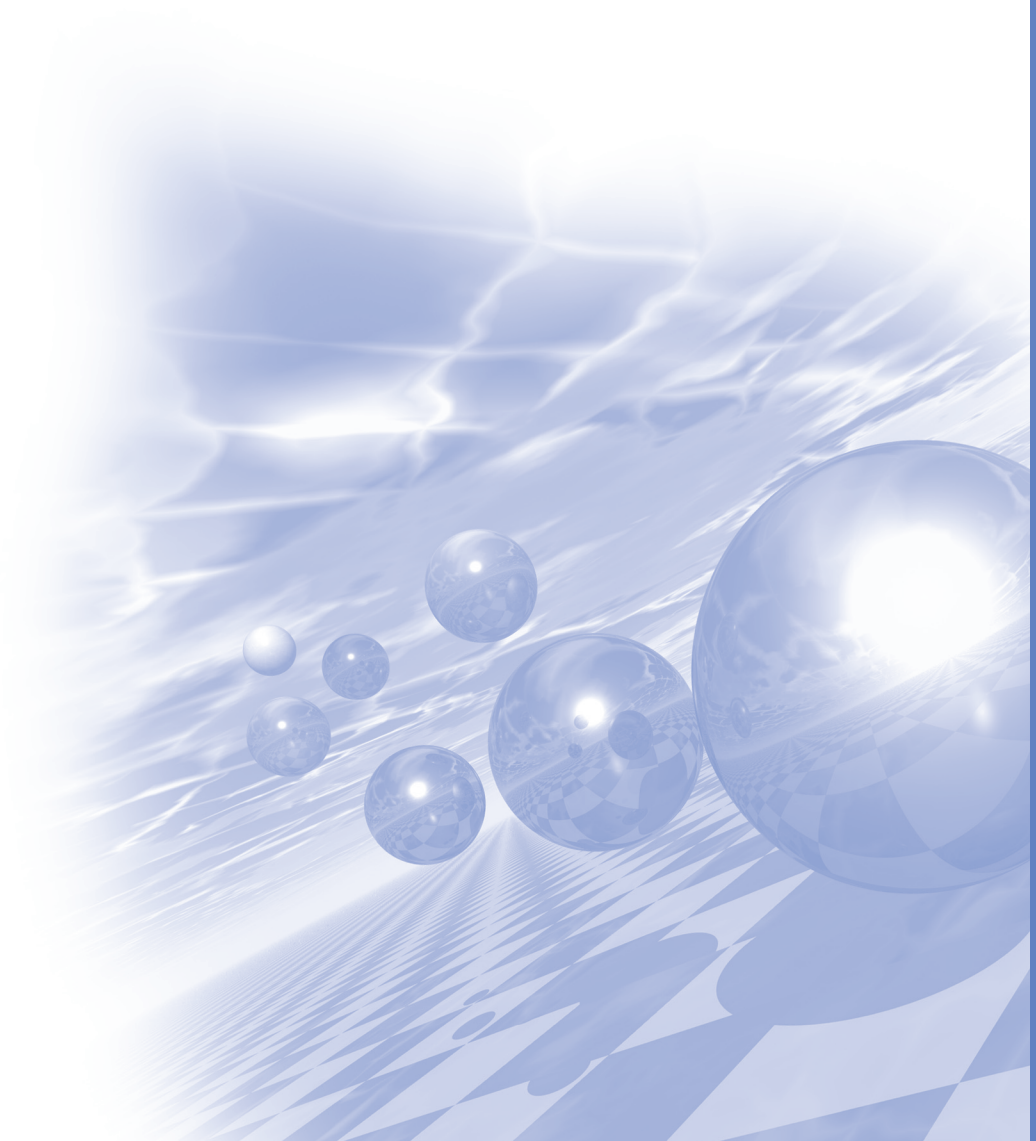

Revisit conventional magnets for tips on finding new permanent magnet material

Hae-Woong Kwon[1*], Jung Gu Lee[2]
[1]Pukyong National University, Busan, Republic of Korea 48513
[2]Korea Institute of Materials Science, Changwon, Republic of Korea 51508

Since its first discovery in 1980s, Nd-Fe-B-type magnet has been making its big time in the high performance permanent magnet market. However, there has always been a chronic apprehension of limited supply and volatile price of raw materials of rare-earth metals, and worse still is that the magnet has poor thermal stability due to low Curie temperature. This poor thermal stability (in particular, unfavourable temperature coefficient of coercivity) has been often an impediment to exploiting the magnet for high performance motor. As such, an extensive effort has been made for finding new alternative rare-earth-free permanent magnet materials, which are meant to replace the current Nd-Fe-B-type magnet, but there are still many obstacles and difficulties that are in the way of their success. Indeed, variety of new materials based on abundant transition metals without rare-earth have been being developed. The researches of finding new rare-earth-free magnet material seemingly have overpromised us, and results of finding new rare-earth-free materials that outperform the current Nd-Fe-B-type magnet seemingly do not meet our initial expectations. The most outstanding position of the Nd-Fe-B-type magnet without comparison is expected to continue over an extended period. We revisit the conventional permanent magnets (Alnico, ferrite, Sm-Co-type, Nd-Fe-B-type, Sm2Fe17Nx-type) to acquire valuable tips for finding new high performance permanent magnet materials.

Progress in ceramic permanent magnets based on M-type hexaferrites

Sang-Im Yoo*, Kang-Hyuk Lee and Sung-Jun Choi
Department of Materials Science and Engineering & Research Institute of Advanced Materials,
Seoul National University, Seoul 151-744, Korea

M-type hexaferrties with the chemical formula of $MeFe_{12}O_{19}$ (Me = Ba, Sr) have been well known as ceramic permanent magnets. Their magnetic properties, including coercivity ($_BH_c$,), remanence (B_r) and the maximum energy product $(BH)_{max}$, have been improved in the order of BaM, SrM, (La,Sr)$(Fe,Co)_{12-x}O_{19}$, and (La,Ca) $(Fe,Co)_{12-x}O_{19}$, which is basically due to the enhancement of the uniaxial magnetocrystalline anisotropy without degrading their saturation magnetization (M_s), leading to improved $_BH_c$, via a cation substitution for both Me^{2+} and Fe^{3+} sites within the unit cell of the magnetoplumbite structure. On the other hand, to achieve a small-grained microstructure, possessing high sintered density with the c-axis alignment of each grain, the forming process under the applied magnetic field is essential, and a small amount of additive must be used. In this talk, first, the progress in the improvement of intrinsic magnetic properties, including M_s and anisotropy field (H_a) through the cation substitution will be explained. Next, I will describe the important factors affecting the extrinsic properties, including $_BH_c$, B_r, and $(BH)_{max}$, for the system of (La,Sr)$(Fe,Co)_{12-x}O_{19}$. Finally, I will discuss the prospect of higher-performance ceramic permanent magnets. This research was supported by Future Materials Discovery Program through the National Research Foundation of Korea (NRF) funded by the Ministry of Science and ICT (2017M3D1A1013748).

1차원 구조를 갖는 교환자기결합형 Sm-Co/Fe-Co 코어쉘 나노섬유의 구현 및 자기적특성

김종렬*
한양대학교 에리카 재료화학공학과

교환자기결합효과(exchange-coupling effect)는 나노 구조를 갖는 연자성 상과 경자성 상의 계면에서 발생하는 교환자기력에 의해, 연자성 상의 높은 포화 자화값과 경자성 상의 높은 보자력이 동시에 구현되어 기존 경자성 소재의 한계를 극복 할 중요한 연구과제로 인식되고 있다. 이러한 효과를 구현하기 위한 다양한 연구가 진행되었으나, 교환자기결합형 영구자석 구현을 위해서는 극복해야 할 다양한 문제가 존재하는 것으로 알려져 있다. 특히, 나노 입자 고유의 응집 특성은 비표면적을 감소시켜 교환자기결합효과의 효율을 감소시키며, 연/경자성 상의 계면 제어(산화물 및 불순물과 같은 제 3상의 유무)와 연자성 상의 균일하고 적절한 두께 제어가 선행되지 않으면 오히려 최대자기에너지적의 열화가 발생되는 것으로 알려졌다. 이러한 기존 연구의 한계를 극복하고자, 본 연구에서는 전기방사법(electrospinning)과 무전해 도금법(electroless plating)을 활용하여 고 분산된 1차원(1-dimensional) 구조의 Sm-Co/Fe-Co 코어-쉘 나노섬유(core-shell nanofiber)를 구현하고자 하였다. 전기방사법에 의해 제조된 경자성의 Sm-Co 나노섬유는 150~200 nm 의 직경을 가지며, 염화암모늄용액을 이용한 표면 개질을 통해 Sm-Co 나노섬유 표면에 잔류하는 불순물 및 산화물을 제거하였다. 연자성의 Fe-Co 쉘의 두께는 무전해도금의 시간에 따라 조절되었고, Sm-Co 나노섬유 표면에 균일하고 연속적으로 형성되었다. 이와 같이 제조된 Sm-Co/Fe-Co 나노섬유의 미세구조 및 자기적 특성의 변화를 TEM(Transmission Electron Microscopy) 분석 및 VSM(Vibrating Sample Magnetometer) 등을 활용하여 분석하였다. 그 결과, Fe-Co 쉘의 두께가 15-20 nm 로 형성되었을 경우, 경자성 Sm-Co 나노섬유의 보자력을 유지하면서 높은 잔류자화의 값을 나타내었으며, 리코일 곡선(recoil curve)으로부터 계산된 가역 자화율(reversible susceptibility)을 통해 교환자기결합효과가 존재함을 확인하였다. 결과적으로, 고 분산 Sm-Co 섬유체의 제조 및 표면 개질, 그리고 균일한 연자성 Fe-Co 쉘의 정밀한 두께 제어를 통하여 최대자기에너지적은 연자성 Fe-Co 쉘의 형성 전과 비교하여 45% 이상의 증가된 값을 보였다. 따라서, 본 연구를 통해 교환자기결합형 영구자석의 한계를 극복할 수 있는 새로운 가능성이 제시되었다고 판단된다.

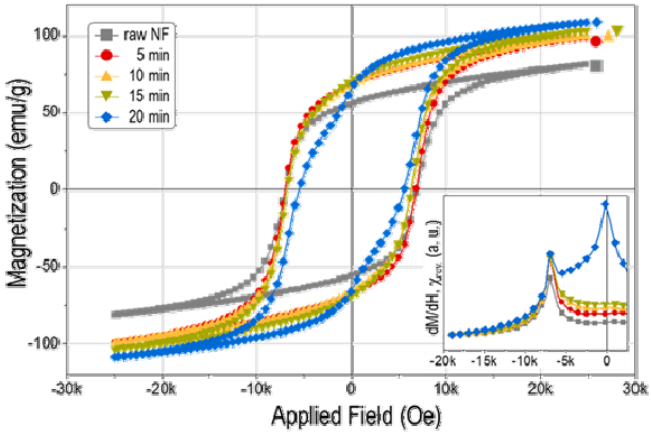

그림 1. 무전해도금 시간에 따른 Sm-Co/Fe-Co 나노섬유의 이력곡선 변화
(삽입된 그래프는 이력곡선의 가역 자화율(reversible susceptibility)을 나타냄.).

Development Status of Rare Earth magnets for Vehicle Motors

Jaeryung Lee*
Hyundai motor, Korea

The use of neodymium magnets is dramatically increasing in the traction motor and various types of high output motors in electrified vehicle future. Magnets used in traction motor have high coercivity not to be demagnetized at high temperatures, so heavy rare earth element should be included in magnets.

Since rare earth resources have difficulty in the unbalance between supply and demand for magnets, rare earth element should be reduced or eliminated. Recently technologies such as grain boundary diffusion method and grain refinement can reduce or be free the use of dysprosium and terbium. In addition, in order to substitute a Neodymium element, magnets with La/Ce, HfMnP, ZnMnP, or L10FeNi have been researched in the world.

If the maximum rising temperature of magnets is reduced during a traction motor is operating, the motor can use at higher energy efficiency, the use of dysprosium and terbium but also can be reduced. The main reason for the temperature rises of magnets in interior permanent magnet (IPM) motors is the eddy current loss of magnet due to harmonics such as slot harmonics and carrier harmonics. In particular, rare earth magnets have high electrical properties so they can easily increase highly the eddy current loss of magnets. The prediction and test technique of eddy current loss considered electric steel core was researched by the relation between surface treatments of divided magnets and electric steel core, and electrical properties of magnets, etc.

Anisotropic Rare-earth Bulk Magnet produced by Hot-deformation Process

Hee-Ryoung Cha[1*], Jae-Gyeong Yoo[1,2], Ga-Yeong Kim[1,2], Youn-Kyoung Baek[1], Hae-Woong Kwon[3], Jung-Goo Lee[1]

[1]Powder & Ceramics Division, Korea Institute of Materials Science, 797 Changwondaero, Changwon 642-831, Korea

[2]Department of Materials Science and Engineering, Pukyong National University, 45 Yongso-ro, Nam-Gu, Busan 48513, Korea

[3]Department of Materials Science and Engineering, Pukyong National University, 45 Yongso-ro, Nam-Gu, Busan 608-737, Korea Affiliation A, Korea

High performance Nd-Fe-B based permanent magnets have major applications in traction motors of hybrid and electric vehicles. Currently, heavy rare earth (HRE) elements such as Dy or Tb have been used in order to enhance the thermal stability of Nd-Fe-B based magnets. However, due to the scarcity and high cost of HRE elements, development of HRE-free high coercive Nd-Fe-B based magnet has become one of the critical issues. Microstructure control such as grain size and grain boundary is necessary to increasing coercivity without HRE element. With regard to grain size, melt-spinning and hydrogenation-disproportionation-desorption-recombination (HDDR) process are known as quite suitable method to decrease grain size. The HDDR powder has coarser-grain (300 nm) compare to melt-spun powder (~40 nm) though much smaller grain size than that of convention sintered magnet. For nano-crystalline powders, hot-deformation process is promising alternative to produce anisotropic bulk magnet. The isotropically oriented grains develop into laterally elongated grains with a strong c-axis texture by hot-deformation process, increasing remanence.

In present study, hot-deformation process was employed to produce anisotropic bulk magnet with melt-spun and HDDR powders. And post treatment was perfomed for coercivity enhancement. Based on the results, we will present an overall study of hot deformation process for high performance rare-earth magnet.

Special Session III

'Bio-Neuro Convergence with Spin Magnetism'

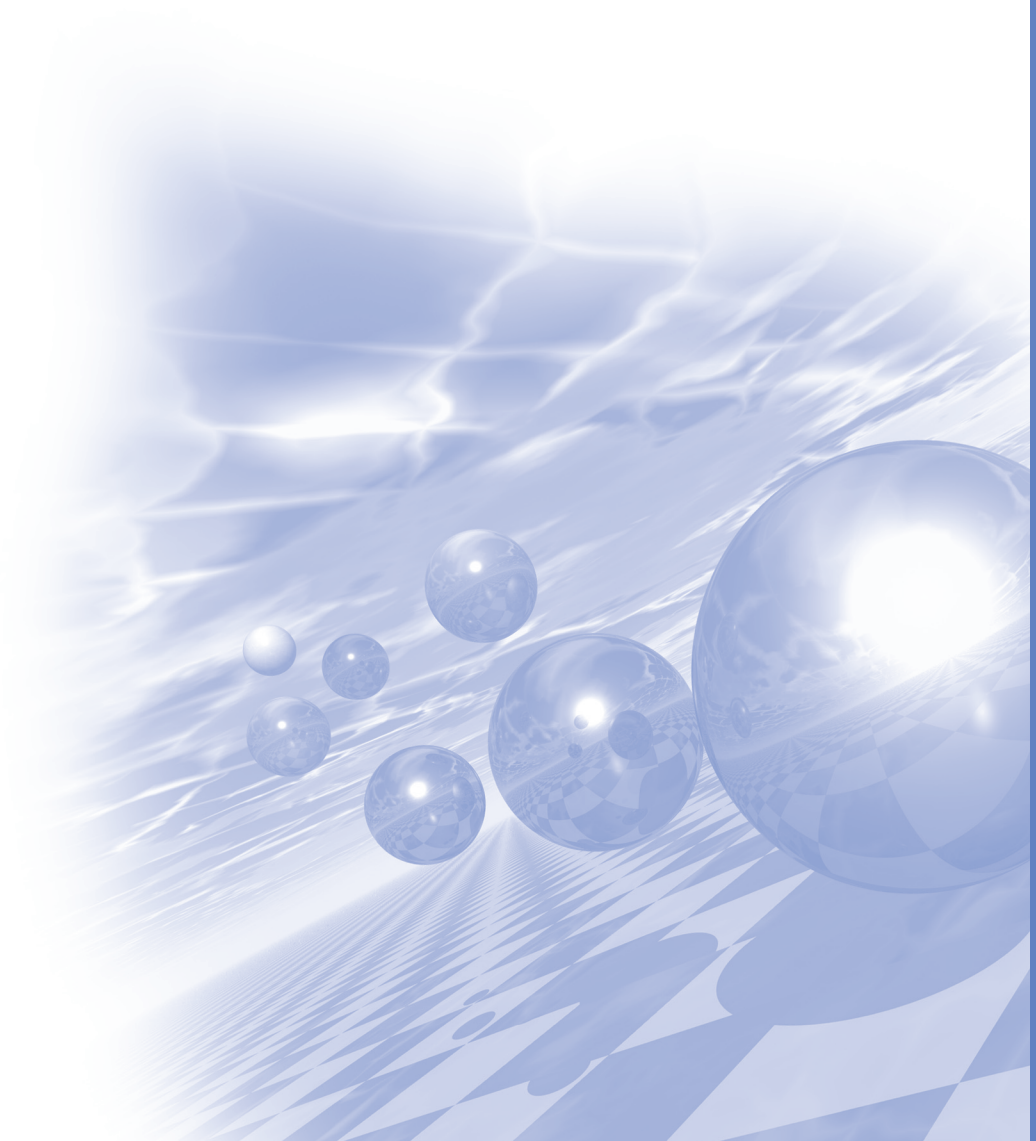

Enhancement of sensitivity of planar Hall effect sensors by optimization of geometry and layer composition: limitations and possibilities

A. D. Talantsev[1*], S. J. Kim[1], M. J. Kim[1], K. W. Kim[1], A. A. Elzwawy[1], S. Oh[3], T. Q. Hung[2], C. G. Kim[1]

[1]Department of Emerging Materials Science, DGIST, Daegu, 42988, Republic of Korea
[2]Institut Charles Gerhardt de Montpellier UMR 5253 Universite de Montpellier 34095 Montpellier, France
[3]Department of Nature-Inspired Nanoconvergence Systems, KIMM, Daejeon, 34103, Republic of Korea

Nanomagnetic sensors are opening a new era in industrial applications, related with information science and technology, bio-medical applications [1], detection of ultra-low magnetic moments [2], remote current sensing in power lines [3], magnetic flux leakage detection for timely elimination of defects in oil and gas pipelines [4] and mechanosensory applications [5]. Hitherto, the key characteristics of planar Hall resistance sensors are underestimated compared with the ones of GMR/TMR sensors, conventionally used in microelectronic logic devices. Indeed, a very high amplitude of response to magnetic field [6], achieved in TMR sensors, serves as a reason of their selection for application in magnetic recording devices, where a “yes-no” logic is needed. However, the gradual switching between “yes” and “no”, and linearity of the response to applied magnetic field is a problem for TMR sensors, because the magnetization reversal in TMR junctions is a multi-domain process with incoherent and stochastic nucleation of reversed magnetization areas.

Magnetic sensors, based on planar Hall effect (planar Hall resistance or PHR sensors), are devoid of this drawback. Coherent magnetization rotation and single domain magnetization reversal in PHR junctions, based on exchange biased bilayers, provide excellent conditions for high linearity of response to magnetic field. As well, the sensitivity and operating field range of PHR sensors are flexible adjustable both by layer composition, and by sensor’s geometry. Adjustment of interface coupling between ferro- and antiferromagnetic layers of junction by the insertion of non-magnetic spacer allows the variation of sensitivity within two orders of magnitude.

The geometry and shape of junction have a crucial effect on the sensor’s sensitivity. For the same occupied area and width of current path, the sensitivity of multi-ring is 2-3 orders of magnitude higher than the one of cross junction [7]. In addition, the magnitude of PHE response can be enhanced by increase of numbers of rings in the multi-ring sensor’s architecture. Particularly, the sensitivity can be adjusted from a few μV/Oe in cross junctions based on NiFe/IrMn bilayers to ~2 mV/Oe in 7-rings sensors, based on NiFe/Cu/IrMn trilayers [8].

One can note, that the ring- and multi-ring type sensors have a Wheatstone bridge architecture. There is a special feature of planar Hall effect bridges (PHEB sensors), compared with magnetoresistive sensors of any other type, connected into a bridge. Only in PHE bridges, the temperature drift of resistance is self-compensated. It means that the drift of PHE signal is of orders of magnitude smaller, than any increment of electrical resistance due to ambient temperature variations. For multi-ring sensors, the PHE signal drift (0.02 Ω/K) was ~10^2 times lower [8], than the drift of electrical resistance (1.5 Ω/K).

In this talk, we will summarize our work on optimization of PHR sensors by variation of layer composition and sensor’s geometry. Effects of material and thickness of FM, spacer and seed layers on the output voltage,

sensitivity and operating field range will be considered. Possibilities of sensitivity enhancement by variation of sensor's geometry will be discussed.

References

[1] K. Kim et al, Lab Chip, **15**, 696-703 (2015).

[2] S. Kamara et al, Adv. Mater. **29**, 1703073 (2017).

[3] P. N. Granell et al. Npj Flexible Electronics **3**, 3 (2019).

[4] H. Pham et al., IEEE Trans. Magn. **54** 6201105 (2018).

[5] S. Oh et al, Sci Rep **7**, 16963 (2017).

[6] S. Ikeda et al. Appl. Phys. Lett. **93, 082508 (2008)**.

[7] T. Q. Hung et al. J. Appl. Phys. **107** 09E715 (2010).

[8] B. Sinha et al, J. of Appl. Phys **113**, 063903 (2013).

PHR 센서의 2차 고조파를 이용한 자성비드 측정

김동영[1*], 윤석수[1], 이재훈[2], 김철기[2]
[1]안동대학교 물리학과
[2]DGIST 신물질과학전공

강자성 단일 박막에서 평면홀 효과(Planer Hall Effect)를 이용한 PHR 센서는 초상자성 특성을 갖는 자성나노비드를 측정하는 초소형 바이오센서에 응용되고 있다. 교류 전류 $I = I_o \sin(\omega t)$를 강자성 박막에 인가한 경우 전류의 방향과 수직인 방향에서 측정한 출력 전압은 1차 고조파와 2차 고조파의 합으로 $V = V_\omega \sin(\omega t) + V_{2\omega} \sin(2\omega t)$로 표현된다[1,2]. $V_\omega = \triangle R I_o$로 일반적인 PHR 신호이며, PHR 센서의 자기장 민감도 특성 분석에 이용하였다. $V_{2\omega}$는 자체 자기장(Self-field)에 의한 2차 고조파 신호이며, 나노비드 신호의 자기장 의존성 분석에 이용하였다.

본 연구에서는 교환결합력을 갖는 NiFe/Cu/MnIr 자성 박막 재료를 사용하여 100 × 200 μm^2 크기의 PHR 센서를 제작하였다. 주파수가 400 Hz인 교류전류를 교환 바이어스 자기장 H_{ex}와 평행하게 인가한 후 Lock-in Amp를 사용하여 1차 및 2차 고조파를 측정하였다. 2차 고조파를 이용하여 측정한 비드 신호는 H=0에서 가장 크게 나타났으며, 자기장의 세기에 따라 감소하여 H=H_{ex}에서 0이 된 후 감소하다가 다시 증가하여 0으로 근접하는 특성으로, 1차 고조파의 미분 형태를 보였다. 이러한 측정 결과로부터 자성비드 신호의 측정은 H=0에서 2차 고조파를 사용하는 것이 최적의 조건임을 알수 있었다. 이러한 측정 조건은 무자장에서 자성 비드를 측정하는 바이오센서에 응용될 수 있다.

References

[1] L. Ejsing, et. al, J. Magn. Magn. Mater. **293**, 667 (2005).
[2] L. Neumann and M. Meinert, AIP Advances **8**, 095320 (2018).

Extremely Low Perpendicular Magnetic Anisotropy and Sustainable Dzyaloshinskii-Moriya Interaction with a Palladium Underlayer

June-Seo Kim*
Intelligent Devices and System Research Group, DGIST, Daegu, Republic of Korea

Skyrmion is a topologically protected spin texture and the Dzyaloshinskii-Moriya interaction (DMI) is an essential ingredient [1]. The skyrmion states has attracted a great deal of attention because of its big potential for future non-volatile memory device, logic gates, even bio-inspired computations. However, the skyrmion state with an interfacial DMI on an ultrathin trilayer system has not been experimentally demonstrated at room temperature. One of main reason is that the perpendicular magnetic anisotropy (PMA) is increased with increasing interfacial DMI [2]. Here, we show a magnetic trilayer, which has an extremely low PMA energy density and a sustainable DMI energy density with introducing a Palladium (Pd) underlayer. Figure 1(a) and (b) show Brillouin light scattering spectra with (a) Pd underlayer and (b) Pt underlayer. Since the frequency difference (Δf) is directly proportional to the interfacial DMI energy density, we confirm that the trilayer with a Pd underlayer has a sustainable DMI energy density like a Pt underlayer system [3-6]. On the other hand, the anisotropy fields (H_k) are drastically decreased with a Pd underlayer as shown in Fig. 1(c). The anisotropy fields measured by performing a vibrating sample magnetometer (VSM) as a function of ferromagnet (Co) thickness are approximately 75% decreased with a Pd underlayer. We now infer through our diverse experimental observations that a skyrmion state at room temperature on a magnetic trilayer system with a Pd underlayer can be nucleated because of its low domain wall energy and it can open an original way to fabricate a lot of exotic spintronic devices for future non-volatile memories and logic applications.

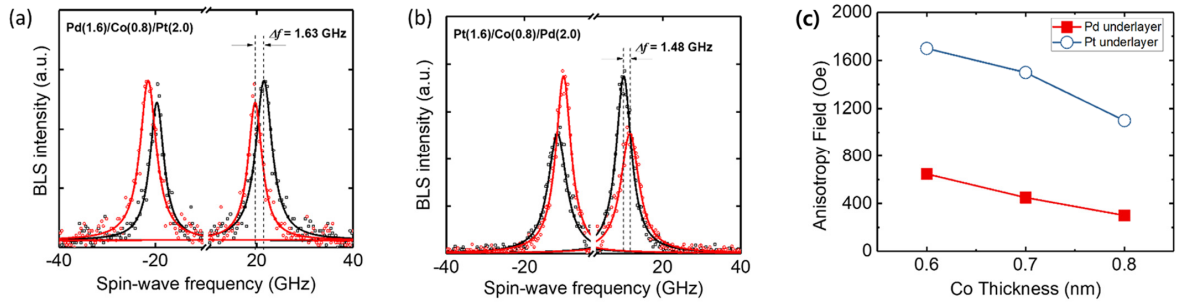

Fig. 1. Brillouin light scattering spectra (a) Pd underlayer system, and (b) Pt underlayer system (c) Anisotropy field (H_k) measurement as a function of ferromagnet (Co) thickness by using vibrating sample magnetometer (VSM)

References

[1] A. Fert, N. Reyren and V. Cros, Nat. Rev. Mater. **2**, 17031 (2017).

[2] N.-H. Kim, D.-S. Han, J. Jung, K. Park, H. J. M. Swagten, J.-S. Kim, and C.-Y. You, Appl. Phys. Express **10**, 103003 (2017).

[3] J. Cho, et al., Nat. Commun. **6**, 7635 (2015).
[4] J. Cho, N.-H. Kim, S. K. Kang, H.-K. Hwang, J. Jung, H. J. M. Swagten, J.-S. Kim, and C.-Y. You, J. Phys. D: Appl. Phys. **50**, 425004 (2017).
[5] R. Lo Conte, et al., AIP Advances **7**, 065317 (2017).
[6] J. Cho, N.-H. Kim, J. Jung, D.-S. Han, H. J. M. Swagten, J.-S. Kim, and C.-Y. You, IEEE Trans. Magn. **54**, 1500104 (2018).

Valley magnetic domain as a pathway to the valleytronic current processing

Youngjae Kim and Jae Dong Lee*
Department of Emerging Materials Science, DGIST, Daegu 42988, South Korea

An interplay between an applied strain and the Berry curvature reconstruction in the uniaxially strained monolayer MoS_2 is explored, which leads to the unbalanced Berry curvatures centered at **K** and **-K** points and eventually the valley magnetization under an external electric field. This finding of the valley magnetoelectric effect (VME) is shown to explain a recent experimental observation of the valley magnetoelectricity [1] and develop a novel concept of the valley magnetic domain (VMD), i.e., a real-space homogeneous distribution of the valley magnetization. Here we discover the anomalous electron dynamics through the VMD activation and achieve a manipulation of the anomalous transverse current perpendicular to the electric field, directly accessible to the signal processing, for instance, the current modulation under the VMD (i.e., the VMD wall) moving and the terahertz (THz) current rectification under the VMD switching. This suggests a concept of VMD to provide new physical insight to the valleytronic functionality and its manipulation to be a key ingredient of potential device applications

Reference

[1] J. Lee, Z. Wang, H. Xie, K.F. Mak, and J. Shan, Nature Mater. **16**, 887 (2017).

Accurate, Hysteresis Free Temperature Sensor for Health Monitoring Using a Magnetic Sensor and Pristine Polymer

Wooseong Jeong*, Mijin Kim, Jae-Hyun Ha, Wooseong Jeong, Nora Asyikin Binti Zulkifli, Jung-Il Hong, Cheol Gi Kim and Sungwon Lee

Department of Emerging Materials Science, Daegu Gyeongbuk Institute of Science & Technology (DGIST)

1. Introduction

To forestall unexpected human health problems, the accurate real-time measurement of body signals is essential. Recently, for application in wearable health-monitoring, a diverse type of temperature sensor embedded in a flexible and stretchable polymer substrate has been researched. In particular, electro-conductive temperature sensors have been reported that consist of a polymer and conductive particle mixture, based on the percolation threshold effect. However, electro-conductive temperature sensors usually face issues such as thermal hysteresis and inaccuracy (±3.1 °C) during repeated heating and cooling.[1-2] To resolve those issues, our group proposed a new concept for an extremely reproducible temperature sensor with high accuracy and no hysteresis.

2. Experiment

A schematic description of our temperature sensor is shown in **Figure 1.** It consists of a magnetic sensor, magnet sheet, and sandwiched polymers, which can accommodate volume expansion from external heat while maintaining its shape by the encapsulation layer. Magnetic sensor detects the variation of magnetic field according to the polymer expansion. A planar Hall resistance (PHR) sensor was used as the magnetic sensor due to its high linearity near zero magnetic fields, low thermal drift, high signal-to-noise ratio, and sensitivity.[3] After fabricating the magnetic sensor, polyethylene glycol (PEG, molecular weight M_w = 1000) was exploited to provide reversible volume control, since it can accommodate ≈2.2 % volume expansion near body temperature (around 35-42 °C).

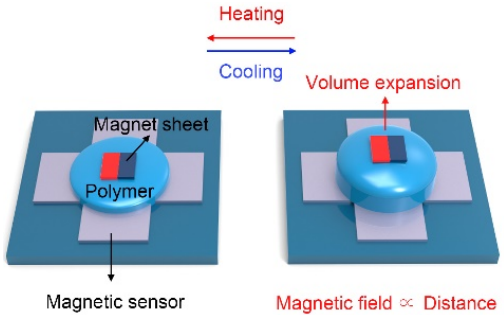

Fig. 1. Schematic description of the temperature sensor using the magnetic sensor and change in structure of polymer with heating.

Parylene C was then deposited by chemical vapor deposition (CVD), to withstand volume expansion and maintain the shape process. A digital photo image of the temperature sensor is shown in Figure 2a. To analyze the PHE voltage depending on temperature, the output signals were normalized. The variation of output signal

was calculated as $\Delta V_{PHE}=V_{PHE,initial} - V_{PHE,final}$, where ΔV_{PHE} is the variation of PHE voltage, and $V_{PHE,initial}$ and $V_{PHE,final}$ are the PHE voltage at 35 °C and the set temperature, respectively. Figure 2b compares the theoretical and experimental output signals of the temperature sensor at 35-42 °C. The experimental and theoretical output signals differ only slightly. Nevertheless, the experimental value shows excellent linearity not only in the range of 35-42 °C but also over a small temperature range with intervals of 0.1 °C, as shown in Figure 2c. This is remarkable, since our sensor can precisely detect displacement of 92.8 nm between the magnet and magnetic sensor. Figure 2d shows that the average response time of the sensor was approximately 1.73 s $°C^{-1}$. The response time was slightly longer at around 38 °C due to the phase transition. Cyclic stability was evaluated from 35 to 42 °C for 1000 cycles while monitoring the output signal. Figure 2e shows the thermal hysteresis loops of the 1st, 100th, and 1000th cycles under continuous heating and cooling. It is notable that the results show almost no hysteresis as well as identical sensitivity through the measurement.

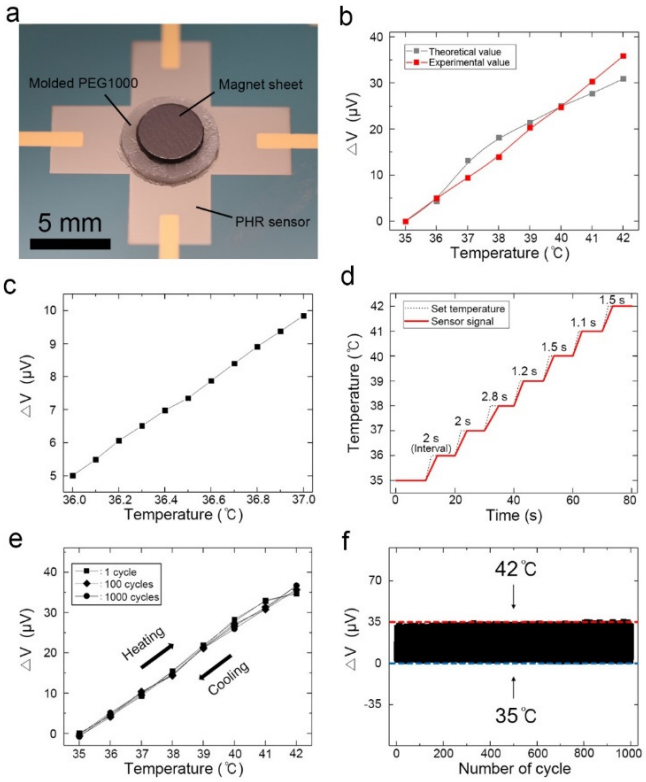

Fig. 2. Normalized electrical performance of new type temperature sensor. a) Photograph of the temperature sensor on wafer. b) Measurements and theoretical calculations of output voltage. c) Output voltage from 36 to 37 °C at intervals of 0.1 °C. d) Response time of the sensor. e) Hysteresis loop, indicating no temperature deviation. f) Cycle test as the temperature changes from 35 to 42 °C.

3. Conclusion

We report an unprecedented design of temperature sensor using a magnetic sensor, magnet sheet, and expanding polymer. The temperature sensor demonstrates attractive properties such as repeatability, tunable temperature ranges, high sensitivity, accuracy, thermal cycling stability, and no thermal hysteresis. Furthermore, we have established a new design which can accommodate reversible volume expansion and also control magnetic field strength depending on temperature.

References

[1] Jeon, J. et al. Flexible wireless temperature sensors based on Ni microparticle-filled binary polymer composites Adv. Mater. **25**, 850 (2013).

[2] Yokota, T. et al. Ultraflexible, large-area, physiological temperature sensors for multipoint measurements PNAS. **112**, 14533 (2015).

[3] Thanh, N. T. et al. Thickness dependence of parallel and perpendicular anisotropic resistivity in Ta/NiFe/IrMn/Ta multilayer studied by anisotropic magnetoresistance and planar Hall effect J. Appl. Phys. **101**, 053702 (2007).

Magneto-optical properties of Bi-YIG thin films prepared by metal-organic decomposition

Viet Dongquoc, Jong-Ryul Jeong*
Department of Materials Science and Engineering, Graduate School of Energy Science and Technology,
Chungnam Nationa University, Daejeon 34134, South Korea

In this study, we have investigated magneto-optical properties of Bi-YIG thin films prepared by metal-organic decomposition(MOD) method. The MOD solution for Bi-YIG thin film was purchased from Kojundu Chemical Laboratory, and it has the composition of Bi:Y:Fe of 1:2:5. The MOD solution was spin coated on the substrate and then was dried at 100°C for 30 min. The spin-coated MOD film was annealed for 1 hour in a tube furnace at oxygen atmosphere at elevated temperature by changing the heating rate. We found that Bi-YIG film annealed with 30°C per minute heating rate at the phase temperature attained the high crystallinity with good morphology. From the measuring of magnetic and Faraday rotation for films made under different heating rates revealed that larger Faraday rotation of -10.5°/μm, attained for 30°C per minute annealed film.

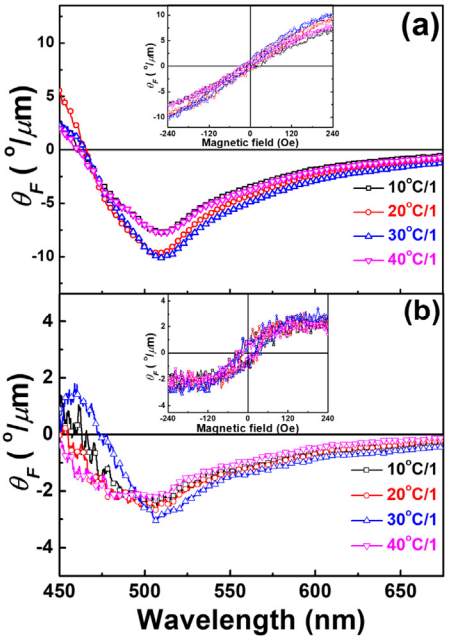

Fig. 1. Faraday rotation spectrum of Bi-YIG thin films
(a) on GGG substrates and (b) on glass substrates by varying heating rate.

KMS 2019 Summer Conference

Special Session Ⅳ

'Magnetization Dynamics'

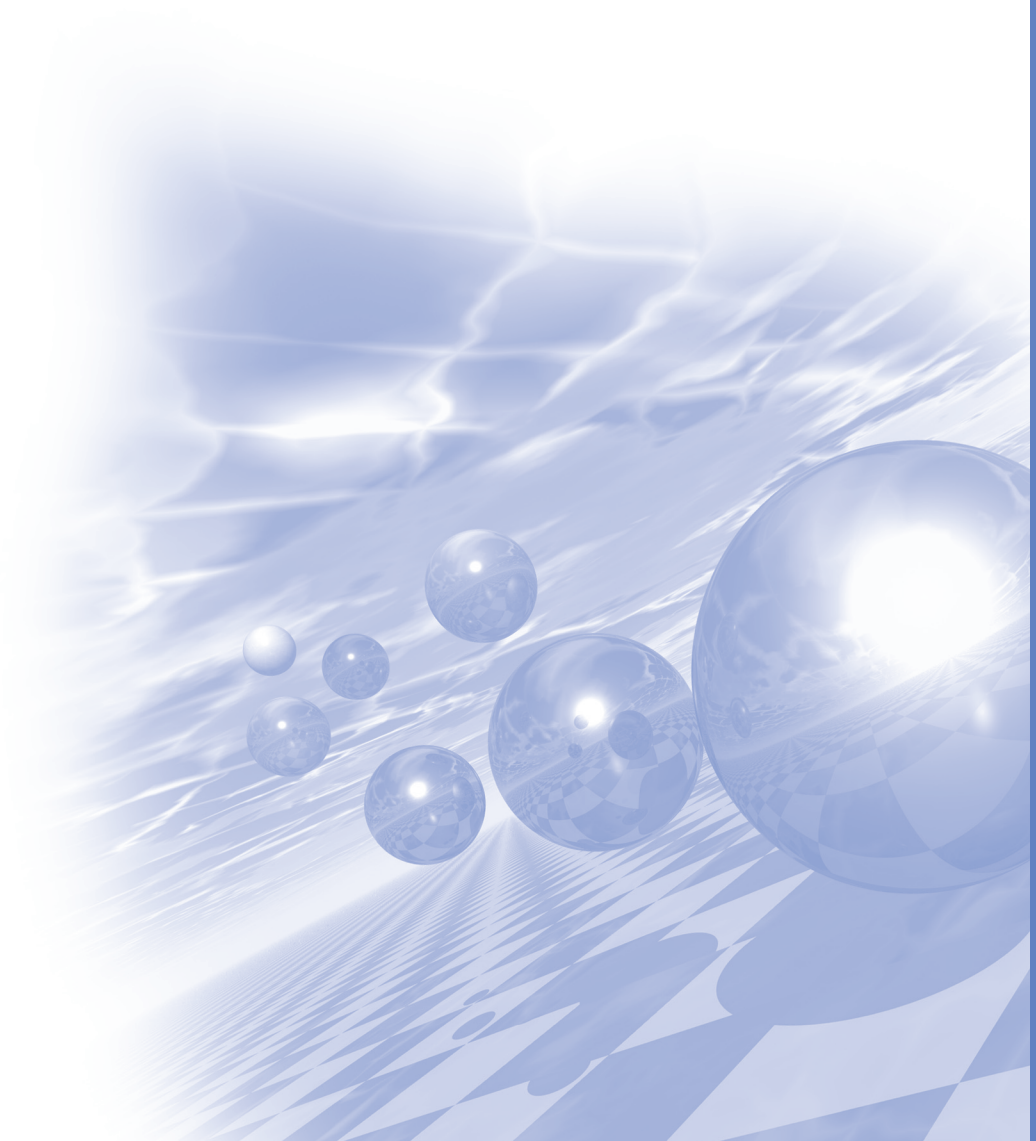

수평자성과 좔로신스키-모리야 상호작용

문경웅*, 김창수, 윤정범, 김동석, 전병선, 이상선, 김동옥, 조재훈, 양승모, 황찬용
한국표준과학연구원

자성체를 박막으로 만들었을 때 면에 수평인 자화방향을 선호하는 성질을 수평자성이라고 한다. 수평자성은 면방향이 안정적이기 때문에 자화방향은 면상에서 360도 자유도를 가진다. 이와 다르게 면에 수직인 방향을 선호하는 성질을 수직자성이라고 한다. 수직자성은 기본적으로 위 또는 아래의 두 가지 방향만 안정적으로 가질 수 있다. 최근 자성분야의 중요한 연구주제는 좔로신스키-모리야 상호작용이다. 이 작용이 수직자성에 적용되면 스커미온 자화상태를 형성한다는 것이 알려져 있다. 이러한 스커미온 자화상태는 자성분야의 또 다른 주요이슈이다. 따라서, 좔로신스키-모리야 상호작용과 스커미온은 최근의 자성동역학의 연구가 주로 수직자성체에 집중되어 진행되고 있는 주요 원인이다. 이번 발표에서는 수평자성에 좔로신스키-모리야 상호작용이 있는 경우 발생하는 몇 가지 흥미로운 상황에 대해 논의하고자 한다. 우선 수평자성체 또한 스커미온 자화상태를 형성 할 수 있다는 결과를 보이고 이를 바탕으로 수평자성에 존재하는 스커미온의 특징을 설명할 것이다. 또 다른 결과로 스핀전달토크가 있을 때 좔로신스키-모리야 상호작용은 안정된 자화방향을 결정 할 수 있음을 발표하고자 한다.

페리자성체/중금속 이종접합에서 마그논(magnon)에 의한 단방향 자기이방성의 거동

이수길[1,2*], 강준호[1], 이재욱[2], 김정목[2], 김상훈[3], 이년종[3], 김창수[4], 문경웅[4], 황찬용[4], 박승영[5], 박병국[2], 김갑진[1]

[1]물리학과, 한국과학기술원
[2]신소재공학과, 한국과학기술원
[3]물리학과, 울산대학교
[4]양자기술연구소, 한국표준연구원
[5]스핀공학물리연구팀, 기초과학지원연구원

반강자성 물질은 THz 영역의 초고속 스핀 동역학을 나타낼 것으로 기대되어 많은 주목을 받고 있다. [1]. 그러나 자화(magnetization)값이 0이고 외부 자계에 쉽게 반응하지 않는 점 때문에 반강자성체를 직접적으로 연구하는 것은 쉽지 않은 실정이다. 페리자성체(ferrimagnet)는 반강자성체에서 기대되는 스핀 동역학을 연구할 수 있는 훌륭한 대안이 될 수 있다. 특히 희토류-전이금속 합금 페리자성체는 반강자성 결합을 가지는 두 개의 이종 원자로 구성되며 조성 및 온도변화에 따라 자화 및 각 운동량이 0이되는 보상 거동을 나타낸다. 이 물질들은 보상점에서 반강자성 스핀동역학을 가질 것으로 이론적으로 예측되거나 실험적으로 증명되어져 왔다. 예를 들어, GdFeCo-페리자성체의 각운동량 보상점에서 1 km/s를 넘는 매우 빠른 자구벽 이동 속도가 실제로 구현되었다 [2]. 하지만 현재 스핀트로닉스 응용의 중심에 다양한 자기저항효과가 자리 잡고 있음에도 불구하고 스핀 동역학이 반강자성 특성을 가지는 물질의 전기저항에 미치는 효과는 상대적으로 연구가 덜 되어 있는 실정이다. 따라서 본 연구에서는 페리자성체에서 스핀 동역학에 의한 자기저항변화가 어떻게 영향을 주는지에 집중했다. 특히, 이러한 연구는 스핀트로닉스에서 반강자성체의 실제적 응용에 대한 단서를 제공 할 수 있다. 강자성체/중금속 이종접합구조에서 최근에 발견 된 단방향 자기저항(unidirectional magnetoresistance)효과는 마그논(magnon)에 의해 유도 될 수 있기 때문에 스핀 동역학과 자기저항효과 사이의 상호 작용을 연구하기 위한 좋은 실험방법이다 [3]. 이 마그논 유도 단방향 자기저항의 기원은 중금속 층에서 페리자성체로의 주입된 스핀 전류가 스핀 플립(spin flip) 프로세스에 의해 마그논을 발생시키거나 제거함에 따라 페리자성체/중금속 이중층의 저항을 변화시키는 것이다. 본 연구발표에서는 스핀 동역학과 전기 수송 사이의 상호 작용을 밝히기 위해 CoGd/Pt 이중층에서 조성과 온도 변화에 따른 마그논 유도 단방향 자기저항효과의 거동을 살펴보고 이를 Brillouin light scattering 스펙트럼과 비교해 보았다.

References

[1] T. Jungwirth, et al, Nature Nanotechnology, 11, 231 (2016).

[2] Kab-Jin Kim, et al, Nature Materials, 16, 1187 (2017).

[3] Kab-Jin Kim, et al, arXiv:1603.08746 (2016); K. Yasuda, et al, Physical Review Letters, 117, 127202 (2016); C. O. Avci, et al, Physical Review Letter, 121, 087207 (2018).

Long-range chiral interlayer exchange coupling in synthetic antiferromagnets

Dong-Soo Han*
Center for Spintronics, Korea Institute for Science and Technology, Seoul, Republic of Korea

The exchange interaction underlies magnetism and thus is responsible for major phenomena in magnetic materials. The exchange coupling combined with spin-orbit coupling comes in two flavours: symmetric and antisymmetric. The symmetric term is the conventional Heisenberg exchange, while the antisymmetric exchange coupling called Dzyaloshinskii-Moriya interaction [1,2] has recently attracted particular interest owing to its major role in rendering topologically non-trivial spin textures[3-5], giving rise to many intriguing phenomena in perpendicularly magnetized multilayers. Beyond the atomic exchange coupling within a single ferromagnetic layer, a symmetric interlayer exchange coupling [6] also leads to ferro- or antiferromagnetic magnetization alignment between individual ferromagnetic thin films. The studies on the interlayer exchange coupling, however, have so far focused only on its symmetric flavour, although from symmetry considerations the interlayer exchange coupling combined with spin-orbit coupling also can lead to the emergence of its antisymmetric component. However, this has so far not been experimentally demonstrated. In this talk, I will present the missing flavour of the antisymmetric interlayer exchange coupling in perpendicularly magnetized synthetic antiferromagnets with parallel and antiparallel couplings.

References

[1] I. A. Dzyaloshinsky, J. Phys. Chem. Solids **4,** 241 (1958).
[2] T. Moriya, Phys. Rev. **120,** 91 (1960).
[3] S. Emori et al., Nat. Mater. **12,** 611 (2013).
[4] S. Woo et al., Nat. Mater. **15,** 501 (2016).
[5] K. Litzius et al. Nat. Phys. **13,** 170 (2016).
[6] P. Bruno et al., J. Magn. Magn. Mater. **121**, 248 (1993).

Low magnetic damping of ferrimagnetic GdFeCo alloys

Duck-Ho Kim[1*], Takaya Okuno[1], Se Kwon Kim[2,3], Se-Hyeok Oh[4],
Tomoe Nishimura[1], Yuushou Hirata[1], Yasuhiro Futakawa[5], Hiroki Yoshikawa[5],
Arata Tsukamoto[5], Yaroslav Tserkovnyak[2], Yoichi Shiota[1], Takahiro Moriyama[1],
Kab-Jin Kim[6], Kyung-Jin Lee[4,7,8] and Teruo Ono[1]

[1]Institute for Chemical Research, Kyoto University, Uji, Kyoto 611-0011, Japan
[2]Department of Physics and Astronomy, University of California Los Angeles, California 90095, USA
[3]Department of Physics and Astronomy, University of Missouri, Columbia, Missouri 65211, USA
[4]Department of Nano-Semiconductor and Engineering, Korea University, Seoul 02841, Republic of Korea
[5]College of Science and Technology, Nihon University, Funabashi, Chiba 274-8501, Japan
[6]Department of Physics, Korea Advanced Institute of Science and Technology, Daejeon 34141, Republic of Korea
[7]Department of Materials Science & Engineering, Korea University, Seoul 02841, Republic of Korea
[8]KU-KIST Graduate School of Converging Science and Technology, Korea University, Seoul 02841, Republic of Korea

Magnetic damping, commonly described by the Gilbert damping parameter, represents the magnetization relaxation phenomenon, describing how quickly magnetization spins reach equilibrium. Understanding the fundamental origin of the damping as well as searching for low damping materials has been a central theme of magnetism research. Several theoretical models for magnetic damping have been proposed and compared with experiments. However, the majority of these studies have focused only on ferromagnetic systems. We investigate the Gilbert damping parameter α for rare earth (RE)-transition metal (TM) ferrimagnets over a wide temperature range [1]. Extracted from the field-driven magnetic domain-wall (DW) mobility, α was as low as 7.2×10^{-3} and was almost constant across the angular momentum compensation temperature T_A, starkly contrasting previous predictions that α should diverge at T_A due to vanishing total angular momentum. Thus, magnetic damping of RE-TM ferrimagnets is not related to the total angular momentum but is dominated by electron scattering at the Fermi level where the TM has a dominant damping role. Furthermore, we investigated α measured by spin-torque (ST)-FMR technique with analysis based on new equation of FMR for ferrimagnets. Therefore, both DW motion and ST-FMR give the same conclusion that the damping parameter is small and remains almost constant with temperature.

Reference

[1] D.-H. Kim et al Phys. Rev. Lett. **122**, 127203 (2019).

Electric field induced spin waves on the CoFeB disk-shaped nanomagnet

조재훈*
한국표준과학연구원

1. Introduction

Voltage control of magnetic properties in metallic ferromagnets is attracting much attention because of its potential to be a key technology in the production of ultralow energy consumption spintronic devices. Voltage control of the exchange stiffness constant, A_{ex}, was first predicted by a theory[1] to explain an experimental result, which shows voltage control of the Curie temperature[2]. The voltage control of the A_{ex} was also evaluated from observations about voltage dependent domain size[3,4]. However, those results may include contradictions. Therefore, here we propose an independent and more precise measurement technique about A_{ex} using a spinwave mode observations[5], and provides reliable experimental data about the voltage modulation of the A_{ex} in the magnetic tunnel junction with perpendicular magnetization.

2. Experimental methods and results

In this study, a 65-nm-diameter magnetic tunnel junction (MTJ) with 1.5-nm-thick CoFeB free layer which has perpendicular magnetic anisotropy was prepared by electron-beam lithography to investigate voltage modulation in A_{ex} and magnetic anisotropy (K_s). The thermally excited ferromagnetic resonance (TE-FMR) measurements were employed to measure the voltage effect on spinwaves in the free layer of the MTJ. Typical TE-FMR spectra which were taken at 6.0 GHz as a function of the external magnetic field under a dc bias of ± 0.52 V as shown in Fig. 1. From voltage effects on the resonance frequency, voltage modulation of A_{ex} and K_s can be determined. The voltage modulation of A_{ex} is determined as 0.31 ± 0.04 pJ/m with a 1 V application through a 1.2 nm-thick-MgO layer. This corresponds to $d(A_{ex})/dE$ = 0.26 ± 0.04 $\times 10^{-21}$J/V for the 1.5 nm CoFeB film. The voltage modulation of A_{ex} corresponds to 8.1 % change under 1 V/nm electric field. In addition, we determined voltage controlled magnetic anisotropy as -60 ± 24 fJ/Vm.

3. Summary

The electric field dependence of the spinwave eigen frequencies showed a different electric field change for different radius nodal modes. Such properties made it possible to independently evaluate the electric field dependence of Aex. The analysis provided an electric field modulation in A_{ex} of 0.26 ± 0.04 $\times 10^{-21}$ J/V for the 1.5 nm CoFeB film. This corresponded to an 8.1 % change in A_{ex} under a 1 V/nm electric field. The effect is useful for controlling the domain size, T_c, and other magnetic properties by the application of an electric field.

Role of the topological singularity in magnetic-vortex dynamics

Hee-Sung Han[1], Mi-Young Im[2], Young-Sang Yu[3], Min-Seung Jung[4], Sooseok Lee[1], Jung-Il Hong[4] and Ki-Suk Lee[1*]

[1]School of Materials Science and Engineering,
Ulsan National Institute of Science and Technology (UNIST), Ulsan 44919, Korea
[2]Center for X-ray Optics, Lawrence Berkeley National Laboratory, Berkeley, CA, 94720, USA
[3]Advanced Light Source, Lawrence Berkeley National Laboratory, Berkeley, CA, 94720, USA
[4]Department of Emerging Materials Science, DGIST, Daegu, 42988, Republic of Korea

A Bloch point (BP) is, as far as we know, the only magnetization singularity in a ferromagnet at which the local magnetization vanishes. Around the BP, magnetizations are formed the unique topological structure having an integer topological number. In nanomagnetic systems, BPs bear critical roles in many dynamical phenomena of spin structures. In general, BPs should be mediated to achieve a change in the topological numbers in spin structures. For example, the switching of magnetic vortex core, which implies the change of the topological number from +1/2 to -1/2 or vice versa, is accomplished through the injection and propagation of the BPs [1-3]. Besides such a vital role in the switching dynamics, it has atomistic nature since the virtual magnetization-vanishing point should be located in the middle of the lattice point. To observe such intrinsic natures of BP, it is indispensable to form a BP in magnetic nanostructures.

In this presentation, we report experimental observation of steady-state BPs in the middle of elongated magnetic vortex cores in asymmetrically shaped Permalloy nanodisks [4] by using the magnetic transmission soft X-ray microscopy (MTXM) at the Advanced Light Source [5]. From time-resolved nanoscale magnetic X-ray imaging combined with micromagnetic simulations, detailed dynamic character of BPs, revealing rigid and limited lateral movements under magnetic field pulses as well as its crucial role in vortex-core dynamics.

References

[1] Thiaville, A. & Miltat, J. Europhys. Lett. 26, 57 (1994).
[2] Wohlhüter, P. et al. Nat. Commun. 6, 7836 (2015).
[3] Noske, M., Stoll, H., Fähnle, M., Hertel, R. & Schütz, G. Phys. Rev. B 91, 014414 (2015).
[4] Im, M., Han, H.-S., et al. Nature Commun. 10, 593 (2019).
[5] Fischer, P. et al. Mater. Today 9, 26-33 (2006).

Plenary Session II

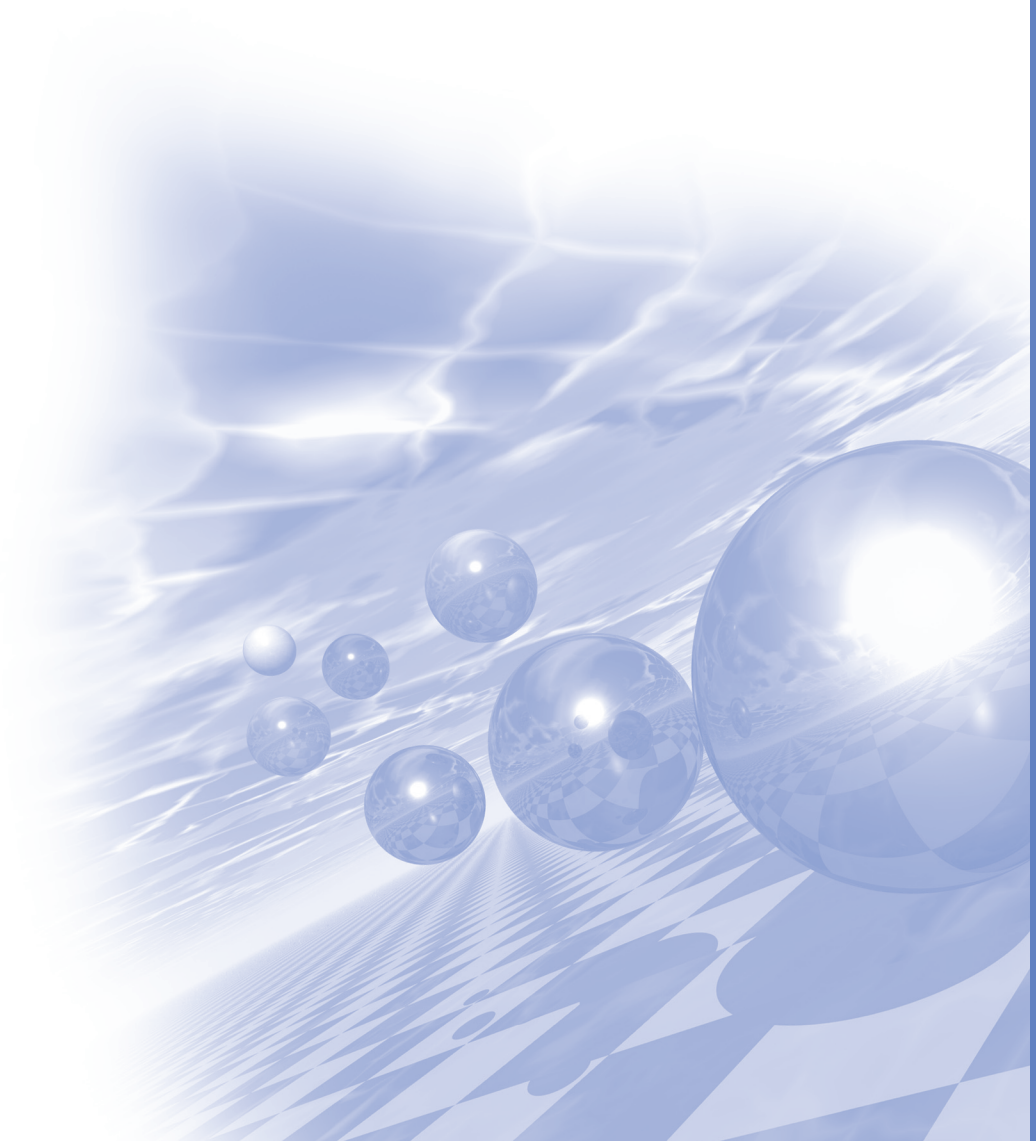

Nanomembranes: From basic concepts to paradigm shifting technologies

Oliver G. Schmidt*
Leibniz-Institut für Festkörper-und Werkstoffforschung Dresden

Nanomembranes are thin, flexible, transferable and can be shaped into unique 3D micro-and nanoarchitectures. This makes them attractive for various scientific disciplines and application scenarios ranging from flexible magnetoelectronics and strainable quantum photonic devices to unique 3D microsystems for functional deployment both on and off the chip.

If assembled into microtubes, rolled-up nanomembranes represent cylindrical microobjects with intriguing optical, plasmonic, electronic and magnetic properties. These lead to exciting application potential in 3D electronics and photonics, sensorics and energy storage units. As off-chip components rolled-up microtubes address novel biophysical and biomedical applications such as biomimetic microelectronics and powerful self-propelling microautonomous systems. Based on these concepts, cellular cyborg machinery is put forth as a new scheme for targeted drug delivery and reproduction technologies.

Prof. Oliver G. Schmidt
Institute Director

Name	Schmidt, Prof. Dr. Oliver G.
Department	4000
Address	IFW Dresden Helmholtzstraße 20
	01069 Dresden
Phone Number	+49-351-4659-800
Email	o.schmidt(at)ifw-dresden.de

Google Scholar Citations

Personal

Name:	Oliver G. SCHMIDT
Date of Birth:	4th July, 1971
Place of Birth:	Kiel, Germany

Awards and Honours

2019	ERC Advanced Grant, European Research Council
2018	Gottfried Wilhelm Leibniz Prize, German Research Foundation
2018	Elected member of the German Academy of Science and Engineering (acatech)
2018	Highly Cited Researcher, Clarivate Analytics
2013	International Dresden Barkhausen Award, Materials Research Network Dresden
2012	New Research Building "Materials, Architectures and Integration of Nanomembranes" (MAIN), Federal state and Free State of Saxony
2011	Honorary Professor, Fudan University, Shanghai, China
2010	Guinness World Record® for the Smallest Man-Made Jet Engine
2010	Ace of Saxony, Free State of Saxony
2010	Nanotechnology Thought Leader, AzoNano
2006	Carus-Prize, City Schweinfurt
2005	Carus-Medal, German Academy of Natural Scientists Leopoldina
2004	Laureate of the competition "Images of Science", Max-Planck-Society
2004	Heinrich-Düker-Prize, Kepler-Seminar for Natural Sciences
2003	Laureate of the Young Scientist competition "Nanotechnology", German Federal Ministry for Education and Research
2002	Philip-Morris Research Award, Philip-Morris GmbH
2000	Otto-Hahn Medal, Max-Planck-Society
1999	*Summa cum laude* for PhD thesis, Berlin University of Technology
1993	Perkin-Elmar-Prize, King's College London

Professional career

2007 -	Director, Institute for Integrative Nanosciences, Leibniz IFW Dresden, Germany
2007 -	Full Professorship, Material Systems for Nanoelectronics, Chemnitz University of

	Technology, Germany
2004 - 2007	Private lecturer, University of Stuttgart
2002 - 2007	Head of research group, Max-Planck-institute for Solid State Research, Stuttgart
2001 - 2002	Research associate, University of Southern California
1999 - 2001	Research associate, Max-Planck-Institute for Solid State Research, Stuttgart
1996 - 1999	Research assistant, Max-Planck-Institute for Solid State Research, Stuttgart

Education

2003	Habilitation (postdoctoral lecture qualification), University of Hamburg, Germany
1999	Graduation to Dr. rer. nat., Berlin University of Technology, German
1996	Diploma in Physics
1993 - 1996	Studies of Physics, Berlin University of Technology, Germany
1993	Bachelor of Science in Physics
1992 - 1993	Studies of Physics, King's College London, England
1990 - 1992	Studies of Physics, Christian-Albrechts-University of Kiel, Germany
1990	"Abitur", German School London, England

Memberships

2019 -	Adjunct Professorship for Nanophysics, Faculty of Physics, TU Dresden
2019 -	Principal Investigator within Cluster of Excellence "Complexity and Topology in Quantum Matter (ct.qmat)", TU Dresden
2018 -	Task Force, Research Center MAIN ("Materials, Archtectures, and Integration of Nanomembranes")
2017 -	Section D, Leibniz Association
2012 - 2019	Principal Investigator within Cluster of Excellence "Center for Advanced Electronics Dresden (CfAED)", TU Dresden
2012 - 2018	Speaker of Center for Materials, Architectures and Integration of Nanomembranes (MAIN)
2012 - 2018	Principal Investigator within Cluster of Excellence "Merge Technologies for Multifunctional Lightweight Structures (MERGE)", TU Chemnitz
2010 -	Institute of Physics, TU Chemnitz
2009 -	Faculty for Natural Sciences, TU Chemnitz
2009 -	Leibniz Institute for Solid State and Materials Research Dresden (Leibniz IFW Dresden)
2007 -	Faculty for Electrical Engineering and Computer Science, TU Chemnitz
1994 -	German Physical Society

Editorial Board Memberships

2017 -	Editorial board member, "Advanced Materials Technologies"
2014 - 2017	Founding editorial board member, "Physical Review Applied"
2012 -	Editorial board member, "Particle"
2007 - 2009	Editorial board member, "Journal of Physics D: Applied Physics"
2006 - 2014	Regional editor (Europe), "Nanoscale Research Letters"

Review services for journals and magazines

- Nature
- Nature Materials
- Nature Nanotechnology
- Nature Photonics
- Nature Physics
- Nature Chemistry
- Nature Communications
- Science Robotics
- Science Advances
- Nano Letters
- ACS Nano
- JACS
- Angewandte Chemie
- Advanced Materials
- Physical Review Letters
- Nanomedicin
- Applied Physics Letters
- and many more…

Review services for foundations

- German Research Society
- European Research Council (ERC)
- European Union
- Alexander von Humboldt Foundation
- United States Department of Energy
- United States National Science Foundation
- US-Israel Binational Science Foundation
- Swiss National Fonds
- and many more…

KMS 2019 Summer Conference

Special Session V

'Advanced Information Technology based on spin-orbit coupling'

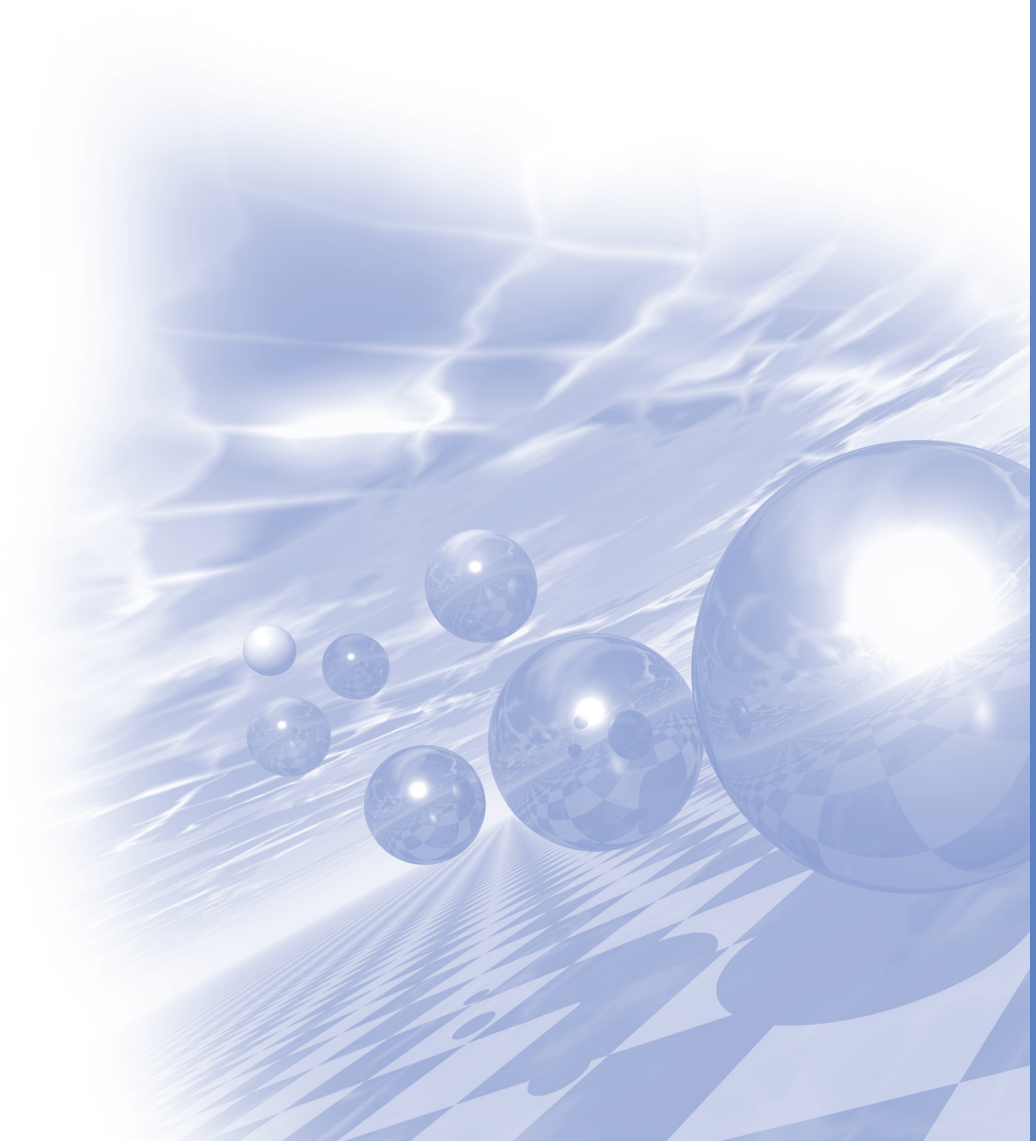

PMA, SOT, and DMI in Non-Centrosymmetric Artificial Superlattices

Teruo Ono[1,2*]

[1]Institute for Chemical Research, Kyoto University, Uji, Kyoto 611-0011, Japan
[2]Center for Spintronics Research Network, Graduate School of Engineering Science, Osaka University, Osaka 560-8531, Japan

Perpendicular magnetic anisotropy (PMA), spin-orbit torque (SOT), and Dzyaloshinskii-Moriya interaction (DMI) are essential ingredients in spintronics. All these effects are known to be a consequence of the inversion symmetry breaking, and main platforms for the investigation of them have been the interfaces of bilayers where the inversion symmetry are locally broken. In this talk, I will introduce a new platform, non-centrosymmetric artificial superlattices, in which the inversion symmetry is broken throughout whole structure, resulting in bulk PMA, SOT and DMI.

Interface-generated spin current and spin-orbit torques

Seung-heon Chris Baek[1,2], Young-Wan Oh[1], Kyung-Jin Lee[3,4] and Byong-Guk Park[1*]
[1]Department of Materials Science and Engineering, KAIST, Daejeon, Korea
[2]School of Electrical Engineering, KAIST, Daejeon, Korea
[3]Department of Materials Science and Engineering, Korea University, Seoul, Korea
[4]KU-KIST Graduate School of Conversing Science and Technology, Korea University, Seoul, Korea

Spin-orbit torque (SOT) arising from spin-orbit coupling has gained much attention because it promises efficient magnetization switching in spintronic devices. It is important for device applications that the SOT switches perpendicular magnetizations without an external magnetic field. In this talk, we demonstrate field-free SOT switching of perpendicular magnetization in ferromagnetic trilayers, in which spin currents generated at the bottom ferromagnet interface transit the spacer layer and exert a torque on the top ferromagnet [1]. In such structures, spin currents have an out-of-plane (z) component of the spin polarization, enabling all-electrical SOT switching of perpendicular magnetization. Our findings of interface-generated spin current broaden the scope of material engineering for energy-efficient SOT-based spintronic devices.

Reference

[1] S.-h. C. Baek, et al., Nat. Mater. **17,** 509 (2018).

Bulk-like spin-orbit torques in ferrimagnets

Hyunsoo Yang*
Department of Electrical and Computer Engineering, National University of Singapore, Singapore
e-mail: eleyang@nus.edu.sg

Spin-orbit torques (SOTs) have been recently studied for its potential applications in memory and logic devices, mostly with ferromagnetic thin films. As the cell size shrinks, these ferromagnetic thin films are thermally unstable due to their sub nano-meter thicknesses. We study SOT-induced magnetization switching and effective fields in rare earth-transition metal (RE-TM) ferrimagnet alloy films and multilayers. We show that devices from the structure of heavy metal/ferrimagnet present a huge switching efficiency and maximum spin-orbit effective fields. It is observed that the switching efficiency and SOT effective fields increase by one order of magnitude as the ferrimagnet approaches compensation. This anomalous increase of the switching efficiency and SOT effective fields is attributed to the negative exchange interaction field due to the antiferromagnetic ordering between the Co and Gd sub-lattices [1]. The negative exchange interaction makes the ferrimagnet thermally stable near compensation by increasing its anisotropy and also provides the exchange coupling torque that assists in switching, effectively increasing the overall switching efficiency of ferrimagnetic SOT devices. We report a long spin coherence length and associated bulk-like torque characteristics in an antiferromagnetically coupled Co/Tb ferrimagnetic multilayer [2]. A strong THz output is also observed from a compensated ferrimagnet /heavy metal bilayer, CoGd/Pt with nearly zero magnetization [3]. It is found that the net spin polarization of the laser induced spin current, rather than the net magnetization, accounts for the THz emission. Our results trigger a ferrimagnet as a core building block in spintronics.

References

[1] R. Mishra et al., Phys. Rev. Lett. **118**, 167201 (2017)
[2] J. Yu et al., Nature Mater. **18**, 29 (2019)
[3] M. Chen et al., Adv. Opt. Mat. **6**, 1800430 (2018)

Abnormal asymmetric motion of magnetic solitons with multiple inversion asymmetries

Kyoung-Whan Kim[1,2*], Seo-Won Lee[3], Kyoung-Woong Moon[4], Jung-Hwan Moon[3], Gyungchoon Go[3], Nico Kerber[2], Jonas Nothhelfer[2], Aurélien Manchon[5], Hyun-Woo Lee[6], Karin Everschor-Sitte[2] and Kyung-Jin Lee[3,7]

[1]Center for Spintronics, Korea Institute of Science and Technology, Korea
[2]Institute of Physics, Johannes Gutenberg University Mainz, Germany
[3]Department of Materials Science and Engineering, Korea University, Korea
[4]Spin Convergence Research Team, Korea Research Institute of Standards and Science, Korea
[5]Computer, Electrical and Mathematical Science and Engineering Division, King Abdullah University of Science and Technology, Saudi Arabia
[6]Department of Physics, Pohang University of Science and Technology, Korea
[7]KU-KIST Graduate School of Converging Science and Technology, Korea University, Korea

Recent interest of spintronics researches has converged to magnetic systems with inversion symmetry breaking. New physical phenomena in these systems, including spin-orbit torque, Dzyaloshinskii-Moriya interaction, magnetic skyrmions, and chiral domain walls, are intensively studied in the past decade and it turns out that they have significant potential for high efficient spintronic devices. The rich physics in chiral magnets originate from the combination of time reversal asymmetry (i.e., magnetism) and spatial inversion asymmetry (i.e. interfaces in thin films).

In this talk, we demonstrate that introduction of another inversion asymmetry makes magnetization dynamics further interesting. We mainly consider two systems, magnetic skyrmion in the presence of both interfacial and bulk inversion symmetry [1] and in-plane magnetic domain wall in the presence of the interfacial Dzyaloshinskii-Moriya interaction [2], and report their counterintuitive behaviors under driving forces.

References

[1] K.-W. Kim, K.-W. Moon, N. Kerber, J. Nothhelfer, and K. Everschor-Sitte, Phys. Rev. B **97**, 224427 (2018).

[2] K.-W. Kim, S.-W. Lee, J.-H., Moon, G. Go, A. Manchon, H.-W. Lee, K. Everschor-Sitte, and K.-J. Lee, Phys. Rev. Lett. in press (arXiv:1803.10776).

Orbital Anisotropic Magnetoresistance

Hye-Won Ko[1*], Hyeon-Jong Park[1], Gyungchoon Go[2], Jung Hyun Oh[2],
Kyoung-Whan Kim[3], Hyun Cheol Koo[3] and Kyung-Jin Lee[1,2]

[1]KU-KIST Graduate School of Converging Science and Technology, Korea University, Seoul 02841, Korea
[2]Department of Materials Science and Engineering, Korea University, Seoul 02841, Korea
[3]Center for Spintronics, Korea Institute of Science and Technology, Seoul 02972, Korea

Based on first-principles calculation, we demonstrate that longitudinal orbital currents in ferromagnets (FMs) depend on the magnetization direction, which contribute to the anisotropic magnetoresistance (AMR). We call this orbital contribution to the AMR as the *orbital anisotropic magnetoresistance* (OAMR). The OAMR occurs due to effective correlation between the orbital and magnetization via a concerted action of the spin-orbit coupling and exchange coupling. Unlike the orbital Hall effect [1,2] for which the orbital hybridization is essential, the OAMR arises from the anisotropic orbital splitting, which is generally present in all materials, but does not need the orbital hybridization.

References

[1] H. Kontani, T. Tanaka, D. S. Hirashima, K. Yamada, and J. Inoue, Phys. Rev. Lett. **102**, 016601 (2009).
[2] D. Go, D. Jo, C. Kim, and H. -W. Lee, Phys. Rev. Lett. **121**, 086602 (2018).

KMS 2019 Summer Conference

Special Session II

'Hard & Soft Magnetic Materials: 고성능 모터용 자석 개발'

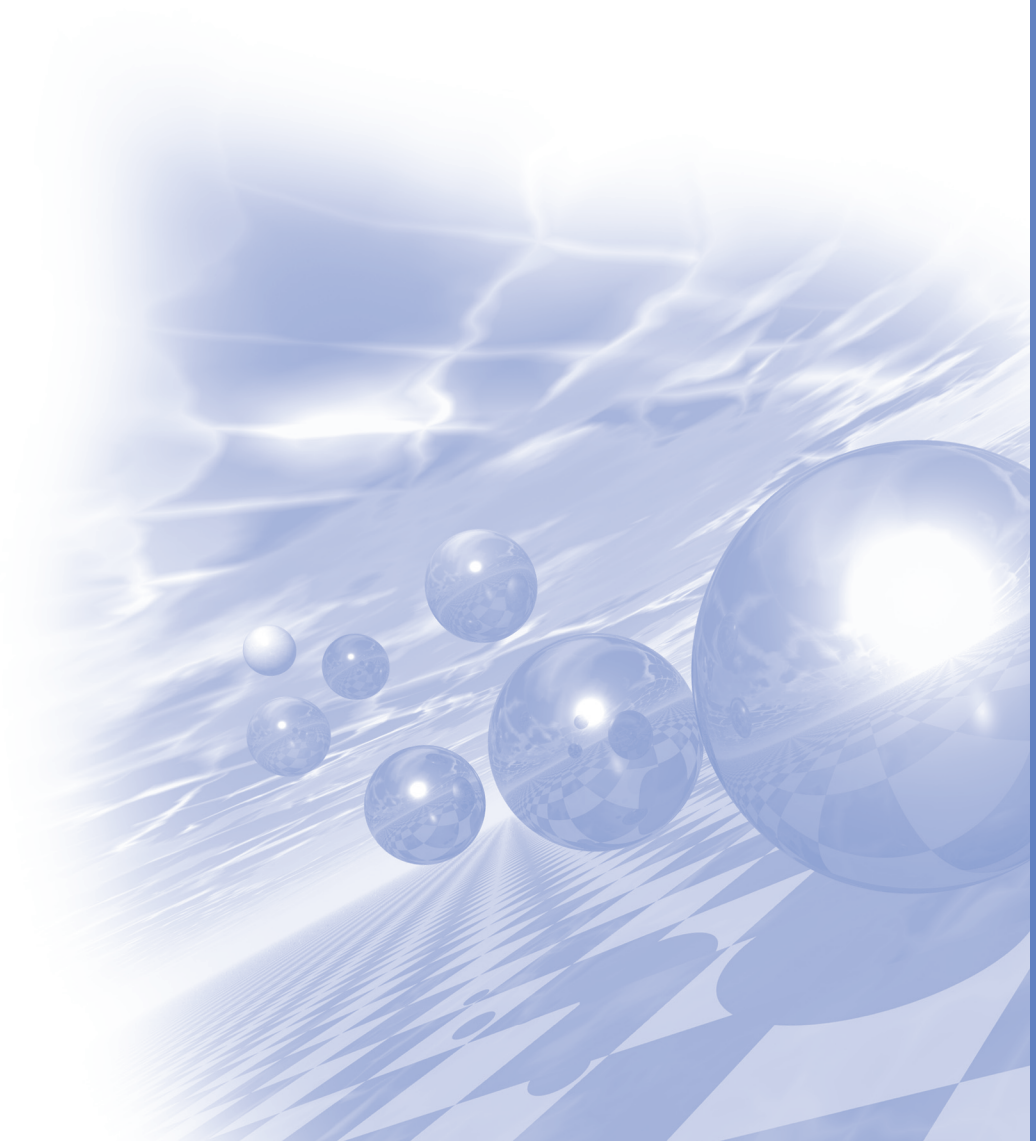

Microstructures and Magnetic Properties of Fe-rich Compounds with $ThMn_{12}$ Structure

Jihoon Park*, Hui-Dong Qian, Jung-Tae Lim, Jong-Woo Kim and Chul-Jin Choi†
Powder & Ceramic Division, Korea Institute of Materials Science, Changwon, Gyeongnam, 51508, South Korea

Iron-rich rare-earth (RE) alloys with tetragonal $ThMn_{12}$ structure have been extensively studied as a potential high performance permanent magnetic material due to its high saturation magnetization of 1.78 T, anisotropy field of 12 T and Curie temperature of 859 K [1]. However, its low intrinsic coercivity prohibits its use as a permanent magnetic material. Therefore, in this work, we have synthesized light RE elements and/or Vanadium doped Sm-Fe-Ti alloys, and modified grain boundaries with Sm-based diffusion materials to investigate microstructure and magnetic properties.

$(Sm_{1-x-y}Re_xZr_y)(Fe_{0.8}Co_{0.2})_{11}Ti_{1-z}V_z$ ribbons were prepared by arc-melting raw material pieces and melt-spinning. The melt-spun ribbons were ground and pressed to produce green bodies, and the green bodies were heat-treated at various temperatures ranging from 800 to 1000 ^oC, followed by water quenching. The synthesized $ThMn_{12}$ structured $(Sm_{1-x-y}Re_xZr_y)(Fe_{0.8}Co_{0.2})_{11}Ti_{1-z}V_z$ were mixed with a grain boundary diffusion material and heat-treated to produce grain boundary modified $(Sm_{1-x-y}Re_xZr_y)(Fe_{0.8}Co_{0.2})_{11}Ti_{1-z}V_z$ bulk.

The hysteresis loops of La and Ce doped samples exhibit enhanced intrinsic coercivity with minor degradation of saturation magnetization. The degrees of the grain boundary diffusion varied based on the diffused materials and heat-treatment conditions. The obtained grain boundary modified $(Sm_{1-x-y}Re_xZr_y)(Fe_{0.8}Co_{0.2})_{11}Ti_{1-z}V_z$ bulks have increased intrinsic coercivity and reduced saturation magnetization. The details of the microstructure and magnetic properties of the synthesized $(Sm_{1-x-y}Re_xZr_y)(Fe_{0.8}Co_{0.2})_{11}Ti_{1-z}V_z$ bulk will be discussed.

Reference

[1] Y. Hirayama, Y. K. Takahashi, S. Hirosawa, and K. Hono, Scripta Materialia, vol. 138, p.62 (2017).

Magnetic Properties of Rare-earth (NdFeB) and Rare-earth-free (Mn-based) Permanent Magnets

Sumin Kim[1*], Hyun-Sook Lee[1], Donghwan Kim[2], Jong Wook Roh[3] and Wooyoung Lee[1†]
[1]Department of Materials Science and Engineering, Yonsei University, Seoul 03722, Republic of Korea
[2]R&D center, Star Group, Daegu 42714, Republic of Korea
[3]School of Nano & Materials Science and Engineering, Kyungpook National University, Gyeongsangbuk-do 37224, Republic of Korea

The realization of efficient electric vehicle motors or power generation systems for wind turbines necessitates the development of high-performance permanent magnets, which is associated with a number of challenges. Since their discovery in 1984, high-coercivity sintered Nd-Fe-B magnets have found numerous practical and industrial applications, e.g., as components of actuators, motors, and generators. And Mn-based, rare-earth free magnetic materials such as MnBi and MnAl are considered to be promising candidates to bridge the gap between Alnico/ferrite-based magnets and rare-earth based magnets, including Sm-Co and Nd-Fe-B, owing to their magnetic properties.

The low-temperature-phase (LTP) of MnBi has attracted much attention as a desirable material for a rare-earth-free permanent magnet that can be used in high-temperature (～200 ℃) applications because of its higher coercivity than Nd-Fe-B magnets at the high temperatures. In this regards, there have been many efforts to obtain the LTP-MnBi bulks and thin films. We report on the magnetic properties of large, compacted, sintered LTP MnBi bulks with dimensions of 20.3×15.3×10.3 mm^3 and multi-layered LTP-MnBi thin films.

The ferromagnetic τ-phase in MnAl with an ordered body-centered tetragonal $L1_0$ structure has attracted much attention because of its high magnetic moment, high magnetic crystalline anisotropy constant, and low density. In particular, it has the advantages of abundant and inexpensive elements, high mechanical strength, and good machinability. We studied on phase stability using formation energy of Mn-Al-C system to find the optimal content of carbon required to stabilize the τ-MnAl phases in Mn-Al-C powders, leading to enhanced magnetic properties (especially, remanence magnetization and saturation magnetization).

Generally, the coercivity of Nd-Fe-B magnets at room temperature can be enhanced by the partial replacement of Nd by Dy, Tb, or both; however, the high cost and scarcity of these rare earths preclude the widespread application of this method and necessitate the development of more economically viable alternatives. One of such alternatives is the reduction of heavy rare earth elements (e.g., Dy and Tb) usage and minimization of remanence and energy product loss via the utilization of the grain boundary diffusion process. Herein, we enhance the not only coercivity, but also thermal stability by grain boundary diffusion process and consecutive heat treatments for application in a high-temperature environment such as electric motors.

Selective Laser Melting Processing of Soft Magnetic Bulk Metallic Glass

Jae Won Jeong[1*], Yeong Gyun Nam[1], Mi Se Chang[1], Sangsun Yang[1], Jung-Goo Lee[2], Yong-Jin Kim[1] and Ji Hun Yu[3]

[1]Metal Powder Department, Korea Institute of Materials Science, 797 changwondae-ro, Seongsan-gu, changwon 51508, Korea

[2]Functional Powder Department, Korea Institute of Materials Science, 797 changwondae-ro, Seongsan-gu, changwon 51508, Korea

[3]3D Printing Materials Center, Korea Institute of Materials Science, 797 changwondae-ro, Seongsan-gu, changwon 51508, Korea

Soft-magnetic bulk metallic glasses (BMG) have been pursued because they exhibit extremely low core loss due to high resistivity originated from disordered atomic arrangement while possessing much higher permeability when compared with conventional electrical steel, and it also can realize 3-dimensial components with optimized magnetic path realizing small, light-weight, and highly efficient devices. However, the actual applications of BMGs have been restricted because glass forming ability is limited and fully amorphous phased BMG could be fabricated only in thickness of several millimeters. As an alternative, successive processing of selective laser melting (SLM) of thin metal powder layers can be a promising solution. SLM process is a kind of rapid melting/quenching process with quenching rate in the degree of 10^3~10^5, which is sufficient for BMG alloys with moderate saturation magnetization (<1.4 T), and might be applicable to high Fe-content amorphous alloys with expected saturation magnetization above 1.6 T. SLM process also can realize 3-dimensional near-shaping of SMC components with optimized magnetic path ways eventually realizing small, light-weight, and highly efficient devices. However, up to date, there are little reports on magnetic and mechanical properties of SLM-processed soft magnetic BMGs, and considerable researches should be done for next step. Here we present a study on microstructure and magnetic properties of partially-crystallized soft magnetic alloys prepared by selective laser melting process adopting double-scan strategy.

Analysis techniques based on magneto-optical Kerr effect

Dong-Hyun Kim*
Department of Physics, Chungbuk National University, Cheongju 28644, Korea

Various analysis technique based on magneto-optical Kerr effect (MOKE) to investigate magnetic materials will be reviewed. MOKE is a surface-sensitive technique, providing a relatively cheap and fast access to exploration of magnetic state of film samples, which allows us to measure numerous valuable magnetic properties such as major/minor magnetic hysteresis curve, relaxation curve, and magnetic domain. Very recently, it has been also known that MOKE can be utilized to investigate ultrafast dynamic properties of magnetic systems on femto/picosecond timescales when combined with a stroboscopic pump-probe measurement technique. In this talk, basic of MOKE measurement/analysis, together with basic understanding of hysteresis, relaxation curve, and magnetic domain formation will be reviewed. Time-resolved MOKE technique will be also reviewed, together with basic understanding of magnetization precession and ultrafast magnetic cooling effect on an ultrafast timescale.

High Performance Magnetic Materials based on Metastable Iron / Iron Oxides

Youn-Kyoung Baek*, Kyung Min Kim and Jung-Goo Lee
Powder & Ceramic Division, Korea Institute of Materials Science (KIMS), Korea

Research on rare-earth free magnetic materials with both high magnetization and coercive field is important for a wide range of applications including clean energy and information processing. Thus, Fe based magnetic material has been suggested as a one of promising candidate due to their advantages such as abundant amount of Fe on the earth and their large saturation magnetization. However, to meet the requirement for a future rare-earth free permanent magnet, it is essential to enhance coercive field. In this study, we have developed Fe or Fe oxide based magnetic particles based on metastable phases to enhance coercive filed via conventional synthetic methods. The strategy in this work would pave the way for the industrial production of rare-earth free high performance magnetic materials based on metastable phases.

This study was supported by the Fundamental Research Program of the Korean Institute of Materials Science (Grant PNK6040)

KMS 2019 Summer Conference

Special Session VI

'뫼스바우어 분광분석을 활용한 융합연구'

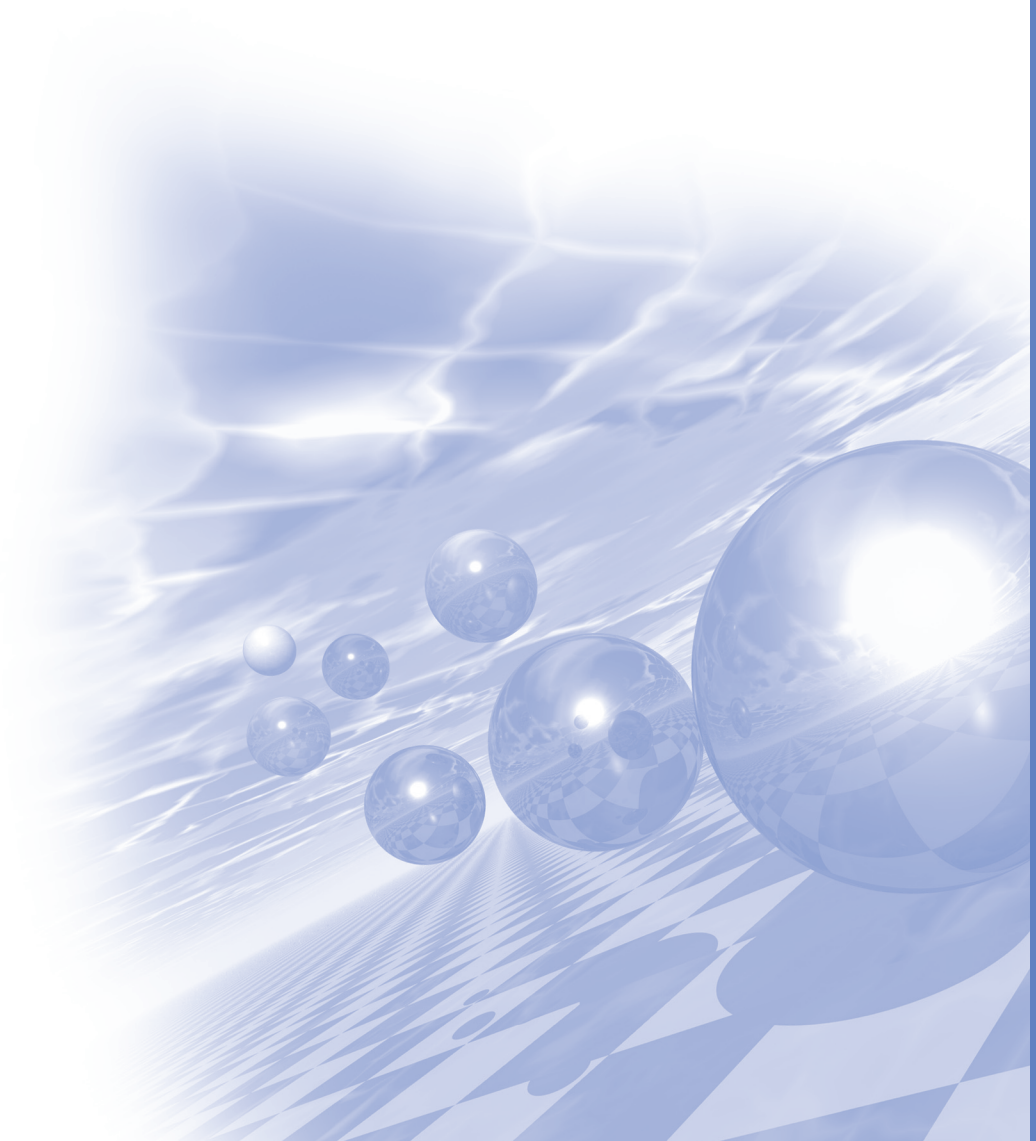

Electrochemically activated cobalt nickel sulfide for an efficient oxygen evolution reaction: partial amorphization and phase control

Sungwook Mhin[1*], Hyuksu Han[2]
[1]Heat Treatment R&D group, Korea Institute of Industrial Technology
[2]Department of Materials Science and Engineering, Hongik University

It has recently been demonstrated that the OER activity of transition metal sulfides (TMSs) could be enhanced by the introduction of a thin amorphous layer on a pristine surface. We report here a novel strategy to enhance the OER by developing cobalt nickel sulfide ($Co_xNi_{1-x}S_2$, CNS) with a high density of crystalline and amorphous phase boundaries. Electrochemical activation (ECA) can partially amorphize hollow CNS nanoparticles derived from surface-selective sulfidation. The ECA-treated CNS (ECA-CNS) electrocatalyst, which is comprised of CNS nanodots separated by thin amorphous layers, shows high densities of crystalline and amorphous phase boundaries. This catalyst shows superior OER catalytic performance with a current density of 10 mA cm^{-2} at a small overpotential of 290 mV, a low Tafel slope of 46 mV dec^{-1}, a high mass activity of 217 A g^{-1}, a high turnover frequency of 0.21 s^{-1} at an overpotential of 340 mV, and excellent stability in alkaline media.

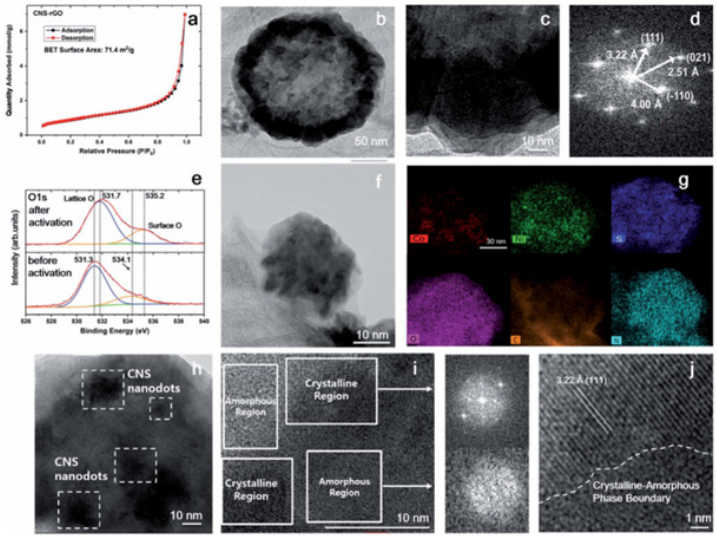

Fig. (a) N_2 adsorption-desorption isotherm of CNS-rGO and (b) TEM image of CNS-rGO with a typical hollow structure. (c) HR-TEM image of CNS-rGO and (d) the corresponding FFT pattern. (e) XPS spectra of CNS-rGO before and after the electrochemical activation process. (f) TEM image of ECA-CNS with the (g) corresponding elemental mapping images for Co, Ni, S, O, S, and N. (h) HR-TEM image of ECA-CNS (i) showing CNS nanodots separated by amorphous phases with (j) a magnified view of the crystalline/amorphous phase boundary.

Reference

[1] S. Mhin et al., Electrochemically activated cobalt nickel sulfide for an efficient oxygen evolution reaction: partial amorphization and phase control, J. Mater. Chem. A, 7(8), 3592 (2019)

Study of exchange interaction strength of $Y_{3-x}R_xFe_5O_{12}$ (R=La, Na, and Gd) using Mössbauer spectroscopy

Young Rang Uhm[1*], Gwang Min Sun[1] and Chul Sung Kim[2]
[1]HANARO Operation and Utilization, Korea Atomic Energy Reasearch Institute, Daejeon, Rep. of Kore
[*]E-mail: uyrang@kaeri.re.kr

Keywords: Rare-earth doped YIG, Super-exchange interaction, Intra-lattice exchange interaction

The magnetic hyperfine field of single phased garnet $Y_{3-x}R_xFe_5O12$ (R=La, Nd, and Gd) was studied using Mössbauer spectroscopy. The $Gd^{3+}$and $Nd^{3+}$are magnetic heavy rare-earth ion, and light rare-earth ion, respectively. While La^{3+} is non-magnetic ion. The Curie temperature was slightly increased substituting rare earth ions such as Gd, Nd, and La with a relatively larger ionic radius than those of Y (yttrium). The magnetic hyperfine fields (H_{hf}) are slightly decreased, as rare earth ions are substituted into YIG. The ionic radius of doped ion in 24(c) site has more immediate and vital influence on the magnetization. This implies that the bond angle of $Fe_{16(a)}$ - O - $Fe_{24(d)}$ is changed, as the 24(c) site is substituted to rare-earth ions with large ionic radius. However, heavy rare-earth ion of Gd^{3+}doped YIG shows the lowest values of H_{hf} at low temperature. The intra-lattice exchange link was focused to clarity magnetic properties of R-YIG (R=La, Nd, and Gd).

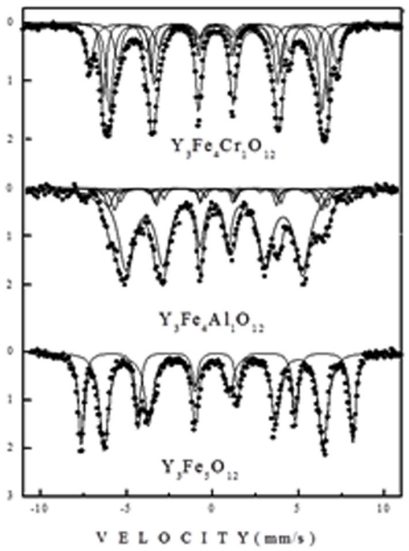

Fig. 1. Mössbauer spectra of R-YIG measured at 293K

Acknowledgments

This work was supported by the National Research Foundation of Korea (NRF) Grant funded by the Korea government (MSIT) (NRF-2018M2A2B3A01071573).

Fe계 신영구자석 개발과 뫼스바우어 분광 연구

임정태[1*], 천휘동[1], 박지훈[1], 김종우[1], 김철성[2], 최철진[1]
[1]재료연구소 분말/세라믹연구본부
[2]국민대학교 물리학과

1. 서론

현재 기술 산업의 발달로 영구자석의 수요가 급증하고 있으나, 기존 사용 중인 희토류 금속 기반의 Nd-Fe-B계 영구자석은 희토류 가격이 급등하여, 이를 근본적으로 해결할 수 있는 차세대 영구자석의 개발이 시급하다. 최근 차세대 영구자석 물질로서 각광받고 있는 Fe계 신영구자석 중에서 $ThMn_{12}$ 구조의 Fe-rich계 화합물은 매우 적은양의 희토류를 포함하고 있으며, 특히 1.78 T에 해당하는 높은 포화자화, 12 T의 높은 자기이방성 및 600 K 이상의 퀴리온도 등의 매우 우수한 자기적 특성을 보이고 있어 많은 연구가 진행 중에 있다. 하지만, $ThMn_{12}$ 구조는 불안정하여 분말로 제조할 때 Fe 원소 일부를 Zr, V, Ti 등의 안정화 원소로 치환해야 하며, 단일상의 제조가 매우 어렵다. 또한, 이론적으로 우수한 특성을 보이는 $ThMn_{12}$ 물질은 현재 예측된 보자력의 약 40%만이 발현되고 있으며 자석의 완전한 잠재력은 아직 실현되지 않았으며, 자기적 특성에 영향을 미치는 초미세 상호작용 및 각각 원소의 부격자 점유도에 대한 연구가 부족한 실정이다. 따라서 본 연구에서는 이를 심도있게 분석하기 위해 뫼스바우어 분광 실험을 수행하였으며, 결정학적 및 자기적 특성의 상관관계를 규명하였다.

2. 실험방법과 결과

$ThMn_{12}$ 합금은 아크 용해와 용융방사법을 통해 제조하였으며, 제조된 리본을 분쇄한 후 다양한 조건에서 열처리를 진행하였다. 제조된 $ThMn_{12}$ 합금에 대해 X-선 회절기 (XRD)와 진동 시료형 자화율 측정기 (VSM) 및 뫼스바우어 분광기를 통해 결정학적 및 자기적 특성에 대해 연구하였다. 비슷한 피크의 위치와 강도를 가지는 $ThMn_{12}$와 Th_2Zn_{17} 구조의 상과 다른 이차상들의 정확한 분석을 위해 Rietvel 정련법을 이용하여 분석하였다. 또한, 뫼스바우어 분광법을 통해 $ThMn_{12}$ 합금의 초미세 상호작용 및 부격자 점유도를 분석하였다.

3. 참고문헌

[1] Y. Hirayama, Y.K. Takahashi, S. Hirosawa, and K. Hono, Scr. Mater. 138, 62 (2017).
[2] T. Kuno, S. Suzuki, K. Urushibata, K. Kobayashi, N. Sakuma, M. Yano, A. Kato, and A. Manabe, AIP Adv. 6, 025221 (2016).

Analysis and Control of Heat Generation of MNPs by Changes in Magnetization for Magnetic Hyperthermia

Sung Hoon Kim*
Department of Electronics Convergence Engineering, Wonkwang University,
460 Iksandae-ro, Iksan, Jeonbuk, 54538, Republic of Korea

This paper presents a new approach for regulating the temperature rise and the specific absorption rate (SAR) produced by superparamagnetic nanoparticles when exposed to an alternating magnetic field, by controlling the magnetization state of the nanoparticles. Throughout this study, it is demonstrated that it is possible to relate the magnetization state of a sample of magnetic nanoparticles rather than just by the magnitude of an applied bias magnetic field. Magnetic heating was produced by applying an alternating magnetic field with a solenoid coil, while magnetization of the nanoparticles was controlled with a static magnetic field generated by a pair of neodymium magnets. Changing the separation distance between the magnets allowed the magnetization state of the nanoparticles to be varied. In the first set of experiments, heating was performed under different amplitudes of alternating magnetic field and magnetization values. The experimental results showed that while the maximum increases in temperature and SAR values are achieved when the magnetization of the nanoparticles is zero, both values decrease as the magnetization increases, tending to zero when the nanoparticles approach their magnetic saturation state. In a second set of experiments, by curve fitting of the experimental data, the required magnetization values to achieve two different specific temperatures and SAR values were calculated. The measured temperature and SAR values were quite similar to the parameters calculated through the curve-fitted data. Overall, the experimental results showed that by controlling the magnetization state of a sample of nanoparticles it is possible to change their heating properties.

Frequency Dependence of Initial Heat Generation in Magnetite Nanoparticles

Sunghyun Yoon[1*] and Chul Sung Kim[2]
[1]Department of Physics, Gunsan National University, Gunsan, 54150, Republic of Korea
[2]Department of Physics, Kookmin University, Seoul, 02707, Republic of Korea
Author to whom correspondence should be addressed. Electronic mail: shyoon@kunsan.ac.kr.

The frequency dependence of heat generation in granular magnetite nanoparticles was studied using vibrating sample magnetometry and the nanoTherics Magnetherm™ hyperthermia testing system. First, the particle size and its distribution were obtained by fitting the *M-H* curve to the classical Langevin function weight-averaged with a modified log-normal size distribution function. Next, the ac power dissipation model for the monodispersed nanoparticle was extended to the polydispersed case, and the volumetric heating rate was predicted as a function of the frequency of the applied field, under the assumption of the Néel relaxation mechanism. Finally, temperature increase with the application of an ac magnetic field was measured experimentally under the frequencies of 50, 112, and 523 kHz, with its amplitude fixed to 250 Oe. It was found that the initial heating rates are in good agreement with the results predicted by the polydispersed power dissipation model.

Half-plenary Session I

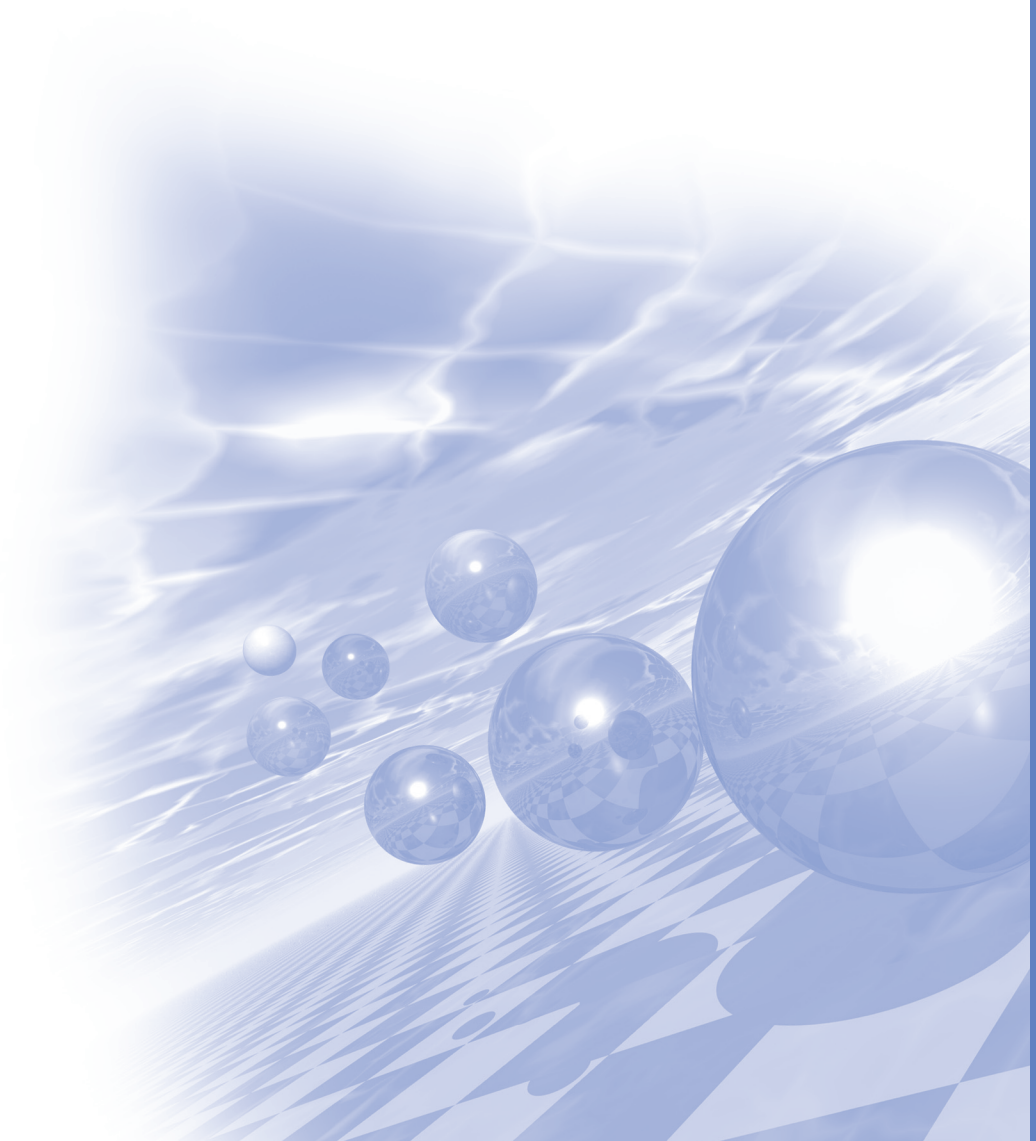

Static and dynamical skyrmions and emergent electromagnetism of moving monopoles in nanowires

Hans-Benjamin Braun*
University College Dublin

Topological defects such as domain walls and skyrmions have gained prominence as they owe their stability to their robustness against continuous deformations of the magnetization field. We first show how dipolar interactions affect the magnetization profile of skyrmions in systems with Dzyaloshinski-Moriya interactions (DMI). While it is generally believed that such parity breaking interactions are necessary for the stabilization of skyrmions, we show that skyrmions surprisingly may also be stabilized entirely dynamically without DMI or dipolar interaction via a purely precessional dynamical mechanism. Being generated in nanocontacts, such dynamical skyrmions may serve as tuneable generators of microwave radiation. As a second example of a topologically nontrival dynamical object in DMI free materials, we discuss the rapid motion of hedgehogs in nanowires. The creation of such hedgehogs is intimately related to the irreversibility of magnetization reversal in generic nanoparticles. Their rapid motion gives rise to a substantial emergent electric field, thus characterizing these hedgehogs as bona-fide monopoles.

Half-plenary Session II

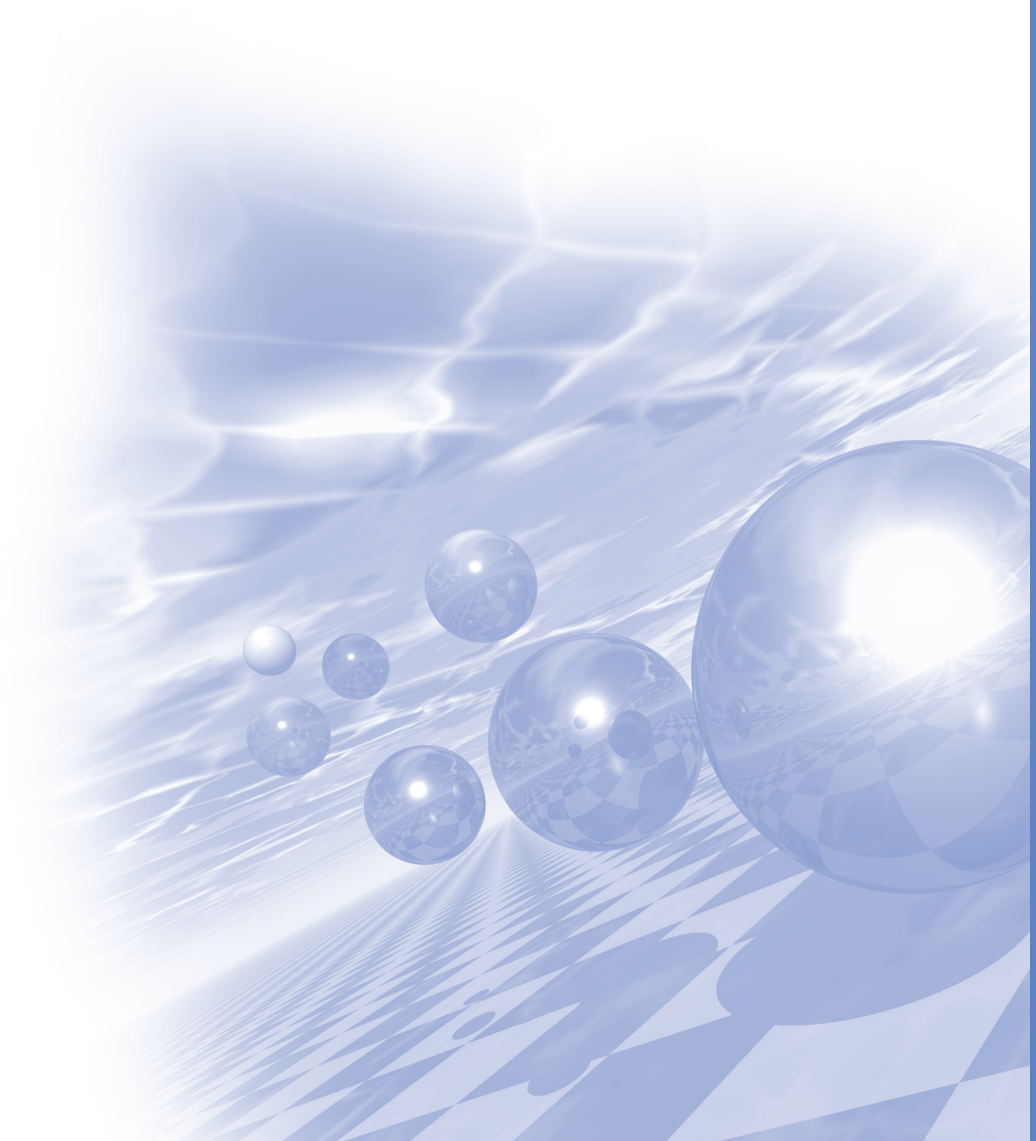

희토류 소재 저감형 신규 모터 설계 기술 연구
A Study on the Advanced Motor Design for Rare Earth Material reduction

유세현*
전자부품연구원 지능메카트로닉스연구센터

1. 서론

최근 중국의 희토류 자원 무기화 정책에 따라 현존하는 최고의 성능을 갖는 희토류 마그네트를 사용하는 영구자석형 모터의 수급 불안이 야기되고 있다. 현재 자동차를 포함하는 로봇, 가전기기 분야에서는 고성능, 고내열성을 위한 Nd 소결 마그네트를 적용한 모터의 사용량이 증가되고 있으나 희토류 소재의 높은 가격 및 수급 불안은 향후 영구자석형 모터 시장의 큰 화두로 거론되고 있다. 본 연구에서는 여러 산업분야에서 희토류 소재를 사용하는 모터 기술을 살펴보고 특히, 차량용 모터를 대상으로 희토류 소재를 저감할 수 있는 본드 마그네트(bonded magnet)를 적용한 모터의 설계 및 그 유용성을 고찰해 본다.

2. 실험방법 및 고찰

본 연구에서는 중희토류(Dy, Tb)를 사용되지 않는 본드 마그네트(Bonded magnet)를 적용한 고성능 전동기 설계를 목표로 하며, 그 유용성 및 성능검증을 위해서는 고출력밀도 특성을 요하는 차량용 ISG(Integrated Starter Generator)를 연구대상 모델로 한다. Nd 소결자석은 보자력 향상을 위한 중희토류 원소(Dy, Tb) 사용이 필수적으로 요구되고 있어, 자원고갈에 따른 수요불안 및 높은 가격상승 문제가 수반되나 본드 자석의 경우 소결 자석에 비하여 에너지적은 작지만 제작 형상의 자유도가 높고, 특히 중희토류(Dy, Tb) 사용 없이 높은 보자력 특성을 갖으며, 입자크기가 작아 와전류손(Eddy current loss)이 없으므로 고내열성의 높은 성능을 요하는 차량용 전동기 분야에는 유용성이 매우 높다.

여기서는 15kW급의 본드 마그네트를 적용한 모터를 설계하고 실험을 통하여 Nd 소결마그네트를 갖는 모터 대비 그 유용성을 확인하였다.

3. 결론

본 연구에서는 희토류 소재를 저감하는 고성능 모터의 기술연구를 위하여 본드 마그네트를 적용한 차량용 15kW급의 모터를 설계하고 시작품 제작을 통한 성능을 고찰 하였다. 그 결과로 본드 마그네트를 적용한 모터는 마그네트의 사용량은 증가되나 성능 측면에서는 소결 마그네트를 사용하는 모터에 준하는 성능을 가질 수 있음을 확인할 수 있었으며, 특히 구조 및 제작성을 고려할 경우 소재 가격과 공정 단가에서 매우 우수한 장점을 보일 것으로 판단할 수 있다.

KMS 2019 Summer Conference

Special Session VII

‘스핀 오비트로닉스: 이론과 실험’

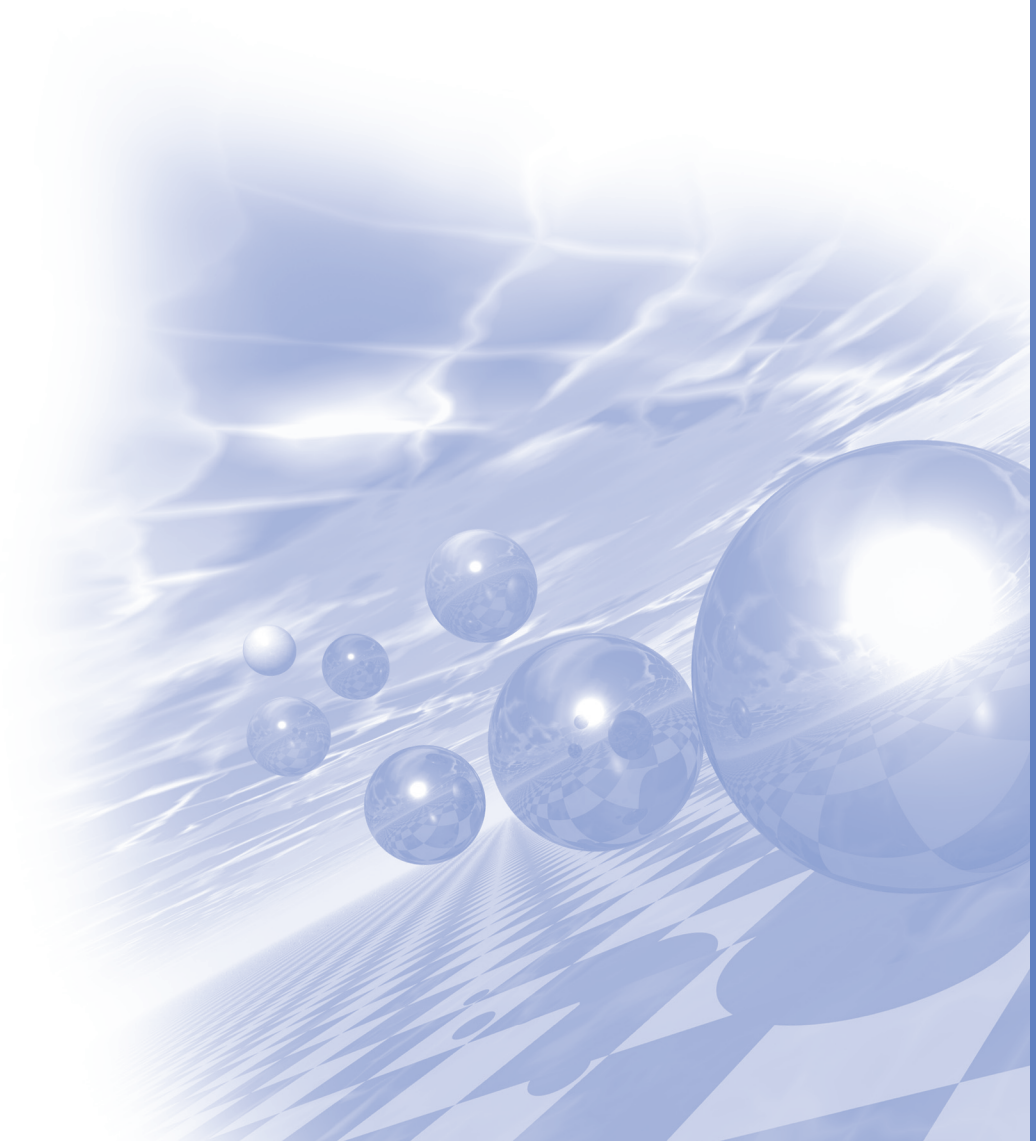

Emergence of robust 2D skyrmions in $SrRuO_3$ ultrathin film

Bongju Kim[1,2*], Byungmin Sohn[1,2], Hai Huang[3], Sang-Jun Lee[3], Se Young Park[1,2], Taeyang Choi[4], Hua Zhou[5], Seo Hyoung Chang[4*], Jung Hoon Han[6*], Jun-Sik Lee[1*] and Changyoung Kim[1,2*]

[1]Department of Physics and Astronomy, Seoul National University, Seoul 08826, Korea
[2]Center for Correlated Electron Systems, Institute for Basic Science, Seoul 08826, Korea
[3]Stanford Synchrotron Radiation Lightsource, SLAC national accelerator Laboratory, Menlo Park, California 94025, USA
[4]Department of Physics, Chung-Ang University, Seoul 06974, Korea
[5]Advanced Photon Source, Argonne National Laboratory, Argonne, IL 60439, USA
[6]Department of Physics, Sungkyunkwan University, Suwon 16419, Korea

We report new findings of magnetic skyrmion formation in a few unit cell of $SrRuO_3$ on top of $SrTiO_3$ substrate without any capping layer. Measurement of the topological Hall effect (THE) reveals a robust stability of skyrmions in this system. THE survives as the field is tilted by as much as 85◦ at with the in-plane magnetic field reaching up to 6.5 T at 10 K. Atomically precise structural determination by the Coherent Bragg Rod Analysis (COBRA) method shows the nontrivial atomic rumpling of the Ru-O lattice plane to be the source of inversion symmetry breaking. First-principles calculations based on the structure obtained from COBRA find significant magnetic anisotropy and precise value of DMI in the $SrRuO_3$ film to be the main source of skyrmion and its robustness. Furthermore, we observed experimental evidence of magnetic skyrmion. These features promise a few-layer $SrRuO_3$ to be an important as a new platform for skyrmionics, without the necessity of introducing the capping layer to boost the spin-orbit coupling strength artificially.

Orbital Spintronics: Non-trivial charge-to-spin conversion in ferromagnetic metal/Cu/oxide trilayers

Junyeon Kim[1*], Dongwook Go[2], Hanshen Tsai[1,3], Kouta Kondou[1],
Hyun-Woo Lee[2], YoshiChika Otani[1,3]

[1]Center for Emergent Matter Science, RIKEN, Japan
[2]Department of Physics, Pohang University of Science and Technology, Korea
[3]Institute for Solid State Physics, University of Tokyo, Japan

The spin/charge interconversion is regarded as an essential mechanism for the development of innovative Spintronic devices [1,2]. Despite the usefulness of the spin/charge interconversion mechanism, the restricted material selection to heavy elements such as Pt, W, or Bi is a potential obstacle for further applications.

In this study, we find a non-trivial spin torque in a CoFe/Cu/Al_2O_3 trilayer without any heavy element. The observation of the charge-to-spin conversion is mainly carried out by the spin torque ferromagnetic resonance technique. Interestingly, the spin torque efficiency (Θ) in this trilayer is 0.13, which is comparable to that for Ta [2]. Additionally, annealing process gives a tremendous enhancement of Θ, and it closes to 0.3 which is similar to that for β-W [3]. In order to understand this anomalous behavior, we propose a novel mechanism induced by the orbital moment generation and transport. In our system, the Cu/Al_2O_3 interface is likely an orbital moment generator by the orbital Rashba and Edelstein effect [4]. Here we note that a chiral orbital texture by the orbital Rashba effect can be achieved without a role by the spin-orbit coupling. The generated orbital moments are injected into the ferromagnetic layer, and induce a change of the magnetization orientation via the L-S coupling [5]. Further discussions will be given during the annual meeting.

References

[1] I. M. Miron et al., Nature **476**, 189 (2011).
[2] L. Liu et al., Science **336**, 555 (2012).
[3] P. Pai et al., Appl. Phys. Lett. **101**, 122404 (2012).
[4] S. R. Park et al., Phys. Rev. Lett. **107**, 156803 (2011).
[5] D. Go et al., arXiv:1903.01085

Linear-response-based DFT+U study on Co-based full Heusler alloy for half-metallic electronic structure

Kenji Nawa[1*], Yoshio Miura[1,2,3]

[1]Research Center for Magnetic and Spintronic Materials, National Institute for Materials Science (NIMS), Japan
[2]Center for Materials research by Information Integration, National Institute for Materials Science (NIMS), Japan
[3]Center for Spintronics Research Network (CSRN), Graduate School of Engineering Science, Osaka University, Japan

The half-metal ferromagnets (HMFs), which are metallic for one spin channel and insulating (semiconducting) for the other spin channel, have attracted much attention because of their potential to produce highly spin-polarized current. Utilizing the HMFs into magnetic tunnel junctions (MTJs) is advantageous for large tunneling magnetoresistance ratio (TMR) and high spin-current-injection efficiency. A large amount of density functional theory (DFT) calculations predicts that Co-based full Heusler alloys Co_2YZ, where Y is transition metal and Z is sp element, are suitable for ferromagnetic electrodes of MTJs due to their nearly half-metal electronic structures and high Curie temperatures. [1] So far, much efforts have been devoted by many experiments for the MTJs with Co_2YZ. At the present stage, the highest TMR of 2610 % were observed at 4.2K for MTJ with Co_2(Fe,Mn)Si electrode, however it decreases to only 429 % at room temperature. [2] The large reduction of the TMR against the temperature increasing is a fundamental problem for Heusler-based MTJ devices. One of the possible reasons is the decrease of the spin polarization in bulk Co_2YZ around the Fermi energy at finite temperature. To suppress the spin polarization reduction with increasing temperature, the HMFs having a wide half-metallic gap and the Fermi energy located at the center of the gap are strongly desired.

In this work, we discuss the origin of the half-metal gap and explore the potential for the HMFs in Co_2YZ alloys on the basis of the DFT+U calculations, in which the Hubbard-type effective on-site Coulomb interactions (U_{eff}) are determined by linear response (LR) approach for better treatment of 3d electron correlations. [3-5] The Co_2MnSi was firstly focused within standard DFT framework. From the calculated electronic band structures, we considered the underlying hybridizations, and found the t_{2g} orbital hybridization between Co and Mn atoms, which is important for the half-metal gap around the Fermi energy. Based on our energy diagram of atomic-orbital hybridizations, the gap is originated from the Co e_u orbital of conduction state and Co-Mn hybridizing $t_{2\mathrm{g}}$ orbitals of valence state at the Fermi energy. Moreover, it is indicated that this band gap is controllable by a select of Y and/or mixing several elements into Y site.

Secondly, the LR calculations were carried out and the U_{eff}s were calculated as reasonable value for Mn (3.53eV) but unexpectedly large for Co (6.57eV), respectively. The band calculation results were compared with experiments. In DFT+U_{Mn} calculation, in which the calculated U_{eff} is applied to only Mn site, obtained total magnetic moment ($m_{\mathrm{spin}} = 5.01\ \mu_{\mathrm{B}}$) and atom-resolved contributions to m_{spin} (0.72 μ_{B} for Mn and 3.63 μ_{B} for Co) are in good agreement with experiments, while the standard DFT result is not consistent with experiment in atom-resolved m_{spin}. We also confirmed the calculated electronic structure correspond to the HAXPES result. On the other hand, DFT+U_{Co} and DFT+$U_{\mathrm{Mn,Co}}$ calculations disagree with experiments; for example, total m_{spin}s are obtained as 6.95 and 8.08 μ_{B} by respective methods where are overestimated compared to experiment (4.97~5.07 μ_{B}). These results imply that the correlation effect of Mn plays a key role for ground-state analysis while the standard DFT and DFT+U method introducing the U_{eff} to Co atom fails to describe electronic and magnetic

properties. As a result, the DFT+U_{Mn} method concluded that the Co_2MnSi is not the HMF, but extremely high value of spin polarization (P = 90 %) is obtained. The results on the half-metallicity, spin polarization, and the size of half-metal gap for the other systems including ternary Co_2YSi and quaternary $Co_2(Y,Mn)Si$ will be discussed.

This work was supported by JSPS KAKENHI Grant Numbers JP16H06332 and JP17H06152.

References

[1] I. Galanakis et al., Phys. Rev. B **66**, 174429 (2002). [2] H. Liu et al., J. Phys. D: Appl. Phys. **48**, 164001 (2015).

[3] M. Cococcioni et al., Phys. Rev. B **71**, 035105 (2005). [4] K. Nawa et al., Phys. Rev. B 97, 035117 (2018).

[5] K. Nawa, and Y. Miura (submitted).

Dynamics of noncollinear antiferromagnetic domain wall driven by spin current injection

Yuta Yamane[1*], Olena Gomonay[2] and Jairo Sinova[2]
[1]RIKEN Center for Emergent Matter Science (CEMS), Saitama 351-0198, Japan
[2]University of Mainz, D-55099 Mainz, Germany

Since the prediction of staggered magnetic order and its experimental observation through 1930s-50s, antiferromagnetic (AFM) materials have occupied a central place in the study of magnetism. The absence of macroscopic magnetization in AFMs, however, indicates that they cannot be effectively manipulated and observed by external magnetic field, which has hindered active applications of AFMs in today's technology. Research in the emergent field of antiferromagnetic spintronics[1] has revealed that electric and spin currents can access AFM dynamics via spin-transfer torques and Neel spin-orbit torques. The studies on current-driven dynamics of AFM textures have opened an avenue toward AFM-based technologies.

Recently, AFMs with noncollinear magnetic configurations are generating increasing attention as they exhibit large magneto-transport[2] and thermomagnetic[3] effects. The studies on current-driven dynamics of AFMs, however, have thus far mostly focused on collinear structures. Understanding the effects of electric and spin currents in noncollinear AFMs is being a crucial issue in the community.

In this talk, we discuss the dynamics of noncollinear AFMs induced by spin current (SC) injection[4], which may be realized by exploiting spin Hall effect in an adjacent nonmagnetic-metal (NM) layer. We derive sine-Gordon type equations of motion for the AFMs, including effective forces due to SC injection, external magnetic field and internal dissipation. Our model is applicable to technologically important triangular AFMs such as Mn3Ir and Mn3Sn, enabling an analytical approach to domain wall (DW) dynamics in those materials. We obtain an expression for DW velocity driven by SC, which is compared to numerical simulations.

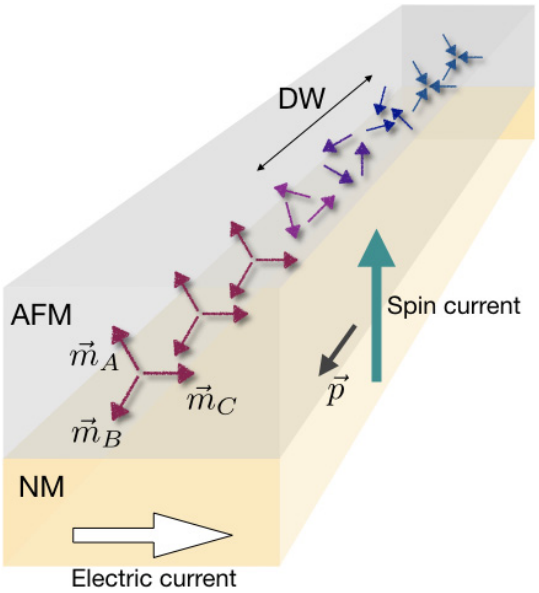

References

[1] V. Baltz et al., Rev. Mod. Phys. 90, 015005 (2018).

[2] S. Nakatsuji et al., Nature 527, 212 (2015).

[3] M. Ikhlas et al., Nat. Phys. 13, 1085 (2017).

[4] Y. Yamane et al., arXiv:1901.05684.

Magnetic spin Hall effects in a non-colinear antiferromagnet

Motoi Kimata*
Institute for Materials Research, Tohoku University, Japan

Spin Hall effects (SHE) are known as interconversion mechanism between spin and charge currents. So far, a lot of studies to reveal their physical mechanisms and/or to achieve high-efficient conversion ratio have been intensively performed. However, previous studies are mainly limited in non-magnetic materials, and thus, the magnetic contribution for the SHE is not fully understood. Here, we report the SHE (direct and inverse SHE) in non-collinear antiferromaget Mn3Sn, where the gigantic anomalous Hall effect is recently observed at room temperature. We observed anomalous sign change of spin accumulation signal (i.e., spin Hall angle) when the triangle magnetic structure is switched by external magnetic field [1]. The observation of this new effect (which we call the magnetic SHE) shows that some magnetic materials have richer spin Hall properties than that in non-magnetic materials. Also, our recent observation will contribute to deeper understanding of charge-spin coupling in magnetic systems.

Reference

[1] M. Kimata et al., Nature 565, (2019) 627-630.

First-Principles Materials Design of Magnetic Anisotropy

D. Odkhuu[1,2*], D. Tuvshin[1], T. Ochirkhuyag[1], Chang Geun Park[1],
T. Tsevelmaa[3], S. H. Rhim[3] and S. C. Hong[3]

[1]Department of Physics, Incheon National University, Incheon 22012, South Korea
[2]Institute of Physics and Technology, Mongolian Academy of Sciences, Ulaanbaatar, Mongolia
[3]Department of Physics, University of Ulsan, Ulsan 44610, South Korea

The magnetic anisotropy and its controllable features have been of significant interests among solid-state physicists and material scientists in the fields of permanent magnet and spintronics. In permanent magnets, for a several decades there have been intense research efforts to replace the *f*-electron or heavy metal compounds with 3*d*-only materials; however no competitive materials have been identified thus far in terms of the magnetic anisotropy. In this talk, we will discuss on our recent highlights and promising approaches to dramatically enhance the magnetic anisotropy without the inclusions of 4f and 4d-to-5d elements in B2-ordered FeCo and L10-ordered FeNi alloys in combination with their high saturation magnetization and Curie temperature. On the other hand, for spintronics research field we will discuss on how the magnetic anisotropy of Co atoms on two-dimensional graphene and *h*-BN layers can be tailored and reoriented from in-plane to perpendicular magnetization by means of degree of the interlayer hybrid bonds at the interface.

This research was supported by Future Materials Discovery Program through the National Research Foundation of Korea (NRF) funded by the Ministry of Science and ICT (2016M3D1A1027831).

KMS 2019 Summer Conference

Special Session VIII

‘Electro-Magnetic Energy Convergence’

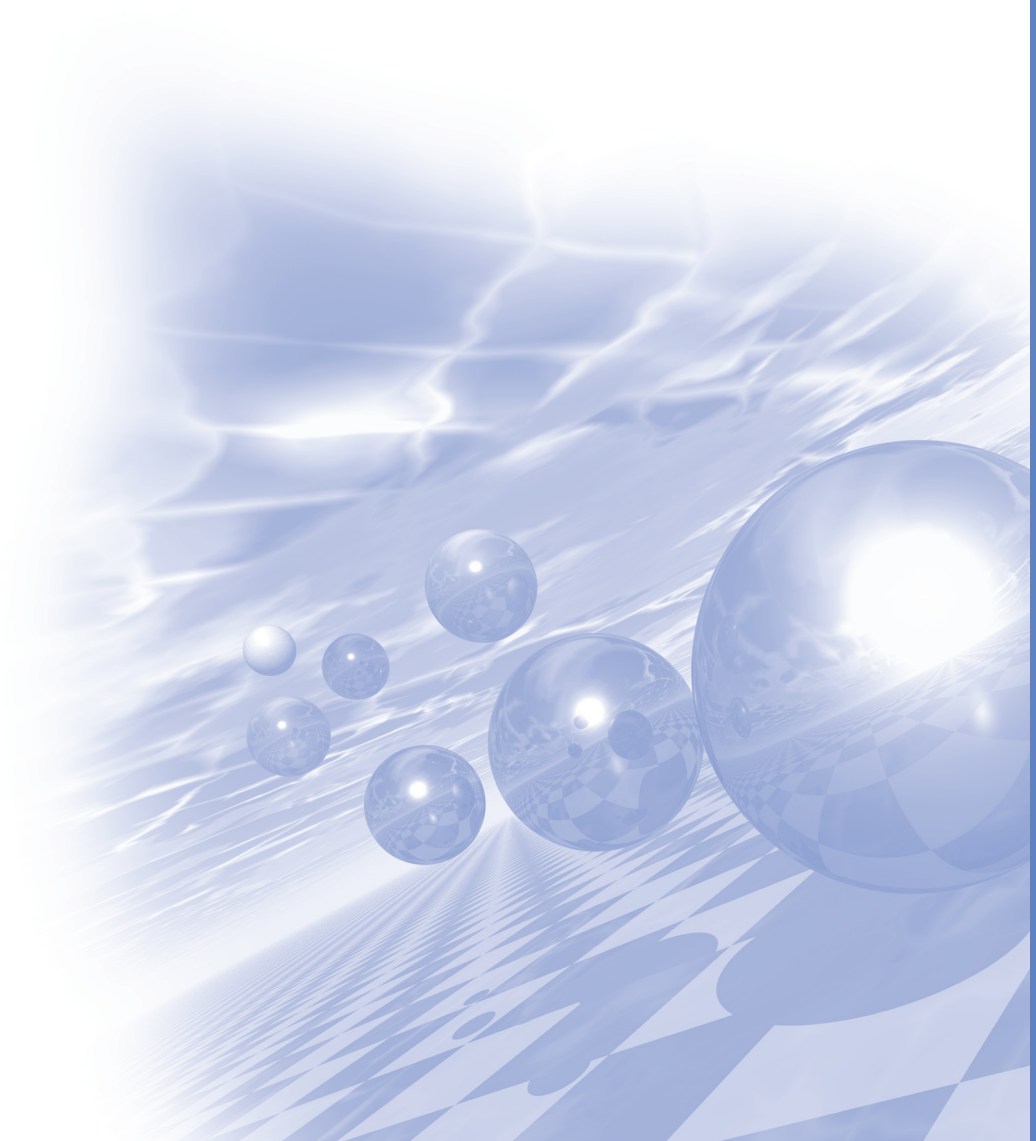

Size Reduction Design of Electric Machine for Rare-earth free applying BSMM

Hyeon-Jin Park[1*], Kyung-Tae Jung[1], Myung-Seop Lim[2], Yun-Yong Choi[3] and Jung-Pyo Hong[1]
[1]Hanyang University, Wangsimni-ro Seongdong-gu Seoul, Korea, 04763
[2]Yeungnam University, Department of Mechanical Engineering,
Daehak-ro, Gyeongsan-si, Gyeongsangbuk-do, Korea, 38541
[3]Drivetech company, Jomaru-ro, Bucheon-si, Gyeonggi-Do, Korea 14558

Rare earth permanent magnets are widely applied to electric machines for reduced size and high power density due to high residual magnetic flux density and coercive force. However, the production sites of rare earth minerals are mainly limited to specific regions. Therefore, supply is unstable due to large price fluctuations. So, many researchers are studying about electric machines with rare earth free.

In particular, motor design researches using ferrite permanent magnets has been actively studied. One of the many studies applying ferrite magnet is multi-layer rotor. This type of motor compensates for the lack of magnetic torque with reluctance torque due to the multi-layer geometry of the rotor. But, this type requires structures of ribs and bridges to ensure strength of the mechanical rotation, these structures create a leakage path in terms of the magnetic circuit, resulting in a lack of torque at the same volume of rare-earth PM motor.

However recent researches on iron core materials have introduced new materials that can overcome these leakage path problems. The new iron core has a non-magnetic property through heat treatment in a specific part, and the mechanical stiffness is strengthened. This is expected to improve the disadvantages of multi-layer rotor.

In this paper, the BSMM(Bi-State Magnetic Material) was applied to the multi-layer rotor to reduce the volume of the motor. Through this, I will study the application of new materials compared with reference model of rare earth permanent magnet motor.

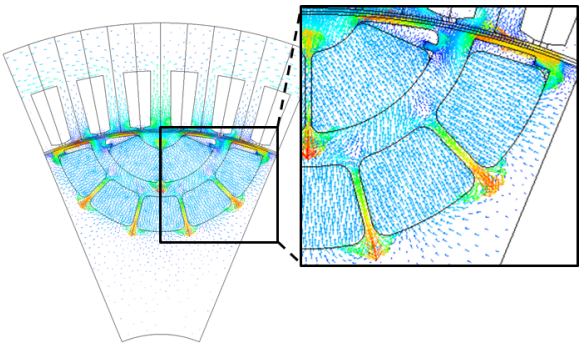

Fig. 1. Multi-layer PMSM and Leakage Flux

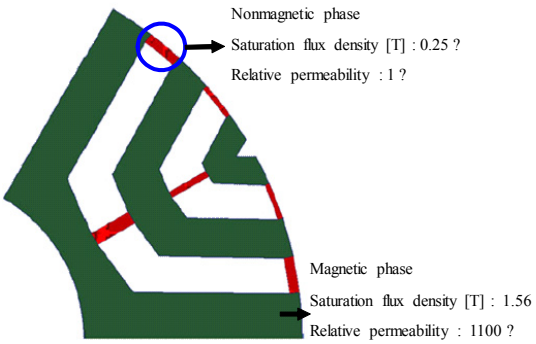

Fig. 2. Characteristic of Bi-state Magnetic Material

Asymmetric Rotor Shape Design for Interior Permanent Magnet Synchronous Motor using Advanced Inverse Cosine Function

Young-Hoon Jung[1], Myung-Seop Lim[2*]
[1]Department of Automotive Engineering, Hanyang University, Korea
[2]School of Mechanical Engineering, Yeungnam University, Korea

An asymmetric rotor design method to reduce the torque ripple as well as harmonics of the induced voltage of an interior permanent magnet synchronous motor (IPMSM) is proposed in this paper. In previous researches, the inverse cosine function (ICF) has been proposed and used for the torque ripple reduction by making a sinusoidal flux density in the air gap under a no-load condition. However, in this paper, the advanced inverse cosine function (AICF) is proposed to design the shape of the core material considering the armature reaction under a load condition. By using the AICF, an asymmetric rotor shape is determined to make a sinusoidal air gap flux density waveform under a certain load condition. In addition to the reduction of the torque ripple, a lower total harmonic distortion (THD) of the induced voltage waveform and a lower iron loss in the core is achieved by applying the AICF, compared to the results of the other conventional design methods. The torque ripple is one of the most important parameters of the electric motor since it affects the performance as well as durability of the mechanical system. In addition, the lower peak value due to the lower THD of the induced voltage are important because they affect the control performance of the motor. The lower iron loss can also lead to a higher efficiency, particularly, in the high-speed operation. To verify the validity of the proposed design method using AICF, the characteristics of 8-pole 12-slot concentrated flux type IPMSM that have various rotor shapes are analyzed using finite element analysis (FEA) as well as experiments.

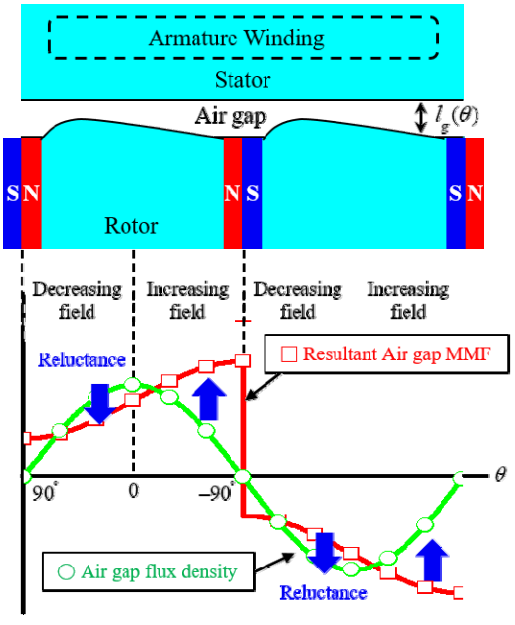

Fig. 1. Effect of the rotor shape design using Advanced Inverse Cosine Function

Study on Slotless Axial Flux Synchronous Motor Using Ceramic Coating Coil

Kyung-Tae Jung[1*], Hyeon-Jun Park[1], Yun-Yong Choi[2], Myung-Seop Lim[3] and Jung-Pyo Hong[1]
[1]Hanyang University, Wangsimni-ro Seongdong-gu Seoul, Korea, 04763
[2]Drivetech company, Jomaru-ro, Bucheon-si, Gyeonggi-Do, Korea 14558
[3]Yeungnam University, Department of Mechanical Engineering,
Daehak-ro, Gyeongsan-si, Gyeongsangbuk-do, Korea, 38541

Slotless synchronous motors have no cogging torque and speed ripple, and mechanical constrains are not tight. Further, the stator core is removed to reduce the weight of the motor. The air gap is larger than that of an electric motor using an iron core, and the air gap flux density is small. Therefore, it is necessary to increase the current for generating the torque. For this purpose, it is important to design the magnetic circuit so that the temperature of the coil does not exceed the allowable value. Until recently, designing the coil temperature so that is does not exceed the allowable temperature depends on experience. Also, in order to confirm that the designed motor is at a stable level, it is actually manufactured and tested. As a result of the experiment, if the coil temperature exceeds the allowable temperature, the design has fail. Based on this, redesign is necessary.

If and electric motor breaks down due to a coil in an industrial field, it can cause financial damage and personal injury. Normally, the allowable temperature of the enamel coating coil is about 200°C. If the coating material is replaced with a ceramic, the allowable temperature of coil can be extended to about 400 to 500 °C.

Increasing the allowable temperature of the coil makes it possible to use the motor more safely. In addition, input current and current density can be increased, which can be expected to increase the output of motor, reduce the size, and reduce weight.

In this paper, the design methods of synchronous motor using ceramic coating coil was studied first. And the prototype motor was fabricated and tested.

Fig. 1. Proto motor

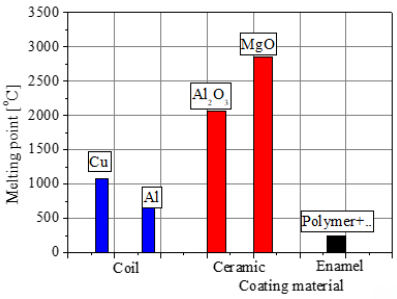

Fig. 2. Coating material melting point comparison

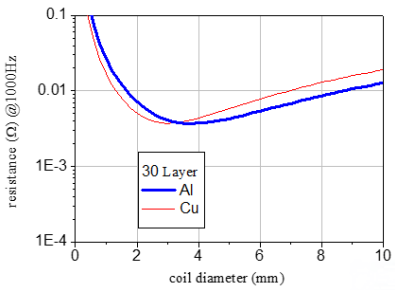

Fig. 3. Aluminium and copper ac resistance depending on layer

해석적 기법을 이용한 마그네틱 랙-피니언 기어의 토크 특성 해석과 실험

Torque Characteristic Analysis and Mesurement of Magnetic Rack-Pinion Gear Using Analytical Method

장강현*, 김창우, 서성원, 신경훈, 윤익재, 최장영
충남대학교 전기공학과

1. 서론

기계식 기어는 현재 동력전달에 폭넓게 사용되고 있으나 기어 치의 파손으로 인해 시스템의 유지보수가 정기적으로 필요하다는 단점이 있다. 한편 영구자석을 이용한 비접촉식 마그네틱 기어는 기계적 기어의 단점을 보완하는 동시에 높은 토크를 전달할 수 있는 장점이 있다. 마그네틱 기어의 장점은 이미 여러 참고 문헌에서 다루고 있다 [1,2]. 마그네틱 기어는 단점 또한 존재한다. 예를 들면 제작의 어려움, 슬립으로 인한 위치 제어의 부정확성, 동작시 발생하는 진동 등이 있다. 이는 향후 마그네틱 기어를 연구할 때 반드시 고려해야 하는 부분이기도 하다. 어려가지 타입의 기어 중 랙-피니언 기어는 선형 및 회전형 기어를 모두 포함한 기어로써 회전운동을 직선운동으로 변환하는데 사용된다. 랙-피니언 기어는 조향 장치, 운반 장치, 공작 기계 및 엘리베이터 등에 사용되어지고 있다. 그러나 평 기어, 동축 기어, 사이클로이드 기어 등의 타입의 마그네틱 기어와는 달리 본 논문에서 제안한 것과 같은 마그네틱 랙-피니언 기어에 관련된 연구는 매우 부족하다 [3]. 따라서 마그네틱 랙-피니언 기어에 대한 해석 및 설계 방법을 연구할 필요성이 있다. 일반적으로 마그네틱 기어의 자기적 특성해석은 유한요소해석(FEM)을 사용하거나 공간고조파법을 기반으로한 해석적 기법을 사용할 수 있다. 설계 초기 단계에서는 다양한 설계 변수에 대해 반복적인 변경과 해석이 필요하다. 이 경우 유한요소 해석법은 해석시간이 매우 오래 걸린다는 단점이 있다. 반면 해석적 기법을 이용한 해석법은 수 초 이내로 해석결과를 얻어 낼 수 있기 때문에 설계 초기 변수에 대한 특성을 확인하는데 매우 유용하다. 또한 멕스웰 방정식을 기반으로한 지배방정식을 이용하여 접근하기 때문에 물리적인 현상을 이해하기 쉽다 [4,5].

본 논문에서는 해석적 기법을 이용하여 마그네틱 랙-피니언 기어의 자계 및 토크특성 해석을 수행하고자 한다. 또한 랙-피니언 기어의 제작과 실험을 통해 그 해석방법의 타당성을 검증하려 한다.

2. 해석방법, 실험방법과 결과

랙-피니언 기어는 회전운동을 선형운동으로 변환 시켜주는 장치이며, 마그네틱 랙-피니언 기어는 영구자석을 사용하여 물리적 접촉 없이 기어의 동작을 할 수 있다. 먼저 해석적 기법을 이용하여 자계 및 토크를 분석하기 위한 마그네틱 랙-피니언 기어의 해석모델을 가정한다. 이 모델을 기반으로 멕스웰 방정식과 각 영역에서의 지배방정식 및 경계조건을 이용하여 각 영역에서의 자계분포를 해석할 수 있다. 영구자석의 자화는 푸리에 급수를 이용하여 간단히 모델링 할 수 있다. 각 영역에서의 자계분포를 해석하게 되면 멕스웰 응력 텐서를 기반으로 랙과 피니언 기어 사이에 발생하는 힘과 토크를 계산할 수 있다. 해석적 기법의 타당성을 입증하기 위하여 설계 사양과 동일한 기어를 제작하고 로드셀과 토크센서를 이용하여 힘과 토크를 측정하여 해석결과와 비교하였다. 해석 및 실험결과 공극자계 분포는 유한요소해석값과 비교하였을 때 잘 일치함을 확인하였고 힘과 토크값은 실험값과 비교하였을 때 마찬가지로 잘 일치함을 확인할 수 있었다.

3. 고찰

공간고조파법을 기반으로한 해석적 방법을 이용하여 마그네틱 기어의 자계특성 분석을 수행하였고 유한요소 해석법의 해석결과와 비교하였을 때 잘 일치함을 확인하였다. 마그네틱 랙-피니언 기어를 제작하여 실험세트를 구성하고 기어의 힘과 토크값을 측정하였다. 측정된 결과값들은 해석적 기법과 유한요소 해석법을 통한 결과와 비교하여 검증되었다. 측정결과는 해석결과와 잘 일치함을 역시 확인하였다.

4. 결론

본 논문은 해석적 기법을 이용한 마그네틱 랙-피니언 기어의 해석과 설계 검증에 대해서 다루었다. 본 논문에서 제시한 마그네틱 랙-피니언 기어의 해석방법은 기어를 설계하는데 유용하게 사용되어 향후 연구에 기초가 될 수 있을 것으로 사료된다. 향후 연구에서는 마그네틱 랙-피니언 기어의 과도상태 해석을 연구 할 예정이다.

5. 참고문헌

[1] Jian-Xin Shen, Hua-Yang Li, He Hao, and Meng-Jia Jin, “A Coaxial Magnetic Gear With Consequent-Pole Rotors,” IEEE Trans. Energy Conv., vol. 32, no. 1, pp. 267-275, Mar. 2017.

[2] Matthew C. Gardner, Benjamin E. Jack, Matthew Johnson, and Hamid A. Toliyat, “Comparison of Surface Mounted Permanent Magnet Coaxial Radial Flux Magnetic Gears Independently Optimized for Volume, Cost, and Mass”, IEEE Trans. Ind. Appl., vol. 54, no. 3, pp. 2237-2245, May/June. 2018.

[3] Kent Davey, Larry McDonald, and Travis Hutson, “Axial Flux Cycloidal Magnetic Gears,” IEEE Trans. Magn., vol. 50, no. 4, 8100607, Apr. 2014.

[4] Seok-Myeong Jang, Jang-Young Choi, and Sang-Sub Jeong “Electromagnetic Analysis and Control Parameter Estimation of Moving-Coil Linear Oscillatory Actuator,” J. Appl. Phys., vol. 99, no 8, 08R307, April 2006.

[5] Boldea and S. A. Nasar, “Linear electric actuators and generators,” IEEE Trans. Energy Conv., vol. 14, no. 3, pp.712-716, 1999.

Magnet Shape Design for SPMSM of EPS System by Using Cycloid Curve

Chung-Seong Lee[1*], Hyeon-Jin Park[2], Yun-Yong Choi[3]
[1]Central R&D Center, Mando, Korea
[2]Department of Automotive Engineering, Hanyang University, Korea
[3]R&D Center, DriveTech, Korea

EPS (Electric Power Steering) system demands are continuously increasing because it has the superior fuel efficiency compared to other electric actuator systems. Reflecting this trend, the quality of EPS system is becoming stricter.

In particular, to improve the steering feel and the stability of the vehicle at high speed, it is required to reduce the cogging torque and the torque ripple characteristics of the motor, which is one of the main parts of the EPS system, and many researchers have studied the design methods therefore.

In this paper, CET (Curtate Eptirochoid) and PET (Prolate Epitrochoid) among cycloid curves applicable to the magnet shape were selected and the magnet shape design method of SPMSM (Surface Permanent Magnet Synchronous Machine) was proposed.

In order to compare and evaluate the cycloid curve with the magnet shape having the conventional curve, the length of air gap on the axis, which is the electrical axis of the magnet, was proposed and applied to it in the same way as conventional curves as shown in Figure 1.

The design results were verified by using FEA (Finite Element Analysis) results as shown in Figure 2. The performances of the prototype with the cycloid curve were improved over the prototype with the eccentric curve through the FEA results of cogging torque, average torque and torque ripple. The proposed magnet shape design will be useful for the tolerance insensitive design considering the improvement of the motor productivity in the future.

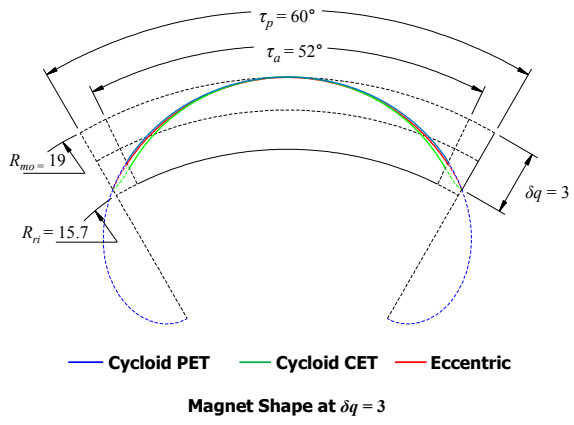

Fig. 1. Magnet Shape for Cycloid and Eccentric Curve

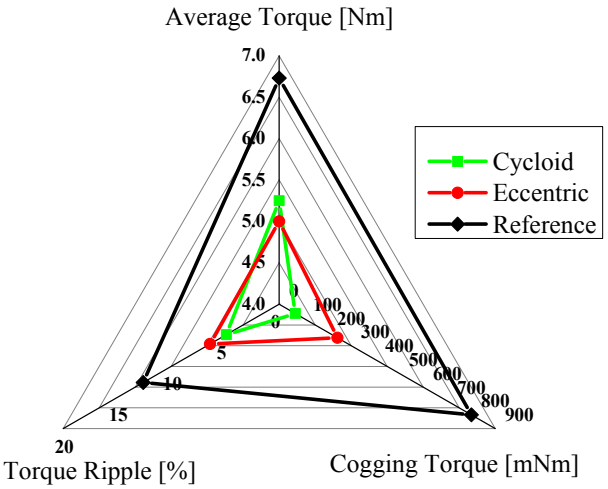

Fig. 2. FEA Results

Design of IE4 Class Line Start Permanent Magnet motor

Jeong-Jong Lee*, Ki-Doek Lee and Se-Hyun Rhyu
Intelligent Mechatronics Research Center, Korea Electronics Technology Institute, Korea
leejj@keti.re.kr

This paper deals with the development of 3-phase line-start permanent magnet motor for IE4 class. LSPM motors use permanent magnets, so high-efficiency operation is possible. In order to design a high efficiency motor, loss analysis method and characteristic analysis method were performed. LSPM motor has similar characteristics such as the synchronous machine in the continuous mode. The LSPM motor has a very large current input at startup. At this time, the probability of occurrence of permanent magnet demagnetizing is very high. Therefore, this paper describes the setting of permanent magnet thickness and the method of motor design to prevent demagnetization of permanent magnet.

Index Terms— Line start permanent magnet, characteristic analysis, demagnetizing, magnetic equivalent circuit

Recently, high efficiency motors have been actively developed to save electric energy. IE4 class is the international motor efficiency classes (IE1- IE4), defined in the Standard IEC60034-30. Line start permanent magnet(LSPM) motor has a great advantage as a kind of these in the electric motor [1-2]. LSPM motor is does not need an inverter because of the starting torque achieved by secondary bar conductor bars in the rotor. Although there has been a lot of research from twenty years before, there are still difficulties in commercialization have a few problems such as a high starting current and demagnetizing of the permanent magnet.

A few papers were published about LSPM motor in the past. The papers suggest the design, analysis and motor parameter extraction of LSPM. A magnetic equivalent circuit model(MEC) of a slotted solid rotor line-start permanent magnet motor is developed[3]. Main characteristics of the device with an emphasis on the demagnetization withstand capability of PMs, are analyzed. Recent, LSPM motor parameter calculation and voltage equation is studied.

The LSPM motor is made like a hybrid between a squirrel-cage induction motor, a synchronous reluctance motor with the permanent magnet synchronous motor as figure 1. This model is based on the induction motor. The rated power is 2.2 kW. Number of slot is 36, pole number is 4. The conductor number is 44. Stack length is 80mm.

Fig. 1 shows the unloaded flux density as a part of the analysis results. At the load condition, the flux density increases to 1.8T. Fig. 5 shows the analyzed efficiency and current. Efficiency exceeds 92%, which is more than 91% of IE4 class. This motor was confirmed through experiments.

In this paper, we summarized about how to analysis of LSPM motor. Even though LSPM motor have the start-up problem, there is a number of advantages in efficiency. Other interesting result and detailed descriptions on experiments and analysis will be included in the full paper.

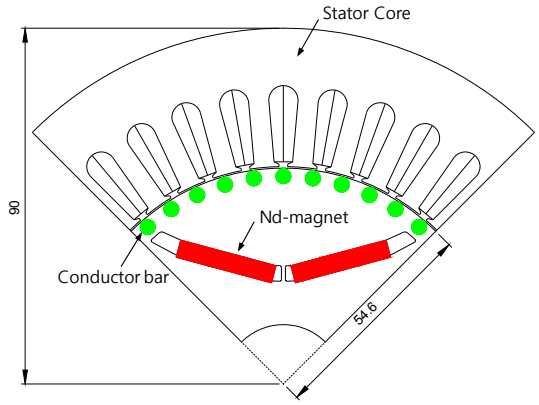

Fig. 1. Quator cross-section of 2.2kW LSPM

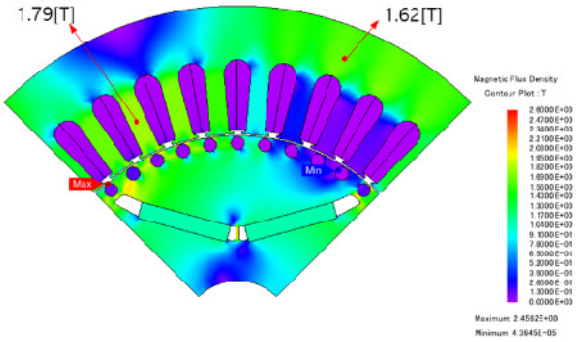

Fig. 2. Flux density at full load condition

Acknowledgment

This work was supported by Korea Institute of Energy Technology Evaluation and Planning(KETEP) grant funded by the Korea government(MOTIE) (2018201010633A, The Development of Design Technology for IE4 Class Motors)

References

[1] Gyu-Hong Kang, Jin Hur, Hyuk Nam, Jung-Pyo Hong, Gyu-Tak Kim, “Analysis of irreversible magnet demagnetization in line-start motors based on the finite-element method”, IEEE Trans. Magn., vol.39, no.3, pp. 1488-1491, May, 2003.

[2] W. Fei, P. C. K. Luk, J. Ma, J. X. Shen and G. Yang “A high-performance line-start permanent magnet synchronous motor amended from a small industrial three-phase induction motor”, IEEE Trans. Magn., vol. 44, no. 10, pp.4724-4727, 2009.

[3] Niazazari M., Mirsalim M., Mohammadi S., “Analytical framework for analysis and demagnetization study of a slotted solid-rotor line-start permanent-magnet synchronous motor”, Power Electronics, Drive Systems and Technologies Conference (PEDSTC), pp. 494-499, 2014.

KMS 2019 Summer Conference

Special Session IX

'Medical Magnetics'

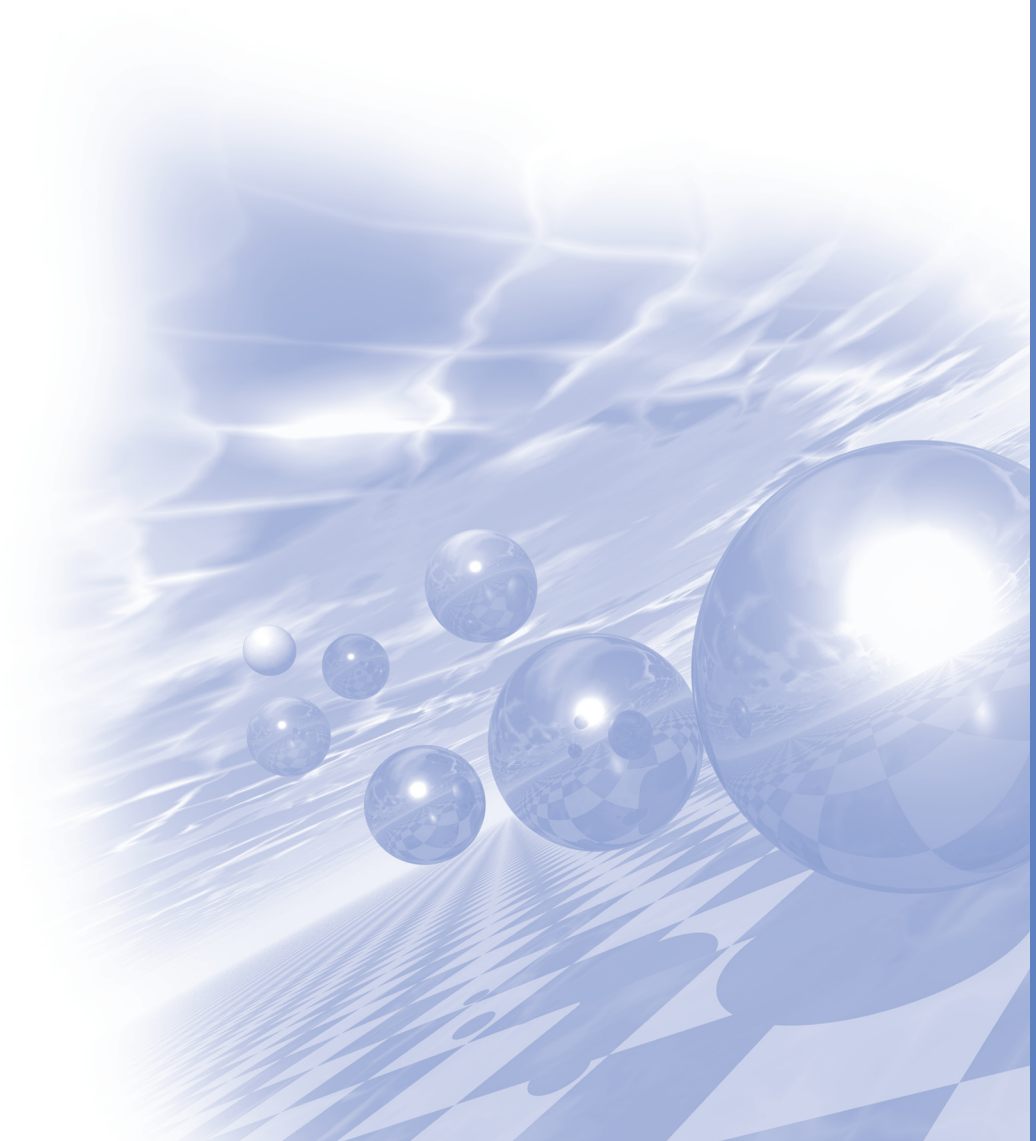

Development of Gamma Camera with a Diverging Collimator Using DMLS 3D Print

Jong-Hun Won[1*], Dong-Hee Han[1], Seung-Jae Lee[3], Cheol-Ha Baek[2]
[1]Department of Medical Health Science, Kangwon National University
[2]Department of Radiological Science, Kangwon National University
[3]Department of Radiological Science, Dongseo University

Gamma imaging is now a rapidly expanding areas of study because of the increase in the radiation applications for medical, environmental monitoring, and research fields. Recently a small and portable gamma camera has been studied for use in gamma imaging systems. The quality of the gamma images depends on the performance of the collimator. A shortcoming of the pinhole collimator is that it loses efficiency rapidly with distance. The diverging collimator is easier to make of DMLS 3D print than existing diverging collimators, and takes advantage of high sensitivity and large FOV. The purpose of this study was to use Monte Carlo simulation to characterize and optimize a design parameters of a diverging collimator. Based on this, the purpose to make an optimized collimator using the 3D printing of Direct Metal Laser-Sintering (DLMS) method. Simulation using the Geant4 Application for Tomographic Emission (GATE) was performed to model the diverging gamma camera system. The gamma camera consists of a diverging shaped tungsten collimator, and a GAGG scintillation crystal with thickness 6.0 mm and area of 25.8 x 25.8 mm. The intrinsic spatial resolution and sensitivity was simulated by changing the collimator height. The point source of ^{99m}Tc was located 10 mm and 20 mm above the center of the collimator and the projection data was estimated for diverging height values from 5 mm ~ 30 mm. The optimal ranges of height and 0.7 mm diameter were determined by evaluation the intrinsic resolution and sensitivity tradeoff curves. The simulation results allowed us to determine the optimal values of diverging diameter and height to be 0.7 mm and 15 mm, respectively, to get intrinsic resolution below 3.0 mm FWHM. Based on optimization design variable values, collimators were designed and built using DMLS, one of the 3D printing techniques. This study produced and developed collimators using DMLS 3D printing techniques. Collimator can be manufactured by optimizing for purpose while maintaining high precision, it is expected to be applied for various fields of medical and industry.

Keywords: DMLS 3D Printing technique, GATE, Collimator Optimization

MR-compatible DOI-PET detector providing multiple spatial resolution

Sungsoo Hong*, Jingyu Yang, Jihoon Kang
Department of Biomedical Engineering, Chonnam National University

1. Introduction and Purpose

There have been great interests in the development of MR-compatible positron emission tomography (PET) to enable improved fusion imaging of function and anatomy of small animals and humans. Although numerous research prototypes have been developed and various scanners were commercialized, there has been considerable interests in the development of the advanced detector design to allow the multipurpose PET image acquisition and spatial resolution improvement. In this study, MR-compatible depth-encoding PET (DOI-PET) detector providing multiple spatial resolution and improving resolution uniformity, was proposed and examined for both clinical and research applications with one camera.

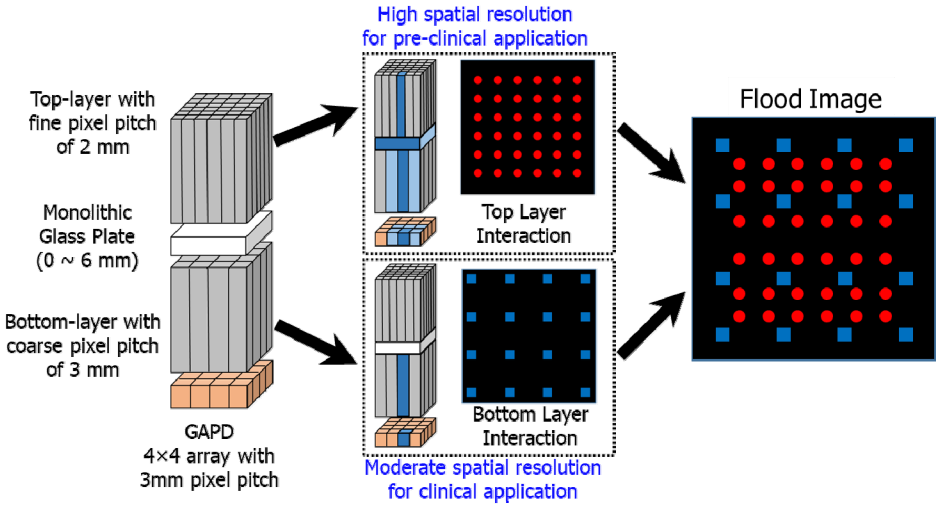

Fig. 1. Principle of the proposed detector to extract 3D information from 2D flood histogram.

2. Materials and Methods

Two layers of pixelated LYSO crystal arrays with different pixel pitch were stacked in the depth direction. Top-layer was a 6 x 6 array of 2 x 2 x 10 mm3 crystals, arranged with a fine pitch of 2.2 mm. Bottom-layer was a 4 x 4 array of 3 x 3 x 10 mm3 crystals, arranged with a coarse pitch of 3.3 mm. The glass plate with the thickness of 4 mm was inserted between the crystal layers and they could generate a unique light response for each discrete scintillator position. Relatively more light was shared when top-layer interacted with the gamma ray, while less light sharing was allowed when bottom-layer interacted with the gamma ray. These light spreading methods allow the extraction of 3D information from a 2D flood histogram. Sixteen output signals from 4x4 GAPD array were multiplexed by the resistive charge division networks, and they were transmitted to remotely located amplifier units using flexible flat cables. The four amplified signals were digitized and were recorded by

the DAQ system. These PET electronics were positioned outside of the 5-Gauss line in the MR to minimize the mutual interference between PET and MRI. In this study, no electromagnetic shielding was introduced to protect the PET components from the MR gradient and RF field.

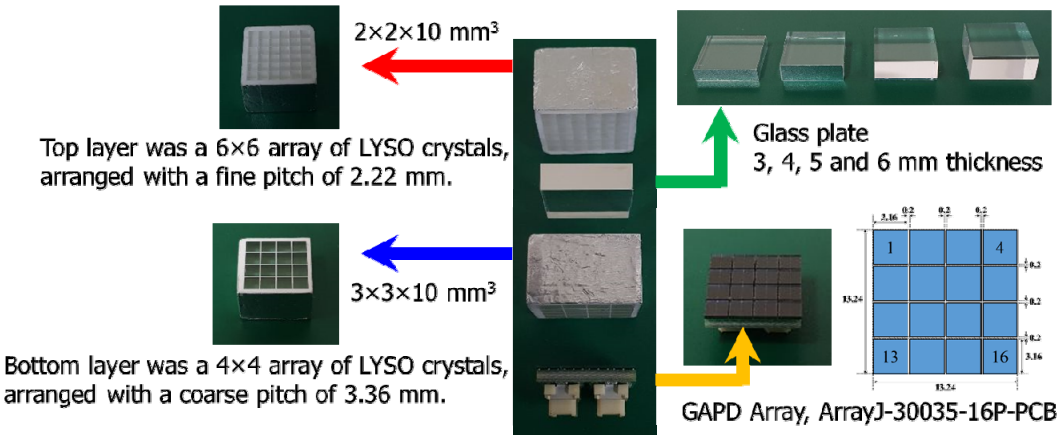

Fig. 2. Images of the prototype detector consists of top-layer with a 6 x 6 LYSO array, the glass plates, bottom-layer with a 4 × 4 LYSO array, and a 4 × 4 GAPD array

3. Results

2D flood histograms without the overlapping of each crystal position were acquired for detectors by inserting the glass plates. Average peak-to-valley ratios of the selected line profiles in DOI-PET detector were 4.5 and 5.4 for top- and bottom-layer, respectively. The mean energy resolution of top-layer providing high spatial resolution and bottom-layer providing moderate spatial resolution were 14.4 ± 1.0% and 13.4 ± 1.4%, respectively. Also, our previous study verified that there was no considerable degradation in PET detector performance and MR phantom image, caused by mutual interference between PET and MRI.

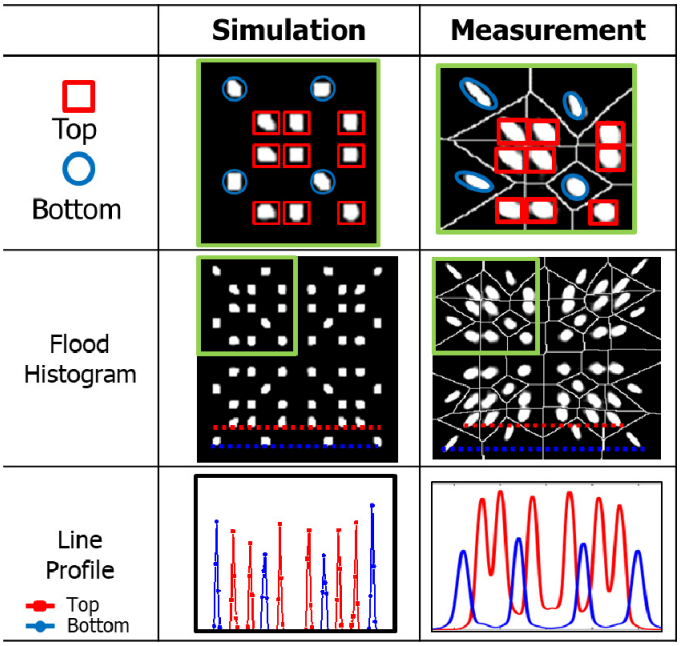

Fig. 3. Flood histograms and line profiles for DOI-PET detector acquired from simulation study and experiment measurement

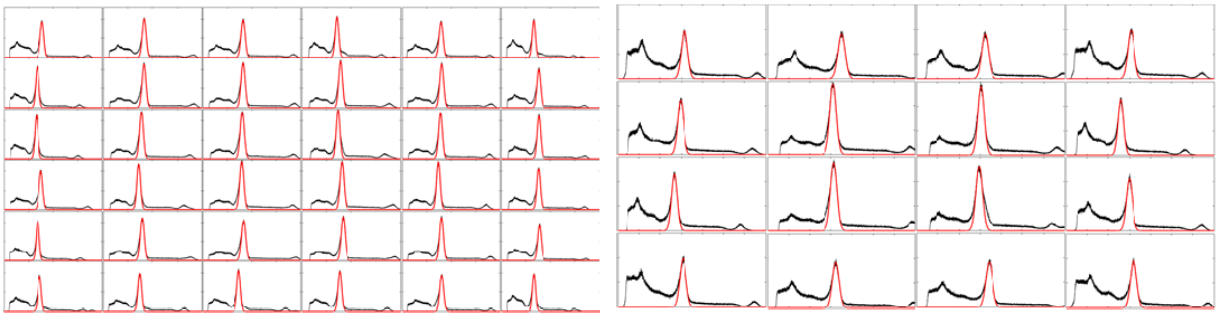

Fig. 4. Energy spectra for top-(left) and bottom-layer(right) for DOI-PET detector

4. Discussions

MR-compatible DOI-PET detector with multiple spatial resolution to provide high versatility for both clinical and research applications was proposed and also examined. 2D flood histograms without the overlapping of each crystal position can be generated for proposed detectors. Therefore, it was feasible to provide multiple spatial resolutions and 2-layer depth positions for the proposed DOI-PET detector using fine- and coarse-pitch crystals and inserting a glass plate between crystal layers.

The other considerable issues are whether potential mutual interference between two modalities can be minimized and whether the individual components can be operated without degrading performance. The charge signal transmission approach, which relays the charge signal from the photosensor to the remotely located preamplifiers for PET signal transmission, was employed in this study. This detector concept could allow the placement of amplifier units at a safe distance for integrated PET-MR scanner, can decrease the space requirements to insert a PET scanner into the restricted MR bore, minimize the mutual interference between PET and MRI, and eliminate the need for placing RF shielding materials close to field of view of the MR scanner.

5. Conclusions

These results demonstrated that the proposed detector design could provide several potential merits and allow the development of hybrid PET-MRI system for both clinical and research applications.

Reference

[1] J. Kang, Y. Choi, K. J. Hong, J. H. Jung, W. Hu, Y. S. Huh, H. K. Lim, B-T Kim, “A feasibility study of photosensor charge signal transmission to preamplifier using long cable for development of hybrid PET-MRI” Medical Physics, 37(11), pp. 5655-5664, Nov. 2010.

[2] J. Kang, Y. Choi, K. J. Hong, W. Hu, J. H. Jung, Y. S. Huh, B-T Kim, “A small animal PET based on GAPDs and charge signal transmission approach for hybrid PET-MR imaging” J. Instrum. 6(8), pp. P08012, August 2011.

Evaluation of Image Distortion according to Difference of Average and Partial Fourier in Gd Contrast Agent in 3D T1 SPACE

Yong Soo Han[1,3*], Cheol Soo Park[1], Man Seok Han[2]

[1]Department of Radiological Science, Hallym Polytechnic University, Chuncheon 24210, Republic of Korea

[2]Department of Radiological Science, Kangwon National University, Samcheok 245-905, South Korea

[3]Department of Medical Device Industry, Dongguk University, Goyang 10326, Republic of Korea

Gd enhancement is used for minimally invasive cancer metastasis and early evaluation on T1 - weighted images. However, in the case of cancer metastasis, the anatomical enhancement is microscopic and the amount of contrast agent is increased in order to enhance the contrast effect, and the 3D sequence is used to increase the detection ability for pathological metastasis and make a more accurate diagnosis.

In 3D T1 SPACE after using Gd contrast agent, image distortions due to difference of average and partial fourier. And Contrast agent phantom was constructed to measure signal intensity change and PSNR by contrast agent concentration.

The data were analyzed by preparing 8 phantoms with a contrast concentration of 3 mL, ranging from 0.1 mmol / mL to 10 mmol / mL, by diluting ProHance and saline in a 1.2 cm diameter cylindrical syringe. Statistical analysis was performed using correlation analysis (Pearson correlation coefficient, SPSS version 22.0 (IBM Co., Armonk, NY, USA).

Experimental results showed that the maximum signal intensity was 0.5mmol in Average 2 and Partial Fourier 8/8 at the time of 3D T1 SPACE test and The image distortion index roundness (%) was decreased to 80% or less after 2mmol. The PSNR was 40.39%, 38.75%, and Signal Intensity was 126.95 and 128.73, respectively, and the roundness (%) was 81.36% and 82.82%, respectively, in the comparison of Average 1.5, Partial Fourier 8/8 and Average 2, Partial Fourier 6/8 showing the same relative SNR (0.870023). Homogeneity index homogeneity was measured as 0.090 and 0.095, respectively.

For small lesions in 3D T1 SPACE after contrast enhancement, reducing the partial fourier rather than reducing the average may be useful for obtaining diagnostic information.

The use of Near Infrared Radiation (NIR) in Reconstructing 3D Oxygenated Images as Biomedical Evidence in Monitoring Diabetic Foot

Mezie Laurence B. Ortiz1[1,2], Axel Yen C. Garcia[1] and Youngjin Jung[1,3*]
[1]Dept. of Multidisciplinary of Radiological Science, Graduate School,
Dongseo University, Busan, 47011, South Korea
[2]College of Medical Radiation Technology, De La Salle Medical and Health Sciences Institute, Cavite, Philippines
[3]Dept. of Radiological Science, Dongseo University, Busan, 47011, South Korea

1. Introduction

This study aims to provide hemodynamic 3D images as clinical evidence using electro-magnetic wave (especially: Near Infrared Radiation) in monitoring diabetic foot which could be of use in improving patient's quality of life for it is portable non-invasive, non-ionizing and not requiring manual calibration, additional medical supplies and specifically trained personnel. Introduction:

Diabetes Mellitus (DM) or Diabetes is said to be the abnormal increase in the glucose concentration in the body. From 415 million people in the year 2015, an increase to 642 million people is expected in the year 2040. Among these individuals suffering from this condition, 25% have a lifetime risks of developing foot diabetes and from this percentage 84% among them have the possibility to undergo amputation of lower extremity. This is considered as the major reasons for non-traumatic amputations. The progressive characteristics of the disease demands for early diagnosis and continuous monitoring. It is undeniably true that radiology and nuclear medicine play an important role in diagnosing and monitoring. However, NIR is a form of non-ionizing radiation that can also be considered. The near infrared light ranging from 650-1000 nm is being used to image the soft-tissues in the body using the technique known as Near Infrared Spectroscopy (NIRS). It is described as portable non-invasive, non-ionizing and not requiring manual calibration, additional medical supplies and specifically trained personnel. NIR specifically works by exploring the oxygenated and deoxygenated hemoglobin concentration in the body which paved way for the measurement of hemoglobin concentration that is used to identify wound healing potential. This also allows the determination of the compression and expansion of blood vessels. NIR Diffuse Optical Tomography (DOT) allowed imaging of biological tissues in the diffusive regime and made the reconstruction of 3D oxygenated dynamic imaging possible to provide biomedical evidence.

2. Materials and Methods

The Toast C++ and MATLAB 2018b software applications were used to reconstruct 3D mesh files of the skin and bones of the foot. Subsequently, Diffuse Optical Tomography (DOT) method was applied on the generated mesh files having the forward and inverse problem for image reconstruction. In forward problem, diffusion equation was applied to predict the emission of NIR light based on the light source and interacting material parameters. Meanwhile, the inverse problem applied the forward problem to reconstruct the optical property distribution of interacting material from a measured data set.

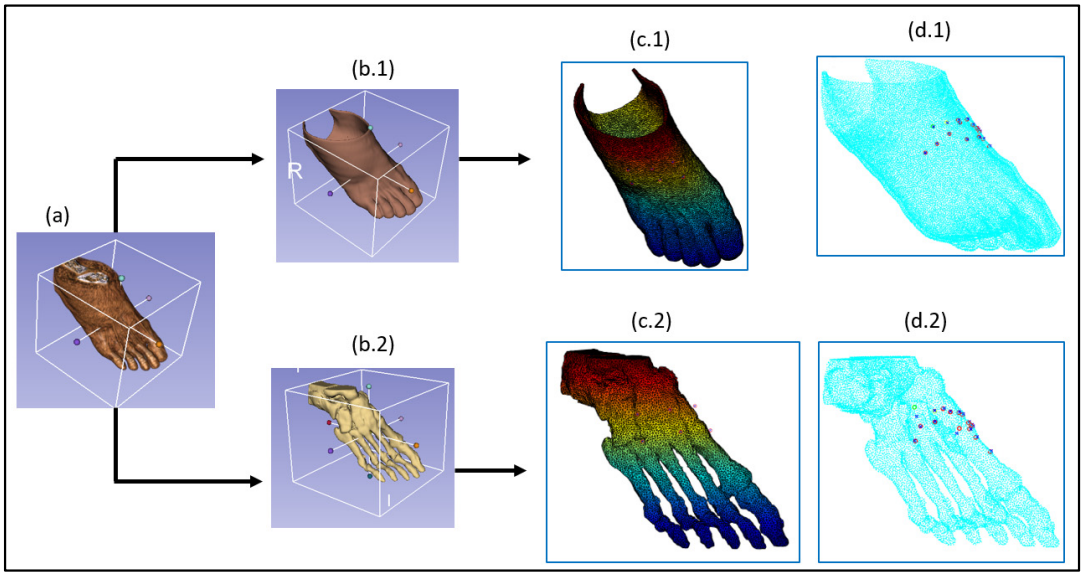

Fig. 1. The process of creating a mesh file starting from (a) foot model, (b.1) skin segmentation, (b.2) bone segmentation process to creation of (c.1) skin polygon mesh model and (c.2) bone polygon mesh model and to final mesh model (d.1, d.2)

3. Results

The hemoglobin concentration measured allowed the 3D reconstruction of oxygenated dynamic imaging, in particular, the absorption recon. The figure illustrates the differences in absorption reconstruction using the NIR and among the four reconstructions, *absorption recon 11* have the highest color map values obtained ranging from 00105 to 0.0105 since interaction happened in superficial area. *Absorption recon 1* have the lowest color map value ranging from 0.100000015 to 0.100000005 for the NIR light interaction happened within the deep seated areas.

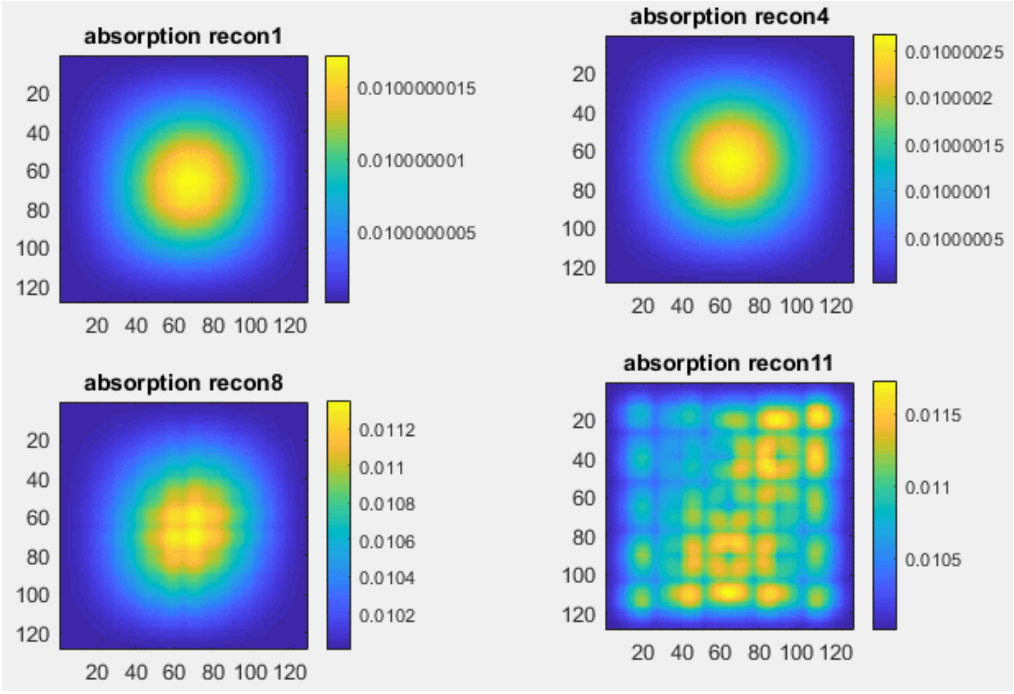

Fig. 2. The Cubic simulation model results.

4. Conclusion

In conclusion, 3D oxygenated dynamic images were reconstructed based on the hemoglobin concentration of the foot particularly the absorption reconstruction using non-ionizing electro-magnetic wave (NIR band). Moreover, the measured hemoglobin concentration could be of use in determining the wound healing potential of diabetic foot based on the ratio of oxygenated and deoxygenated hemoglobin in the blood. Contact and Remote based Near Infrared Spectroscopy could be of use in monitoring diabetic foot.

Radiation Dosimetry for medical field using Alanine/ESR System

Han-Ki Jang[1*], Ki-Tak Han[1], Woo-sang Ahn[2]
[1]Radiation Technology and Research Center, Korean Association for Radiation Application, Korea
[2]Department of Radiation Oncology, Gangneung Asan Hospital, University of Ulsan College of Medicine, Korea

Electron Spin Resonance(ESR) is one of the physical detection methods using spectroscopic technique to detect unpaired electrons in materials. In the field of radiation dosimetry for irradiated materials, ESR dosimetry have demonstrated as a versatile and key tool for dose assessment. Especially, alanine/ESR system is the most well known substances as free radical dosimeter. Also, alanine/ESR system is recommended by the International Atomic Energy Agency(IAEA) as a standard for high dose measurements. The alanine dosimeter can be used with an absorbed dose range of 1 to 200 kGy for photon, electron, and neutron. Also, Alanine/ESR dosimetry systems are used in reference or transfer-standard or routine dosimetry systems in radiation applications such as, food irradiation, medical therapy, and radiation damage studies in materials. In Korea, various dosimetry studies have been carried out using the Alanine/ESR system and reference irradiation system. Especially, in the KREDOS EPR working group, active research is being conducted on the Alanine/ESR dose assessment system through intercomparison using alanine samples. In this study, to evaluate the response of the alanine/ESR system to the photon and electron beams, we used a clinical linear accelerator(CLINAC) installed in a domestic hospital. Irradiation doses were set to 1 to 10 Gy for the energies of 6, 12 and 20 MeV electron beams and 4, 6, 10 and 15 MV photon beams. And, the experiment was performed after setting the dose rate range from 100 to 600 MU/min using 6 MV photon and 12 MeV electron beams in order to evaluate the dependence on the dose rate. In the case of alanine samples, we used two types of alanine sample manufactured by Bruker and Magnettech, respectively. The final goal of this research is to apply the alanine/ESR system to therapeutic radiation.

자기공명영상(MRI) 기반의 영상유도방사선치료 기법 및 응용

정도일*, 오성훈
(주)한빔테크놀로지

기존의 영상유도 방사선치료(image guided radiation therapy)는 X-ray 영상장치를 이용하여 치료 전 종양의 위치를 확인하는데 널리 사용되고 있다. 하지만, 획득된 영상은 연부조직(soft tissue)에 대한 대조도가 낮아 정확한 구분이 어려우며, 치료 기간 동안 반복되는 환자의 위치 확인을 위한 추가적인 방사선 피폭이 불가피하다. X-ray 영상장치의 한계점을 극복하기 위하여 자기공명영상(magnetic resonance imaging, MRI) 장치와 선형가속기(linear accelerator, LINAC)를 결합된 최첨단 MR-LINAC 방사선 치료 시스템이 최근 실제 임상에 사용되고 있는 상황이다.

기존 LINAC 장비에 대한 MR의 간섭을 최소화하기 위해 Magnet Free Zone에서 작동하도록 설계되어 있으며, O-ring gantry에 장착되어 기계적 중심축(isocenter)에 대한 정확도가 우수한 특징을 지닌다. MR-LINAC 장비를 이용한 영상유도방사선치료는 MRI를 이용하기 때문에 콘빔(cone-beam) CT(computed tomography) 또는 X-ray 영상에 비해 표적(target volume)이 되는 종양을 보다 정확하고 세밀한 조준이 가능하며, 더불어 환자의 치료부위 위치 확인을 위한 추가적인 방사선 피폭을 줄일 수 있다 것이 장점이다. 여러 번 반복되는 방사선 치료 중에 발생하는 종양의 위치나 크기, 형태의 변화는 물론 주변 정상 조직의 위치와 형태 변화까지 실시간으로 확인이 가능하며, 필요시 치료계획을 재수립하여 방사선 치료를 시행할 수 있는 실시간 맞춤형 방사선치료가 가능하다는 것이 특징적이다.

실제 종양의 움직임을 MRI로 실시간 추적(tracking)이 가능하기에 호흡동조 방사선치료(respiratory gated radiotherapy)에서도 큰 효과를 기대할 수 있을 것이다.

KMS 2019 Summer Conference

Special Session X

'Magnetics for IoT'

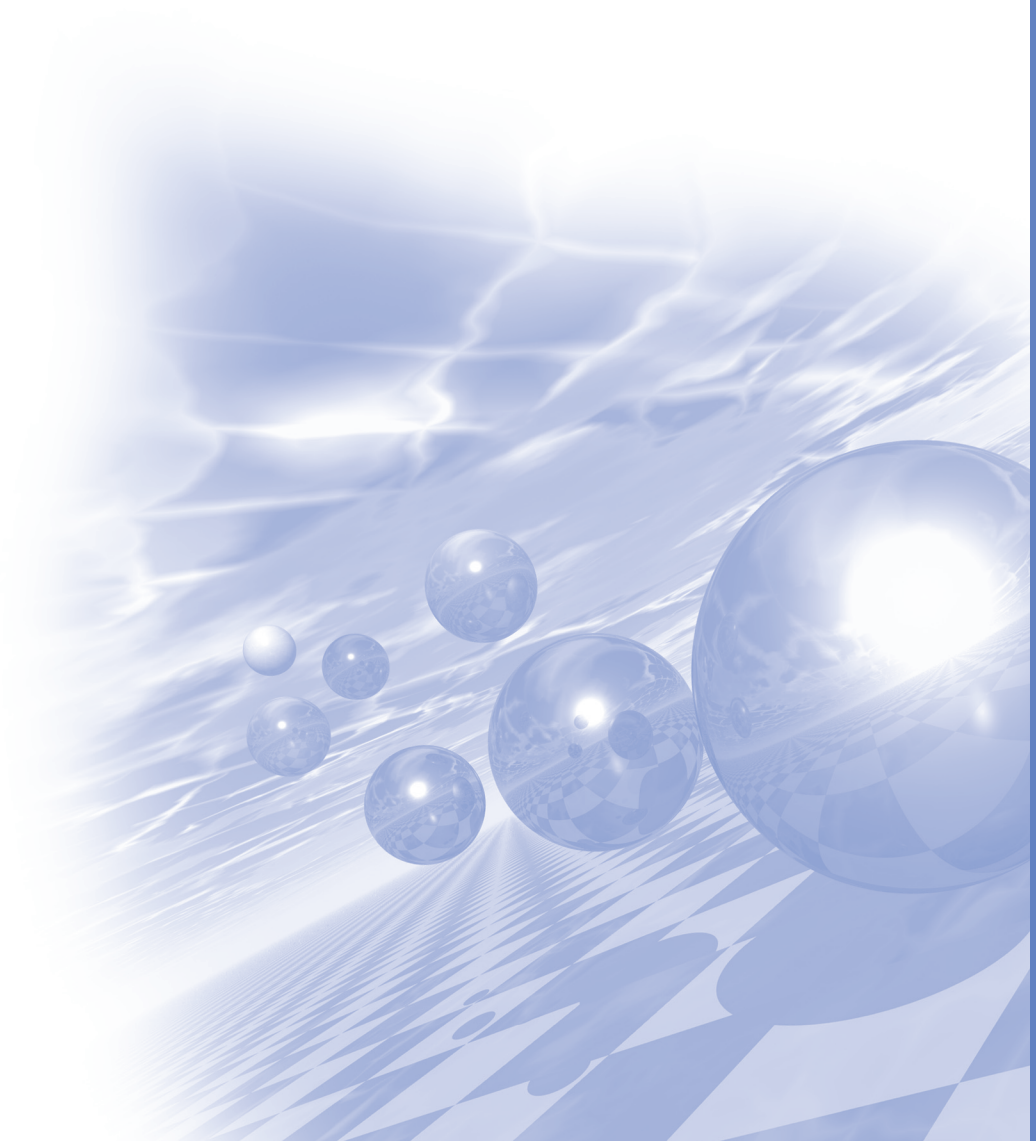

함정 전자기 신호 피탐 성능 분석 기법 연구

양창섭[1*], 정현주[1], 배기웅[1], 정우진[1], 이현진[2], 표성영[2]
[1]국방과학연구소 제6기술연구본부
[2]대양전기공업(주)

1. 서론

대부분의 군사 선진국은 전자기위협 무기체계로부터 자국 함정의 생존성 극대화와 이를 통한 전투력 향상을 위해 함정 전자기 스텔스 기술 및 핵심 장비들을 독자 개발하여 운용하고 있다. 국방과학연구소는 '15년 9월부터 '18년 8월까지 전자기 위협 무기체계로부터 국내 함정의 생존성 향상을 위한 연구의 일환으로 '함정자장제어기술' 과제를 수행하였다. 본 논문에서는 과제 세부 핵심 연구 내용 중에서 실 함정 대상의 전자기 신호 피탐 성능 분석 기법 연구 결과에 대해 기술하고자 한다.

2. 함정자장제어기술 과제 현황

함정자장제어기술 과제는 감시체계 및 기뢰체계 등의 위협세력으로부터 함정의 생존성 확보를 위한 수중 전자기 스텔스 기술을 국내 독자 개발하는 내용이다. 본 과제에서는 먼저 함정 전자기 수치해석 모델 설계를 통해 예측되는 실함 해석 신호와 해군 자기측정시설로부터 확보된 실함 계측 신호로부터 임의 작전 환경 하에서의 함정에서 발생되는 수중 전자기 신호의 특성을 사전 예측하였다. 또한 위협세력(기뢰, 항공/수중감시체계 등)의 탐지센서 수준별 함정 자장제어 전/후의 신호 피탐 성능을 예측하였다. 아울러 현재 국내 함정에서 전량 국외 도입되어 운용되고 있는 소자장비(Degaussing System) 국산화 기반 구축을 위해 축소함용 소자/탈자장비 제작을 통한 핵심 알고리즘 연구와 실함용 소자장비 핵심부품(2종) 제작 및 실함 대상 소자장비 개념설계를 추가 수행하였다.

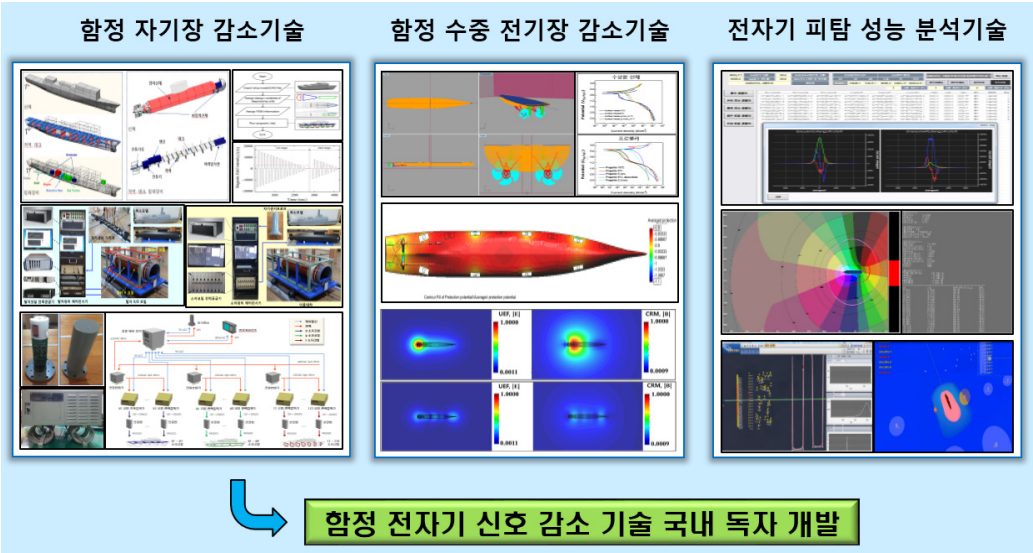

그림 1. 과제 개념도

3. 함정 전자기 신호 피탐 성능 분석 방안 및 결과

함정 전자기 신호 피탐 성능 분석 연구는 함정 전자기 신호원의 특성 및 전자기 위협원의 특성을 수학적으로 모델링한 후, 이를 바탕으로 위협 무기체계의 탐지 수준별 대상 함정의 피탐 성능을 예측하기 위한 기법을 개발하는 내용이다. 본 연구의 결과를 요약하면 다음과 같으며, 개발된 기법의 완성도를 높이기 위해 실함 대상의 해군 전자기 신호 DB 활용은 물론 위협 무기체계의 전자기 신호 탐지 성능을 종합 반영하였다.

- 함정 전자기 신호원 특성 모델링

함정 전자기 신호원 특성 모델링은 소요군의 자기시험시설로부터 확보된 대상 함정의 전자기 신호로부터, 수학적인 등가 전자기 모델링을 수행한 후 대상 함정의 운용 조건(수심, 거리)별 전자기 신호를 계산하였다.

- 전자기 위협세력 특성 모델링

기존 전자기 위협 세력의 주요 탐지 성능 요소를 설계에 반영하여 모델링하였으며, 위협세력에서 향후 활용 가능한 탐지 성능 요소를 추가 식별하여 범용성 및 확장성을 고려하였다.

- 전자기 위협세력별 피탐 성능 시뮬레이션

대상 함정의 전자기 신호 특성 모델링과 위협 세력 특성 모델링 결과로 부터, 전자기 위협세력 대비 대상 함정의 피탐 성능에 대한 시뮬레이션을 수행하였다. 그림 2는 가상의 위협 기뢰체계에 대한 함정 자기장 감소기법 적용 전/후의 피탐 성능 분석 결과를 보여주고 있으며, 동일한 함정에 대해 자장제어 전 대비 자장제어 후에는 피격 확률이 크게 감소됨을 확인할 수 있었다.

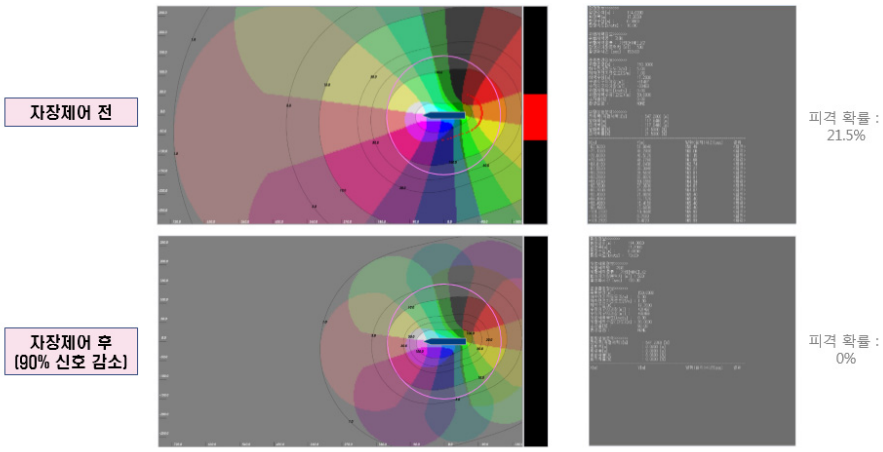

그림 2. 함정 자기장 감소기법 적용 전/후의 피탐 성능 분석 결과

4. 결론

본 논문에서는 함정자장제어기술 과제의 일환으로 수행된 함정 전자기 신호 피탐 성능 분석 연구 결과에 대해 기술하였다. 본 연구를 통해 가상의 위협무기체계에 대비하여 다양한 운용 환경에서의 대상 함정의 전자기 신호 피탐 성능 시뮬레이션이 가능하게 됨으로써 향후 국내 함정의 작전 수행 능력 향상과 전투력 증강에 크게 기여할 수 있을 것으로 판단된다.

5. 참고문헌

[1] 양창섭, 정현주, 정우진, 한국자기학회지, **24**(4), 114(2014)

[2] 양창섭, 정현주, 조동진, 정우진, 한국자기학회 2016년 하계학술연구발표회, 11(2016)

[3] 양창섭, 정현주, 조동진, 정우진, 2016년 한국군사과학기술학회 추계학술대회, 1(2016)

[4] 양창섭, 2017년 함정기술 무기체계 세미나, 168(2017)

3-축 Flux-gate 마그네토미터를 이용한 지하매설 불발병기(DXO)탐지에 관한 연구

손대락[1*], 김은애[2], 김상준[2]
[1]한남대학교
[2]주)센서피아

1. 서론

일반적으로 땅속에 표면에 있는 금속물체는 금속탐지기를 사용하여 탐지가 가능하다. 그러나 땅속 깊이 매설되어 있는 불발병기의 경우 일반적인 금속탐지기로는 탐지가 불가능하여, 전통적으로 불발병기가 철로 되어 있는 점에 착안을 하여 불발병기에 의하여 발생되는 비정상적인 자기장의 분포를 측정하여 불발병기를 탐지하는 기술로 사용되고 있다. 자기장의 측정방법으로는 1축의 마그네토미터를 2개 사용하는 magnetic gradiometer 방식을 사용 주변 환경자기장 효과를 최소화하고, 불발병기에 의하여 발생되는 자기장의 분포를 측정하고 있다. 그러나 1-축의 자기장센서의 경우 한계가 있어서 여러 개의 magnetic gradiometer를 나열하여 분석을 하고 있다.

2. 실험 및 결과

본 연구에서는 직각도를 보정하여 직각도가 0.05도 이상인 3-축의 flux-gate magnetometer를 1 m 간격으로 배치하여 total field의 gradient를 측정하게 하여, 드론과 같은 무인기에 장착하여도 이들 비행물체에 의한 진동이나 흔들림에 의하여도 total field의 크기는 변화하지 안기 때문에 무인기를 사용한 자기장 탐사가 가능하여진다. 그림 1은 본 연구에서 제작 된 3-축의 flux-gate magnetometer를 2개 사용한 gradiometer의 사진이고 그림 2는 길이 5m의 승용차를 드론을 사용하여 8m 상공에서 자기장의 gradient를 측정한 결과이다.

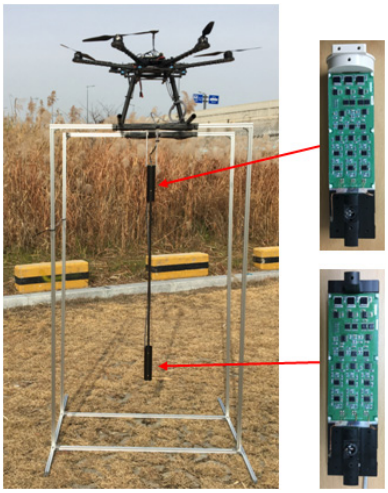

그림 1. 본 연구에서 제작한 3-축 flux-gate magnetometer 2개를 사용한 gradiometer

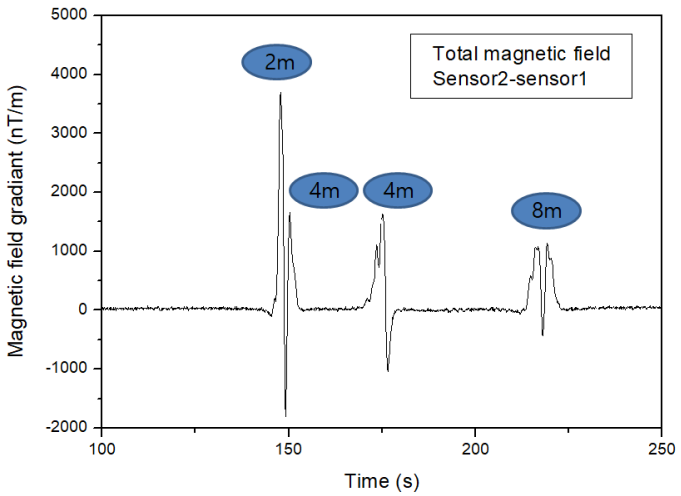

그림 2. 길이 5m의 승용차를 드론을 사용하여 2-8m 상공에서 측정한 total field의 qradiant

함정용 소자장비 핵심기술 개발

표성영[1*], 이현진[1], 정봉출[1], 정현주[2], 양창섭[2]
[1]대양전기공업(주) 1연구소
[2]국방과학연구소 제6기술연구본부 3부

1. 서론

해군 함정에서 수중으로 방사되는 정 자기장 신호는 기뢰와 같은 위협세력의 탐지원이 된다[1]. 이러한 정 자기장 신호를 감쇄시켜 함정의 생존성을 높이기 위해 함정에 소자장비를 탑재한다.

함정 소자장비 국산화를 위해 지속해서 많은 연구가 이루어지고 있다[2-4]. 이에 맞추어 당사 연구소는 소자장비 개발에 필요한 핵심기술을 파악하고 이에 대한 기술 확보를 수행하였다. 본 발표에서는, 함정용 소자장비를 국산화하기 위한 개발의 일환으로써, 축소함용 소자장비와 함정용 소자장비 핵심부품을 설계·제작한 내용을 소개한다.

2. 실험방법과 결과

수상함과 잠수함 형태의 축소모델은 강자성 재질이고, 소자코일에 전력을 공급할 전력공급기와 소자 제어기는 캐비닛에 설치되는 형태로 개발되었다.

그림 1. 축소함용 소자장비 구성

지구 자기장과 함정 방향에 따라 변화하는 함정 유도 자기장과 함정 탈자 후 잔류 영구 자기장을 효과적으로 보상하기 위해 소자코일을 V-A-L 형식으로 배치 설계하였다. 축소함용 소자장비의 자기장 감쇄 능력은 시험을 통해 확인되었다.

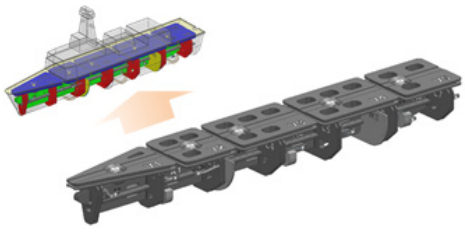

그림 2. 소자코일 조립체

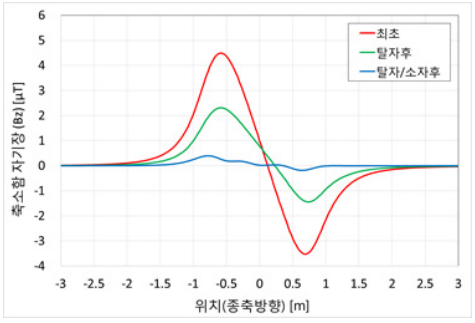

그림 3. 축소함 자기장 감소 시험

함정 자기 요구수준을 만족하는 함정용 소자장비 개발을 위한 단계적 접근 방안으로 소자장비의 핵심부품이라 할 수 있는 자기센서 프로브와 소자코일 전력증폭기를 설계·제작하였다. 두 개의 핵심부품은 성능시험과 환경시험에서 요구사항을 모두 충족하였다.

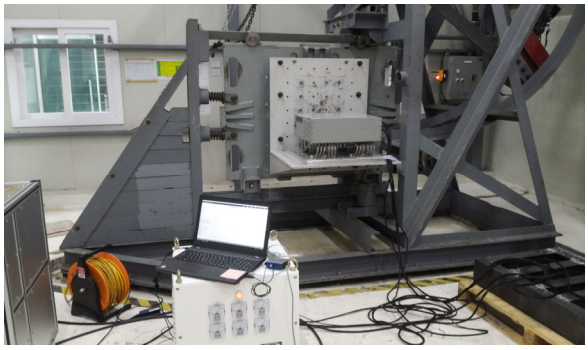

그림 4. 소자코일 전력증폭기 충격시험

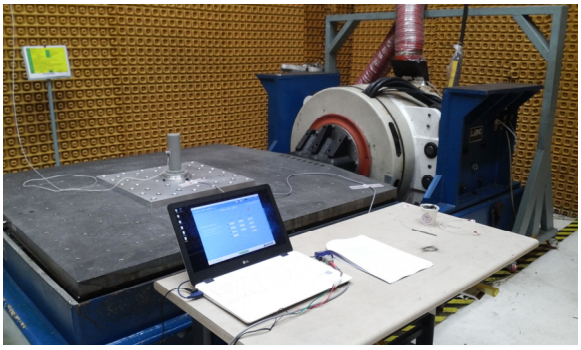

그림 5. 자기센서프로브 진동시험

3. 고찰

개발된 축소함용 소자장비의 목표 소자 성능의 충족을 확인하였다. 실함 탑재용으로 개발한 소자장비의 핵심부품인 자기센서 프로브와 소자코일 전력증폭기는 설계 제원상의 성능을 충족하였고 군사규격의 충격시험, 진동시험 그리고 온습도시험 인증까지 받아서 함정에 탑재가 가능한 수준이다.

4. 결론

축소함용 소자장비 개발을 통하여 함정용 소자장비 국산화를 위한 핵심기술을 확보하고, 실함용 소자장비 핵심부품인 자기센서 프로브와 소자코일 전력증폭기 시제도 제작하여 함정 소자장비 국산화 개발 가능성을 더욱 높이게 되었다. 향후 지속적으로 장비 개발을 추진하여 장비 국산화를 완료할 계획이다.

5. 참고문헌

[1] John J. Holmes, Exploitation of a Ship's Magnetic Field Signatures, Morgan & Claypool (2006) pp. 19-23.
[2] 조동진, Journal of the Korean Magnetics Society 27(2), 63-69 (2017).
[3] 양창섭, 정현주, Journal of the Korean Magnetics Society, Volume 21, Number 5, Oct. 2011.
[4] 양창섭, 정현주, Journal of the Korean Magnetics Society, Volume 17, Number 6, Dec. 2007.

함정의 두께와 반자장에 따른 탈자 영향 분석

박관수[1*], 임상현[1], 이호영[1], 정현주[2]
[1]부산대학교
[2]국방과학연구소

1. 서론

함정은 강자성체로 이루어지고, 강자성체의 특징에 따라 제조 공정 및 외부 자기장에 의하여 착자되게 된다. 이렇게 착자되어진 함정은 수중 자기장을 이용하여 공격하는 기뢰, 어뢰, 대잠 초계기 등의 무기들에 의하여 피해를 받을 위험이 있다. 수중 무기에 의한 피해를 줄이기 위해서는 함정의 자기장을 줄이는 방법이 필요하고, 이를 탈자라고 한다. 탈자는 외부에서 교번하고 감소하는 자기장을 인가하여 자성체의 히스테리시스 특성에 따라 잔류 자화값을 0으로 만드는 과정을 뜻한다.

현재 세계적으로 함정의 탈자를 연구하기 위하여 등가모델로써 속이 빈 원통 시편을 이용하여 탈자 프로토콜의 변수들의 영향에 대하여 연구를 진행하고 있다. 하지만 시편을 이용하게 될 경우 탈자 연구에 큰 문제점이 발생하게 된다. 양 끝 단이 개방되어 있기 때문에 필연적으로 내부 반자장이 발생하게 되므로, 시편 내부에서는 외부에서 인가한 자기장보다 작은 자기장이 실제로 인가되게 된다. 이에 따라 연구 목적과는 다른 연구 결과가 발생하게 된다. 그러므로, 함정의 두께가 탈자에 미치는 영향에 대한 연구가 필요하다.

본 연구에서는 다양한 두께의 시편을 이용하여 동일한 탈자 프로토콜을 인가함으로써 두께에 따른 탈자 영향을 분석하였다. 또한, 수식과 FEM을 통하여 시편의 내부 반자장 계수를 분석하고, 이를 고려하여 탈자를 수행함으로써 다른 탈자 프로토콜을 인가하여 동일한 탈자 결과가 발생하는 것을 확인하였다.

2. 실험방법과 결과

본 연구에서는 다양한 두께를 가지는 속이 빈 원통 시편을 이용하여 동일한 탈자 프로토콜을 인가하고 난 뒤 탈자 결과를 분석하였다. 또한 내부 반자장 계수를 고려한 탈자 프로토콜을 각각 인가한 뒤 동일한 탈자 결과가 발생하는 것을 확인하였다. 자세한 탈자실험 과정은 다음과 같다.

1) 아래의 시편과 축소함에 동일한 탈자 프로토콜을 인가한 뒤, 수직 방향 18cm 떨어진 위치에서 수평 자기장 성분 Bx 및 수직 자기장 성분 Bz 값을 비교한다.

2) 내부 반자장 계수를 고려하여 탈자 프로토콜을 각각 수정한 뒤, 각 탈자 프로토콜을 인가한 뒤 자기장 값을 측정한다.

3) 각각의 탈자 결과를 비교 분석한다. 동일한 탈자 프로토콜을 인가하면 실제 내부에는 다른 자기장이 인가되기 때문에 각각 다른 탈자 결과가 발생하는 것을 확인하였다. 내부 반자장을 고려한 프로토콜을 인가하게 되면 동일한 탈자 결과가 발생하는 것 또한 확인하였다.

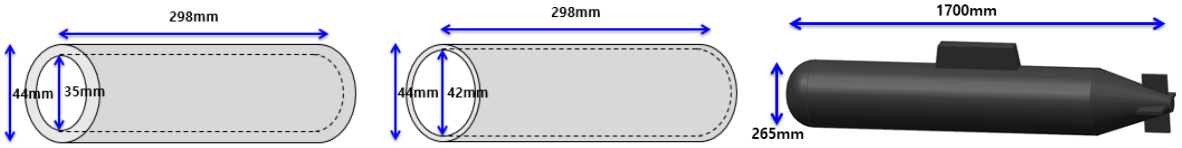

<그림 1>

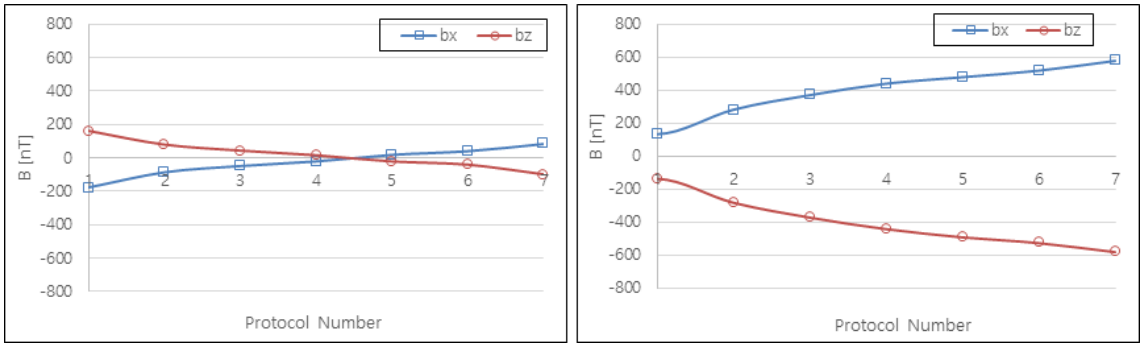

(a) 시편 1 (b) 시편 2

그림 2. 시편의 두께에 따른 탈자 결과

3. 고찰

그림 2에서 알 수 있듯이, 동일한 탈자 프로토콜을 두께가 다른 시편들에 인가하게 되면, 다른 탈자 결과가 발생하게 된다. 자기장의 크기는 시편의 부피에 따라 달라질 수 있지만, 전체적인 변화의 경향성을 분석하면 전혀 다른 탈자 결과가 발생하였다고 할 수 있다. 반면 내부 반자자을 고려하여 탈자 프로토콜을 인가하게 되면, 전체적인 자기장 크기는 다르지만, 동일한 경향이 발생하는 것을 알 수 있다.

4. 결론

본 논문에서는 함정의 두께에 따른 반자장이 탈자 결과에 미치는 영향에 대하여 분석하였다. 다양한 두께의 시편과 축소함을 이용한 실험을 통하여 동일한 탈자 프로토콜을 인가하더라도 내부 반자장에 따라 다른 결과가 발생하게 된다는 것을 확인하였다. 또한 반자장을 고려하여 탈자를 수행하게 되면 두께가 다르더라도 동일한 탈자 결과가 발생하는 것 또한 확인하였다. 이러한 결과를 바탕으로, 향후 탈자 연구를 수행할 경우 내부 반자장을 고려하여 탈자를 수행하여야만 할 것이다.

5. 참고문헌

[1] H. Won, H. S. Ju, S. Park and G. S. Park, IEEE Trans. Magn. 49(5), 2045 (2013).

[2] 한국자기학회, 한국자기학회 학술연구발표회 논문개요집, 2014.5, 132-133 (2 pages)

[3] 원혁, “강자성체의 자화 역학 구조에 따른 히스테리시스 현상의 수치 모델링에 관한 연구”, 공학 박사 학위 논문, 부산대학교, 2010

선체 부식으로 인한 수중 전자기 신호 특성 및 감소 기법 연구

정현주*, 양창섭
국방과학연구소

1. 서론

수중 무기체계에서 표적 탐지가 가능한 전/자기 신호원으로는 강자성 선체에 의한 정 자기장(Static magnetic field) 신호가 대표적이다. 그러나 최근 함정 자기처리(deperming) 및 소자(degaussing) 등과 같은 함정의 정 자기장 신호에 대한 스텔스 능력이 지속적으로 향상되면서 강자성 선체에 의한 정 자기장 신호를 탐지하기가 날로 어려워지고 있다. 이러한 문제를 극복하기 위하여 미국, 영국, 중국, 러시아 등 군사 선진국들은 표적으로부터 발생되는 수중 전기장 신호를 탐지할 수 있는 센서들을 개발하여 무기체계에 적용하고 있다[1]. 아울러 이러한 무기체계에 대항하기 위한 방안으로 선체 부식에 의한 수중 전/자기 신호를 최소화하여 아함의 생존성을 극대화하기 위한 노력도 함께 병행하고 있다[2]. 따라서 본 논문에서는 선체의 부식 및 부식방지 장치에 의해 수중에서 발생되는 수중 전/자기 신호의 발생원리 및 특성을 소개하고, 감소 기법에 대한 내용을 기술하였다.

2. 선체 부식으로 인한 수중 전자기 신호 특성

선체의 부식은 부식의 여러 현상 중에서 갈바닉 부식에 해당된다. 그림 1은 선체 갈바닉 부식의 원리를 나타내는 그림이다. 프로펠러를 구성하는 청동합금(NAB, Nickel Aluminum Bronze)에 비해 상대적으로 낮은 전위를 가지는 선체를 구성하는 철은 부식이 진행되는 중 이온화(Fe → Fe2+ + 2e-)되며, 이온화 과정에서 발생된 전자는 프로펠러 축계를 거쳐 프로펠러로 이동하고, 철 이온은 해수를 통해 프로펠러로 이동한다. 이러한 원리로 선체-해수-프로펠러-프로펠러 축계-선체로 연결되는 폐 루프(Closed loop)를 형성하며 전류가 흐르게 되고, 이 전류에 의해 함정으로부터 전기장 및 자기장이 발생된다.

선체의 부식을 방지하기 위한 방법으로는 갈바닉 전위가 낮은 금속들을 인위적으로 선체에 부착하여 선체를 보호하는 수동 부식방지장치와 기준 전극을 통해 선체 표면의 전위를 모니터링하고 비소모성 양극을 통해 전류를 흘려줌으로써 선체 부식이 일어나지 않는 전위 조건으로 항상 유지시켜 주는 능동 부식방지장치가 사용되고 있다. 수동 음극부식방지장치의 경우는 시간이 경과함에 따라서 희생양극이 점진적으로 소모됨으로 인해 함정 상가 시 정기적인 정비 및 교체가 필수적이다. 반면, 능동 음극부식방지장치는 비소모성 양극 금속, 기준 전극 및 전원 공급기를 사용함으로서 초기 설치비용은 수동 음극부식방지장치보다 증가하지만 유지비용이 감소한다는 장점이 있다. 따라서 최근 대부분의 중대형 선박에서는 능동 음극부식방지장치를 주로 사용하고 있다. 능동부식방비장치는 선저표면의 전위를 부식이 발생하지 않는 일정한 값으로 유지하여 선체를 부식으로부터 보호하는 장치로서, ICCP(Impressed Current Cathodic Protection) 장치가 여기에 해당된다. ICCP 장치는 선저 주요 부위에 장착된 기준전극(Reference Electrode)이 각 부위의 직류 전압을 감지하고, 선체 전위가 -0.8 V가 유지되도록 ICCP 양극과 해수를 통해 강제로 선체외부에 전류를 흘려줌으로서 선체를 부식으로부터 보호하게 한다. 이렇게 강제로 흘려주는 전류에 의해서 수중에는 전기장과 자기장이 발생하게 된다. 또한, 함정 프로펠러 축계의 회전에 의한 선체 부식방지전류의 변조 현상에 의해 수십 Hz대역까지의 교류 전기장 및 자기장 신호가 발생될 수 있으며, 능동 부식방지장치의 전원 필터 특성이 나쁜 경우에 수백Hz 대역까지의 교류 신호가 발생된다.

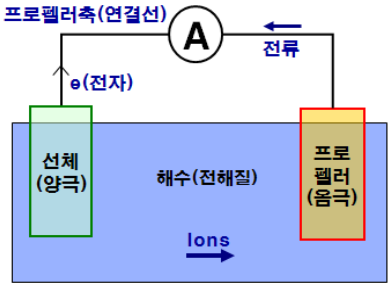

그림 1. 선체의 갈바닉 부식 모델

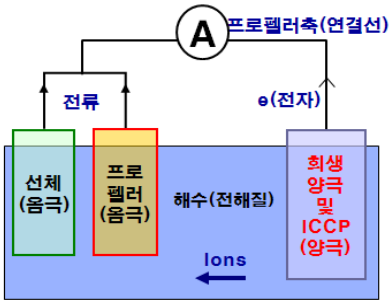

그림 2. 부식방지장치에 의한 갈바닉 부식

3. 선체 부식으로 인한 수중 전자기 신호 감소 기법

선체 부식에 의한 수중 전/자기 신호를 감소시키는 대표적인 방법은 ICCP 장비의 양극 개수를 증대시키고, 또 양극과 기준전극의 위치를 최적화하는 것이다. 임의 함정을 대상으로 그림 3과 ICCP 양극의 개수를 2 pairs, 3 pairs 및 4 pairs로 배치한 세 가지 경우에 대해서 수중 전/자기 신호 전용 해석 도구인 영국 FNC사의 FNREMUS 소프트웨어를 사용하여 해석한 결과를 표 1에서 비교하였다. 표 1에서 알 수 있듯이 ICCP 미 동작 시와 동작 시 ICCP 양극 배치 조건별로 수중 전기장 크기를 비교하면 ICCP 양극의 개수가 증가함에 따라 그 크기가 감소함을 알 수 있는데 4 pairs ICCP 양극 배치의 경우, 2 pairs 대비 수평 종축 성분(x축)은 대략 46 % 수준까지 감소하고, 수직 성분(z축)은 대략 42 % 수준까지 감소함을 알 수 있었다.

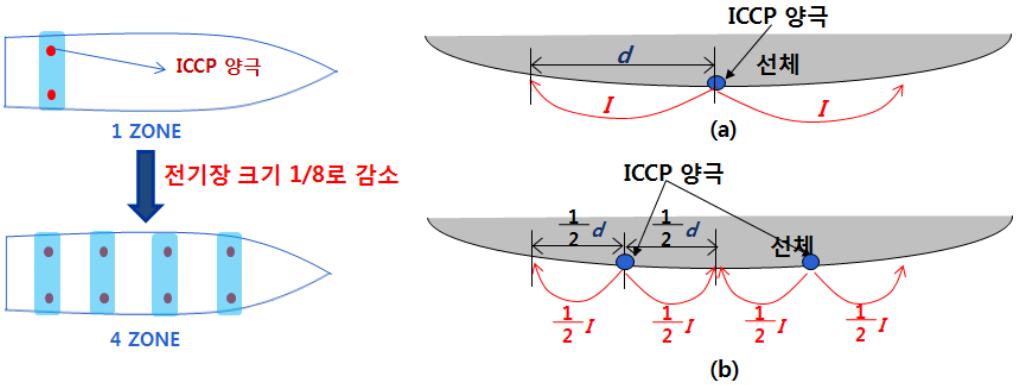

그림 3. ICCP 양극 배치 개념

표 1. ICCP양극 배치 조건에 따른 수중 전기장 신호 크기

항목	수평성분(Ex)	수직성분(Ez)
ICCP 미 작동	0.25	0.45
2 pairs	0.56	0.79
3 pairs	0.33	0.46
4 pairs	0.26	0.33

4. 참고문헌

[1] H. Jones, “Development of a low a noise electric field sensor for measurement and ranging applications”, MARELEC 2004, 17-18th March 2004.

[2] Richard Holt, “The source of electric fields in seawater, and Their Measurement”, Warship Cathodic Protection 2001, 21-23 August 2001.

NextSAT2 호기용 TAM 및 EMTB에 관한 연구

김은애[1*], 김상준[1], 손대락[2]
[1]주)센서피아
[2]한남대학교

1. 서론

차세대 소형위성 1호기(NEXTSat1)가 제작되어 2018년 11월에 성공적으로 발사되어 작동 운용이 되고 있다. 차세대 소형위성 2호기(NEXTSat2)의 경우 차세대 소형위성 1호기와는 조금 다른 규격으로 설계요구사양이 변경되었다. EMTB(Electro-Magnetic Torque Bar)의 경우 운용 전압이 28 V에서 15 V로 변화되었으며, TAM(Three Axis magnetometer)의 경우 측정자기장의 범위는 ±60 uT로 같으나 치수와 입력 전원이 변동되었으며, 전워은 15 V_{dc}에서 소비전력이 1 W로 구동이 되게 변동되었다.

2. 실험 및 결과

제작된 되면서 EMTB의 경우 최대 magnetic diopole moment가 ±15 Am²이고 ±15 V 에서는 ±12 Am² 이 발생될 수 있게 제작을 하였다. TAM의 경우 측정자기장의 범위는 ±60 uT이고 직각도가 1° 이상, 성형도가 0.1% 이상dl되고 interfaces는 RS422로 baud rate는 38400bps 이고 측정 자기장 값은 binary로 출력되게 하였다. 제작된 EMTB와 TAM의 환경시험은 열진공시험 및 진동시험을 수행하였다. 열진공시험의 경우 진공도 : <1.0E-5 torr 이하에서, 온도 : -40˚C ~ +53˚C 주기 : 2.5, 담금시간 : 6시간 이상 수행하였다. 진동시험의 경우 20~2000 Hz 범위에서 total rms 값이 16.05g에서 2분간 수행하였다.

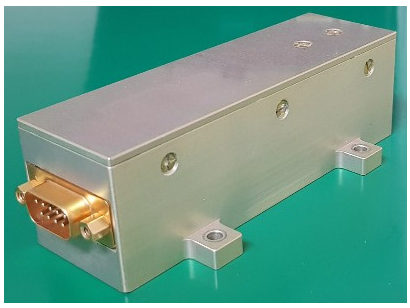

그림 1. NEXTSat-2용으로 제작된 TAM의 사진

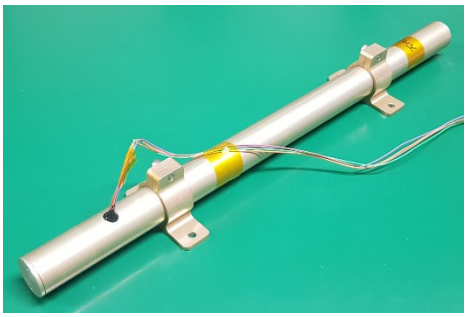

그림 2. NEXTSat-2용으로 제작된 EMTB의 사진

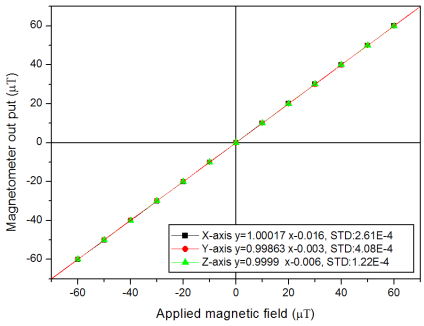

그림 3. TAM의 선형도 특성

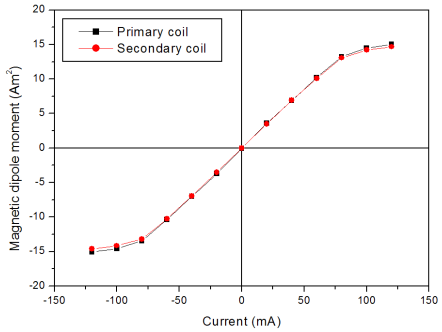

그림 3. EMTB의 *m-I* 특성

Author Index

Name	Abstract ID	Page
Abert, Claas	MD08	44
Ahn, Woo-sang	초S-IX-5	207
Arifiadi, Anindityo Nugra	NS03	82
Bae, Geonhee	SA04	91
Baek, Cheol-Ha	초S-IX-1	199
Baek, Seung-heon Chris	초S-V-2	148
Baek, Youn-Kyoung	HM04	50
Baek, Youn-Kyoung	초S-II-10	159
Baek, Youn-Kyoung	초S-II-5	117
Bhoi, Biswanath	MD06	40
Bhoi, Biswanath	MD07	42
Bhoi, Biswanath	NS03	82
Braun, Hans-Benjamin	HP-1	171
Braun, Hans-Benjamin	T-3	5
Byun, Sang Won	NS02	81
Cha, Hee-Ryoung	HM03	49
Cha, Hee-Ryoung	MT05	14
Cha, Hee-Ryoung	초S-II-5	117
Chang, Mi Se	초S-II-8	157
Chang, Seo Hyoung	초S-VII-1	179
Cho, Daegill	HM02	48
Cho, Jin-Hyung	HM07	54
Cho, Young-Jun	MD02	35
Choe, Sug-bong	MD09	45
Choi, Chul-Jin	초S-II-6	155
Choi, Min	MT17	26
Choi, Mi-Young	MT11	20
Choi, Seong Jin	SA03	90
Choi, Sungjoon	SA03	90
Choi, Sung-Jun	초S-II-2	114
Choi, Taeyang	초S-VII-1	179
Choi, Taeyoung	초S-I-1	105
Choi, Y. J.	NS01	80
Choi, Yun-Yong	초S-VIII-1	189
Choi, Yun-Yong	초S-VIII-3	191
Choi, Yun-Yong	초S-VIII-5	194
Choi-Yim, Haein	HM10	58
Cuong, Do Duc	MT18	27
Djuanda, Dagus R.	HM06	52
Do, Thi Nga	SO01	74
Dongquoc, Viet	초S-III-6	130
Elzwawy, A. A.	초S-III-1	121
Everschor-Sitte, Karin	초S-V-4	150

Name	Abstract ID	Page
Futakawa, Yasuhiro	초S-IV-4	136
Garcia, Axel Yen C.	초S-IX-4	204
Go, Dongwook	초S-VII-2	180
Go, Gyungchoon	초S-V-4	150
Go, Gyungchoon	초S-V-5	151
Gomonay, Olena	초S-VII-4	183
Ha, Jae-Hyun	초S-III-5	127
Han, Dong-Hee	초S-IX-1	199
Han, Dong-Soo	초S-IV-3	135
Han, Hee-Sung	MT04	12
Han, Hee-Sung	초S-IV-6	138
Han, Hyuksu	초S-VI-1	163
Han, Jonghee	HM10	58
Han, Jung Hoon	초S-VII-1	179
Han, Ki-Tak	초S-IX-5	207
Han, Man Seok	초S-IX-3	203
Han, Yong Soo	초S-IX-3	203
Heo, Yun-Seok	SM01	60
Hirata, Yuushou	초S-IV-4	136
Ho, Thi H.	MT09	18
Ho, Thi H.	MT13	22
Hong, Jinki	SS02	72
Hong, Jisang	MT01	9
Hong, Jisang	MT08	17
Hong, Jung-Il	초S-III-5	127
Hong, Jung-Il	초S-IV-6	138
Hong, Jung-Pyo	초S-VIII-1	189
Hong, Jung-Pyo	초S-VIII-3	191
Hong, Mun Bong	MT03	11
Hong, S. C.	MT03	11
Hong, S. C.	MT09	18
Hong, S. C.	MT10	19
Hong, S. C.	MT13	22
Hong, S. C.	MT14	23
Hong, S. C.	초S-VII-6	186
Hong, Soon Cheol	MT02	10
Hong, Soon Cheol	MT18	27
Hong, Sungsoo	초S-IX-2	200
Huang, Hai	초S-VII-1	179
Huh, Seok Hwan	MT16	25
Hung, T. Q.	초S-III-1	121
Im, Mi-Young	초S-IV-6	138
Jang, Han-Ki	초S-IX-5	207

Name	Abstract ID	Page
Jeen, Hyoungjeen	HM02	48
Jeen, Hyoungjeen	HM07	54
Jeen, Hyoungjeen	SM01	60
Jeon, Haechan	MD05	38
Jeon, Jeehoon	SS02	72
Jeong, Jae Won	초S-II-8	157
Jeong, Jong-Ryul	초S-III-6	130
Jeong, Wooseong	초S-III-5	127
Jeong, Wooseong	초S-III-5	127
Jin, Hyo-Sun	MT12	21
Jiralerspong, Trivoramai	NS03	82
Jiralerspong, Trivoramai	SA04	91
Joo, Sungjung	SS02	72
Jung, Kyung-Tae	초S-VIII-1	189
Jung, Kyung-Tae	초S-VIII-3	191
Jung, Min-Seung	초S-IV-6	138
Jung, Young-Hoon	초S-VIII-2	190
Jung, Youngjin	초S-IX-4	204
Kang, Jihoon	초S-IX-2	200
Kang, Kung wan	HM07	54
Kang, M. S.	HM06	52
Kerber, Nico	초S-V-4	150
Khairani, Inna Yusnila	NS03	82
Khan, Imran	MT01	9
Khan, Imran	MT08	17
Kim, Bongju	초S-VII-1	179
Kim, Bosung	MD06	40
Kim, Bosung	MD07	42
Kim, Bumseop	MT17	26
Kim, C. G.	SA02	89
Kim, C. G.	초S-III-1	121
Kim, Changyoung	초S-VII-1	179
Kim, Cheol Gi	MT07	16
Kim, Cheol Gi	초S-III-5	127
Kim, Chul Sung	초S-VI-2	164
Kim, Chul Sung	초S-VI-5	167
Kim, Dae-Yun	MD09	45
Kim, Donghwan	HM08	55
Kim, Donghwan	초S-II-7	156
Kim, Dong-Hyun	초S-II-9	158
Kim, Duck-Ho	초S-IV-4	136
Kim, Ga-Yeong	HM03	49
Kim, Ga-Yeong	MT05	14
Kim, Ga-Yeong	초S-II-5	117
Kim, H. J.	HM06	52
Kim, Hi-Jung	O-1	97
Kim, Hyeonsal	MT07	16
Kim, Hyun Jung	HM02	48
Kim, Jiho	MT19	28
Kim, Jihye	HM10	58
Kim, Jong-Woo	초S-II-6	155
Kim, Jun Sung	초S-I-5	109
Kim, June-Seo	초S-III-3	124
Kim, Junhoe	MD08	44
Kim, Junyeon	초S-VII-2	180
Kim, K. W.	초S-III-1	121
Kim, Kab-Jin	MD04	37
Kim, Kab-Jin	초S-IV-4	136
Kim, Keonmok	MT07	16
Kim, Kyoung-Whan	초S-V-4	150
Kim, Kyoung-Whan	초S-V-5	151
Kim, Kyung Min	HM04	50
Kim, Kyung Min	초S-II-10	159
Kim, M. J.	초S-III-1	121
Kim, Mijin	초S-III-5	127
Kim, Mingu	MT19	28
Kim, Min-Kwan	MD01	33
Kim, Namkyu	MT04	12
Kim, S. J.	SA02	89
Kim, S. J.	초S-III-1	121
Kim, Sang-Koog	MD01	33
Kim, Sang-Koog	MD02	35
Kim, Sang-Koog	MD03	36
Kim, Sang-Koog	MD05	38
Kim, Sang-Koog	MD06	40
Kim, Sang-Koog	MD07	42
Kim, Sang-Koog	MD08	44
Kim, Sang-Koog	MT20	30
Kim, Sang-Koog	NS03	82
Kim, Sang-Koog	SA04	91
Kim, Sangsu	SS02	72
Kim, Se Kwon	초S-IV-4	136
Kim, Seo-Jin	MT06	15
Kim, Sumin	HM08	55
Kim, Sumin	초S-II-7	156
Kim, Sung Hoon	초S-VI-4	166
Kim, Sung Jong	SS01	71
Kim, T. W.	SA05	93
Kim, Tae Hee	SO01	74
Kim, Taeyueb	SS02	72
Kim, Y. K.	SA05	93
Kim, Yang-Do	HM03	49
Kim, Yong-Jin	초S-II-8	157
Kim, Young Keun	NS02	81
Kim, Youngjae	초S-III-4	126
Kimata, Motoi	초S-VII-5	185

Name	Abstract ID	Page
Ko, Hye-Won	초S-V-5	151
Ko, Min Jun	NS02	81
Kondou, Kouta	초S-VII-2	180
Koo, Hyun Cheol	SS01	71
Koo, Hyun Cheol	SS02	72
Koo, Hyun Cheol	초S-V-5	151
Kulahlioglu, Adem Halil	MT17	26
Kwon, H. W.	HM06	52
Kwon, Hae-Woong	초S-II-1	113
Kwon, Hae-Woong	초S-II-5	117
Kwon, Seoyeon	SM02	61
Lee, B. W.	NS01	80
Lee, Changgu	초S-I-4	108
Lee, Chung-Seong	초S-VIII-5	194
Lee, Donghun	초S-I-2	106
Lee, Geun-Hee	MD04	37
Lee, H. N.	SA05	93
Lee, Hyun-Sook	HM08	55
Lee, Hyun-Sook	초S-II-7	156
Lee, Hyun-Woo	초S-V-4	150
Lee, Hyun-Woo	초S-VII-2	180
Lee, J. G.	HM06	52
Lee, J. H.	SA02	89
Lee, Jae Dong	초S-III-4	126
Lee, Jae S.	HM02	48
Lee, Jae-Hyeok	MD01	33
Lee, Jae-Hyeok	MT20	30
Lee, Jaehyeok	NS03	82
Lee, Jaekwang	HM02	48
Lee, Jaekwang	HM07	54
Lee, Jaeryung	초S-II-4	116
Lee, Jeong-Jong	초S-VIII-6	195
Lee, Ji Eun	MT16	25
Lee, Jieun	초S-I-6	110
Lee, Jong-Hyuk	MD03	36
Lee, June Hyuk	HM07	54
Lee, Jung Goo	HM04	50
Lee, Jung Gu	초S-II-1	113
Lee, Jung-Goo	HM03	49
Lee, Jung-Goo	MT05	14
Lee, Jung-Goo	초S-II-10	159
Lee, Jung-Goo	초S-II-5	117
Lee, Jung-Goo	초S-II-8	157
Lee, Jun-Sik	초S-VII-1	179
Lee, Kang-Hyuk	HM01	47
Lee, Kang-Hyuk	초S-II-2	114
Lee, Ki-Doek	초S-VIII-6	195
Lee, Ki-Suk	MT04	12
Lee, Ki-Suk	초S-IV-6	138
Lee, Kwan-Woo	MT06	15
Lee, Kwan-Woo	MT11	20
Lee, Kwan-Woo	MT12	21
Lee, Kyung-Jin	초S-IV-4	136
Lee, Kyung-Jin	초S-V-2	148
Lee, Kyung-Jin	초S-V-4	150
Lee, Kyung-Jin	초S-V-5	151
Lee, Oukjae	SS01	71
Lee, Sang-Jun	초S-VII-1	179
Lee, Seong-Hyub	MD09	45
Lee, Seo-Won	초S-V-4	150
Lee, Seung Min	HM04	50
Lee, Seung-Jae	초S-IX-1	199
Lee, Soo Seok	MT04	12
Lee, Sooseok	초S-IV-6	138
Lee, Sungwon	초S-III-5	127
Lee, Suyoun	SS01	71
Lee, Wooyoung	HM08	55
Lee, Wooyoung	초S-II-7	156
Lim, Jung-Tae	초S-II-6	155
Lim, Myung-Seop	초S-VIII-1	189
Lim, Myung-Seop	초S-VIII-2	190
Lim, Myung-Seop	초S-VIII-3	191
Manchon, Aurélien	초S-V-4	150
Mhin, Sungwook	초S-VI-1	163
Min, Byoung-Chul	MD09	45
Miura, Yoshio	초S-VII-3	181
Moon, Jung-Hwan	초S-V-4	150
Moon, Kyoung-Woong	초S-V-4	150
Moriyama, Takahiro	초S-IV-4	136
Nam, Yeong Gyun	초S-II-8	157
Nam, Yune-Seok	MD09	45
Nawa, Kenji	초S-VII-3	181
Nguyen, Quynh Anh T.	MT13	22
Nishimura, Tomoe	초S-IV-4	136
Nothhelfer, Jonas	초S-V-4	150
Ochirkhuyag, T.	초S-VII-6	186
Odkhuu, D.	초S-VII-6	186
Oh, Jung Hyun	초S-V-5	151
Oh, S.	초S-III-1	121
Oh, Se-Hyeok	초S-IV-4	136
Oh, Young-Wan	초S-V-2	148
Okuno, Takaya	초S-IV-4	136
Okyay, Mahmut Sait	MT17	26
Ono, Teruo	초S-IV-4	136
Ono, Teruo	초S-V-1	147
Ortiz, Mezie Laurence B.	초S-IX-4	204

Name	Abstract ID	Page
Otani, YoshiChika	초S-VII-2	180
Park, Bum Chul	NS02	81
Park, Byong-Guk	초S-V-2	148
Park, Chang Geun	초S-VII-6	186
Park, Cheol Soo	초S-IX-3	203
Park, Hyeon-Jong	초S-V-5	151
Park, Hyeon-Jin	초S-VIII-1	189
Park, Hyeon-Jin	초S-VIII-5	194
Park, Hyeon-Jun	초S-VIII-3	191
Park, Hyeon-Kyu	MD03	36
Park, Hyun Soon	T-2	4
Park, Je-Geun	초S-I-3	107
Park, Jihoon	초S-II-6	155
Park, Jin Sik	MT02	10
Park, Jun Kue	HM02	48
Park, Minkyu	MT15	24
Park, Noejung	MT17	26
Park, Se Young	초S-VII-1	179
Park, Seung-Young	SA03	90
Park, Sungkyun	MT01	9
Park, Tae-Eon	SS01	71
Park, Yong-Keun	MD09	45
Pham, Thi Kim Hang	SO01	74
Phan, T. L.	NS01	80
Pyo, Min Ji	HM04	50
Qian, Hui-Dong	초S-II-6	155
Rhie, Kungwon	MT19	28
Rhim, S. H.	MT02	10
Rhim, S. H.	MT03	11
Rhim, S. H.	MT09	18
Rhim, S. H.	MT10	19
Rhim, S. H.	MT13	22
Rhim, S. H.	MT14	23
Rhim, S. H.	MT18	27
Rhim, S. H.	초S-VII-6	186
Rhim, Sung Hyon	MT15	24
Rhyu, Se-Hyun	초S-VIII-6	195
Roh, Jong Wook	HM08	55
Roh, Jong Wook	초S-II-7	156
Ryu, Sangkyun	HM02	48
Ryu, Sangkyun	HM07	54
Schmidt, Oliver G.	P-2	141
Shin, Dongbin	MT17	26
Shin, Jae Cheol	SS02	72
Shiota, Yoichi	초S-IV-4	136
Sim, Jaegun	MD01	33
Sim, Jaegun	MD02	35
Sim, Jaegun	MT20	30
Sim, Jaegun	NS03	82
Sinova, Jairo	초S-VII-4	183
Sohn, Byungmin	초S-VII-1	179
Song, Young-Joon	MT12	21
Subhan, Fazle	MT08	17
Suess, Dieter	MD08	44
Sun, Gwang Min	초S-VI-2	164
Talantsev, A. D.	초S-III-1	121
Thuy, Hoang Thu	MT10	19
Tran, N.	NS01	80
Tsai, Hanshen	초S-VII-2	180
Tserkovnyak, Yaroslav	초S-IV-4	136
Tsevelmaa, T.	초S-VII-6	186
Tsukamoto, Arata	초S-IV-4	136
Tuvshin, D.	초S-VII-6	186
Uhm, Young Rang	초S-VI-2	164
Ul-ain, Qurat	MT14	23
Won, Jong-Hun	초S-IX-1	199
Yamane, Yuta	초S-VII-4	183
Yang, Hyunsoo	P-1	101
Yang, Hyunsoo	초S-V-3	149
Yang, Jaehak	MD03	36
Yang, Jaehak	MD08	44
Yang, Jingyu	초S-IX-2	200
Yang, Sangsun	초S-II-8	157
Yim, Haein	SM02	61
Yoo, Jae-Gyeong	MT05	14
Yoo, Jae-Gyeong	초S-II-5	117
Yoo, Sang-Im	HM01	47
Yoo, Sang-Im	SA03	90
Yoo, Sang-Im	초S-II-2	114
Yoon, Jongwan	MT07	16
Yoon, Sunghyun	초S-VI-5	167
Yoshikawa, Hiroki	초S-IV-4	136
You, Jae-Hyoung	SA03	90
Yu, Jaejun	MT14	23
Yu, Ji Hun	초S-II-8	157
Yu, Ji-Sung	MD09	45
Yu, Young-Sang	초S-IV-6	138
Yun, Changjin	MT19	28
Zhou, Hua	초S-VII-1	179
Zulkifli, Nora Asyikin Binti	초S-III-5	127
강병욱	BM02	86
강병욱	SM05	66
강준호	초S-IV-2	134
김갑진	초S-IV-2	134
김경모	SM06	68
김경원	SA01	88

Name	Abstract ID	Page
김규섭	HM09	56
김규식	HM09	56
김규원	SS03	73
김남규	T-1	3
김동석	초S-IV-1	133
김동영	초S-III-2	123
김동옥	초S-IV-1	133
김민석	SA01	88
김상국	MT21	32
김상준	초S-X-2	213
김상준	초S-X-6	220
김상훈	초S-IV-2	134
김수철	HM09	56
김영근	SS03	73
김용진	SS03	73
김은애	초S-X-2	213
김은애	초S-X-6	220
김정목	초S-IV-2	134
김정훈	SM03	62
김종렬	HM05	51
김종렬	초S-II-3	115
김종우	초S-VI-3	165
김주성	SO04	79
김창수	초S-IV-1	133
김창수	초S-IV-2	134
김창우	초S-VIII-4	192
김철기	초S-III-2	123
김철성	SM03	62
김철성	SO02	75
김철성	SO03	77
김철성	초S-VI-3	165
김태현	SS03	73
김택수	HM11	59
남선우	HM11	59
남영균	SM04	64
목진원	BM01	84
문경웅	초S-IV-1	133
문경웅	초S-IV-2	134
민병철	SO04	79
박관수	초S-X-4	216
박규영	MT21	32
박덕근	SM06	68
박병국	초S-IV-2	134
박승영	SO02	75
박승영	초S-IV-2	134
박예라	SM06	68
박용근	SO04	79
박정현	SO04	79

Name	Abstract ID	Page
박지훈	초S-VI-3	165
방승환	BM01	84
배기웅	초S-X-1	211
서성원	초S-VIII-4	192
서재연	SO02	75
손대락	SM06	68
손대락	초S-X-2	213
손대락	초S-X-6	220
신경훈	초S-VIII-4	192
신광호	SA01	88
신정우	SM06	68
양상선	SM04	64
양승모	초S-IV-1	133
양창섭	초S-X-1	211
양창섭	초S-X-3	214
양창섭	초S-X-5	218
오성훈	초S-IX-6	208
유세현	HP-2	175
유지훈	SM04	64
윤석수	초S-III-2	123
윤익재	초S-VIII-4	192
윤정범	초S-IV-1	133
이기석	T-1	3
이년종	초S-IV-2	134
이병화	HM09	56
이상석	BM02	86
이상석	SM05	66
이상선	초S-IV-1	133
이수길	초S-IV-2	134
이재욱	초S-IV-2	134
이재훈	초S-III-2	123
이지민	HM05	51
이현숙	BM01	84
이현진	초S-X-1	211
이현진	초S-X-3	214
이호영	초S-X-4	216
임상현	초S-X-4	216
임정태	초S-VI-3	165
장강현	초S-VIII-4	192
전병선	초S-IV-1	133
정대한	T-1	3
정도일	초S-IX-6	208
정봉출	초S-X-3	214
정우진	초S-X-1	211
정재원	SM04	64
정현주	초S-X-1	211
정현주	초S-X-3	214
정현주	초S-X-4	216

Name	Abstract ID	Page
정현주	초S-X-5	218
조재훈	초S-IV-1	133
조재훈	초S-IV-5	137
조주영	HM11	59
좌용호	HM05	51
좌용호	HM11	59
차인호	SS03	73
천휘동	초S-VI-3	165
최석봉	SO04	79
최장영	초S-VIII-4	192
최종구	BM02	86
최종구	SM05	66
최철진	초S-VI-3	165
최현경	SO03	77
카지드마	SM05	66
표성영	초S-X-1	211
표성영	초S-X-3	214
한승현	BM01	84
한희성	T-1	3
황찬용	초S-IV-1	133
황찬용	초S-IV-2	134
황현석	SO04	79

Digests of the KMS 2019 Summer Conference

The Korean Magnetics Society

사단법인 한국자기학회

2019년도 하계학술연구발표회 논문개요집 제 29권 1호

(06130) 서울특별시 강남구 테헤란로 7길 22(역삼동635-4) 한국과학기술회관 신관 905호

TEL. (02)3452-7363, **FAX.** (02)3452-7364

E-mail. komag@unitel.co.kr, **Home-page.** www.komag.org

PHILIPS

Digital MRI - Compressed SENSE

Without Compressed SENSE

Total
16:52

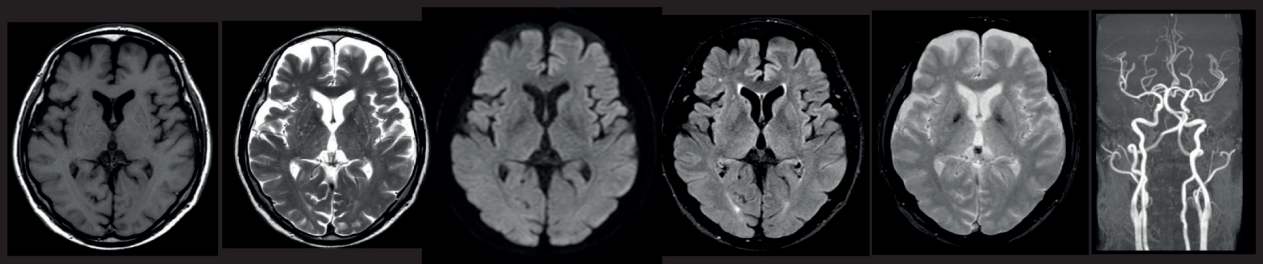

T1W SE
2.35 min

T2W TSE
2.04 min

DWI (b1000)
0.45 min

T2W FLAIR
2.12 min

T2W FFE
1.15 min

3D MRA
7.11 min

With Compressed SENSE

Total
9:06

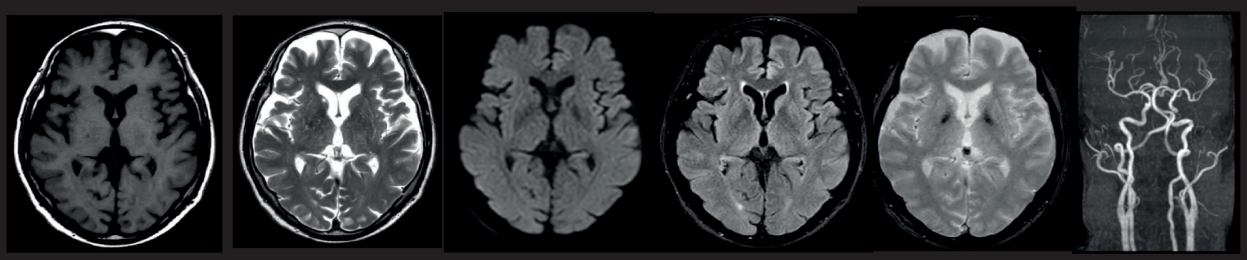

T1W SE
1.14 min

T2W TSE
1.30 min

DWI (b1000)
0.45 min

T2W FLAIR
1.30 min

T2W FFE
0.49 min

3D MRA
3.06 min

Speed done right.
Every time.
Compressed SENSE

innovation + you